STUDY OF DAMPING IN LAYERED AND WELDED BEAMS

Bhagat Singh

DEPARTMENT OF MECHANICAL ENGINEERING
NATIONAL INSTITUTE OF TECHNOLOGY
ROURKELA - 769008, ODISHA, INDIA

NOVEMBER 2011

STUDY OF DAMPING IN LAYERED AND WELDED BEAMS

A THESIS SUBMITTED TO THE
NATIONAL INSTITUTE OF TECHNOLOGY, ROURKELA
IN PARTIAL FULFILMENT OF THE REQUIREMENTS
FOR THE DEGREE OF

DOCTOR OF PHILOSOPHY

IN

MECHANICAL ENGINEERING

BY

Bhagat Singh
(Roll- 508ME104)

UNDER THE GUIDANCE OF

Prof. Bijoy Kumar Nanda

DEPARTMENT OF MECHANICAL ENGINEERING
NATIONAL INSTITUTE OF TECHNOLOGY
ROURKELA - 769008, ODISHA, INDIA

NOVEMBER 2011

DEDICATED TO MY PARENTS

Department of Mechanical Engineering
National Institute of Technology
Rourkela-769008, Odisha, India

Certificate

This is to certify that the thesis titled **"Study of damping in layered and welded beams"** being submitted to the National Institute of Technology, Rourkela (India) by **Mr. Bhagat Singh** for the award of the degree of **Doctor of Philosophy (Mechanical Engineering)** is a record of bonafide research work carried out by him under my supervision and guidance. Mr. Singh has worked for more than three years on the above problem and the work has reached the standard fulfilling the requirements and regulations for the degree. To the best of my knowledge, the work incorporated in this thesis has not been submitted in part or full to any other University or Institute for the award of any degree or diploma.

N.I.T. Rourkela (Prof. Bijoy Kumar Nanda)

Date: Supervisor

Acknowledgement

First and foremost, I express my deep sense of indebtedness and gratitude to Dr. B.K. Nanda, Professor, Department of Mechanical Engineering, National Institute of Technology, Rourkela for kindly providing me an opportunity to work under his supervision and guidance. His keen interest, invaluable guidance and immense help have helped for the successful completion of the thesis.

I express my sincere thanks to Prof. S.K. Sarangi, Director, NIT, Rourkela for creating healthy working environment in the campus and giving permission to use the facilities available in the institute for this study.

I would also like to thank Prof. K.P. Maity, Head of the Department, Prof. N. Kavi, and other faculty and staff members of the department for their help and cooperation during the progress of the work. I am immensely grateful to Dr. S.C. Mohanty, Professor-in-charge of Dynamic Laboratory and his staffs for their cooperation and support in conducting the experiments.

I also acknowledge the help extended by my colleagues Mr. L.N. Patra, Mr. Ramesh Mohanty and Mr. C.R. Deo of the department for providing friendship, moral support and good times during the course of this work.

Special thanks to my parents, brothers and sisters for their love, affection and understanding.

I wish to thank my wife for sharing all the good and bad moments and for her love, sacrifice and understanding. Without her full support and encouragement, this thesis would not have been brought to completion.

This thesis is dedicated to my beloved son Samay and daughters Diya and Siya. I love them more than I can express.

N.I.T. Rourkela (Bhagat Singh)

Abstract

Vibration and noise reduction are crucial in maintaining high performance level and prolonging the useful life of machinery, automobiles, aerodynamic and spacecraft structures. Notwithstanding the variety and immensity of work done within this domain of study, and despite all possibly most accurate solutions and arduous experiments, many aspects related to damping remain poorly examined. In fact, the damping and its improvement in machines or structures are one of the biggest challenges to the practicing engineers. Following the requirements of modern technology, there is an increasing demand for machine tools and fabricated structures with high stiffness, high damping capacity and light weight. Such requirements necessitated the use of layered and welded cantilever beams as structural members. Alternatively, cast cantilever beams can be used, but unfortunately, these are more expensive to manufacture. As a result, the deployment of welded layered beams is becoming increasingly common in the machine tool industry and fabricated construction. Many structures are made by connecting structural members through joints. Due to very low material damping of built-up structures, sufficient damping has to come from the joints. Damping in built-up structures is often caused by energy dissipation due to micro-slip along frictional interfaces (e.g., at welded joints), which provides a beneficial damping mechanism and plays an important role in the vibration behavior of such structures.

The research presented in this thesis is devoted to the problem of damping estimation in engineering structures, typically welded and layered cantilever beams, through analytical and experimental work. The ultimate goal of this project is to develop a damping model that is capable of describing the effects of welded joints on a vibrating structure. In order to do this, it is not necessary to model the actual physics at the microscopic level, instead, the macroscopic effects of the joint on the gross vibration characteristics of the structure are considered and a way for modeling these effects is sought. A careful theoretical and experimental study to quantify the effects of the joints on the structural damping is an integral part of this effort. This thesis consists of two different parts: a theoretical analysis of the problem and an experimental work. The theoretical analysis proposes three different methods to evaluate damping:

classical, finite element and response surface method. It is a general fact that the theoretically computed results will differ from the actual values due to the assumptions made in the theoretical analyses. In view of this discrepancy in results, experiments are conducted for different set of mild steel and aluminium specimens under different vibrating conditions. Time and frequency domain approaches have been adopted to experimentally evaluate the damping capacity. Both the numerical and experimental results are compared for authentication. Finally, useful conclusions have been drawn from both the numerical and experimental results.

The damping characteristics in jointed structures are influenced by the intensity of pressure distribution, micro-slip and kinematic coefficient of friction at the interfaces and their correct assessment is very important to understand the mechanism of damping in such structures. All the above vital parameters are largely influenced by the thickness ratio of the beam and thereby affect the damping capacity of the structures. In addition to this, number of layers, cantilever length and beam thickness also play key roles on the damping capacity of the jointed structures quantitatively. The effect of all these parameters is studied vividly in the present investigation. It is established that the damping capacity can be enhanced appreciably using larger cantilever length and lower thickness ratio of the beams. Further improvement in damping is possible with the use of more number of layers compared to its equivalent solid one. This design concept of using layered structures with welded joints can be effectively utilized in trusses and frames, automobiles, aerodynamic and spacecraft structures, bridges, machine members, robots and many other applications where higher damping is required.

CONTENTS

List of Figures

List of Tables

Nomenclature

English Symbols

A	Area of cross-section of the beam
$\boldsymbol{d}^e$	Nodal displacement vector of an element
b	Width of the beam
$\mathbf{C}$	Damping matrix
$\mathbf{q}^e$	Nodal displacement vector
$\boldsymbol{D}$	Global displacement vector
$\ddot{\boldsymbol{D}}$	Global acceleration vector
E	Static bending modulus of elasticity
E_{loss}	Total energy loss per cycle
E_{ne}	Maximum strain energy stored in the system
$f(t)$	Forcing time dependent displacement function
F_0	Amplitude of forcing time dependent displacement function
$2h$	Overall thickness of the beam of the welded beam
$H(t)$	Heaviside function
I	Moment of inertia of the cross-section of the beam
k	Static bending stiffness of the layered and jointed beam
k'	Static bending stiffness of the solid beam
$\mathbf{k}^e$	Element stiffness matrix
$\mathbf{K}$	Global stiffness matrix
l	Length of the layered and welded beam individual
m	Number of layers in a jointed beam
$\mathbf{m}^e$	Element mass matrix

M	Global mass matrix
n	Number of finite elements
p	Interface pressure
P	Static load applied at the free end of the cantilever beam
P_c	Critical static load applied at the tip of the welded cantilever beams
u_1	Displacement in the x-direction of points on the upper beam
u_2	Displacement in the x-direction of points on the lower beam
v_1	Vertical deflection of upper laminate
v_2	Vertical deflection of lower laminate
$X_i(x)$	Modal function
N_1, N_2, N, N'	Cubic shape functions
t	Time coordinate
u_r	Relative dynamic slip at the interfaces
W	Static load
x_1, x_{z+1}	Amplitude of first cycle and last cycle, respectively
$y(l, 0)$	Initial free end displacement
z	Number of cycles

Greek Symbols

α	Dynamic slip ratio
δ	Logarithmic decrement of the system
Δ	Deflection due to static load
μ	Kinematic coefficient of friction
η_s	Loss factor
ω	Excitation frequency

ω_n	Natural frequency of vibration
ω_d	Damped frequency of vibration
$\boldsymbol{\phi}$	Eigenvector or modal displacement
$\varphi_i(t)$	Time-dependent function
ρ	Mass density
σ_{x_1}	In-plane bending stress on the upper laminate
σ_{x_2}	In-plane bending stress on the lower laminate
τ_{xy}	Shear stress at the interfaces
θ_1, θ_2	Slope at the nodes of an element
ψ	Damping ratio

Superscripts

e	Element

Operators

‘.’	$\frac{\mathrm{d}}{\mathrm{dt}}$
‘..’	$\frac{\mathrm{d}^2}{\mathrm{dt}^2}$
‘,’	$\frac{\mathrm{d}}{\mathrm{dx}}$
‘,,’	$\frac{\mathrm{d}^2}{\mathrm{dx}^2}$
‘,,,’	$\frac{\mathrm{d}^3}{\mathrm{dx}^3}$
‘,,,,’	$\frac{\mathrm{d}^4}{\mathrm{dx}^4}$
T	Transpose of a matrix

1

INTRODUCTION

1.1 Background

Studies on vibration damping in fabricated structures can be dated back to a few decades ago. Problems associated with vibration damping and noise control in these structures has been a subject of comprehensive interest of scientists and researchers for a long time. Engineering structures are generally fabricated using a variety of fasteners such as bolted, riveted, welded joints etc. Joints are an integral part of most of the real structures. However, its behavior under dynamic condition has not yet been fully understood by the researchers. This is an impediment to accurate modeling. Joints have a great potential for reducing the vibration levels of a structure thereby attracting the interest of many researchers. These connections are recognized as a good source of energy dissipation and greatly affect the dynamic behavior in terms of natural frequency and damping [1-3]. This structural damping offering excellent potential for large energy dissipation is associated with the interface shear of the joint. It is thus recognized that the provision of joints can effectively contribute to the damping of all fabricated structures.

The damping and its improvement in structural applications poses the biggest challenge to the practicing engineers. Usually, such structures possess both low structural weight and damping. This situation calls for use of additional measures to improve the damping characteristics by dissipating more energy. However, increasing the damping capacity of a structure is not always easy and may often lead to the waste of energy during normal operating conditions. The monolithic structures can be used as a replacement, but unfortunately they possess very low inherent material damping and are not cost-effective. One of the techniques used for improving damping is fabricating these structures in layers by means of joints which provide suitable means of energy dissipation. The introduction of joints promotes the flexibility of the assembled structures and contributes adequately to the damping properties. The low

material damping of assembled structures are thus compensated. Therefore, the use of joints is becoming increasingly significant in most of the engineering applications.

However, the use of joints has its own drawbacks causing fretting corrosion at the interfaces, reducing stiffness and presenting difficulty in analysis due to nonlinearity [4]. Beards [5] has pointed out that any loss of static stiffness of a structure will not necessarily affect the integrity of the structure if the joints are carefully designed. The effect of friction joints on the reduction of vibration level have attracted great interests from many researchers in the past and present [6-16]. A detailed discussion on joint damping is presented in the next chapter.

Although most of the inherent damping occurring in real structures arises in the joints, but little effort has been made to study this source of damping because of complex mechanism occurring at the interfaces due to coefficient of friction, relative slip and pressure distribution characteristics. It is therefore important to focus the attention on these parameters for accurate assessment of damping capacity of structures. The role of friction is of paramount importance in controlling the dynamic characteristics of engineering structures. In applications where relative motion between surfaces in contact occurs, the effect of frictional forces, whether desirable or not, cannot be ignored. The friction mechanism has a tendency to reduce the vibratory response of the structures and provide the energy dissipation at the interfaces. These effects are desirable in applications where friction reduces large resonant stresses and high cycle fatigue, such as built-up structures.

The contact pressure between the surfaces is generated by the clamping action of the joints and plays a vital role in the joint properties. Under such circumstances, the profile of the interface pressure distribution assumes a significant role, especially in the presence of slip for dissipation of vibration energy. In the past few decades, several researchers have tried to investigate the nature of pressure distribution at the interfaces of the assembled structures. Almost all previous researchers have idealized the joints by assuming a uniform pressure profile without considering the effects of surface irregularities and asperities [17-22].

The presence of friction in connecting joints has a strong impact on the system dynamics and largely contributes to the majority of the damping capacity of the system. It is understood that the joint friction arises only when the contacting layers

tend to move relatively under the action of transverse vibration and serves as a catalyst for energy dissipation. For most of the analysis, the Coulomb's friction law is widely used to represent the dry friction at the contacting surfaces. Many authors have carried out an elaborate review of research on the effects of joint friction on structural damping in built-up structures [2, 3, 23-25].

Micro-slip is the mechanism by which mechanical joints dissipate energy and therefore, a better understanding of its phenomenon is required for the study of damping effects in the jointed structures. Joints seem to exhibit two types of motion during vibration: microslip and macroslip [26]. When the dynamic load is increased or decreased within a threshold range, slip along the frictional joint interfaces occurs locally at the joints. This situation is called micro-slip, where the slip along the interface is localized in the slip region while the rest of the interface is in the stick region. When the load reaches beyond the threshold range, a larger portion of the interface will break free and slip. Eventually, slip along the entire interface takes place which is referred to as macro-slip. While both micro and macro-slip causes energy dissipation thus providing the dominant damping mechanism in a built-up structure but the latter is generally avoided as it leads to structural damage of the joints. The contribution of the micro-slip on the overall system damping is significant in spite of its low magnitude and is generally promoted in structural joint designs.

The origin and mechanism of damping are complex and sometimes difficult to comprehend. The energy of the vibrating system is dissipated by various mechanisms and often more than one mechanism may be present at the same time. Although the knowledge on the friction joint is limited, efforts have been made in the present investigation to study the damping aspect of the friction joints in built-up structures.

1.2 Motivation

Built-up structures are fabricated using many types of fasteners such as bolted, riveted and welded joints. Welded joints are extensively used to fabricate assembled structures in machine tools, automotive, aerospace and many such industries requiring high damping. Vibration attenuation in these structures can enhance the dynamic stability significantly. It has been observed that friction damping at the interfaces in built up structures provides a beneficial role in reducing the adverse effects of vibrations thereby enhancing their life. The dynamics of bolted and riveted structures

have been studied by many investigators as evident from the wealth of published literatures. However, a little amount of research has been reported till date on the mechanism of damping in layered and welded symmetrical structures. No work has been reported till date on the damping mechanism of layered and tack welded beams of unequal thickness subjected to various kinds of loading. Moreover, surface roughness is an important factor influencing the microslip phenomenon in the jointed structures that has been overlooked by most of the earlier researchers and little work has been reported on this aspect till date. The motivation for the present investigation lies in developing the theory of damping mechanism in both symmetrical and unsymmetrical welded beam structures using classical, finite element method and response surface methodology approach under the consideration of surface roughness parameter.

1.3 Linear Problem

Generally, the structural problems are divided into two categories i.e., linear and nonlinear systems. In linear systems, the excitation and response are linearly related and their relationship is given by a linear plot. For many cases, this assumption is valid over certain operating ranges. Working with linear models is easier from both an analytical and experimental point of view. For a linear system, the principle of superposition holds which means that doubling the excitation will approximately double the levels of the response. For beams undergoing small displacements, linear beam theory is used to calculate the natural frequencies, mode shapes and the response for a given excitation. Linear and nonlinear systems agree well at small values of excitation, while they deviate at higher levels. The nonlinear beam theory is used for larger displacements where the superposition principle is not valid. The linear vibration theory is used when the beam is vibrated at small amplitudes and lower modes of vibration. The present investigation mainly focuses on the study of damping of jointed and welded cantilever beams at lower excitation levels which can be well considered as linear.

1.4 Beam Theories

The beam is one of the fundamental elements of an engineering structure and finds wide applications in structural members. These beam-like structures are typically subjected to dynamic loads. Therefore, studying the static and dynamic response, both

theoretically and experimentally, of these structural components under various loading conditions would help in understanding and explaining the behavior of more complex and real structures.

The popular beam theories used are: (a) Euler-Bernoulli beam theory and (b) Timoshenko beam theory. Dynamic analysis of beams is generally based on one of the above beam theories. If the lateral dimensions of the beam are less than one-tenth of its length, then the effects of shear deformation and rotary inertia are neglected for the beams vibrating at low frequency [27]. The no-transverse-shear assumption means that the rotation of cross section is due to bending alone. A beam based on such conditions is called Euler-Bernoulli beam or thin beam.

If the cross-sectional dimensions are not small compared to the length of the beam, the effects of shear deformation and rotary inertia are to be considered in the analysis. Timoshenko [28] included these effects and obtained results in accordance with the exact theory. The hypothesis presented by Timoshenko is known as thick beam theory or Timoshenko beam theory.

The present investigation is based on the assumptions of Euler-Bernoulli beam theory as the beam is vibrated at low frequency and the dimensions of test specimens are much smaller in the lateral directions compared to length, thus satisfying the condition of thin beam theory.

1.5 Modeling of a Structure

It is essential to have a theoretical model to represent the damping mechanism of jointed structures. Theoretical modeling of the present problem considers two approaches using the Euler-Bernoulli beam theory: continuous and finite element models. Both these approaches are used in the present investigation.

A continuous model is characterized by a partial differential equation with respect to spatial and time coordinates which is often used for studying simple structures such as a uniform beam. Exact solutions of such equations are possible only for a limited number of problems with simple geometry, boundary conditions and material properties.

However, real-life engineering structures are generally very complex in geometry, boundary conditions and material properties. For this reason, normally some kind of

other approximate method is needed to solve a general problem. In contrast to the continuous model, the system is characterized by a finite element model which consists of one-dimensional elements. Each element consists of two nodes with three degrees of freedom, i.e., rotation, transverse and axial displacement at each node. In this case, the equations of motion are expressed by a set of coupled ordinary-differential equations.

The damping model of jointed structures is also developed based on the experimental data. In the present work, response surface methodology has also been adopted to develop the damping models of layered and jointed welded structures. Response surface methodology (RSM) is a technique used to determine and represent the cause and effect of relationship between true mean responses and input control variables influencing the responses as n-dimensional hyper surface. Response surface methodology is a new statistical approach in which the experimental results of damping capacity are statistically analyzed considering the various factors affecting the damping.

In order to validate the developed theoretical models experiments have been performed. Several experimental techniques are in use to quantify the level of damping in a structure. The most popular experimental techniques are the frequency and time domain approaches.

In time domain, the damping ratio is identified using the logarithmic decrement method. The time domain methods are based on the observation of the time history of energy dissipation which results in the decay of amplitude of oscillation. Time signals can also be processed using Time-Frequency Transforms when several frequencies or nonlinear behaviors are taken into account [29]. This method is generally applied to lightly damped structures excited at low amplitude and frequency.

The frequency domain analysis is based on frequency response and forced vibration is the main concept behind this method. In frequency domain, the loss factor is evaluated using the half power band width method. The frequency domain method is based on the decaying of the amplitudes at the various modal frequencies. In the frequency domain, it is possible to estimate the damping ratio by analyzing the experimental Frequency Response Functions (FRF) [8,30]. There are several approaches that have been utilized to identify joint parameters. These approaches rely

on the experimental measurements of FRFs. In the present work, both the approaches have been used to evaluate the damping capacity of layered and welded structures.

1.6 Aims and Objectives of this Research

Following the requirements of modern technology, there is an increasing demand for machine tools and fabricated structures with high stiffness, high damping capacity and light weight. Such requirements necessitated the use of layered and welded cantilever beams as structural members. Alternatively, cast cantilever beams can be used, but unfortunately, these are more expensive to manufacture. As a result, the deployment of welded layered beams is becoming increasingly common in the machine tool industry and fabricated construction. Many structures are made by connecting structural members through joints. Due to very low material damping of built-up structures, sufficient damping has to come from the joints. Damping in built-up structures is often caused by energy dissipation due to micro-slip along frictional interfaces (e.g., at welded joints), which provides a beneficial damping mechanism and plays an important role in the vibration behavior of such structures.

The research presented in this thesis is devoted to the problem of damping estimation in engineering structures, typically welded and layered cantilever beams, through analytical and experimental work. The ultimate goal of this project is to develop a damping model that is capable of describing the effects of welded joints on a vibrating structure. In order to do this, it is not necessary to model the actual physics at the microscopic level, instead, the macroscopic effects of the joint on the gross vibration characteristics of the structure are considered and a way for modeling these effects is sought. A careful theoretical and experimental study to quantify the effects of the joints on the structural damping is an integral part of this effort.

The damping characteristics in layered and welded structures are influenced by the intensity of pressure distribution, relative dynamic slip and kinematic coefficient of friction at the interfaces and their correct assessment is very important to understand the mechanism of damping in such structures. All the above vital parameters being largely influenced by the thickness ratio of the beam has been critically studied in subsequent chapters.

This thesis consists of two different parts: a theoretical analysis of the problem and an experimental work. The theoretical analysis proposes three different methods to

evaluate damping: classical, finite element and response surface method. The validity of the theoretical methods has been validated by conducting the experiments. Time and frequency domain approaches have been adopted to experimentally evaluate the damping capacity. Both the numerical and experimental results are compared for authentication. Finally, useful conclusions have been drawn from both the numerical and experimental results.

1.7 General Assumptions

In the present analysis, certain assumptions are made while exploring the joint dynamics. These include:

(1) Each layer of the beam undergoes the same transverse deflection.

(2) The initial excitation at the free end of the beam is of small amplitude.

(3) There is no gross or macro-slip at the joint.

(4) The local mass of the joint area is not considered as significant in altering the behavior of the beam.

(5) The effect of residual stress due to tack welding is neglected.

(6) There is no displacement and rotation of the beam at the clamped end.

(7) The Coulomb law of friction is used.

(8) The material behaves linearly.

(9) The deflections are small compared to the beam thickness.

(10) The effects of rotary inertia and shear deformation are neglected.

(11) The material and support damping are neglected.

1.8 Thesis Outline

The research presented in this thesis provides a framework to study the damping capacity and its improvement in welded structures due to joint friction and micro-slip. The investigation as outlined in this thesis is broadly divided into eleven chapters. The thesis is organized as follows:

Chapter 1: This chapter serves as a brief introduction to the thesis work and summarizes the importance, motivation, aims and objectives of the present investigation.

Chapter 2: This chapter contains a detailed survey of relevant literature on various aspects of vibration analysis of layered and jointed structures. Most of the past and present important researches carried out by various investigators have been presented in details. This chapter is divided into different sections emphasizing types of damping, mechanisms of damping, various vibration terminologies and techniques used for improving the damping.

Chapter 3: This chapter gives a detailed description of the theoretical analysis by classical approach considering dynamic slip ratio for determining the damping capacity in welded cantilever beams. The theoretical expression for the uniform pressure distribution has been found out by considering the flat bodies in perfect contact. This pressure distribution has been further utilized to estimate the logarithmic decrement for two as well as multi-layered tack welded beams.

Chapter 4: In this chapter a different approach has been adopted to explore the mechanism of slip damping in two layered welded symmetrical beams with single interface. The relative dynamic slip at the interface has been ascertained considering the in-plane bending stress and expressions for the slope and deflection of the welded beams have been developed. This relative slip is further used to estimate the loss factor of jointed symmetrical beams with single interface for both the cases of static and dynamic loadings.

Chapter 5: In this chapter, a detailed static and dynamic analysis considering in-plane bending stress has been presented for damping mechanism in multilayered symmetrical beams. The expression for relative slip and transverse response have been developed which is further used to develop the damping model of multilayered welded beams. Moreover, in this chapter effect of number of layers on the damping capacity has been studied vividly.

Chapter 6: In this chapter, a detailed analysis has been presented for the estimation of damping in layered and welded beams with unequal thickness. The factors governing the damping capacity of welded unsymmetrical beams are identified considering in-plane bending stress for both free and forced vibration conditions. Further, the findings are compared with that of the equivalent welded symmetrical beams.

Chapter 7: This chapter deals with the solution of the present problem using the finite element method and extends the results of Chapters 3-6 to a welded beam structure represented by a discrete model. The "Minimum Potential Energy" approach has been used to formulate the dynamic equation of free vibration of a welded cantilever beam. In this method, the beam is discretized into finite number of one-dimensional elements and a suitable solution is assumed within each element. Two-node Euler-Bernoulli linear elements of equal length are utilized for the calculations.

Chapter 8: There are number of parameters affecting slip damping in jointed structures which cannot be assessed correctly using the classical theory. Alternatively, experiments are performed and results are analyzed by using suitable technique such as Response Surface Methodology (RSM) to ascertain the effectiveness of these parameters on the damping of layered and jointed structures. The present chapter highlights the use of RSM by designing a three-factor three-level Full Factorial and Central Composite rotatable design matrix with full replication of planning, conducting, executing and developing the mathematical models utilizing the experimental results. This is useful for predicting the mechanism of interfacial slip damping in layered and welded structures. The design utilizes the number of tack welded joints, initial amplitude of excitation, natural frequency and surface roughness at the interfaces as well as the material property to develop a damping model for the layered and welded structures.

Chapter 9: This chapter outlines the details of the experimental set-up, instrumentation, specimen preparation and testing procedure for the measurement of damping. In practice, the experimental measurement of vibration becomes necessary because of the fact that the theoretically

computed damping capacity of a machine or structure may be different from that of the actual values due to assumptions made in the theoretical analysis. Damping of these structures has been experimentally measured in terms of logarithmic decrement and loss factor using the free decay time signals and frequency response functions, respectively. Experimental results for different set of layered and jointed mild steel and aluminium specimens have been compared with the corresponding numerical values obtained in chapters 3-8, for establishing the authenticity of the theory developed. These comparative results are presented in graphical and tabular forms.

Chapter 10: This chapter elaborates the discussions on the results obtained from the theoretical and experimental analysis as outlined in chapters 3-9.

Chapter 11: This chapter summarizes the important conclusions drawn from the observations discussed in the chapter 10 along with some suggestions for continuing the future research in this field.

2

LITERATURE SURVEY

2.1 Preamble

Damping in structures has historically been of great importance in nearly all branches of engineering endeavors, and it also happens to be one of the most difficult parameters to predict. Problems associated with vibration damping and noise control in structures has been a subject of comprehensive interest of scientists and researchers for a long time. Notwithstanding the variety and immensity of work done within this domain of study, and despite all possibly most accurate solutions and arduous experiments, many aspects related to damping remain poorly examined. The study of damping and its improvement in many engineering structures is of paramount importance for controlling excessive vibration. In the present investigation, the effects of welding on damping of fabricated structures have been studied vividly. The reported literature presented in the current chapter deals with the theoretical and experimental findings by various investigators on the interfacial slip damping in built-up structures. At the end of the chapter a summary of the literature survey and the knowledge gap in the earlier investigations are presented.

2.2 Vibration Attenuation

Studies on vibration phenomena can be dated back to a few centuries ago. It has long been observed that when a structure is subjected to a periodic load, it can vibrate violently. Consequently, high levels of stress and noise are built up. Unlike static deformation, the vibration magnitude of a structure is determined by both the magnitude and the period (or frequency) of the excitation. For each structure, there are always some special frequencies; if the frequency of an excitation load happens to coincide with (or be close to) one of these special frequencies, the structure will vibrate at an exceedingly high level due to resonance. These special frequencies are called the natural frequencies and they are the inherent properties of structures.

Usually, corresponding to kinetic energy, potential energy and energy dissipation, the properties of a structure can be defined by mass, stiffness and damping. However, it is also worth mentioning that if some parts of the structure are rotating, other forces such as centrifugal force can be involved. Accordingly, other properties should be used.

Problems involving vibration occur in many areas of mechanical, civil and aerospace engineering: wave loading of offshore platforms, cabin noise in aircrafts, earthquake and wind loading of cable stayed bridges and high rise buildings, performance of machine tools – to pick only a few random examples. Quite often vibration is not desirable and the interest lies in reducing it by dissipation of energy or damping. Characterization of damping forces in a vibrating structure has long been an active area of research in structural dynamics. Since the publication of Lord Rayleigh's classic monograph 'Theory of Sound (1877)', a large body of literature can be found on damping. Although the topic of damping is an age old problem, the demands for modern engineering have led to a steady increase of interest in recent years. Studies of damping have a major role in vibration isolation of automobiles under random loading due to surface irregularities and buildings subjected to earthquake loadings. The recent developments in the fields of robotics and active structures have provided impetus towards developing procedures for dealing with general dissipative forces in the context of structural dynamics. Besides these, in the last few decades, the sophistication of modern design methods together with the development of improved composite structural materials instilled a trend towards lighter structures. At the same time, there is also a constant demand for larger structures, capable of carrying more loads at higher speeds with minimum noise and vibration level as the safety/workability and environmental criteria become more stringent. Unfortunately, these two demands are conflicting and the problem cannot be solved without proper understanding of energy dissipation or damping behaviour.

Structural systems always have very low inherent damping capacities. Hence, passive or active damping techniques are widely used in practice in order to protect structures from hazards of unwanted vibrations [31-32]. Passive damping involves the use of add-on materials with very high damping capacities. For example, high damping viscoelastic materials are often incorporated during fabrication of many structures for the purpose of vibration control. In general, the passive damping is a well developed

technique and cost-effective [33]. Among passive damping treatments, the use of layered constructions connected with mechanical joints is the most commonly used method. On the other hand, active damping refers to the energy dissipation from the system by external means such as actuators and sensors for vibration detection and control.

The origin and mechanism of damping are complex and sometimes difficult to comprehend. The energy of the vibrating system is dissipated by various mechanisms and often more than one mechanism may be present simultaneously. For convenience, damping is generally divided into two major groups identified as: (a) material damping and (b) structural damping.

2.2.1 Material Damping

Material damping is related to the energy dissipation within the volume of material. This mechanism is usually associated with the internal reconstructions of micro and macro structure ranging from crystal lattice to molecular scale effects, thermo-elasticity, grain boundary viscosity, point-defect relaxation, etc. [34, 35]. The majority of published information on material damping is of empirical nature and the underlying physical effects are not fully understood. Besides, there are two types of material damping: hysteretic damping and viscoelastic damping.

When materials are critically stressed, energy is dissipated internally within the material itself. The damping caused by the friction between the internal planes that slip or slide as the material deforms is called the hysteretic damping. Experiments by several investigators indicate that for most structural systems, the energy dissipated per cycle is independent of the frequency and approximately proportional to the stiffness of the system and square of amplitude of vibration. Internal damping fitting to this classification is termed as hysteretic damping. The energy loss per cycle is expressed as $E = \pi k \lambda A^2$, where k, λ and A are the stiffness of the system, dimensionless damping factor depending on the property of the material and amplitude of vibration, respectively. The magnitude of this damping is very small as compared to other types of damping. When a body undergoing material damping is subjected to vibration, the stress-strain diagram shows a hysteresis loop whose area denotes the energy lost per cycle due to damping. The stress (σ) and strain (ε) relations at a point in a vibrating body possess a hysteresis loop as shown in Fig. 2.1.

The area of the hysteresis loop gives the energy dissipation per unit volume of the material per stress cycle [36, 37]. This is termed as specific damping capacity (Ψ) and given by the cyclic integral $\psi = \oint \sigma \, d\varepsilon$.

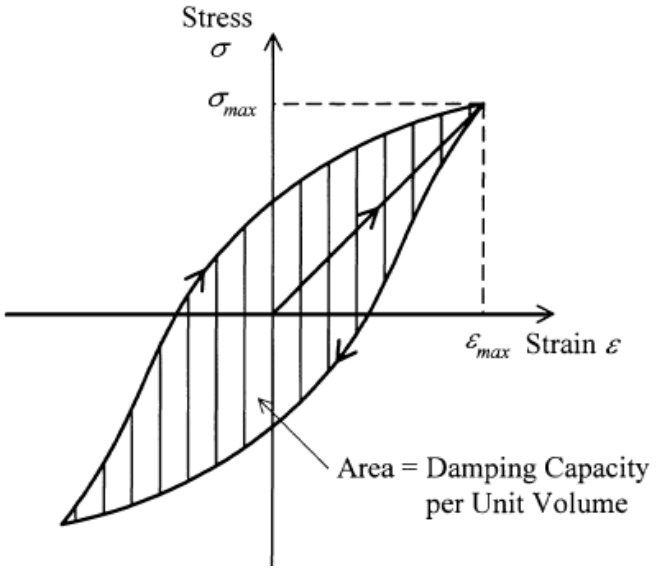

Fig. 2.1 A typical hysteresis loop for material damping

Passive damping using viscoelastic materials (VEM's) is widely used in both commercial and aerospace applications. Viscoelastics are elastomeric materials whose long-chain molecules cause them to convert mechanical energy into heat when they are deformed. The relation between the stress and strain of a viscoelastic damping material is expressed by a linear differential equation with respect to time. The most widespread model used for viscoelastic damping is the Kelvin-Voigt model as it gives the most accurate results for practical purposes [37]. The stress-strain relationship given by this model is $\sigma = E\varepsilon + E^* \dfrac{d\varepsilon}{dt}$, where E and E^* are the Young's modulus and complex modulus of the material, respectively. The term "$E\varepsilon$" represents the elastic behavior of the material with no contribution to damping, while the second term $E^* \dfrac{d\varepsilon}{dt}$ is responsible for damping. The damping capacity per unit volume is expressed as $d_v = E^* \oint \dfrac{d\varepsilon}{dt} d\varepsilon$.

2.2.2 Structural Damping

In most of the real fabricated structures, vibration attenuation is attributed to the slip damping at the joints and interfaces [37]. It is the result of energy dissipation caused by rubbing friction resulting from relative motion between components and by intermittent contact at the joints in a mechanical system. However, the energy dissipation mechanism in a joint is a complex phenomenon being largely influenced by the interface pressure and degree of slip at the interfaces. It is this slip phenomenon occurring in the presence of friction at the joint interface that causes the energy dissipation and nonlinearity in the joints.

Rubbing friction or contact among different elements in a mechanical system causes structural damping. Since the dissipation of energy depends on the particular characteristics of the mechanical system, it is very difficult to define a model that represents perfectly a structural damping. The Coulomb-friction model is a rule used to describe energy dissipation caused by rubbing friction. Regarding structural damping, energy dissipation is determined by means of the coefficient of restitution of the two components that are in contact.

Structural damping is usually estimated by measuring the decaying signal and number of cycles but the measured values represents the total damping in the mechanical system. Consequently, it is necessary to estimate the values for the other types of damping and to subtract them from the measured value in order to obtain a value for structural damping. Structural damping is much greater than the material damping and it represents a large portion of energy dissipation in mechanical structures.

As mentioned above, different factors such as rubbing friction or impacts cause structural damping. The most important form of structural damping is the slip damping. This form of damping is caused by Coulomb friction at a structural joint. It depends on many factors such as joint forces or surface properties. Assuming an ideal Coulomb friction, the damping force at a joint can be expressed through the following expression;

$$f = c \cdot \operatorname{sgn}\left(\dot{q}\right)$$

where:

f = damping force

q = relative displacement at the joint

c = friction factor

and the signum function is defined by:

$$\operatorname{sgn}(x) = 1 \quad \text{for } x \geq 0$$

$$\operatorname{sgn}(x) = -1 \quad \text{for } x < 0$$

The slight rubbing or interfacial slip of the two surfaces nominally at rest with respect to each other results in the corrosion damage of the asperities at the contact surfaces which is technically termed as fretting corrosion [38]. It is recognized that joint damping depends on the rubbing at the interfaces and always occurs in association with fretting corrosion. The fretting corrosion occurring in a structural joint poses a serious problem for the successful joint design. Joint surface prepared from cyanide hardening and electro-discharge machining considerably reduces the fretting effect and also results in enhanced joint damping [39]. The inclusion of joints results in the lowering of the stiffness of the structures. However, this sacrifice in stiffness can be appreciably lowered if the joints are carefully designed. It is often unnecessary to include a special damping device to a structure for increasing the friction damping. Instead, it is easy and cheap to enhance the inherent damping in a structure by utilizing damping in joints ensuring adequate stiffness. This damping mechanism is most effective at low frequencies and first few modes of vibration as the vibration amplitudes are large enough to allow significant slip [38].

2.3 Methods to Enhance Damping of Structures

Vibration and noise reduction in structures can significantly enhance dynamic stability. Vibration attenuation in structures is an important aspect of mechanical design. It has been well established that the extent of inherent damping in structures is very low and various other external means are incorporated in the parent system to improve the damping. A number of techniques have been developed in practice to enhance the damping level of the structures. These include;

- Use of viscoelastic layers
- Use of special high damping inserts
- Use of layered and jointed constructions

2.3.1 Use of Viscoelastic Layers

A viscoelastic material is characterized by possessing both viscous and elastic behavior. This has been illustrated in Fig. 2.2, which shows the behavior of various materials in the time domain.

A purely elastic material is one in which all the energy stored in the sample during loading and is returned during unloading. As a result, the stress and strain curves for elastic materials move completely in phase. For elastic materials, Hooke's Law is applicable, where the stress is proportional to strain, and the modulus is defined as the ratio of stress to strain.

A complete opposite to an elastic material is a purely viscous material as shown in Fig. 2.2 which does not return any of the energy stored during loading. All the energy is lost as "pure damping" once the load is removed. In this case, the stress is proportional to the rate of strain, and the ratio of stress to strain rate is known as viscosity, μ. These materials have no stiffness component except the damping.

For all others materials that do not fall to any one of the above category are called the viscoelastic materials. Some of the energy stored in a viscoelastic system is recovered upon removal of the load, and the remainder is dissipated in the form of heat. The cyclic stress at a loading frequency of ω is out-of-phase with the strain by some angle ϕ, (where $0 < \phi < \pi/2$). The angle ϕ is a measure of the materials damping level; the larger the angle the greater the damping.

One of the unique characteristics of viscoelastic materials is that their properties are influenced by many parameters. They can include: frequency, temperature, dynamic strain rate, static pre-load, time effects such as creep and relaxation, aging, and other irreversible effects. In working with this class of materials, it is necessary to define the materials complex modulus (stiffness and damping properties) as a function of these parameters. Viscoelastic materials are typically characterized by their behavior as shown in Fig. 2.3. These materials exist in various unique states or "phases" over the broad temperature and frequency ranges in which they are used. These regions are typically referred to as the Glassy, Transition, Rubbery, and Flow Regions. Viscoelastic materials behave differently in these regions depending on the types of their applications.

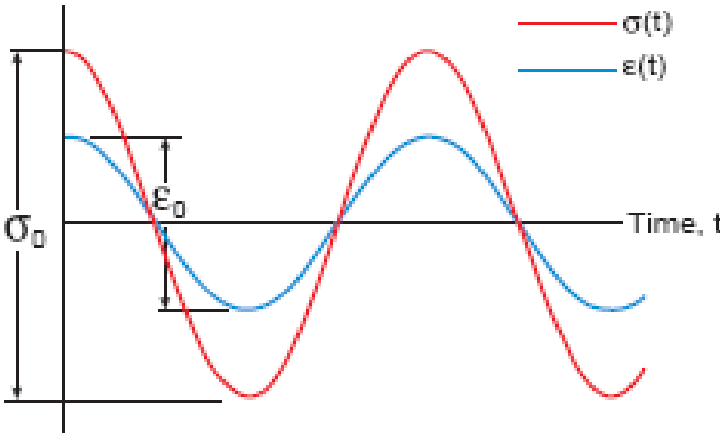

a. Elastic Material

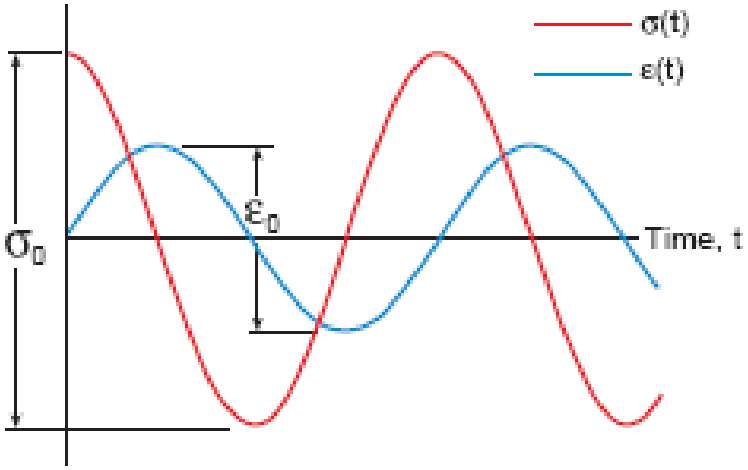

b. Viscous Material

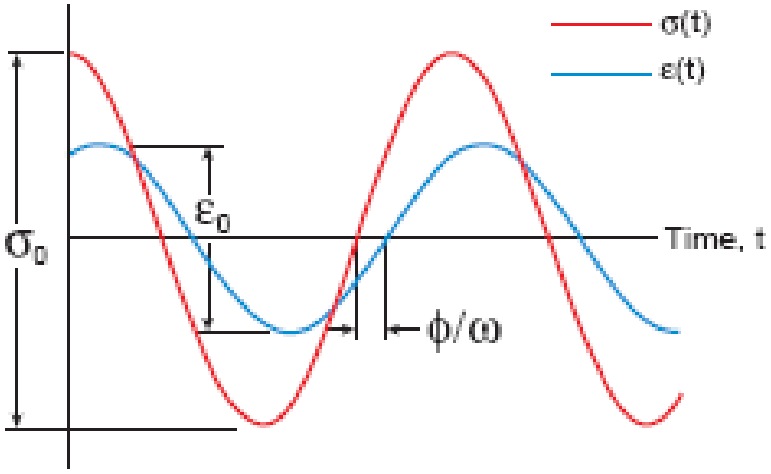

c. Viscoelastic Material

Fig. 2.2 Cyclic stress and strain curves versus time for various materials

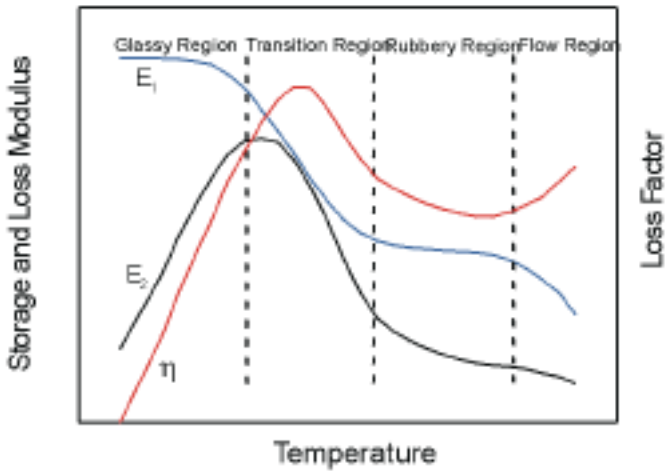

Fig. 2.3 Variation of complex modulus with temperature for viscoelastic material

Viscoelastic damping, also known as passive layer damping, is the most common form of damping treatment and is widely used in various engineering fields [40, 41]. When exposed to vibrations, the high polymeric molecular properties exhibited by the viscoelastic materials enhance the system damping, thereby dissipating considerable amount of vibration energy. Two types of composite constructions widely used in practice are extensional (termed as unconstrained layer) construction where the damping material is applied as a layer on the structural surface and the sandwich construction (termed as constrained layer) where the damping material is sandwiched between elastic layers. The vibratory energy is dissipated due to direct strains in case of the former and predominantly by shear strains in case of the later [42].

For the same mass of applied damping material, sandwich constructions are known to yield significantly larger system damping compared to extensional layer damping treatments. Moreover, the presence of constraining layer results in an additional mass of the sandwich panels. However, unconstrained damping treatments are preferred to sandwich panels in many practical applications due to simplicity.

2.3.1.1 Free - layer or Extensional Damping

Extensional damping is one of the simplest energy control technique as shown in Fig. 2.4. It involves attaching a material with a strong adhesive to the surface of a structure. Alternatively, the structure may be dipped into a vat of heat-liquefied material that hardens upon cooling. Energy is dissipated as a result of extension and compression of the damping material under flexural stress from the base structure. In

such applications, damping performance increases with damping layer thickness. Changing the composition of a damping material may also alter its effectiveness. In order to optimize the system damping, the damping layer must be as rigid as possible. Ideally, the rigidity of the damping layer should match the rigidity of the substrate. Unfortunately, materials with high levels of damping, such as elastomers, plastics and adhesives, typically are significantly less stiff than the substrates to which they are attached, i.e., aluminum fuselage.

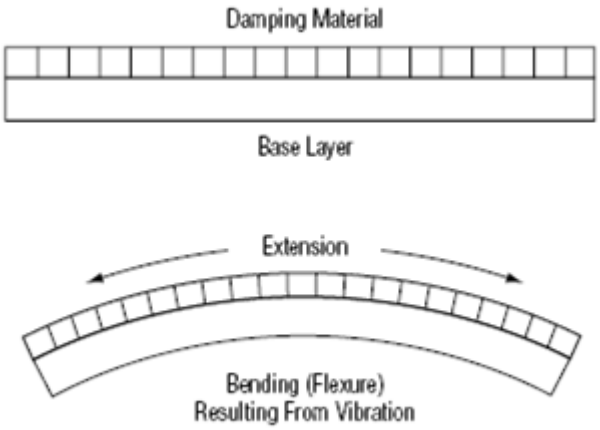

Fig. 2.4 An extensional damping system

In the past few decades' extensional damping constructions have received a considerable amount of interest and extensive investigations have been reported [43, 44]. The addition of damping material results in an increase in the structural mass, which has to be comprehended in the design of lightweight structural configurations, especially in the aerospace and automotive industries. In view of the above considerations, the damping material is applied over a certain area of the structural surface, where the extensional deformation is more effective. Reddy et al. [45] and Parthasarathy et al. [46] through theoretical and experimental investigations have evaluated the effectiveness of unconstrained layer damping treatments in achieving damping when applied to rectangular plates. They have shown that the application of damping material increases the modal loss factor and decreases the modal frequencies.

2.3.1.2 Constrained-layer Damping

Constrained-layer damping systems are usually used for very stiff structures or when a lightweight damping treatment is required. A "sandwich" is formed by laminating

the base layer to the damping layer and adding a third constraining layer as shown in Fig. 2.5. When the system flexes during the vibration, shear strains develop in the damping layer. Energy is lost through shear deformation, rather than extension, of the material. The effect of the outer elastic layer (constraining layer) is to increase the deformation in the viscoelastic core, thus resulting in higher energy dissipation in the viscoelastic material. Constrained damping treatments are employed on the skin of the aircraft as well as the decorative and structural interior trim panels.

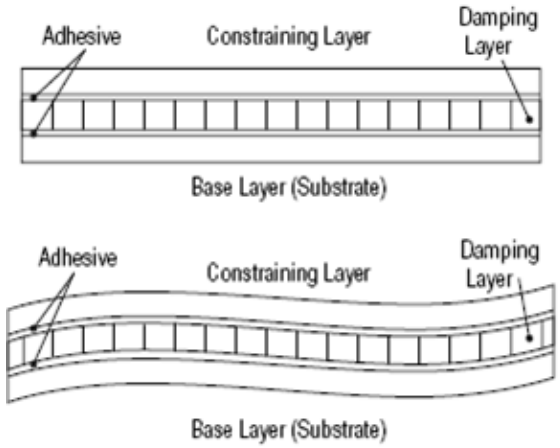

Fig. 2.5 Constrained-layer damping system

A lot of work has been carried out in the past on the viscoelastic sandwich damping systems. The fundamental work in this field was pioneered by Ross et al. [43], who used a three-layer model to predict damping in plates with constrained layer damping treatments. Kerwin [47] was the first to present a theoretical approach of damped thin structures with a constrained viscoelastic layer. He stated that the energy dissipation mechanism in the constrained core is attributable to its shear motion. He presented the first analysis of the simply supported sandwich beam using a complex modulus to represent the viscoelastic core. Several researchers such as; DiTaranto [48] and Mead and Markus [49] extended Kerwin's work using his basic assumptions. DiTaranto proposed an exact sixth-order theory for the unsymmetrical three-layer beam, and this was subsequently refined [50-52]. Douglas and Yang [53] and Douglas [54] have presented a mathematical model for damping of three-layer beams. Sylwan [55] has developed a model considering shear and compression damping effects in layered beams with thin damping cores showing increased losses over a wide frequency range. More recently, Lee and Kim [56] have presented mathematical results in the

analysis of beams and plates with constrained viscoelastic damping layers and obtained good results with the use of very thin viscoelastic layers.

2.3.2 Use of Special High Damping Inserts

Using the inserts of special high damping materials is another way to achieve substantial damping in structural members [57-59]. The inserts are considered to be both welded and press-fit to the parent members. It has been observed that the effectiveness of the press-fit inserts is much more than that of the welded inserts. The damping capacity of a member can be considerably increased with inserts without any significant loss in static rigidity [59]. Rahmathullah and Mallik [60] have experimentally studied the damping capacity of aluminium cantilever strips by using high damping inserts of different materials namely Cast Iron, Bakelite and Perspex. They have reported that with a proper choice of insert material, considerable improvement in damping capacity can be attained by using very little amount of high damping material.

2.3.3 Use of Layered and Jointed Constructions

Another way of achieving considerable vibration attenuation in structural members is layered construction made possible by holding the members together by means of suitable fasteners. This can be achieved by bonded (welded), bolted and riveted connections with appropriate locations along the layered interface. Under such circumstances, the profile of the interface pressure assumes a significant role, especially in the presence of slip, to dissipate the vibration energy. It is a general fact that the total damping in a structure is always much more than the sum of the material damping of individual elements of the structure. It is therefore recognized that the damping is largely caused due to the inclusion of mechanical joints or fasteners in the structure. Since 1970, the effects of slip at the friction joint interfaces on the control of vibration of mechanical structures have attracted the attentions of many researchers [6-14, 61, 62]. Various structures have been tested and the great potential for a friction joint to reduce vibration level has been observed.

The damping in beam type structures is increased by fabricating the same in several layers bolted, riveted and welded together so that the interfacial slip occurs between the layers during vibration, thus giving rise to frictional damping. Many researchers in

this field [63-65] have suggested that the presence of joints offers most of the damping in a typical jointed layered structure and plays a major role in passive vibration control. The energy dissipation is mainly caused due to the inclusion of joints that produce local stiffness and damping in assembled structures. This energy dissipation, although undesirable when one wishes to avoid fretting corrosion, is usually desirable since it acts to limit the vibration amplitudes [1]. A great deal of research works [64-70] have been reported through the theoretical and experimental studies focusing on the joint damping.

The energy dissipation mechanism in a joint is a complicated phenomenon being largely influenced by the interface pressure and slip between the contacting surfaces. Although the energy dissipation is related to many physical phenomena, the friction between the layers is considered to be the most important factor [25]. It is always difficult to assess theoretically the damping arising in joints because of variations in the coefficient of friction under dynamic conditions. However, it is generally accepted that the friction force generated between the joint interfaces is usually dependent on the materials in contact and proportional to the normal force across the interface. At the specified joint clamping pressure, sliding takes place on a micro scale and the Coulombs law of friction is assumed to be valid.

Although a lot of work has been done within this domain of study but many aspects related to damping due to joints remain poorly examined. There is a wide range of dynamic systems and structures such as beam systems, machine tools, frameworks, gas turbines, automobiles and aerospace structures that would benefit from increased joint damping. The research presented in this thesis primarily emphasizes on the use of welded connections in built-up structures to achieve increased damping. A vast amount of relevant literature study on the interfacial joint damping is enumerated in the succeeding section.

2.4 Literature Review on Joint Damping in Built-up Structures

In reality, almost all structures are composed of substructures and parts that are joined together with a multitude of different connections – screwed, nailed, glued, interference fit, bolted, riveted, welded, etc. Joints are inherently present in the assembled structures which contribute significantly to the slip damping in most of the fabricated structures. Joints have a great potential for reducing the vibration levels of a

structure thereby attracting the interest of many researchers. These connections are recognized as a good source of energy dissipation and greatly affect the dynamic behavior in terms of natural frequency and damping [1-3]. This structural damping offering excellent potential for large energy dissipation is associated with the interface shear of the joint. It is thus recognized that the provision of joints can effectively contribute to the damping of all fabricated structures. Damping in such jointed structures mainly originates from two sources. One is the internal or material damping which is inherently present in the material and is very low [71] and the other one is the structural damping arising due to joints [17]. The latter one offers an excellent source of energy dissipation, thereby adequately compensating the low material damping of structures. It is estimated that structures consisting of bolted, riveted and welded members contribute about 90% of the damping through the joints [23, 63-65].

In the last few decades, the effects of slip at the friction joint interfaces to control the vibration of mechanical structures have attracted the attentions of many researchers [6-14, 61, 62]. Various structures have been tested and the great potential for a friction joint to reduce vibration level has been observed. The problems in utilizing a friction joint as a tool to control the vibration of a fabricated structure have been summarized by Beards [5] as:

- Fretting corrosion at joint interface;
- Loss of static stiffness of the structure; and
- Difficulty in design and analysis due to problems of nonlinearity.

Beards [5, 7] has shown that fretting damage can be minimized by providing a layer of low modulus or yield strength at the joint interface. Non-metallic or metal coatings can also be used to prevent the fretting crack from propagating through the whole joint. Surface preparations such as shot peening, blasting and metal sprays also reduce the fretting damage. Cyanide hardening and electro discharge machining are also very effective in minimizing the fretting damage.

Beards [5] also pointed out that any loss of static stiffness of a structure did not necessarily affect the integrity of the structure if the joints are carefully located. Accordingly, the major obstacle in the application of the friction joint in vibration control

is the problem of nonlinearity. In dealing with this nonlinear problem, attention has been paid to the following:

- Modelling the properties of a joint.
- Calculating the response of a fabricated structure when the properties of all the joints are known.

Quasi-static experiments have been carried out on various friction joints [68, 69, 72-77]. It has been found that the relationships between the load and deformation in the directions normal and parallel to the interfaces are not linear. In the direction parallel to the interfaces, energy is dissipated when a cyclic load is applied. When the deformation magnitude is small, Coulomb's dry friction law is not adequate and the microslip mechanism is responsible for the characteristics of the friction joint. The effects of the joint mass [78] and variable normal load [11, 12, 79] on the property of the joint have also attracted the attention of some researchers. Two-dimensional motion at the joint has also been investigated [80, 81]. The effects of a friction force on the stability of a structure have also been studied [82-85]. For most of the analysis on friction joint related problems, only qualitative agreements between the theoretical analysis and the experiment have been achieved. Quantitative agreement is still lacking.

The modeling of structural joint is very important for accurate analysis. The joint problem is difficult to solve. Joint physics are affected by many parameters including interface area, normal force and the surface finish at the interfaces. Several experiments have shown that the joint physics may be history-dependent, meaning that the physics may change over time. The effect also depends on the magnitude and type of force applied. All of these variables pose difficulty in examining and modeling the joints. Several approaches can be used for investigating the joints. One of the techniques is to identify the actual physics taking place within the joint on a micro-scale [86-88]. An alternative approach is to look at the effect of the joint on the overall dynamics of the structure. In this approach, the micro-physics need not necessarily be considered (or modeled) in details, but the overall dynamical effect of the full joint needs to be examined. The present investigation follows the second approach. All the previous works have focused on axial and torsional motion at the joints. Little work has been done with joints in bending. The scope of this thesis is to perform an investigation into welded joints in bending. The overall goal of the project

is to develop a model capable of incorporating the effects of the welded joint into a model of a simple welded and jointed beam configuration. In order to achieve this both theoretical and experimental study have been carried out to determine the loss factor in welded beams with joints. The modeling of structural joint is very important for accurate analysis. A good knowledge of the joint characteristics is necessary to devise an efficient model considering slip associated energy dissipation. Many investigators [25, 89-91] have contributed significantly on the models with joint friction of built-up structures. Song et al. [92] have proposed the Adjusted Iwan Beam Element (AIBE) model considering nonlinearity effects of an assembled bolted structure. Hartwigsen et al. [93] have investigated experimentally to quantify the effects of nonlinearity on shear lap joints of two structures: a beam with a bolted joint at its center and a frame with a bolted joint at one of its members. Both structures are subjected to a variety of dynamical tests to determine the effects of nonlinearity of the joints. Their experimental results discuss several important parameters influencing the effective stiffness and damping of lap joints. Miller and Quinn [94] have presented a two-sided interface model based on a series-series Iwan system in which the parameters are physically motivated. This interface model is then incorporated into a large structural model to calculate the damping arising from micro-slip. Khattak et al. [95] have developed a parameter-free and physics-based model of the joint dynamics considering shear lap joints with reasonable accuracy. This model can be applied for different loading and joint parameters, i.e., different joint geometries, friction coefficients and clamping pressures.

Although most of the inherent damping occurring in real structures arises in the joints, but a little effort has been made to study this source of damping because of complex mechanism occurring at the interfaces due to coefficient of friction, relative slip and pressure distribution characteristics. It is therefore important to focus the attention on these parameters for accurate assessment of damping capacity of structures. The role of friction is of paramount importance in controlling the dynamic characteristics of engineering structures. In applications where relative motion between surfaces in contact occurs, the effect of frictional forces, whether desirable or not, cannot be ignored. The friction mechanism has a tendency to reduce the vibratory response of the structure and provide the energy dissipation at the interface. These effects are desirable in applications where friction reduces large resonant stresses and high cycle

fatigue, such as built-up structures. However, in shear lap joints for example, the presence of relative motion with friction will compromise the structural stiffness, thereby making frictional effects undesirable. The balance between the stiffness and damping is a direct function of the desired application, since the two effects are competitive. Friction joints strongly influence the dynamic response of the structures. In particular, transient interface friction phenomena provide overall structural stiffness and energy dissipation. Friction damping through partial slip of mechanical joints is attractive for large built-up structures because it provides passive vibration control. Friction damping is also tunable through variations of the joint clamp load, but this has the consequence of altering structural stiffness as well. Light clamp loads promote interfacial slip but compromise stiffness, while heavy clamp loads make a stiff but lightly damped structure. The design challenge therefore is to optimize joint clamp load to introduce significant energy dissipation while providing adequate structural stiffness. The Coulomb's law of friction is widely used to represent the dry friction at the contacting surfaces. Den Hartog [96] has analytically solved the steady state response of a single degree of freedom system with friction damping subject to harmonic excitation. The approach was based on an assumption of Coulomb friction law at the interface, with the sticking and slipping conditions explicitly defined by a coefficient of friction. The solution was pieced together for each subinterval of the cycle for which the analytical result has been obtained to form the solution for the complete cycle. The method illustrated by Den Hartog accounted for only two stick-slip transitions per cycle. In theory, however multiple transitions can take place. This problem was addressed by Pratt and Williams [97]. They have illustrated the change in response to variations in friction coefficient, excitation frequency, and natural frequencies of the bodies in frictional contact and shown that the response behavior of the system under multiple stick-slip transitions substantially varies from the results of Den Hartog. Reviews on the effects of joint friction on structural damping in built-up structures have been presented by many researchers [3, 24, 25, 36, 98, 99]. Their findings have shown that the friction in structural joints is regarded as a major source of energy dissipation in assembled structures.

An important feature of built-up structures is the existence of slip at the interfaces of the structural components. The energy in such structures is dissipated through slipping, thereby emphasizing the need to study the mechanism of slip at the

interfaces. Joints seem to exhibit two types of motion during vibration: microslip and macroslip [26]. When the dynamic load is increased or decreased within a threshold range, slip along the frictional joint interfaces occurs locally at the joints. This situation is called micro-slip, where slip along the interface is localized in the slip region while the rest of the interface is in the stick region. When the load reaches beyond the threshold range, a larger portion of the interface will break free and slip. Eventually, slip along the entire interfaces take place which is referred as macro-slip. While both micro and macro-slip causes energy dissipation providing the dominant damping mechanism in a built-up structure, the latter is generally to be avoided as it leads to structural damage of the joints.

In built-up structures, interface undergoes partial slip, in which a portion of the interface slips while another portion sticks. Moreover, the boundary partitioning the interface into sticking and slipping zones is a function of the prevailing forces acting on the structure and can be a general function of time. Because energy dissipation takes place only in the interface slip zones, the difficulty of the analysis becomes clear. Rigorous continuum approaches must track the stick-slip boundary location, as well as calculate interface slip displacements, dynamically as a function of time. The numerical intensity of such an approach leads naturally to the investigation of models for dynamic interface behavior. Such models for dynamic friction at the interfaces include both macroslip and microslip approaches. Macroslip models consider all points on the interface to respond in unison, resulting in either a pure slip or pure stick interface response. As such, they can be viewed as point contact models, and partial slipping situations cannot be modeled using a macroslip element. Microslip models consider the spatially-distributed interface response and capture partial slipping situations, and therefore require a multi-point contact modeling approach. The suitability of these modeling approaches is dictated largely by the magnitude of the contact normal force. Macroslip approaches are well suited for scenarios in which the interface responds in either pure stick or pure slip, corresponding to a very large or small contact normal force. In these circumstances, the interface response is not spatially distributed and a point contact approach is appropriate and reliable. For intermediate values of normal load substantial localized interface stick-slip takes place and a microslip model will provide greater fidelity and improved performance predictions by capturing the interface response details.

Behavior of the two models can be compared from the force - displacement curves of Fig. 2.6. For the macroslip model Fig. 2.6(a), the friction interface is characterized by a constant stiffness as indicated by the piecewise linear nature of the force displacement behavior. At a critical value of breakaway friction force the whole interface slips is indicated by the horizontal segments of the hysteresis loop. In the case of the microslip model Fig. 2.6(b), the interface has maximum stiffness at the no slip condition. As soon as microslip is initiated, the stiffness of the interface decreases and the force displacement curve shows a softening behavior. The length of the slip zone grows, consequently reducing the contact stiffness of the interface. For both macroslip and microslip formulations, it is observed that the loading and unloading curves for force - displacement do not overlap. After an initial loading, followed by unloading the applied force to zero and it is observed that there is some residual displacement at the interface. A similar behavior can be observed when the load is decreased to a negative maximum and then increased to zero. As such the interface displacement is path dependent on the load and this results in what is called the hysteresis behavior. The simplest explanation for the hysteresis loops is the fact that frictional resistance always acts opposite to the applied force and is an energy dissipation mechanism. The area included in the hysteresis loop represents the energy dissipated in a single loading cycle.

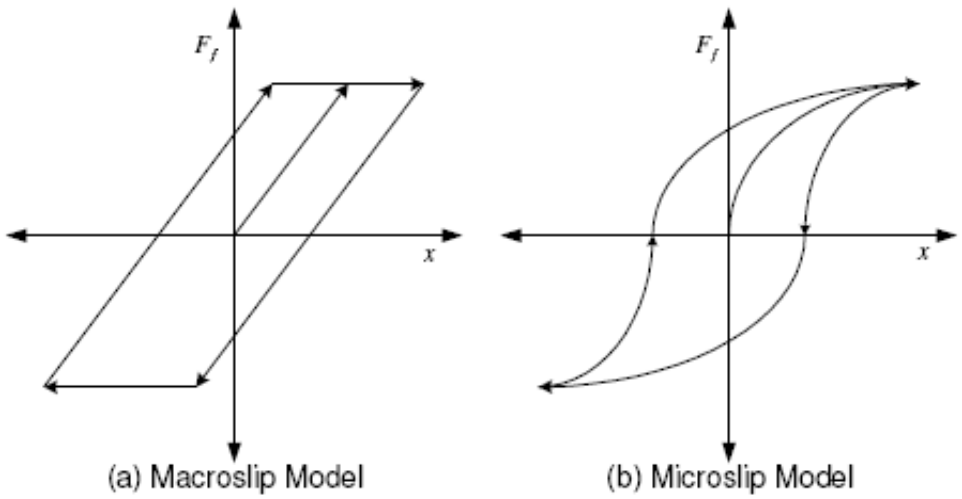

Fig. 2.6 Hysteresis behavior for macroslip and microslip models

Over the past few decades, most of the work has been confined to the area of micro- and macro-slip phenomena [93, 100]. Several workers [10, 101-107] have investigated using the macro-slip approach, modeling the friction interface as a rigid body. This model is generally adopted when the normal load at the interface is small. On the other hand, many researchers [11, 12, 108-114] have utilized the micro-slip concept considering the friction surface as an elastic body. In this case, the interface undergoes partial slip at high normal load. Masuko et al. [19] and Nishiwaki et al. [21, 22] have found out the energy loss in jointed cantilever beams considering micro-slip and normal force at the interfaces. Olofsson and Hagman [115] have shown that the micro-slip at the contacting surfaces occur when an optimum frictional load is applied. They have also presented a model for micro-slip between the flat smooth and rough surfaces covered with ellipsoidal elastic bodies.

The nature of pressure distribution at the interfaces of the jointed beams is another important aspect governing the damping capacity of built-up structures. In the past few decades, several researchers have tried to investigate the nature of pressure distribution at the interfaces of the assembled structures. Almost all previous researchers have idealized the joints by assuming a uniform pressure profile without considering the effects of surface irregularities and asperities [17-22]. In fact, many researchers [116-122] have conducted experiments to know the exact pressure distribution characteristics. These experiments have confirmed that the interface pressure is hardly constant in actual situation. In particular, Gould and Mikic [123] and Ziada and Abd [124] have reported that the pressure distribution at the interfaces of a bolted joint is parabolic in nature circumscribing the bolt which is approximately 3.5 times the bolt diameter. The pressure profile is also reported to be independent of the applied tightening load. Hisakado and Tsukizoe [125] have presented a simple method for measuring the interface pressure distribution of bolted joints. Their experimental results show that the interface pressure distribution is almost independent of the surface roughness. They measured the pressure distribution of two metals in contact by using the impressions of the softer surface formed by the penetrations of harder asperities.

Recently, Nanda and Behera [110] have developed a theoretical expression for the pressure distribution at the interfaces of a bolted joint by curve fitting the earlier data reported by Ziada and Abd [124]. They have obtained an eighth order polynomial

even function in terms of normalized radial distance from the centre of the bolt such that the function assumes its maximum value at the centre of the bolt and decreases radially away from the bolt. They have used Dunn's curve fitting software to calculate the exact spacing between bolts that would result in a uniform interfacial pressure distribution along the entire length of the beam. Using exact spacing of 2.00211 times the diameter of the connecting bolts, Nanda and Behera have been successful in simulating uniform interface pressure over the length of the beam. Thereafter, they have investigated the effect of interface pressure on the behavior of interfacial slip damping.

Damisa et al. [126] have also recently carried out an analysis to study the effect of non-uniform pressure distribution on the mechanism of slip damping for layered beams, but their analysis is limited to static load. Later, they have extended their analysis to realistic dynamic loading for estimating the interfacial slip damping in clamped layered beams [127]. They have shown that under the action of dynamic loads, the factors like non-uniform pressure distribution as well as frequency variation have a significant effect on both the energy dissipation and logarithmic decrement associated with the mechanism of slip damping in layered structures. They have further reported that the amount of energy dissipation through slip damping under externally applied dynamic load is less than that of the corresponding static load. Olunloyo et al. [128] have used other forms of pressure distributions such as polynomial or hyperbolic representations but the results obtained have demonstrated that the effects of these distributions in comparison with the linear profile are largely incremental in nature.

The aim of the present thesis is to devise mathematical models to evaluate slip damping in welded structures. In the present analysis, the welded beams are considered to be in contact with each other because of perfect flatness and same condition of flatness is maintained under excitation due to welding. Since perfect contact is maintained under both the static and dynamic conditions, the pressure at the interfaces is assumed to be uniform. The contact pressure for flat surfaces with rounded corners has been found out by Ciavarella et al. [129], which shows a non-uniform distribution pattern at the interfaces. Contrary to this, the pressure distribution at the interfaces of flat surfaces is uniform owing to the contact of the upper layer over the lower one as established by Johnson [130] and Giannakopoulos

et al. [131]. The present investigation uses the pressure distribution given by Johnson [130] and Giannakopoulos et al. [131] for flat surfaces in contact with each other.

In the analysis of the vibration of structure assemblies, the problem of estimating the damping remains the biggest challenge. In built-up structures, damping mainly results due to the energy loss owing to the slippage at the interfaces. Energy dissipation resulting from slip and pressure distribution in jointed structures has been the subject of many studies [19, 21, 22, 75, 132-134]. Some researchers [2,135,136] have reported different mechanisms of energy dissipation that might take place depending on the clamping pressure. Typically, the normal interfacial pressure at the jointed interface is not uniformly distributed. Under high pressure, the slip is small, while under low pressure the shear due to friction is small. An optimal clamping force exists somewhere between these two limits under which a joint dissipates maximum vibration energy. Beards [63] has looked into this aspect and recognized the existence of an optimum joint force for maximum energy dissipation. Jezequel [134] has proposed an algorithm for calculating the energy loss due to slip in bolted plates. It has been found that the joint friction exhibits viscous-like damping characteristics when the normal force is allowed to vary with the relative slip [68, 69, 137-141]. Researchers at Sandia National Laboratories have performed experiments to investigate the damping due to micro-slip at joints and established a power law relation between the energy dissipation and lateral load [86, 87].

Recently, Heller et al. [142] have used an experimental procedure to determine the nonlinear damping capacity of built-up structures due to friction joints. They have conducted experiments on a simple built-up structure consisting of two bolted beams to analyze the influence of interface pressure and contact area on its dynamic behavior. Their experiment has confirmed that the frictional joints are the main source of energy dissipation in built-up structures due to relative motion between the components. The recent experimental investigation of Walker et al. [143] discusses the joint parameters affecting the damping of aerospace structures. They have studied the importance of joint stiffness on the damping of the jointed structures. They have established that the built-up structures with higher stiffness results in lower energy loss. Moreover, Mohanty and Nanda [144,145] used the classical energy approach to estimate the damping capacity of layered and riveted symmetrical and unsymmetrical

beams. They have studied the importance of input excitation, rivet diameter and spacing on the damping of the riveted structures.

There are several approaches to evaluate the energy loss. Most researchers considered a continuous description of the joint in their analysis [4, 18, 110, 144-146]. The dissipated energy is nil when the surfaces stick and is positive when the surfaces partially slide. The transition from the sticking position to the moment when the body begins to slip depends on the normal stress between the two contacting surfaces. In assemblies, normal stresses are time-dependent and space-dependent. Previous works have distinguished the cases in which normal stresses are:

- Constant (time-independent) and uniformly distributed (space-independent) [18, 110, 146].
- Constant and non-uniformly distributed [107,147,148].
- Non-constant and non-uniformly distributed (computed with discrete models), Yang et al. [149].

To obtain and solve the model equations with constant and uniformly distributed normal stresses, several authors used analytical or semi-analytical approaches. The aim is to determine a parametric function of damping [103,110]. When the normal stress is non-uniformly distributed, the researchers used the Finite Element Method (FEM) [4, 147, 148]. The finite element method is one of the numerical techniques for solving many boundary and initial value engineering problems. However, its application in damping analysis is relatively recent. Gaul and Lenz [90] have worked in detail on the finite element models considering slip mechanisms to study the dynamic response of assembled structures. Sainsbury and Zhang [150] have used the finite element procedure through Galerkin element method (GEM) to carry out the dynamic analysis of damped sandwich beam structures. Lee et al. [151] have used the finite element model of a jointed beam to obtain the natural frequencies and mode shapes. Hartwigsen et al. [93] have found out the contact area of bolted joint interfaces using finite element analysis and further conducted experiments to verify the same. Chen and Deng [4] have carefully studied the micro-slip phenomenon using the finite element method under plane stress conditions. They have carried out investigations on two classical joint configurations for modeling: the press-fit joint and lap-shear joint. They have focused their work to evaluate the effect of dry friction and slip on the damping response of joints for quantifying the energy dissipation

during cyclic loading. Oldfield et al. [152] have analyzed the effect of dynamic friction on energy dissipation of a bolted joint under harmonic loading by finite element method using Jenkins elements. They have studied the effect of preload on the interface pressure affecting the response of the joint. At high preload, little sliding occurs at the joint interface producing less frictional energy. Further, Mohanty and Nanda [153] investigated the damping mechanism in layered and riveted cantilever beams using finite element approach. In their analysis, they have adopted Galerkin's method of residual approach considering the dynamic slip ratio to evaluate the damping matrix and energy dissipation in jointed structures.

The FEM computation codes include the contact between the parts [30] and allow more complex shapes to be taken into account. However, this kind of simulation presents two difficulties. First, it requires a very fine mesh of the contact area, which may lead to a high number of degrees of freedom in the modeling of the contact but is not convenient for modeling vibration. Second, the time increment must be sufficiently small to ensure the convergence of the algorithm which leads in turn to a large number of iterations. As a result, the FEM simulation of an assembly structure often demands unreasonable computational time. Currently, research is being conducted to divide the structure into substructures to facilitate the computations [147,148].

Response surface methodology is a new statistical approach which has been adopted by many researchers [68,154-157] to explore the vibration characteristics in various built-up structures. Response surface methodology (RSM) is a technique used to determine and represent the cause and effect of relationship between true mean responses and input control variables influencing the responses as a n-dimensional hyper surface. Liang et al. [158] used the response surface methodology to analyze the effect of design parameters on sound radiation from a vibrating panel. Li and Liang [159] utilized the response surface methodology to analyze the design parameters and optimize the vibro-acoustic properties of damped structures. Further, the response surface methodology has gained importance in structural dynamics of damped structures using the finite element models. In this context, Ren and Chen [160] presented a response surface-based finite element model updating procedure for civil engineering structures by formulating explicitly an optimization technique. In the present work, the response surface methodology has been used to explore the

mechanism of damping in layered and welded structures subjected to static and dynamic vibration conditions.

It is very difficult to assess the joint properties correctly from the theoretical models and therefore, experiments are performed to verify the same. The main purpose of joint identification is to estimate the joint parameters that minimize the differences between the measured assembly response characteristics and those predicted analytically or numerically. The damping of a structure is experimentally measured either by time or frequency domain methods.

In time domain, the modal damping ratio can be identified using the logarithmic decrement method. Time signals can also be processed using Time-Frequency Transforms when several frequencies or nonlinear behaviors are taken into account [29]. This method is generally applied to lightly damped structures excited at low amplitude and frequency. Many researchers have conveniently used this technique for estimating damping experimentally [1, 2, 25, 110]. Nishiwaki et al. [21] have developed an improved band-width method to measure experimentally the damping capacity in terms of logarithmic decrement of a bolted cantilever beam at first, second and third modes of vibration. Masuko et al. [19] and Nishiwaki et al. [22] have theoretically calculated the logarithmic decrement of a jointed cantilever beam considering the normal force and micro-slip at the interfaces. Recently, Olunloyo et al. [161] have analytically investigated the slip damping of layered viscoelastic beam-plate structures using the logarithmic decrement approach. Damisa et al. [127] have performed a dynamic analysis of slip damping in clamped layered beams with non-uniform pressure distribution at the interfaces. They have shown that under dynamic loads, the frequency variation and non-uniformity in pressure distribution can have significant effect on both the energy dissipation and logarithmic damping decrement.

It is also possible to estimate the damping ratio by analyzing the experimental Frequency Response Functions (FRF) [8, 30] in the frequency domain. There are several approaches that have been utilized to identify joint parameters. These approaches rely on the experimental measurements of FRFs. Yoshimura [66,162] conducted a series of experimental investigations to measure dynamic characteristics and quantitative values of the stiffness and damping of a bolted joint, welded joint, and representative joints in machine tool structures. Wang and Chuang [163] and Tsai and Chou [119] have proposed a frequency domain method to study the stiffness and

damping of a single bolted joint directly from the frequency response function (FRF) of the structures. They have used FRFs in different frequency ranges to extract the joint properties so that the joint dynamic behavior is well represented over the frequency range. Yin et al. [164] have introduced a method based on the wavelet transform of FRFs for linear systems to estimate the natural frequency and damping. They have used Cauchy's integral formula for calculating the continuous wavelet transform of the FRFs for any complex function. Hwang [165] has developed a response model in frequency domain to identify the stiffness constant and damping coefficient parameters of connections using the experimental data. Ahmadian and Jalali [166] have presented a parametric model for an Euler-Bernoulli beam with bolted lap joint in the mid span. The solution provides the FRF of the beam at any desired point due to excitation at a certain location. This FRF is compared with the corresponding experimental results to identify the parameters of the bolted joint interface affecting damping. Measured modal parameters have been used in several studies to identify joint structural parameters [167,168]. For example, Inamura and Sata [169] proposed a joint structural parameter identification approach based on the use of the complete mode shapes and eigenvalues. Yuan and Wu [170] and Kim et al. [171] used a condensed FE model and incomplete mode shapes to identify joint stiffness and damping properties. These methods require accurate modal parameters, which are difficult to extract especially in cases of closely coupled or heavily damped modes. In order to overcome the difficulties encountered in extracting accurate modal parameters, some methods based on FRFs for determining joint properties have been proposed in the literature [30,120,172,173]. Mottershead and Stanway [172] have proposed an algorithm for obtaining structural parameters from FRF measurements.

As evident from the preceding discussions, built-up structures are generally assembled by bolted, riveted and welded connections representing a significant source of damping. The dynamics of bolted and riveted structures have been studied by many investigators as evident from the wealth of published literatures. However, a little amount of research has been reported till date on the mechanism of damping in layered and jointed welded structures. Aoki [174] studied the effect of welding on dynamic characteristics of welded cantilever beam structures and established that the damping ratio increases when welding is used for the fabrication of the structures. Carey [175] studied the effects of welding on damping in several beam-stiffened

plates. He ascertained that at frequencies below 500 Hz, welding causes an increase in damping in the plates. Ehnes [176] extended the work of Carey [175] and found that welded joints do increase the damping of built-up structure and that Rayleigh damping is an appropriate model for its analysis. The study indicates that damping is relatively high in the low frequency domain while decreasing exponentially at the higher frequencies. The damping emanating from the welds increases the damping of the overall system but does not show any positional damping. Damping found near the point of excitation are similar to damping values of positions separated from the point of excitation by multiple welds. The study of slip damping in welded structures is very vital for achieving maximum vibration attenuation in automotive and aerospace industries where these structures are extensively used. Masuko et al. [19] and Nishiwaki et al. [21] have established that the welded steel structures can be used in machine tool structures as a substitute for monolithic cast iron material to compensate for damping. The steel plates used in the welded machine tool structures, however, have a low inherent damping as compared to the cast iron. The low damping of mild steel can be compensated largely by using the layered structures with suitable welded joint as the damping in such structures are due to micro-slip and kinematic coefficient of friction at the interfaces. Welded joints being one of the methods, the damping of such joints with steel structures can be brought to its counterpart cast iron by employing proper design and techniques of welding. Apart from this, steel has the other advantages of higher strength and unit rigidity under static and dynamic loading over cast iron. Moreover, considerable amount of saving in material can be achieved by using steel structures instead of cast iron for heavy machine tools thus reducing the overall cost. No work has been reported till date on the damping mechanism of layered and tack welded beams of unequal thickness subjected to various kinds of loading. Moreover, surface roughness is an important factor influencing the microslip phenomenon in jointed structures that has been overlooked by most of the earlier researchers and little work has been reported on this aspect till date. The motivation for the present investigation lies in developing the theory of damping mechanism in both symmetrical and unsymmetrical welded beam structures using classical, finite element method and response surface methodology approach under the consideration of surface roughness parameter. The results so obtained are validated experimentally.

2.5 Summary

Vibration and noise reduction in structures can significantly enhance dynamic stability. Vibration attenuation in structures is an important aspect in the area of mechanical design. It has been well established that the extent of inherent damping in structures is very low and various external means are incorporated in the parent system to improve the damping. The use of layered and jointed construction serves this purpose to a larger extent. The efficient utilization of damping from joint configurations provides an accurate prediction of dynamic responses of assembled structures subjected to external excitation. Notwithstanding the variety and immensity of work done within this domain of study, and despite all possibly most accurate solutions and arduous experiments, many aspects related to slip damping remain poorly examined. Therefore, the prediction of damping in built-up structures is always challenging due to limited knowledge of joint physics. It is therefore necessary to analyze the damping mechanism theoretically along with the influencing parameters and authenticate the results experimentally.

It is evident from the literature survey that the presence of joints offers a major potential for passive vibration control. The damping arising from these joints is always dominant compared to the low inherent material damping. It is the outcome of energy dissipation during the vibration of a structure when some relative movement takes place at the joint interfaces in the presence of friction. This energy dissipation is desirable as it results in limiting vibration amplitudes thereby enhancing the useful life of the structures. Extensive research has been carried out in the past decades on the damping of bolted and riveted structures. However, the information available on the damping behavior of welded joints is rather limited and insufficient. The aim of the present investigation is to assess energy dissipation in the layered and jointed welded structures through analytical and experimental work. The behavior of welded joints in structural dynamic system has been simulated to include accurate damping models for welded joints to predict dynamic response. Extensive experiments have been conducted to validate the damping model developed for layered and welded beams.

3

DAMPING ESTIMATION OF WELDED SYMMETRICAL BEAMS WITH SINGLE AND MULTIPLE INTERFACES CONSIDERING DYNAMIC SLIP RATIO

3.1 Introduction

Damping capacity of the jointed structures is governed by a number of parameters such as; intensity of pressure distribution, micro-slip and kinematic coefficient of friction at the interfaces. The effects of all these parameters are to be considered for accurate evaluation of energy loss in assembled structures. This chapter presents a detailed description of the theoretical analysis by considering the dynamic slip ratio for determining the damping capacity of layered and jointed cantilever beams with welded joints. A cantilever beam model representing a continuous system based on Euler-Bernoulli theory has been used for deriving the necessary formulations.

3.2 Beam Theories

A bar that carries loads by undergoing flexural deformation (transverse displacement) is commonly referred to as a beam. There are a number of beam theories that are used to represent the kinematics of deformation. To describe beam theories, the following coordinate systems are introduced. The x, y, and z coordinates are taken along the length, thickness and width of the beam, respectively. All the applied loads and geometry are such that the displacement (u, v, and w) along the coordinates (x, y, and z) are functions of 'x' and time't' as shown in Fig. 3.1. In the current development, it is assumed that the kinematical quantities do not vary in the 'z' direction.

3.2.1 Classical Beam Theory

The most commonly used beam theory is the Euler-Bernoulli classical beam theory. This is referred to as classical beam theory. The fundamental kinematical assumption

for classical beam theory is that the planar cross-sections maintain their shape and remain perpendicular to the centroidal axis when the beam undergoes deformation. Hence, the displacement is expressed as;

$$u = u_0 - \mathrm{y}\frac{\partial v}{\partial x}, \qquad v = v_0 \tag{3.1}$$

where u_0 and v_0 are the axial and transverse normal components of the displacement of points on neutral axis of the beam. As a result of this assumption, the displacement of any point in the beam is kinematically related to the displacement of centroid. It is evident from expression (3.1) that all strains except 'ε_{xx}'are zero. This theory of bending is widely used for thin beams.

3.2.2 Timoshenko Beam Theory

In Timoshenko beam theory, plane sections originally perpendicular to the longitudinal axis of the beam remain plane, but not necessarily perpendicular to the longitudinal axis of the beam. The displacement is expressed as;

$$u = u_0 - \mathrm{y}\,\theta, \qquad v = v_0 \tag{3.2}$$

where 'θ' denotes the total rotation of a cross section of the beam as shown Fig. 3.1. The classical beam theory assumes that the shear stress distribution is not accompanied by a shear strain although the cross-sections carry a resultant shear force. In actuality, the shear stress and strain vary over the cross-section as the shear stress is zero at the upper and lower surfaces of the bar. Timoshenko approximated the effect of shear as an average over the cross-section, implying that each cross-section rotates independently of the slope of the centroidal axis in the deformed state. In order to incorporate corrections to the classical beam theory, rotary inertia of cross-sections is considered in the formulations. In the present thesis, Euler-Bernoulli classical beam theory has been adopted to evaluate the damping capacity of layered and welded beams.

3.3 Types of Beam Model

Models of vibrating systems are generally divided into two classes, i. e., discrete and continuous depending on the nature of parameters.

3.3.1 Discrete or Lumped Parameter System

In case of discrete or lumped parameter system, the mass is assumed to be rigid being concentrated at individual points and the stiffness is considered to be mass less springs connecting these rigid masses. The motion of discrete systems is governed by ordinary differential equations and the number of masses generally defines the number of degrees of freedom of the system. The solution of discrete systems is approximate and has been considered in details using the finite element approach in the succeeding chapter.

3.3.2 Real or Continuous Systems

In real or continuous systems, the mass and elasticity are considered as distributed or continuous parameters. This distribution of the mass and elasticity requires partial differential equations to describe the vibration. Systems with distributed parameters are characterized by an infinite number of degrees of freedom. If the model is linear, the number of its natural frequencies and modes are equal to its degrees of freedom. Indeed, the displacement depends on two independent variables, namely spatial and time variables, x and t, respectively. The time‘t’ is an independent variable in a dynamic response problem. As a result, the motion of continuous systems is governed by partial differential equations satisfying the whole domain. This chapter is entirely devoted to continuous systems producing exact solutions.

3.4 Dynamic Equations of Free Transverse Vibration

Figure 3.1 shows a cantilever beam undergoing free vibration with transverse displacement $y(x, t)$.

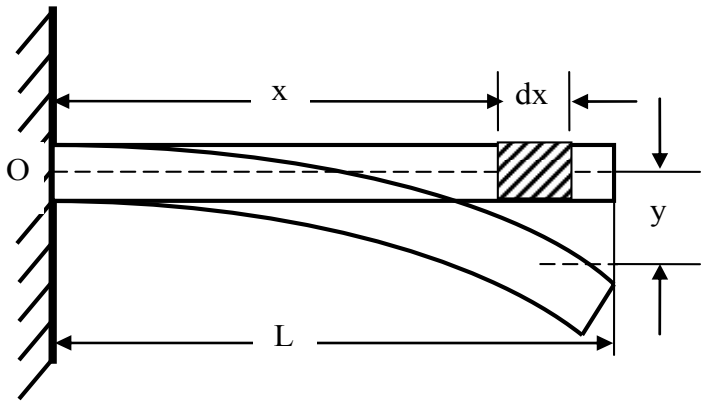

Fig. 3.1 Differential analysis of a beam

In formulating the dynamic equations, Euler-Bernoulli beam theory is used on the assumptions that the rotation of the differential element is negligible compared to translation and the angular distortion due to shear is small in relation to bending deformation. This assumption is valid when the ratio of the length of beam to its depth is relatively large as in case of the present investigation.

The beam vibration is governed by partial differential equations in terms of spatial variable x and time variable t. Thus, the governing differential equation for the free transverse vibration is given by;

$$c^2 \frac{\partial^4 y(x,t)}{\partial x^4} = -\frac{\partial^2 y(x,t)}{\partial t^2} \tag{3.3}$$

where $c = \sqrt{EI/\rho A}$ and E, I, ρ and A are modulus of elasticity, second moment of area of the beam, mass density and cross-sectional area, respectively. The free vibration given by the expression (3.3) contains 4^{th} spatial derivatives and hence requires four boundary conditions for getting a solution. The presence of 2^{nd} time derivatives again requires two initial conditions, one for the displacement and another for velocity.

The above expression is solved using the technique of separation of variables. In this method, the displacement $y(x,t)$ is written as the product of two functions, one depending only on x and the other depending only on t. Thus, the solution is expressed as;

$$y(x,t) = F(x)G(t) \tag{3.4}$$

where $F(x)$ and G(t) are the space and time functions, respectively.
Substituting expression (3.4) into (3.3) results;

$$c^2 F''''(x) G(t) = -F(x) \ddot{G}(t) \tag{3.5}$$

Dividing expression (3.5) by $F(x)G(t)$ on both the sides, the variables are separated as;

$$c^2 \frac{F''''(x)}{F(x)} = -\frac{\ddot{G}(t)}{G(t)} = \omega_n^2 \tag{3.6}$$

where the term ω_n^2 is the separation constant representing the square of natural frequency. As the first term in this equation is a function of x only and the second term is a function of t only, the entire equation can be satisfied for arbitrary values of x and t only if each term is a constant.

This expression yields two ordinary differential equations and the first one is given by;

$$F''''(x) - \left(\frac{\omega_n}{c}\right)^2 F(x) = 0 \tag{3.7}$$

Taking $\lambda^2 = \frac{\omega_n}{c}$, expression (3.7) is rewritten as;

$$F''''(x) - \lambda^4 F(x) = 0 \tag{3.8}$$

This expression is solved in the usual way considering $F(x)$ consisting of the sum of four terms. The required solution is simplified as;

$$F(x) = A_1 \cosh \lambda x + A_2 \sinh \lambda x + A_3 \cos \lambda x + A_4 \sin \lambda x \tag{3.9}$$

where constants A_1, A_2, A_3 and A_4 are determined from the boundary conditions of the cantilever beam.

The second expression is given as;

$$\ddot{G}(t) + \omega_n^2 G(t) = 0 \tag{3.10}$$

which is the familiar free vibration expression for an undamped single degree of freedom system having the solution

$$G(t) = A_5 \cos \omega_n t + A_6 \sin \omega_n t \tag{3.11}$$

where constants A_5 and A_6 are evaluated from the initial conditions.

Substituting the expressions for space and time functions as given by expressions (3.9) and (3.11), respectively, into expression (3.4), the complete solution for the deflection of a beam at any section is given by;

$$y(x,t) = (A_1 \cosh \lambda x + A_2 \sinh \mu x + A_3 \cos \lambda x + A_4 \sin \lambda x) \times (A_5 \cos \omega_n t + A_6 \sin \omega_n t) \quad (3.12)$$

It is noted that the model of the transverse vibration of the beam presented in expression (3.3) ignores the effects of shear deformation and rotary inertia. If these effects are considered, more accurate Timoshenko beam theory is to be used.

3.4.1 Evaluation of Constants A_1, A_2, A_3 and A_4

Considering the expression for space function as given by equation (3.9) and taking the successive derivatives, the following relations are derived;

$$F(x) = A_1 \cosh \lambda x + A_2 \sinh \lambda x + A_3 \cos \lambda x + A_4 \sin \lambda x \quad (3.13a)$$

$$F'(x) = \lambda (A_1 \sinh \lambda x + A_2 \cosh \lambda x - A_3 \sin \lambda x + A_4 \cos \lambda x) \quad (31.3b)$$

$$F''(x) = \lambda^2 (A_1 \cosh \lambda x + A_2 \sinh \lambda x - A_3 \cos \lambda x - A_4 \sin \lambda x) \quad (3.13c)$$

$$F'''(x) = \lambda^3 (A_1 \sinh \lambda x + A_2 \cosh \lambda x + A_3 \sin \lambda x - A_4 \cos \lambda x) \quad (3.13d)$$

The four boundary conditions for a cantilever beam are given by:

At the fixed end: $x = 0$, $F(0)=0$, $F'(0) = 0$

At the free end: $x = l$, $F''(l) = 0$, $F'''(l) = 0$

Putting the above boundary conditions, expression (3.11) is reduced to;

$$F(0) = A_1 + A_3 = 0 \quad (3.14a)$$

$$F'(0) = A_2 + A_4 = 0 \quad (3.14b)$$

$$F''(l) = \lambda^2 (A_1 \cosh \lambda l + A_2 \sinh \lambda l - A_3 \cos \lambda l - A_4 \sin \lambda l) = 0$$

i.e., $A_1 \cosh \lambda l + A_2 \sinh \lambda l - A_3 \cos \lambda l - A_4 \sin \lambda l = 0 \quad (3.14c)$

$$F'''(l) = \lambda^3 (A_1 \sinh \lambda l + A_2 \cosh \lambda l + A_3 \sin \lambda l - A_4 \cos \lambda l) = 0$$

i.e., $A_1 \sinh \lambda l + A_2 \cosh \lambda l + A_3 \sin \lambda l - A_4 \cos \lambda l = 0 \quad (3.14d)$

The expression (3.14) can be written in a compact matrix form as;

$$\begin{bmatrix} 1 & 0 & 1 & 0 \\ 0 & 1 & 0 & 1 \\ \cosh \lambda l & \sinh \lambda l & -\cos \lambda l & -\sin \lambda l \\ \sinh \lambda l & \cosh \lambda l & \sin \lambda l & -\cos \lambda l \end{bmatrix} \begin{bmatrix} A_1 \\ A_2 \\ A_3 \\ A_4 \end{bmatrix} = \begin{bmatrix} 0 \\ 0 \\ 0 \\ 0 \end{bmatrix} \tag{3.15}$$

This vector equation has a nonzero solution for the vector $\begin{bmatrix} A_1 & A_2 & A_3 & A_4 \end{bmatrix}^T$ only if the determinant of the coefficient matrix vanishes, i.e., singular. Setting the determinant equal to zero, the characteristic equation is given as;

$$\cos \lambda l . \cosh \lambda l = -1 \tag{3.16}$$

This transcendental equation is the required condition for the co-efficient matrix to give a non-trivial solution and can be further used to determine the frequencies of vibration.

The expression (3.15) is expressed into four algebraic equations. The constants A_1, A_2 and A_3 are dependent parameters and A_4 is an independent parameter. A_4 may have any value. Taking A_4=1, the values of constants of A_1, A_2, A_3 and A_4 are found as;

$$A_1 = \left(\frac{\sin \lambda l + \sinh \lambda l}{\cos \lambda l + \cosh \lambda l} \right),\ A_2 = -1,\ A_3 = -\left(\frac{\sin \lambda l + \sinh \lambda l}{\cos \lambda l + \cosh \lambda l} \right) \text{and } A_4 = 1$$

The space function as given in expression (3.9) is modified by putting the values of various constants as;

$$F(x) = \left(\frac{\sin \lambda l + \sinh \lambda l}{\cos \lambda l + \cosh \lambda l} \right) \cosh \lambda x - \sinh \lambda x - \left(\frac{\sin \lambda l + \sinh \lambda l}{\cos \lambda l + \cosh \lambda l} \right) \cos \lambda x + \sin \lambda x$$

$$\text{i.e., } F(x) = \frac{(\cosh \lambda x - \cos \lambda x)(\sin \lambda l + \sinh \lambda l) + (\sin \lambda x - \sinh \lambda x)(\cos \lambda l + \cosh \lambda l)}{\cos \lambda l + \cosh \lambda l} \tag{3.17}$$

This equation gives different mode shapes of vibration.

3.4.2 Evaluation of Constants A_5 and A_6

The general expression for deflection at any section of the beam as given in expression (3.12) is rewritten as;

$$y(x,t) = F(x)\left(A_5 \cos \omega_n t + A_6 \sin \omega_n t\right) \tag{3.18}$$

Taking derivatives with respect to time, the above equation is reduced to;

$$\frac{dy(x,t)}{dt} = F(x)\left(-A_5 \omega_n \sin \omega_n t + A_6 \omega_n \cos \omega_n t\right) \tag{3.19}$$

The expression (3.19) represents the velocity of deflection at any section of the beam. However, from the initial condition of the cantilever beam, the velocity of deflection at the free end is zero, i.e., $\frac{dy(l,0)}{dt} = 0$, which yields $A_6 = 0$.

Hence, the expression (3.18) is reduced to;

$$y(x,t) = F(x).A_5 \cos \omega_n t \tag{3.20}$$

The initial deflection at the free end of the beam is taken equal to $F(l)$ and substituting the same in expression (3.20), the equation is modified as;

$y(l,0) = F(l).A_5$, which gives $A_5 = \frac{y(l,0)}{F(l)}$

Substituting the value of A_5 in expression (3.20), the final equation for deflection is found to be;

$$y(x,t) = F(x)\left[\frac{y(l,0)}{F(l)}\right]\cos \omega_n t \tag{3.21}$$

This is the generalized deflection equation at any section of a cantilever beam.

3.5 Mechanisms of Micro-slip

The mechanism of micro-slip at the interfaces presents a very complicated characteristics and a thorough understanding of this phenomenon is required for

correct assessment of energy dissipation. Therefore, different theories have been proposed for the possible cause of micro-slip at the interfaces of connecting members.

In practice, the interfaces are microscopically irregular and contain asperities of different size and shape. When two interfaces are pressed together and vibrate, big asperities get compressed and deform first in the tangential direction. Due to different physical properties, the nature of the deformation of the asperities is different; some deform elastically, few plastically and others break up completely. These deformations introduce a partial slippage over a small area at the interfaces. Therefore, even though there is no deformation of the component members being jointed, micro-slip can still occur. However, this may not be the only cause of micro-slip and possibly there are other mechanisms responsible for its occurrence.

Another mechanism states that the micro slip can also occur when the joints connecting the members are semi-rigid and a small relative motion is allowed at the interfaces. Under the action of the transverse load in the jointed beams, slippage occurs over a fraction of the region of contact and is referred to as micro-slip. The occurrence of micro-slip is mainly controlled by the interface pressure provided by the welded joints. When the joint is appreciably rigid, no frictional sliding takes place at the interfaces and the two beam components is considered as a monolithic cantilevered structure. Moreover, when the slip occurs over the entire interface, it is termed as macro-slip which has not been considered in the present investigation.

From the above discussions, it is established that the cause of micro-slip is due to several effects such as; i) different properties of the asperities at the interfaces, ii) semi-rigid nature of joints joining different layers and iii) pressure distribution at the interfaces. It is the micro-slip at the jointed interface which is mainly responsible for the cause of energy dissipation. Moreover, the micro-slip between the connecting members occurs only at lower excitation levels. When the excitation level is increased, both micro- and macro-slips occur at the jointed interfaces. Usually, the macro-slip is avoided because it may lead to structural damage of the joint. On the other hand, micro-slip provides a good level of energy dissipation without causing any adverse effect to the joints. The contribution of micro-slip to the overall system damping is significant in spite of its low magnitude in real applications.

3.5.1 Evaluation of Relative Dynamic Slip

In order to simplify the theoretical analysis, it is assumed that each layer of the jointed cantilever beam being vibrated has the equal bending stiffness and is in the same bending condition. Further it is assumed that each layer of the beam shows no extension of the neutral axis and no deformation of the cross-section. When the jointed cantilever beam is given an initial excitation at the free end, the contacting surfaces undergo relative motion called micro-slip. This relative displacement *u(x, t)* at any distance *x* from the fixed end is equal to the sum of Δu_1 and Δu_2 as shown in Fig. 3.2 and at a particular position and time is given by;

$$u(x,t) = \Delta u_1 + \Delta u_2 = 2h \tan[\partial y(x,t) / \partial x] \tag{3.22}$$

where *h* is the half of the thickness of beam cross-section

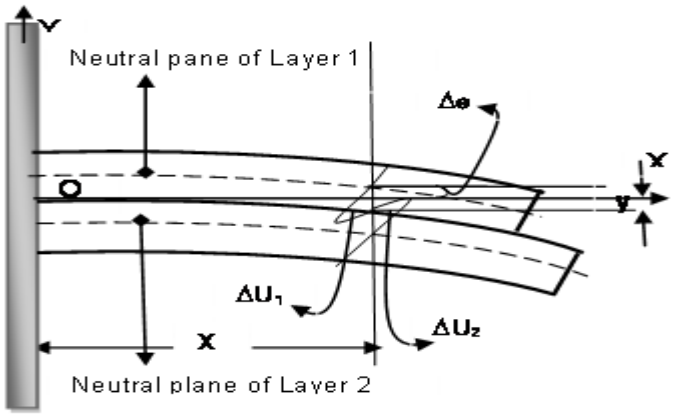

Fig. 3.2 Mechanism of relative dynamic slip at the interfaces

However, the actual relative dynamic slip [$u_r(x, t)$] at the interfaces during the vibration will be less and is found out by subtracting the elastic recovery part of the relative displacement from u(x, t) and is rewritten as

$$u_r(x,t) = \alpha u(x,t) = 2\alpha h \tan[\partial y(x,t) / \partial x] \tag{3.23}$$

where, α is the dynamic slip ratio.

This mechanism of slip is shown in Fig. 3.3 by using the hysteresis loop and the area OAB shows the loss energy dissipated by the micro-slip and the area ABH shows the elastic recovered energy.

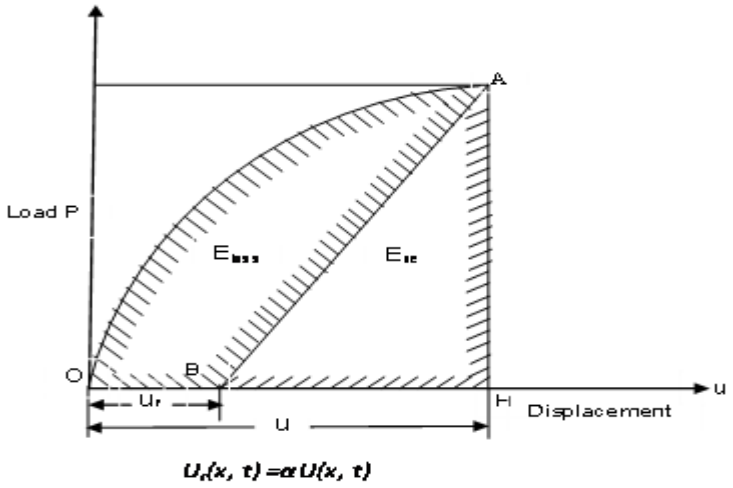

Fig. 3.3 Relationship between u_r and u

3.6 Pressure Distribution at the Jointed Interfaces

A layered and jointed construction is made by welding which holds the members together at the interfaces. Under such circumstances, the profile of the interface pressure distribution assumes a significant role, especially in the presence of slip, to dissipate the vibration energy. Consequently, it is necessary to examine the exact nature of the interface pressure profile and its magnitude across a beam layer for the correct assessment of the damping capacity of a jointed structure. As discussed in the previous chapter, almost all earlier analyses have examined the effect of pressure distribution on slip damping in a jointed beam with bolted and riveted joints but no significant work has been reported till date on the similar beams jointed with welded joints.

3.6.1 Determination of Pressure Distribution at the Interfaces

For experimental flat-on- flat geometry, it is assumed that some rounding of corners is present due to machining. This alleviates the stress singularities at the edges of contact and normal pressure falls to zero. The solution of contact pressure for flat surfaces with rounded corners is found out by Ciavarella et al. [129]. The geometry of such a flat surface with rounded corners is shown in Fig. 3.4.

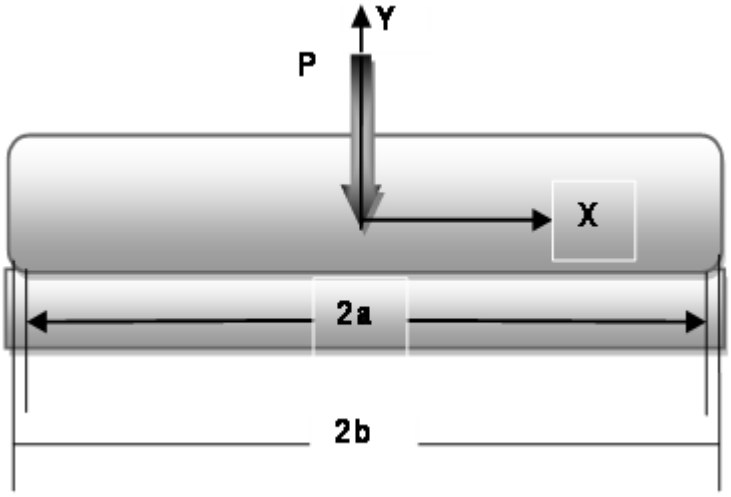

Fig. 3.4 Flat-on-Flat contacts of finite bodies

The actual width of contact is given by '2*b'* under normal load "P" per unit length, which envelopes the flat portion of width '2a' of the flat body and extends into the rounded geometry.

A co-ordinate system for such geometry is given by;

$$\sin\phi = \frac{x}{b}, -b \le x \le b \tag{3.24}$$

$$\sin\phi_0 = \frac{a}{b} \tag{3.25}$$

The contact pressure with half space is given by Ciavarella et al. [129] as;

$$\frac{bp(\phi)}{P} = -\frac{2/\pi}{\pi - 2\phi_o - \sin 2\phi_o}\left\{(\pi - 2\phi_o)\cos\phi + \ln\left[\left|\frac{\sin(\phi+\phi_o)}{\sin(\phi-\phi_o)}\right|^{\sin\phi}\left|\tan\left(\frac{\phi+\phi_o}{2}\right)\tan\left(\frac{\phi-\phi_o}{2}\right)\right|^{\sin\phi_o}\right]\right\} \tag{3.26}$$

Fig. 3.5 shows the pressure distribution for a/b ratio equal to 0, 0.25, 0.5, 0.75,1, i.e., ranging from the Hertzian case to the limit flat profile case. From the figure it is quite obvious that the pressure is not constant and further more pressure at the edges tends to infinity as a/b tends to1 and falls to zero at the edges for a/b<1.

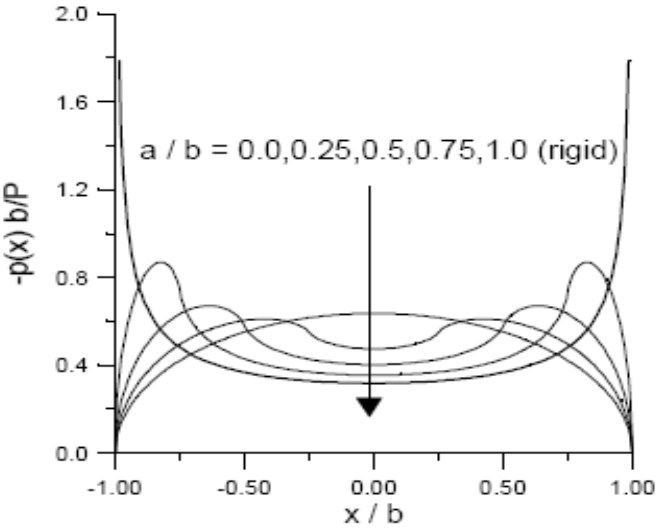

Fig. 3.5 Pressure distribution for rounded edge flat body at various geometric ratio a/b

Further, in Fig. 3.6, the maximum pressure p_{max} is plotted as a function of the ratio a/b, which tends to infinity as a/b tends to 1 and to the Hertzian value as a/b decreases.

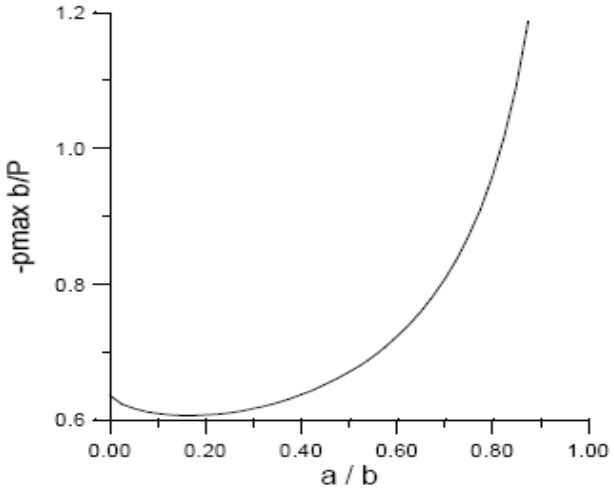

Fig. 3.6 Maximum pressure as a function of the geometric ratio a/b

In this case, the pressure profile falls to zero at the contact edges for a/b<1 with no stress singularities and tends to infinity as a/b tends to infinity. Since for the above case, the pressure distribution is not constant rather depends on the roundness of the edges, i. e., ratio a/b, hence the above pressure distribution is not considered for the present case of flat bodies in contact. However, for flat bodies, the pressure

distribution remains constant and is found out by Johnson [130] and Giannakopoulos et al. [131] as shown in Fig. 3.7 and is given as;

$$p(x) = \frac{P}{2a} \tag{3.27}$$

In the present analysis, the welded beams are considered to be in contact with each other because of perfect flatness and same condition of flatness is maintained under excitation due to welding. Since perfect contact is maintained under both the static and dynamic conditions, the pressure at the interfaces is assumed to be uniform. The contact pressure for flat surfaces with rounded corners has been found out by Ciavarella et al. [129], which shows a non-uniform distribution pattern at the interfaces. Contrary to this, the pressure distribution at the interfaces of flat surfaces is uniform owing to the contact of the upper layer over the lower one as established by Johnson [130] and Giannakopoulos et al. [131]. The present investigation uses the pressure distribution given by Johnson [130] and Giannakopoulos et al. [131] for flat surfaces in contact with each other.

3.7 Energy Dissipation due to Friction and Micro-slip

Structural joints are regarded as a potential source of energy dissipation in assembled structures. During vibration, a jointed beam oscillates about its mean position in the transverse direction. As a result, the different layers constituting the jointed beam undergo a small relative motion (micro-slip) at the interfaces. Friction will arise due to this relative motion of the components in contact and its presence results in the energy losses. The friction, although is viewed to have deteriorating effects on the performance of various systems, but it can also be used to enhance the system performance due to its damping properties. The energy loss of a structure is found out by measuring the area of the hysteresis loop obtained from the friction force vs. relative displacement plot as given in Fig. 3.3 earlier.

3.7.1 Determination of Energy Dissipation per Cycle of Vibration

Energy is dissipated due to the relative dynamic slip at the interfaces. Considering the cantilever beam as shown in Fig. 3.2, the interface pressure at x is expressed as p(x) and assuming that p(x) is constant in z-direction (the direction to the width of beam), the normal load acting on the length of dx is p(x)$b$dx, where b is the width of beam.

Thus, the frictional force at the interfaces is given by $\mu p(x)b\mathrm{d}x$. Assuming that the interface pressure is uniformly spread over all the contact area (bl), pressure $p(x)$ yields p. The energy loss due to the frictional force at the interfaces per half-cycle of vibration is found out considering uniform pressure distribution at the interfaces (p) and is given by;

$$E_{loss} = \int_0^{\pi/\omega_n} \int_0^{l} \mu pb\left[\left\{\partial u_r(x,t)/\partial t\right\} dxdt\right] \tag{3.28}$$

However, the energy introduced into the layered and jointed cantilever beam in the form of strain energy per half-cycle of vibration is given by;

$$E_{ne} = \left(3EI/l^3\right) y^2(l,0) \tag{3.29}$$

From the above expressions (3.28) and (3.29), the ratio of energy (E_{loss}/E_{net}) is found to be;

$$\frac{E_{loss}}{E_{ne}} = \int_0^{\pi/\omega_n} \int_0^{l} \left[\mu pb\left\{\partial u_r(x,t)/\partial t\right\} dxdt\right] \Big/ \left[\left(3EI/l^3\right) y^2(l,0)\right] \tag{3.30}$$

Considering uniform pressure distribution throughout the contact area of the interfaces and assuming dynamic slip ratio, α, to be independent of the distance from the fixed end of the cantilever beam and time, the above expression (3.30) is modified using expression (3.23) as;

$$\frac{E_{loss}}{E_{ne}} = \left[2\mu bhp\alpha \Big/ \left\{\left(3EI/l^3\right) y^2(l,0)\right\}\right] \int_0^{\pi/\omega_n} \int_0^{l} \left[\partial\left\{\tan \partial y(x,t)/\partial x\right\} dxdt\right] \Big/ \partial t \tag{3.31}$$

The slope of the cantilever beam $\partial y(x,t)/\partial x$ being quite small, the same is modified as; $\tan \partial y(x,t)/\partial x \simeq \partial y(x,t)/\partial x$

Therefore, expression (3.31) is modified to

$$\frac{E_{loss}}{E_{ne}} = \left[2\mu bhp\alpha \Big/ \left\{\left(3EI/l^3\right) y^2(l,0)\right\}\right] \int_0^{\pi/\omega_n} \int_0^{l} \left[\left\{\partial^2 y(x,t)/\partial x \partial t\right\} dxdt\right] \tag{3.32}$$

Using the expression (3.21) in expression (3.32) and changing the limits of the time interval from 0 and π/ω_n to 0 and $\pi/2\omega_n$ and multiplying the expression by two for yielding definite solution we get;

$$E_{loss}/E_{ne} = \frac{4\mu bh\alpha}{\left(3EI/l^3\right)y^2(l,0)} \int_0^{\pi/\omega_n} \int_0^{l} \partial^2 \left[F(x)\left\{ y_0/F(l)\right\} \cos\omega_n t \right] dxdt \Big/ \left[\partial x/\partial t\right] \tag{3.33}$$

Substituting expression (3.15) in (3.33) and simplifying we get;

$$E_{loss}/E_{ne} = \left[4\mu bhp\alpha\, y(l,0)\right] \Big/ \left[3\left(EI/l^3\right) y^2(l,0)\right] \tag{3.34}$$

Replacing, $3EI/l^3 = k$ i.e., the equivalent spring constant (static bending stiffness) of the layered and jointed beam, the above expression (3.34) reduces to;

$$E_{loss}/E_{ne} = \left[4\mu bhp\alpha\right] \Big/ \left[ky(l,0)\right] \tag{3.35}$$

3.8 Determination of Logarithmic Damping Decrement

For a lightly damped linear system, the damping capacity of a jointed beam is usually determined from the logarithmic decrement method. This approach is generally used to estimate the damping from the experiments in which the decaying amplitude is recorded from the time history plot. For the theoretical evaluation of damping, the energy approach is popular because the logarithmic decrement is fundamentally equal to the energy loss per cycle of vibration.

Logarithmic damping decrement is used as a measure of damping capacity of a structure and is influenced by dynamic slip and interface pressure at the contacting surfaces. The logarithmic damping decrement, δ, is usually expressed as, $\delta = \ln(a_n/a_{n+1})$ where a_n is an amplitude of vibration at certain time and a_{n+1} is the amplitude of vibration after one cycle passed. If the energy stored in the system when amplitude of vibration is a_n, is denoted as E_n, it is easily known that $E_n = E_{ne} + E_{loss}$ and $E_{n+1} = E_n - E_{loss}$. Therefore, assuming that the energy stored in the system is proportional to the square of the corresponding amplitude, the relationship between logarithmic damping decrement and damping ratio is written as;

$$\delta = \ln(a_n / a_{n+1}) = \ln\left(E_n / E_{n+1}\right)^{1/2} = \left[\ln\left\{1/(1-\psi)\right\}\right]/2 \tag{3.36}$$

In case of $\psi \ll 1$, Maclaurin expansion of expression (3.36) is given by;

$$\delta = \frac{1}{2}\left(\psi + \frac{1}{2}\psi^2\right) \tag{3.37}$$

where the high order terms, i. e., more than ψ^2 are ignored.

The damping ratio, ψ, is expressed as the ratio of energy dissipated due to the relative dynamic slip at the interfaces and the total energy introduced into the system and is found to be;

$$\psi = \left[E_{loss}/\left(E_{loss} + E_{ne}\right)\right] = 1/\left[1 + E_{ne}/E_{loss}\right] \tag{3.38}$$

where E_{loss} and E_{ne} are the energy loss due to interface friction and the energy introduced during the unloading process, respectively.

Putting the values of E_{loss}/E_{ne} from expression (3.35) in (3.38) we get;

$$\psi = \frac{1}{1 + \left[ky(l,0)\right]/\left[4\mu bph\alpha\right]} \tag{3.39}$$

Since, the above expression is valid for two-layered and jointed cantilever beam, a generalized expression has been developed for a multi-layered and jointed cantilever beam as given by;

$$\psi = \frac{1}{1 + \left[ky(l,0)\right]/\left[4(m-1)\mu bph\alpha\right]} \tag{3.40}$$

where, 'm' is the number of layers.

The energy dissipation principally depends upon the kinematic coefficient of friction (μ) and dynamic slip ratio (α) at the interfaces. It is very difficult to assess the damping produced in the joints due to variations of the above two vital parameters under dynamic conditions. These two parameters are inter-dependent and inversely related, i.e., if one is increasing, the other is decreasing and vice versa. However, their product ($\alpha.\mu$) is found to be constant for a particular specimen irrespective of the

surface condition. Thus, this product $\alpha.\mu$ is found out modifying expressions (3.36) and (3.39) as;

$$\alpha.\mu = k\left(1-e^{-2\delta}\right)y(l,0)\Big/4bphe^{-2\delta} \tag{3.41}$$

This product has been found out from the experimental results of logarithmic decrement for a particular welded beam of 3 mm thickness using the expression (3.41) and subsequently used to find out the numerical values of the logarithmic decrement for other conditions of the beam using expressions (3.36) and (3.40).

3.9 Summary

In this chapter, an exact solution is presented considering the distributed-parameter model for the beam structure. The governing equations for the transverse vibration have been derived assuming the Euler-Bernoulli beam theory neglecting the effects of shear deformation and rotary inertia. Further, the total relative dynamic slip at the interfaces has been evaluated considering the expressions for the slope and deflection. It is found that the total slip is a function of the distance from the fixed end. The interface pressure distribution has been determined and is found to be uniformly distributed. Subsequently, the equations for logarithmic decrement for two as well as multi-layered welded beams have been developed. It is established that the micro-slip, kinematic coefficient of friction and the nature of pressure distribution at the interfaces, cantilever length and number of layers play major roles in quantifying the damping of the welded beam structures. Therefore, an extensive study on all the above vital parameters has been carried out in the present investigation.

4

DAMPING ESTIMATION OF WELDED SYMMETRICAL BEAMS WITH SINGLE INTERFACE CONSIDERING IN-PLANE BENDING STRESS

4.1 Introduction

In the previous chapter, a detailed static analysis has been presented for the evaluation of damping mechanism in layered and welded beams considering the dynamic slip ratio. In the present chapter a different approach has been adopted to explore the mechanism of slip damping in two layered welded symmetrical beams with single interface. In the present chapter damping capacity has been evaluated for the layered and welded symmetrical beams subjected to both static and dynamic loading conditions. Relative dynamic slip has been ascertained considering the in-plane bending stress and expressions for the slope and deflection of the jointed beams. This relative slip is further used to estimate the loss factor of jointed symmetrical beams with single interface for both the cases of static and dynamic loadings.

4.2 Single Interface

The two layered and tack welded cantilever beam model with thickness 2*h*, width *b*, and length *l* as shown in Fig. 4.1(a) is considered to find out the damping ratio. The loading consists of uniformly distributed pressure at the interfaces due to perfect contact between two flat bodies, and a concentrated load *P* applied at the free end, x= *l*. Each of the two halves of thickness *h* is considered separately with the loading as depicted in the Fig. 4.1(b). The continuity of stress and vertical displacement '*v*' is imposed at the interfaces. At some finite value of *P*, the shear stress at the interfaces will reach the critical value for slip $\tau_{xy} = \mu p$, where μ and p are the kinematic co-efficient friction and interface pressure, respectively. Additional static force due to excitation will produce a relative displacement $\Delta u(x)$ at the interfaces.

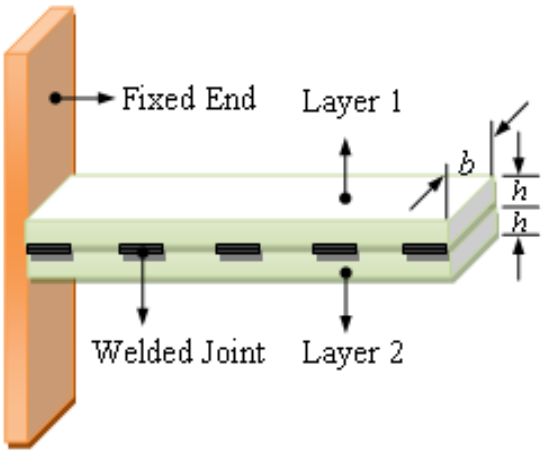

Fig. 4.1(a) Two layered tack welded cantilever beam model

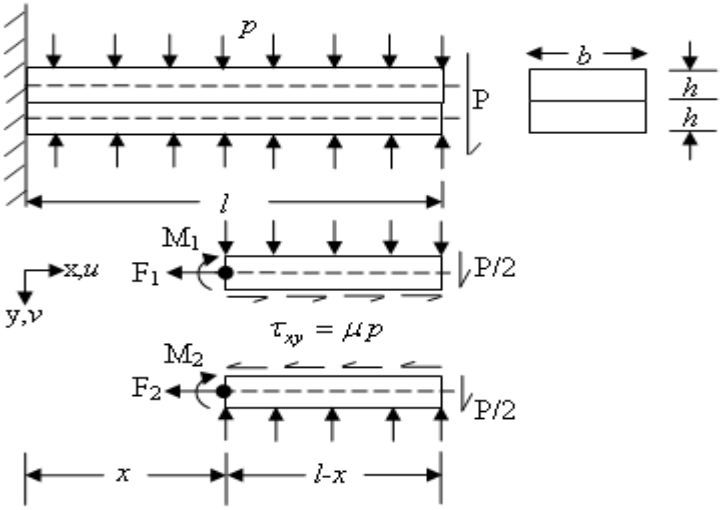

Fig. 4.1(b) Two halves of the beam depicting load and co-ordinates

4.2.1 Static Analysis

In the present section a detailed static analysis of the two layered jointed and welded beams with single interface has been presented. In the static analysis the beams has been assumed to be initially excited with constant static force and the damping is then evaluated in terms of the loss factor.

4.2.1.1 Interface Pressure Distribution

The pressure distribution at the interfaces is assumed to be uniform owing to the contact of the upper layer over the lower one. The relation for uniform pressure

distribution as given by Johnson [130] and Giannakopoulos et al. [131] due to contact of two flat bodies has been considered as discussed in details (expression 3.27) in the previous chapter.

4.2.1.2 Analysis of Static Response

The layered and jointed welded beams are initially excited by a transverse static load and then released. The transverse bending of the jointed beams takes place which is considered as the static response. The static response under the action of transverse static load is evaluated by considering the equilibrium of the various forces acting on the jointed beam as presented in the Fig. 4.1(b).

The resultant moment at the centroid of each laminate as shown in Fig. 4.1(b) is given by;

$$M_1 = M_2 = M = \frac{P}{2}(l-x) - \mu pb\frac{h}{2}(l-x) \tag{4.1}$$

where the subscripts 1 and 2 refer to the upper and lower laminates, respectively.

Invoking the relation between bending moment and curvature as derived by Warburton [177], we get;

$$M = -EI\frac{d^2v}{dx^2} \tag{4.2}$$

where E is the modulus of elasticity

Putting expression (4.2) in (4.1) the following expression is obtained;

$$\frac{d^2v}{dx^2} = \frac{6}{Ebh^3}(P - \mu pbh)(l-x) \tag{4.3}$$

where $I = bh^3/12$ is the moment of inertia of the cross-section of the beam.

Integrating expression (4.3) once we get;

$$\frac{dv}{dx} = \frac{6}{Ebh^3}(P - \mu pbh)\left(lx - \frac{x^2}{2}\right) + C_1 \tag{4.4}$$

where C_1 is the integration constant and is evaluated to be zero by putting the boundary condition, $\left(dv/dx\right)\Big|_{x=0} = 0$ in the expression (4.4).

Further, integration of expression (4.4) yields;

$$v = \frac{3}{Ebh^3}\left(P - \mu pbh\right)\left(lx^2 - \frac{x^3}{3}\right) + C_2 \tag{4.5}$$

where the integration constant, $C_2 = 0$ since $v\big|_{x=0} = 0$.

Putting the value of C_2 in the expression (4.5) and simplifying, the static deflection mode shape expression is given by;

$$v(x) = \frac{\left(P - \mu pbh\right)l^3}{Ebh^3}\left[3\left(\frac{x}{l}\right)^2 - \left(\frac{x}{l}\right)^3\right] \tag{4.6}$$

The two dimensional parameters Q and R are defined as presented below;

$$Q = \mu pbh \tag{4.7a}$$

$$R = \frac{Ebh^3}{l^3} \tag{4.7b}$$

Putting the expressions (4.7a) and (4.7b) in (4.6) and simplifying we get;

$$v(x) = \frac{P - Q}{R}\left[3\left(\frac{x}{l}\right)^2 - \left(\frac{x}{l}\right)^3\right] \tag{4.8}$$

4.2.1.3 Evaluation of Relative Slip

Relative slip at the interfaces is an important parameter affecting the slip damping in jointed structures. Relative slip at the interfaces is dependent on the type of loading and varies along the length of the beam. Correct assessment of this parameter is important for the evaluation of damping in the built-up structures. In the present analysis the slip at the interfaces has been evaluated considering the slope, transverse deflection and in-plane bending stress.

The displacements at any axial position x and $y_{1,2} = \mp h/2$ are given by;

$$u_1 = \frac{1}{E}\int_0^x \sigma_{x_1} dx - \frac{h}{2}\frac{dv_1}{dx} \tag{4.9a}$$

$$u_2 = \frac{1}{E}\int_0^x \sigma_{x_2} dx + \frac{h}{2}\frac{dv_2}{dx} \tag{4.9b}$$

These displacements are produced by the resultant axial force $F_{1,2}$ and moment $M_{1,2}$, about the centroid of each half of the beam as shown in Fig. 4.1(b).

where v_1, v_2 are the vertical deflections, E is the modulus of elasticity and $\sigma_{x_1}, \sigma_{x_2}$ are the in-plane bending stresses. It is assumed that the continuity equation prevails, i.e., $v_1 = v_2 = v$

From the force equilibrium, the in-plane bending stresses in the upper and lower laminates are computed as follows:

$$\sigma_{x_1} = \frac{\mu p}{h}(l - x) \tag{4.10}$$

$$\sigma_{x_2} = -\frac{\mu p}{h}(l - x) \tag{4.11}$$

Combining expressions (4.8), (4.9), (4.10) and (4.11) and simplifying, the relative slip displacement at the interfaces is given by;

$$\Delta u = u_2 - u_1 = \frac{3h}{Rl}\left[P - \frac{4}{3}Q\right]\left[2\left(\frac{x}{l}\right) - \left(\frac{x}{l}\right)^2\right] \tag{4.12}$$

Slip will occur only if $P > P_c = {}^{4Q}\!/_{3}$

where P_c is the critical static load applied at tip of the welded cantilever beams.

4.2.1.4 Analysis of Energy Dissipated

The energy is dissipated due to friction and relative dynamic slip at the interfaces. For completely reversed loading, the product of the shear force, μp and the relative displacement, Δu integrated over the length of the beam is equal to one-fourth of the energy dissipated in a complete cycle.

Thus, energy dissipation per cycle as established by Goodman and Klumpp [17] is given by;

$$E_{loss} = 4b\int_0^l \tau_{xy}\Delta u(x)\,dx = 4\mu pb\int_0^l (u_2 - u_1)\,dx \tag{4.13}$$

where u_1 and u_2 are the displacements in the x-direction between the points on the adjacent faces of the upper and lower half beam, respectively.

Substituting the expression (4.12) in (4.13) considering the beam to be loaded cyclically between the loads $\pm P_m$ and integrating, the energy dissipation per cycle in terms of static load is given by;

$$E_{loss} = \frac{8Q}{R}\left(P_m - \frac{4Q}{3}\right) \tag{4.14}$$

where P_m is the maximum static load applied at the tip of the welded cantilever beam. The maximum tip displacement v_m corresponding to $P = P_m$ is obtained from (4.8) by putting $x = l$ and is given by;

$$v_m = \frac{2}{R}(P_m - Q) \tag{4.15a}$$

Rearranging expression (4.15a), P_m in terms of v_m is found to be;

$$P_m = \frac{Rv_m}{2} + Q \tag{4.15b}$$

Putting the expression (4.15b) in (4.14), the energy dissipation in terms of displacement is given by;

$$E_{loss} = 4Q\left(v_m - \frac{2Q}{3R}\right) \tag{4.16}$$

From the expression (4.16), it is evident that slip will occur only if $v = v_c = \frac{2Q}{3R}$, where v_c is the critical tip displacement.

The load-deflection curve for the beam is shown in Fig. 4.2.

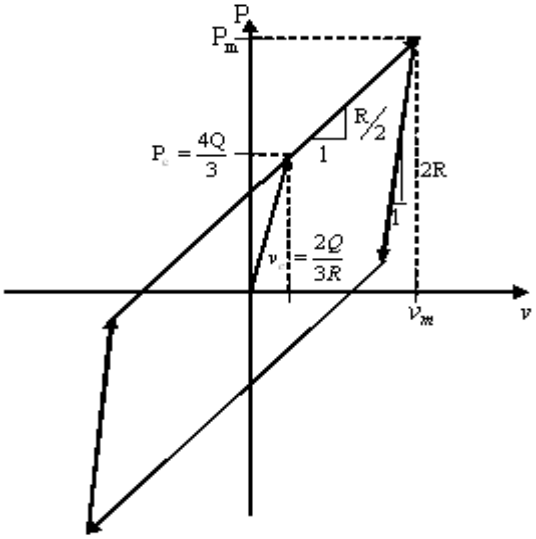

Fig. 4.2 Static load versus tip deflection for cantilever beam

The curve is bilinear with elastic compliance $C_1 = \frac{1}{2R}$ and slip compliance $C_2 = \frac{2}{R}$.

Slip is initiated at the critical load $P_c = \frac{4Q}{3}$ and tip displacement $v_c = \frac{2Q}{3R}$.

4.2.1.5 Evaluation of Damping Ratio

In vibration problems, it is most convenient to express the dissipative properties of the system in terms of a non-dimensional quantity such as the damping ratio "ψ" and loss factor "η_s", defined by;

$$\psi = \frac{E_{loss}}{E_{ne}} \tag{4.17a}$$

$$\eta_s = \frac{E_{loss}}{2\pi E_{ne}} = \frac{\psi}{2\pi} \tag{4.17b}$$

where E_{ne} is the maximum strain energy stored in the system.

The maximum strain energy stored in the system in terms of maximum load and tip deflection is given by;

$$E_{ne} = \frac{1}{2} P_m \left(\frac{v_c}{P_c} \right) P_m = \frac{P_m^2}{4R} \tag{4.18a}$$

$$E_{ne} = \frac{1}{4R}\left(\frac{Rv_m}{2} + Q\right)^2 \tag{4.18b}$$

Putting expressions (4.14), (4.16) and (4.18) in expression (4.17) and simplifying, the damping ratio in terms of tip displacement and load is given by;

$$\psi = \frac{64\left(\frac{Rv_m}{Q} - \frac{2}{3}\right)}{\left(\frac{Rv_m}{Q} + 2\right)^2} \tag{4.19a}$$

$$\psi = 32\left[\left(\frac{Q}{P_m}\right) - \frac{4}{3}\left(\frac{Q}{P_m}\right)^2\right] \tag{4.19b}$$

Putting expressions (4.18) and (4.19) in (4.17), the expression for loss factor for two layered welded structures is given by;

$$\eta = \frac{32}{\pi}\frac{\left(\frac{Rv_m}{Q} - \frac{2}{3}\right)}{\left(\frac{Rv_m}{Q} + 2\right)^2} \tag{4.20a}$$

$$\eta = \frac{16}{\pi}\left[\left(\frac{Q}{P_m}\right) - \frac{4}{3}\left(\frac{Q}{P_m}\right)^2\right] \tag{4.20b}$$

These relations are plotted in Fig. 4.3. The arrows indicate the direction of increasing load or deflection with point **A** corresponding to the onset of slip. The energy dissipation per cycle always increases with increasing load or deflection, the loss factor increases in the region **AB** and then decreases with further increase in load or deflection. The point **B** at which a maximum loss factor occurs depends upon the values of the dimensional and material parameters of the beam as well as the loading.

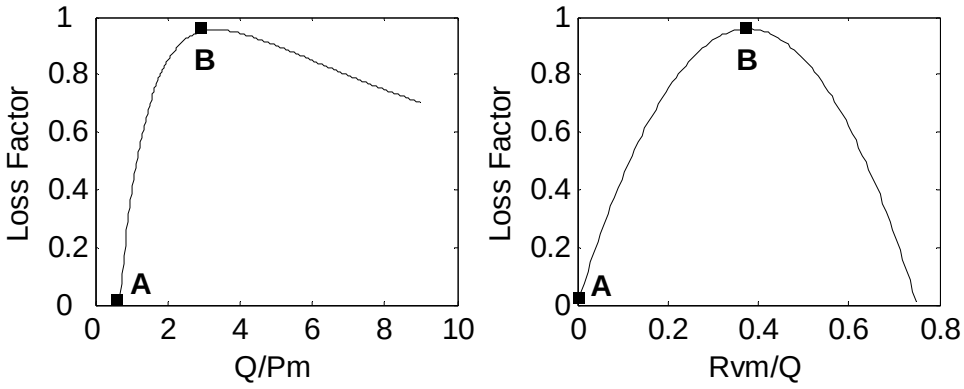

Fig. 4.3 Loss factor versus load and displacement parameter

4.2.2 Dynamic Analysis

In the present section, a detailed analysis has been presented for the dynamic analysis of the two layered welded beams with single interface. For the forced vibration of a cantilever beam, the static analysis has been extended to include distributed inertia forces and examine their effect on the mode shape, relative slip distribution and energy dissipation due to slip. In the present analysis two types of loading has been considered; Heaviside and harmonic loading. The analysis developed here follows the static analysis developed in the preceding sections for the beam as shown in Fig. 4.1.

4.2.2.1 Analysis of Dynamic Response

The two layered and jointed welded beams are initially excited at the free end by a time varying dynamic transverse force of Heaviside and harmonic nature. The transverse bending of the jointed beams takes place which is referred to as the dynamic response. The dynamic response under the action of transverse dynamic load is evaluated by considering the equilibrium of the various forces acting on the jointed beam as presented in the Fig. 4.1(b). The forced vibration of the beam produced by a time-dependent displacement at the unsupported end has been considered such that;

$$v\big|_{x=l} = f(t) \tag{4.21}$$

Following Timoshenko [28], the dynamic displacement is composed of two parts;

$$v = v_{\mathrm{I}} + v_{\mathrm{II}} \tag{4.22}$$

where

$$v_{\mathrm{I}} = \left[\frac{3}{2}\left(\frac{x}{l} \right)^2 - \frac{1}{2}\left(\frac{x}{l} \right)^3 \right] f(t) \tag{4.23}$$

The term in the bracket represents the static mode function and satisfies the end conditions;

$$v_{\mathrm{I}}\big|_{x=0} = 0; \frac{\mathrm{d}\, v_{\mathrm{I}}}{\mathrm{d}\, x}\bigg|_{x=0} = 0; \frac{\mathrm{d}^2 v_{\mathrm{I}}}{\mathrm{d}\, x^2}\bigg|_{x=l} = 0; v_{\mathrm{I}}\big|_{x=l} = 0; \tag{4.24}$$

but does not satisfy the dynamic equilibrium equation;

$$EI \frac{\partial^4 v}{\partial x^4} + \rho A \frac{\partial^2 v}{\partial t^2} = 0 \tag{4.25}$$

where EI and ρ are the flexural rigidity and density of the beam, respectively.
The displacement v_{I} produces the dynamic loads as given by;

$$-A\rho \left[\frac{3}{2}\left(\frac{x}{l} \right)^2 - \frac{1}{2}\left(\frac{x}{l} \right)^3 \right] \ddot{f}(t) \tag{4.26}$$

where A is the cross-sectional area of the beam.
Moreover, the displacement (v_{II}) representing vibrations produced by the force function (4.26) is expressed as;

$$v_{\mathrm{II}} = \sum_i \varphi_i(t) X_i(x) \tag{4.27}$$

where $X_i(x)$ and $\varphi_i(t)$ are the modal and time-dependent functions, respectively.

v_{II} must satisfy the end conditions as follows;

$$v_{\mathrm{II}}\big|_{x=0} = 0; \frac{\mathrm{d}\, v_{\mathrm{II}}}{\mathrm{d}\, x}\bigg|_{x=0} = 0; \frac{\mathrm{d}^2 v_{\mathrm{II}}}{\mathrm{d}\, x^2}\bigg|_{x=l} = 0; v_{\mathrm{II}}\big|_{x=l} = 0; \tag{4.28}$$

$X_i(x)$ are the solutions of the expression (4.25) and satisfies the end condition (4.28).
Thus we get;

$$X_i = \sinh k_i l \sin k_i (l-x) - \sin k_i l \sinh k_i (l-x) \tag{4.29}$$

where k_i are the roots of the following expression;

$$\tanh k_i l = \tan k_i l \tag{4.30}$$

The total displacement is then obtained by putting expressions (4.23) and (4.27) in (4.22) and the same is given by;

$$v = \left[\frac{3}{2}\left(\frac{x}{l}\right)^2 - \frac{1}{2}\left(\frac{x}{l}\right)^3 \right] f(t) + \sum_i \varphi_i(t) X_i(x) \tag{4.31}$$

Applying the principle of virtual work, Timoshenko [28] has shown that the time-dependent functions $\varphi_i(t)$ must satisfy the differential equation

$$\ddot{\varphi}_i + \frac{EIk_i^4}{A\rho}\varphi_i = -b_i \ddot{f}(t) \tag{4.32}$$

where the dot superscripts denote differentiation with respect to time. The coefficients b_i are obtained by expanding the force function (4.26) in a series of the normal functions, X_i. Thus,

$$-A\rho\ddot{f}(t)\left[\frac{3}{2}\left(\frac{x}{l}\right)^2 - \frac{1}{2}\left(\frac{x}{l}\right)^3 \right] = -A\rho\ddot{f}(t)\sum_i b_i X_i \tag{4.33}$$

and the coefficients b_i are obtained from the following expression;

$$b_i = \frac{\int_0^l X_i \left[\frac{3}{2}\left(\frac{x}{l}\right)^2 - \frac{1}{2}\left(\frac{x}{l}\right)^3 \right] \mathrm{d}x}{\int_0^l X_i^2 \, \mathrm{d}x} \tag{4.34}$$

Integrating the expression (4.34), b_i is finally given by;

$$b_i = \frac{2}{k_i l (\sinh k_i l - \sin k_i l)} \tag{4.35}$$

The general solution of expression (4.32) is given by;

$$\varphi_i(t) = A_i \cos p_i t + B_i \sin p_i t - \frac{b_i}{p_i}\int_0^t \ddot{f}(t)\sin p_i(t-\tau)\,\mathrm{d}\tau \tag{4.36}$$

where

$$p_i = \left(\frac{EI}{A\rho}\right)^{1/2} k_i^2$$

Constants A_i and B_i are evaluated from the initial conditions;

$$v(0) = U(x,0) \tag{4.37a}$$

$$\dot{v}(0) = V(x,0) \tag{4.37b}$$

Putting expression (4.31) in expression (4.37), U and V are given by;

$$U = \left[\frac{3}{2}\left(\frac{x}{l}\right)^2 - \frac{1}{2}\left(\frac{x}{l}\right)^3\right] f(0) + \sum_i X_i \{A_i\} \tag{4.38a}$$

$$V = \left[\frac{3}{2}\left(\frac{x}{l}\right)^2 - \frac{1}{2}\left(\frac{x}{l}\right)^3\right] \dot{f}(0) + \sum_i X_i \{B_i p_i\} \tag{4.38b}$$

Moreover;

$$\left[\frac{3}{2}\left(\frac{x}{l}\right)^2 - \frac{1}{2}\left(\frac{x}{l}\right)^3\right] = \sum_i b_i X_i \tag{4.39}$$

Putting expression (4.39) in (4.38) and simplifying we get;

$$U(x,0) = \sum_i X_i \{A_i + b_i f(0)\} \tag{4.40a}$$

$$V(x,0) = \sum_i X_i \{B_i p_i + b_i \dot{f}(0)\} \tag{4.40b}$$

Putting the initial conditions U=V=0, the constants A_i and B_i are evaluated as;

$$A_i = -b_i f(0) \tag{4.41a}$$

$$B_i = -\frac{b_i}{p_i}\dot{f}(0) \tag{4.41b}$$

Substitution of expressions (4.36) and (4.41) in (4.31) yields;

$$\begin{aligned} v(x,t) &= \left[\frac{3}{2}\left(\frac{x}{l}\right)^2 - \frac{1}{2}\left(\frac{x}{l}\right)^3\right] f(t) - f(0)\sum_i b_i X_i \cos p_i t \\ &- \dot{f}(0)\sum_i \frac{b_i}{p_i} X_i \sin p_i t - \sum_i \frac{b_i}{p_i} X_i \int_0^t \ddot{f}(\tau)\sin p_i (t-\tau)\,\mathrm{d}\tau \end{aligned} \tag{4.42}$$

Integrating and simplifying the expression (4.42), the transverse deflection is finally found to be;

$$v(x,t) = \left[\frac{3}{2}\left(\frac{x}{l}\right)^2 - \frac{1}{2}\left(\frac{x}{l}\right)^3\right] f(t) - \sum_i b_i X_i f(t) + \sum_i b_i X_i p_i \int_0^t f(\tau)\sin p_i (t-\tau)\,\mathrm{d}\tau \tag{4.43}$$

4.2.2.2 Evaluation of Dynamic Slip

The relative slip at the interfaces of jointed beams subjected to time dependent loading is a complex phenomenon. The relative slip under dynamic loading is a time dependent phenomenon and is invariant at each and every moment of time. The correct evaluation of dynamic slip is vital for the estimation of damping in the layered and tack welded cantilever beams. In the present section, the relative dynamic slip at the interface of two layered and welded beams has been evaluated considering the external loading and in-plane bending stresses developed during this loading.

The relative dynamic slip at the interfaces under dynamic condition is evaluated by combining the expressions (4.9), (4.10) and (4.43). The relative slip at the interfaces is given by;

$$\Delta u_x = u_2 - u_1 = -\frac{\mu p l^2}{Eh}\left(\frac{2x}{l} - \frac{x^2}{l^2}\right) + h\frac{\mathrm{d}v}{\mathrm{d}x} \tag{4.44}$$

Utilizing the expression for mode shape as given by (4.43) in (4.44), the relative slip is modified as;

$$\Delta u_x = \left[-\frac{\mu p l^2}{Eh} + \frac{3h}{2l} f(t) \right] \left(\frac{2x}{l} - \frac{x^2}{l^2} \right) + h \sum_i b_i k_i \left[\sinh k_i l \cos k_i (l-x) - \sin k_i l \cosh k_i (l-x) \right] \times \left[f(t) - p_i \int_0^t f(\tau) \sin p_i (t-\tau) \, \mathrm{d}\tau \right] \tag{4.45}$$

4.2.2.3 Analysis of Energy Dissipation

The dissipation of energy is due the relative dynamic slip and the dynamic friction at the interfaces of the layered and tack welded beams. The energy dissipation per cycle has been evaluated considering the relation developed by Goodman and Klumpp [17] as presented in the preceding section.

Substituting the expression (4.45) in (4.12), the energy dissipation per cycle is given by;

$$E_{loss} = 4\mu p b \int_0^l \left\{ \begin{array}{l} \left[-\frac{\mu p l^2}{Eh} + \frac{3h}{2l} f(t) \right] \left(\frac{2x}{l} - \frac{x^2}{l^2} \right) \\ + h \sum_i b_i k_i \left[\sinh k_i l \cos k_i (l-x) - \sin k_i l \cosh k_i (l-x) \right] \\ \times \left[f(t) - p_i \int_0^t f(\tau) \sin p_i (t-\tau) \, \mathrm{d}\tau \right] \end{array} \right\} \mathrm{d}x \tag{4.46}$$

Rearranging expression (4.46) we get;

$$\begin{aligned} E_{loss} &= 4\mu p b \int_0^l \left\{ \left[-\frac{\mu p l^2}{Eh} + \frac{3h}{2l} f(t) \right] \left(\frac{2x}{l} - \frac{x^2}{l^2} \right) \right\} \mathrm{d}x \\ &+ 4\mu p b h \sum_i b_i k_i \int_0^l \left\{ \begin{array}{l} \left[\sinh k_i l \cos k_i (l-x) - \sin k_i l \cosh k_i (l-x) \right] \\ \times \left[f(t) - p_i \int_0^t f(\tau) \sin p_i (t-\tau) \, \mathrm{d}\tau \right] \end{array} \right\} \mathrm{d}x \end{aligned} \tag{4.47}$$

Modifying expression (4.47) we have;

$$\begin{aligned} E_{loss} &= 4\mu p b \int_0^l \left\{ \left[-\frac{\mu p l^2}{Eh} + \frac{3h}{2l} f(t) \right] \left(\frac{2x}{l} - \frac{x^2}{l^2} \right) \right\} \mathrm{d}x \\ &+ 4\mu p b h \sum_i \left\{ \begin{array}{l} b_i k_i \left[\int_0^l \left\{ \sinh k_i l \cos k_i (l-x) \, \mathrm{d}x \right\} - \int_0^l \left\{ \sin k_i l \cosh k_i (l-x) \, \mathrm{d}x \right\} \right] \\ \times \left[f(t) - p_i \int_0^t f(\tau) \sin p_i (t-\tau) \, \mathrm{d}\tau \right] \end{array} \right\} \end{aligned} \tag{4.48}$$

Integrating the expression (4.48) we get;

$$E_{loss} = 4\mu pb\left[-\frac{\mu pl^2}{Eh}+\frac{3h}{2l}f(t)\right]\left[\frac{2l}{3}\right] \\ +4\mu pbh\sum_i\left\{b_i k_i\left[\frac{\sinh k_i l\sin k_i l}{k_i}-\frac{\sin k_i l\sinh k_i l}{k_i}\right]\times\left[f(t)-p_i\int_0^t f(\tau)\sin p_i(t-\tau)\,\mathrm{d}\tau\right]\right\} \tag{4.49}$$

Simplification of expression (4.49) yields;

$$E_{loss} = 4\mu pb\left[-\frac{\mu pl^2}{Eh}+\frac{3h}{2l}f(t)\right]\left[\frac{2l}{3}\right] \tag{4.50}$$

Rearranging the expression (4.50) we get;

$$E_{loss} = 4\mu pbh\left[-\frac{2\mu pbh}{\frac{3Ebh^3}{l^3}}+f(t)\right] \tag{4.51}$$

The expression (4.51) is modified putting two dimensional parameters Q and R as given by expressions {4.7(a) and 4.7 (b)} and the same is given as;

$$E_{loss} = 4Q\left(f(t)-\frac{2Q}{3R}\right) \tag{4.52}$$

4.2.2.4 Evaluation of Loss Factor

The damping capacity of the layered and welded cantilever beams with single interface subjected to the various types of loading has been evaluated in the present section. The dissipative properties of this system is evaluated in terms of non-dimensional quantities such as the damping ratio "ψ" and loss factor "η_s", as defined in the expression (4.17). The maximum strain energy stored in the system in terms of dynamic deflection at the tip of the beam is given by;

$$E_{ne} = \frac{1}{4R}\left(\frac{Rf(t)}{2}+Q\right)^2 \tag{4.53}$$

Putting expressions (4.52) and (4.53) in expression (4.17a) and simplifying, the damping ratio in terms of dynamic tip displacement is given by;

$$\psi = \frac{64\left(\frac{Rf(t)}{Q} - \frac{2}{3}\right)}{\left(\frac{Rf(t)}{Q} + 2\right)^2} \tag{4.54}$$

Putting expression (4.54) in expression (4.17b) and simplifying, the loss factor in terms of dynamic tip displacement is given as;

$$\eta_s = \frac{32\left(\frac{Rf(t)}{Q} - \frac{2}{3}\right)}{\pi\left(\frac{Rf(t)}{Q} + 2\right)^2} \tag{4.55}$$

4.2.2.5 Types of Loading Considered In the Analysis

A little amount of work has been reported on the mechanism of damping in layered and welded structures subjected to forced vibration. In the present chapter, a detailed theoretical analysis has been presented for static loading, which is further extended to evaluate the mechanism of damping in layered and jointed structures vibrating under dynamic conditions. The result for loss factor clearly indicates that the value for expression (4.55) cannot be fully determined unless the forcing time dependent displacement function $f(t)$ is specified. Consequently, we limit our analysis to the following cases namely:

(a) $f(t) = F_0 H(t - t_0)$ (4.56a)

where $H(t)$ is the Heaviside function and F_0 is the amplitude

(b) $f(t) = F_0 \, e^{i\omega t}$ (4.56b)

where ω is the excitation frequency

The dynamic response, slip and the loss factor have been evaluated for the above two cases of $f(t)$ putting the expressions {4.56(a) and 4.56(b)} in (4.43), (4.45) and (4.55).

4.3 Summary

In this chapter, static and dynamic analysis has been presented for layered and welded beams with single interface. The governing equations of the transverse vibration and relative dynamic slip under static and dynamic loading have been derived considering the in-plane bending stress and neglecting the effects of shear deformation and rotary inertia. It is found that the total slip is a function of the distance from the fixed end for static loading and time at dynamic loading. The loss factor has been evaluated considering Heaviside and harmonic loadings. The interface pressure distribution has been determined and is found to be uniformly distributed. It is established that the micro-slip, kinematic coefficient of friction and the nature of pressure distribution at the interfaces, cantilever length and type of loading play major roles in quantifying the damping of such welded beam structures. Therefore, an extensive study of all the above vital parameters has been carried out in the present investigation.

5

DAMPING ESTIMATION OF WELDED SYMMETRICAL BEAMS WITH MULTIPLE INTERFACES CONSIDERING IN-PLANE BENDING STRESS

5.1 Introduction

In the past decades, a lot of work has been reported on the mechanism of slip damping in layered and jointed structures with single interface. A very few researchers [110, 113,144] have reported on the mechanism of slip damping in multilayered structures. However, their work is limited to the multilayered bolted and riveted beams subjected to static load. Moreover, in their analysis, they neglected the effect of in-plane bending stress on the damping mechanism of multilayered and jointed structures. All of their analysis was based on the natural free vibration of these structures. Study on damping mechanism of multilayered and welded beams subjected to forced vibration has not been reported till date. In the present chapter, a detailed static and dynamic analysis has been presented for damping mechanism in multilayered symmetrical beams.

5.2 Multiple Interfaces

In the present chapter, a detailed static and dynamic analysis has been carried out considering the in-plane bending stress at the various interfaces about the centroid of the jointed beam. A detailed description has been presented for the mechanism of slip damping in multilayered structures as the formulation is entirely different from that as discussed in the previous chapter. Further, this also gives an insight to the slip mechanism, magnitude of critical load and amplitude for both the odd and even number of layers. In order to study the mechanism of slip damping in multilayered built-up structures with multiple interfaces, the tack welded cantilever beam model as shown in Fig. 5.1(a) is considered with overall thickness $2h$, width b, length l with

'm' number of laminates of equal thickness (2*h*/m), so that the slip is occurring on (m-1) number of interfaces simultaneously. The interface pressure is also considered to be uniformly distributed as enumerated earlier. The continuity of stress and vertical displacement '*v*' is imposed at the interfaces. Each of the laminates of thickness 2*h*/m is considered separately with the loading as depicted in the Fig. 5.1(b).

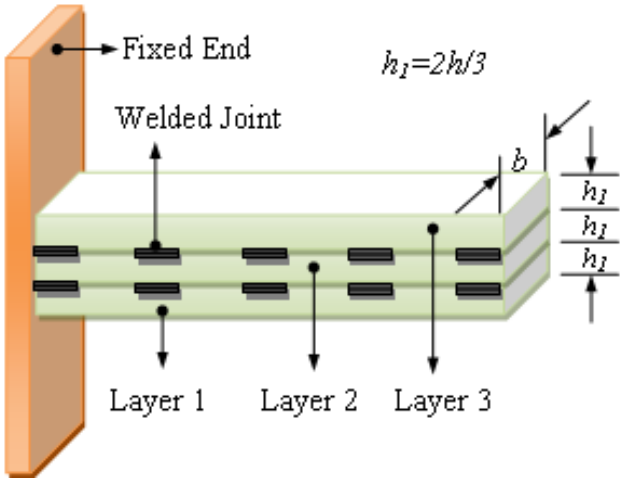

Fig. 5.1(a) Three layered tack welded cantilever beam model

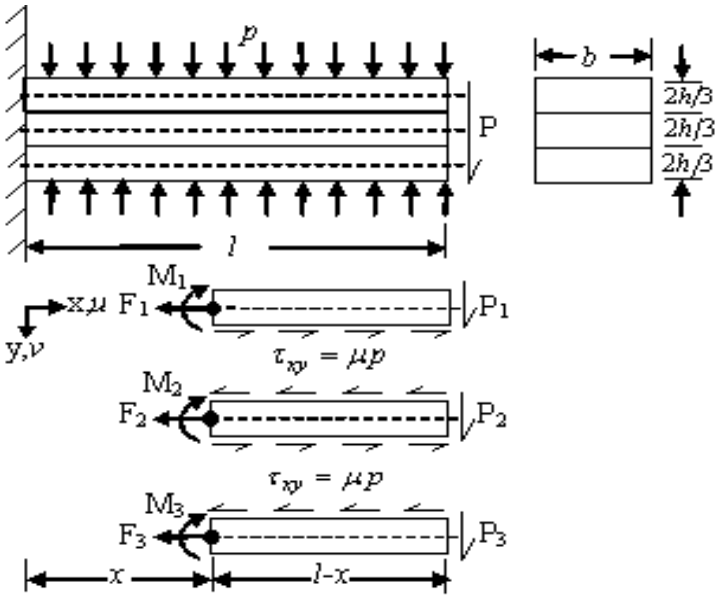

Fig. 5.1(b) Three layers of the jointed beam depicting load and co-ordinates

5.2.1 Static Analysis

In the present section, a detailed static analysis of the multilayered and welded symmetrical beams with multiple interfaces has been presented.

5.2.1.1 Interface Pressure Distribution

The relation for uniform pressure distribution as given by Johnson [130] and Giannakopoulos et al. [131] due to contact of two flat bodies has been considered as discussed in details in the previous chapter.

5.2.1.2 Analysis of Static Response

The static response under the action of transverse static load is evaluated by considering the equilibrium of the various forces acting on the multilayered beam as presented in the Fig. 5.1(b). The resultant bending moment about the centroid of each laminate is found to be;

$$M_{\mathrm{m}} = \frac{1}{\mathrm{m}}\left[P - \frac{2(\mathrm{m}-1)\mu pbh}{\mathrm{m}}\right](l-x) \tag{5.1}$$

Considering the relation between bending moment and curvature as derived by Warburton [177] and presented in expression (4.2) we get;

$$M = -EI\frac{d^2v}{dx^2}$$

Putting expression (4.2) in (5.1) the following expression is obtained;

$$\frac{\mathrm{d}^2 v}{\mathrm{d}x^2} = \frac{1}{\mathrm{m}EI}\left[P - \frac{2(\mathrm{m}-1)\mu pbh}{\mathrm{m}}\right](l-x) \tag{5.2}$$

where $I = b\left(\frac{2h}{\mathrm{m}}\right)^3 \Big/ 12$ is the moment of inertia of the cross-section of each beam.

Integrating expression (5.2) once we get;

$$\frac{\mathrm{d}v}{\mathrm{d}x} = \frac{3\mathrm{m}^2}{2Ebh^3}\left[P - \frac{2(\mathrm{m}-1)\mu pbh}{\mathrm{m}}\right]\left(lx - \frac{x^2}{2}\right) + C_1 \tag{5.3}$$

where C_1 is the integration constant and evaluated to be zero by putting the boundary condition, $\left(\mathrm{d}v/\mathrm{d}x\right)\Big|_{x=0} = 0$ in the expression (5.3).

Further, integration of expression (5.3) yields;

$$v = \frac{3\mathrm{m}^2}{2Ebh^3}\left[P - \frac{2(\mathrm{m}-1)\mu pbh}{\mathrm{m}}\right]\left(\frac{lx^2}{2} - \frac{x^3}{6}\right) + C_2 \tag{5.4}$$

Putting the value of C_2 in the expression (5.4) and simplifying, the static deflection mode shape is given by;

$$v = \frac{l^3}{Ebh^3}\left[P - \frac{2(\mathrm{m}-1)\mu pbh}{\mathrm{m}}\right]\left[\frac{3\mathrm{m}^2}{4}\left(\frac{x}{l}\right)^2 - \frac{\mathrm{m}^2}{4}\left(\frac{x}{l}\right)^3\right] \tag{5.5}$$

The two dimensional parameters "Q" and "R" as defined by expression (4.7) in the previous chapter is given by;

$$Q = \mu pbh$$

$$R = \frac{Ebh^3}{l^3}$$

Putting the expressions (4.7a) and (4.7b) in (5.5) and simplifying, the static deflection mode shape of the multilayered welded beams is found to be;

$$v = \frac{1}{R}\left[P - \frac{2(\mathrm{m}-1)Q}{\mathrm{m}}\right]\left[\frac{3\mathrm{m}^2}{4}\left(\frac{x}{l}\right)^2 - \frac{\mathrm{m}^2}{4}\left(\frac{x}{l}\right)^3\right] \tag{5.6}$$

5.2.1.3 Evaluation of Relative Slip

In the multiple interfaces the relative slip is dependent on the number of layers as the distance of the centroidal plane of each laminate from the centroid of the cross-section of the overall jointed beam is different. The relative displacement for even and odd number of laminates, at any axial position "*x*" has been evaluated considering the in-plane bending stresses and the curvature of the bent cantilever beam.

5.2.1.3.1 *Slip in Even Number of Laminates*

The relative slip for the even number of laminates is given by;

$$\Delta u = \frac{-1}{E}\int_0^l 2(\mathrm{m}-1)\sigma_x \,\mathrm{d}x + 2(\mathrm{m}-1)\frac{h}{\mathrm{m}}\left(\frac{\mathrm{d}v}{\mathrm{d}x}\right) \tag{5.7}$$

where σ_x is the in plane bending stress.

From the force equilibrium, the in-plane bending stresses in the respective laminates are computed as follows:

$$\sigma_x = \frac{\mathrm{m}\,\mu p(l-x)}{2h} \tag{5.8}$$

Combining expressions (5.6), (5.7) and (5.8) and simplifying, the relative slip displacement at the interfaces for even number of laminates is given by;

$$\Delta u = \frac{3\,\mathrm{m}(\mathrm{m}-1)h}{2Rl}\left[P - \frac{(7\,\mathrm{m}-6)Q}{3\,\mathrm{m}}\right]\left[\left(\frac{2x}{l}\right) - \left(\frac{x}{l}\right)^2\right] \tag{5.9}$$

Slip will occur only if $P > P_{ce} = \dfrac{(7\,\mathrm{m}-6)Q}{3\,\mathrm{m}}$ (5.10)

where P_{ce} is the critical static load applied at tip of the welded cantilever beams with even number of laminates.

5.2.1.3.2 *Slip in Odd Number of Laminates*

The relative slip for the odd number of laminates is given by;

$$\Delta u = \frac{-1}{E}\int_0^l 2(\mathrm{m}-2)\sigma_x \,\mathrm{d}x + 2(\mathrm{m}-1)\frac{h}{\mathrm{m}}\left(\frac{\mathrm{d}v}{\mathrm{d}x}\right) \tag{5.11}$$

Combining expressions (5.6), (5.8) and (5.11) and simplifying, the relative slip displacement at the interfaces for odd number of laminates is given by;

$$\Delta u = \frac{3\,\mathrm{m}(\mathrm{m}-1)}{2Rl}\left[P - \frac{(7\,\mathrm{m}^2-14\,\mathrm{m}+6)Q}{3\,\mathrm{m}(\mathrm{m}-1)}\right]\left[\left(\frac{2x}{l}\right) - \left(\frac{x}{l}\right)^2\right] \tag{5.12}$$

Slip will occur only if $P > P_{co} = \dfrac{\left(7\,\mathrm{m}^2 - 14\,\mathrm{m} + 6\right)Q}{3\,\mathrm{m}\left(\mathrm{m}-1\right)}$

where P_{co} is the critical static load applied at tip of the welded cantilever beams with odd number of layers.

5.2.1.4 Analysis of Energy Dissipated

Energy dissipation in the multilayered jointed beams is evaluated by considering the expression for energy loss developed by Goodman and Klumpp [17] as discussed in details (expression 4.13) in the previous chapter. The relative slip in multilayered jointed beams depends on the number of laminates whether even or odd. Therefore, in the present analysis the expression for energy loss has been evaluated considering the number of layers and relative slip.

5.2.1.4.1 *Energy loss in Even Number of Laminates*

The energy loss in jointed beam with even number of laminates is evaluated by considering the friction force and relative slip developed at the interfaces of even number of laminates.

Substituting the expression (5.9) in (4.13) considering the beam to be loaded cyclically between the loads $\pm P_m$ and integrating, the energy dissipation per cycle in terms of static load for even number of laminates is given by;

$$E_{loss} = \frac{4\,\mathrm{m}\left(\mathrm{m}-1\right)Q}{R}\left[P_{\mathrm{m}} - \frac{\left(7\,\mathrm{m}-6\right)Q}{3\,\mathrm{m}}\right] \tag{5.13}$$

where P_m is the maximum static load applied at the tip of the welded cantilever beams.

The maximum tip displacement v_m, corresponding to $P = P_m$ is obtained from (5.6) by putting $x = l$ as follows;

$$v_{\mathrm{m}} = \frac{\mathrm{m}^2 P_{\mathrm{m}}}{2R} - \frac{\mathrm{m}\left(\mathrm{m}-1\right)Q}{R} \tag{5.14a}$$

On rearranging expression (5.14a), P_m in terms of v_m is given by;

$$P_{\mathrm{m}} = \frac{2Rv_{\mathrm{m}}}{\mathrm{m}^2} + \frac{2(\mathrm{m}-1)Q}{\mathrm{m}} \tag{5.14b}$$

Putting the expression (5.14b) in (5.13), the energy dissipation in terms of tip displacement for even number of laminates is given by;

$$E_{loss} = \frac{8(\mathrm{m}-1)Q}{\mathrm{m}}\left[v_{\mathrm{m}} - \frac{\mathrm{m}^2 Q}{6R} \right] \tag{5.15}$$

From the expression (5.15), it is evident that slip will occur only if $v \geq v_{ce} = \frac{\mathrm{m}^2 Q}{6R}$, where v_{ce} is the critical tip displacement in even number of layers.

5.2.1.4.2 *Energy loss in Odd Number of Laminates*

The energy loss in jointed beam with odd number of laminates is evaluated by considering the friction force and relative slip developed at the interfaces of odd number of laminates.

Substituting the expression (5.11) in (5.12) and integrating, the energy dissipation per cycle in terms of static load for odd number of laminates is given by;

$$E_{loss} = \frac{4\mathrm{m}(\mathrm{m}-1)Q}{R}\left[P - \frac{(7\mathrm{m}^2 - 14\mathrm{m} + 6)Q}{3\mathrm{m}(\mathrm{m}-1)} \right] \tag{5.16}$$

Putting the expression (5.14b) in (5.16), the energy dissipation in terms of tip displacement for odd number of laminates is given by;

$$E_{loss} = \frac{8(\mathrm{m}-1)Q}{\mathrm{m}}\left[v_{\mathrm{m}} - \frac{\mathrm{m}^2(\mathrm{m}-2)Q}{6(\mathrm{m}-1)R} \right] \tag{5.17}$$

From the expression (5.17), it is evident that slip will occur only if $v \geq v_{co} = \frac{\mathrm{m}^2(\mathrm{m}-2)Q}{6(\mathrm{m}-1)R}$, where v_{co} is the critical tip displacement in the odd number of layers.

5.2.1.5 Evaluation of Damping Ratio

The damping capacity of the multilayered structures subjected to static loading is evaluated considering the energy losses in even and odd number of laminates. The maximum strain energy stored in the system in terms of static deflection at the tip of the beam is given by;

$$E_{ne} = \frac{1}{4R}\left(\frac{Rv_{\mathrm{m}}}{2} + Q\right)^2 \tag{5.18}$$

5.2.1.5.1 *Loss Factor in Even Number of Laminates*

The loss factor of layered and welded structures with even number of laminates subjected to static loading has been found out by considering the energy loss in even number of laminates.

Putting expressions (5.15) and (5.18) in expression (4.17) and simplifying, the loss factor in terms of dynamic tip displacement for even number of laminates is given by;

$$\eta_s = \frac{64(\mathrm{m}-1)\left(\frac{Rv_{\mathrm{m}}}{Q} - \frac{\mathrm{m}^2}{6}\right)}{\mathrm{m}\pi\left(\frac{Rv_{\mathrm{m}}}{Q} + 2\right)^2} \tag{5.19}$$

5.2.1.5.2 *Loss Factor in Odd Number of Laminates*

The loss factor of layered and welded structures with odd number of laminates subjected to static loading has been found out by considering the energy loss in odd number of laminates.

Putting expressions (5.17) and (5.18) in expression (4.17) and simplifying, the loss factor in terms of dynamic tip displacement for odd number of laminates is given by;

$$\eta_s = \frac{64(\mathrm{m}-1)\left(\frac{Rv_{\mathrm{m}}}{Q} - \frac{\mathrm{m}^2(\mathrm{m}-2)}{6(\mathrm{m}-1)}\right)}{\mathrm{m}\pi\left(\frac{Rv_{\mathrm{m}}}{Q} + 2\right)^2} \tag{5.20}$$

5.2.2 Dynamic Analysis

In the present section, a detailed analysis has been presented for the dynamic analysis of the multilayered welded beams with multiple interfaces. In the present analysis, two types of loading has been considered; Heaviside and harmonic loading.

5.2.2.1 Types of Excitation Forces Considered In the Analysis

In the present work, the following time dependent displacement function $f(t)$ is considered;

(a) $f(t) = F_0 H(t - t_0)$ (5.21a)

where $H(t)$ is the Heaviside function and F_0 is the amplitude

(b) $f(t) = F_0 \, e^{i\omega t}$ (5.21b)

where ω is the excitation frequency

5.2.2.2 Analysis of Dynamic Response

The dynamic response under the action of transverse dynamic load is evaluated by considering the equilibrium of the various forces acting on the jointed beam as presented in the Fig. 5.1(b).

The forced vibration of the beam produced by a time-dependent displacement at the unsupported end has been considered such that;

$$v\big|_{x=l} = f(t) \tag{5.22}$$

Following Timoshenko [28], the dynamic displacement is composed of two parts;

$$v = v_{\mathrm{I}} + v_{\mathrm{II}} \tag{5.23}$$

where

$$v_{\mathrm{I}} = \left[\frac{3\,\mathrm{m}^2}{4} \left(\frac{x}{l} \right)^2 - \frac{\mathrm{m}^2}{4} \left(\frac{x}{l} \right)^3 \right] f(t) \tag{5.24}$$

The term in the bracket represents the static mode function and satisfies the end conditions;

$$v_{\mathrm{I}}\big|_{x=0}=0;\left.\frac{\mathrm{d}\,v_I}{\mathrm{d}\,x}\right|_{x=0}=0;\left.\frac{\mathrm{d}^2\,v_{\mathrm{I}}}{\mathrm{d}\,x^2}\right|_{x=l}=0;v_{\mathrm{I}}\big|_{x=l}=0; \tag{5.25}$$

but does not satisfy the dynamic equilibrium equation;

$$EI\frac{\partial^4 v}{\partial x^4}+\rho A\frac{\partial^2 v}{\partial t^2}=0 \tag{5.26}$$

where EI and ρ are the flexural rigidity and density of the beam, respectively.

The displacement v_{I} produces the dynamic loads as given by;

$$-A\rho\left[\frac{3\,\mathrm{m}^2}{4}\left(\frac{x}{l}\right)^2-\frac{\mathrm{m}^2}{4}\left(\frac{x}{l}\right)^3\right]\ddot{f}(t) \tag{5.27}$$

where A is the cross-sectional area of the beam.

Moreover, the displacement (v_{II}) representing vibrations produced by the force function (5.27) is expressed as;

$$v_{\mathrm{II}}=\sum_i \varphi_i(t)\,X_i(x) \tag{5.28}$$

where $X_i(x)$ and $\varphi_i(t)$ are the modal and time-dependent functions, respectively.

v_{II} must satisfy the end conditions;

$$v_{\mathrm{II}}\big|_{x=0}=0;\left.\frac{\mathrm{d}\,v_{\mathrm{II}}}{\mathrm{d}\,x}\right|_{x=0}=0;\left.\frac{\mathrm{d}^2\,v_{\mathrm{II}}}{\mathrm{d}\,x^2}\right|_{x=l}=0;v_{\mathrm{II}}\big|_{x=l}=0; \tag{5.29}$$

$X_i(x)$ are the solutions of the expression (5.26) and satisfies the end condition as given in (5.29). Thus we get;

$$X_i=\sinh k_i l\sin k_i(l-x)-\sin k_i l\sinh k_i(l-x) \tag{5.30}$$

where k_i are the roots of the following expression;

$$\tanh k_i l=\tan k_i l \tag{5.31}$$

The total displacement is then obtained by putting expressions (5.24) and (5.28) in (4.22) and the same is given by;

$$v = \left[\frac{3\mathrm{m}^2}{4}\left(\frac{x}{l}\right)^2 - \frac{\mathrm{m}^2}{4}\left(\frac{x}{l}\right)^3 \right] f(t) + \sum_i \varphi_i(t) X_i(x) \tag{5.32}$$

By applying the principle of virtual work, Timoshenko [28] has shown that the time-dependent functions $\varphi_i(t)$ must satisfy the differential equation given by;

$$\ddot{\varphi}_i + \frac{EIk_i^4}{A\rho}\varphi_i = -b_i \ddot{f}(t) \tag{5.33}$$

where the dot superscripts denote differentiation with respect to time. The coefficients b_i are obtained by expanding the force function as given in expression (5.27) in a series of the normal functions, X_i. Thus,

$$-A\rho\ddot{f}(t)\left[\frac{3\mathrm{m}^2}{4}\left(\frac{x}{l}\right)^2 - \frac{\mathrm{m}^2}{4}\left(\frac{x}{l}\right)^3 \right] = -A\rho\ddot{f}(t)\sum_i b_i X_i \tag{5.34}$$

The coefficients b_i are obtained from the following expression;

$$b_i = \frac{\int_0^l \{X_i\}\left[\frac{3\mathrm{m}^2}{4}\left(\frac{x}{l}\right)^2 - \frac{\mathrm{m}^2}{4}\left(\frac{x}{l}\right)^3 \right] \mathrm{d}x}{\int_0^l X_i^2 \,\mathrm{d}x} \tag{5.35}$$

Integrating the expression (5.35) b_i is finally found to be;

$$b_i = \frac{m^2}{k_i l(\sinh k_i l - \sin k_i l)} \tag{5.36}$$

The general solution of expression (5.33) is given by;

$$\varphi_i(t) = A_i \cos p_i t + B_i \sin p_i t - \frac{b_i}{p_i}\int_0^t \ddot{f}(t)\sin p_i(t-\tau)\,\mathrm{d}\tau \tag{5.37}$$

where $p_i = \left(\frac{EI}{A\rho}\right)^{1/2} k_i^2$

Constants A_i and B_i are evaluated from the initial conditions;

$$v(0) = U(x,0) \tag{5.38a}$$

$$\dot{v}(0) = V(x,0) \tag{5.38b}$$

Putting expression (5.32) in (5.38), U and V are evaluated as;

$$U = \left[\frac{3\mathrm{m}^2}{4}\left(\frac{x}{l}\right)^2 - \frac{\mathrm{m}^2}{4}\left(\frac{x}{l}\right)^3\right] f(0) + \sum_i X_i \{A_i\} \tag{5.39a}$$

$$V = \left[\frac{3\mathrm{m}^2}{4}\left(\frac{x}{l}\right)^2 - \frac{\mathrm{m}^2}{4}\left(\frac{x}{l}\right)^3\right] \dot{f}(0) + \sum_i X_i \{B_i p_i\} \tag{5.39b}$$

Moreover, from the expression (5.34) we get;

$$\left[\frac{3\mathrm{m}^2}{4}\left(\frac{x}{l}\right)^2 - \frac{\mathrm{m}^2}{4}\left(\frac{x}{l}\right)^3\right] = \sum_i b_i X_i \tag{5.40}$$

Putting expression (5.40) in (5.39) and simplifying we get;

$$U(x,0) = \sum_i X_i \{A_i + b_i f(0)\} \tag{5.41a}$$

$$V(x,0) = \sum_i X_i \{B_i p_i + b_i \dot{f}(0)\} \tag{5.41b}$$

Putting the initial conditions U=V=0, the constants A_i and B_i are found as;

$$A_i = -b_i f(0) \tag{5.42a}$$

$$B_i = -\frac{b_i}{p_i} \dot{f}(0) \tag{5.42b}$$

Substitution of expressions (5.37) and (5.38) in (5.32) yields;

$$\begin{aligned} v(x,t) = &\left[\frac{3\mathrm{m}^2}{4}\left(\frac{x}{l}\right)^2 - \frac{\mathrm{m}^2}{4}\left(\frac{x}{l}\right)^3\right] f(t) - f(0)\sum_i b_i X_i \cos p_i t \\ &- \dot{f}(0)\sum_i \frac{b_i}{p_i} X_i \sin p_i t - \sum_i \frac{b_i}{p_i} X_i \int_0^t \ddot{f}(\tau) \sin p_i (t-\tau)\, \mathrm{d}\tau \end{aligned} \tag{5.43}$$

Integrating and simplifying the expression (5.43), the transverse deflection is finally found to be;

$$v(x,t)=\left[\frac{3m^2}{4}\left(\frac{x}{l}\right)^2-\frac{m^2}{4}\left(\frac{x}{l}\right)^3\right]f(t)-\sum_i b_i X_i f(t)$$
$$+\sum_i b_i X_i p_i \int_0^t f(\tau)\sin p_i(t-\tau)\,\mathrm{d}\tau \tag{5.44}$$

5.2.2.3 Evaluation of Relative Dynamic Slip

The relative dynamic slip at the interfaces of the multilayered welded beams subjected to dynamic loading is evaluated for even and odd number of layers.

5.2.2.3.1 *Dynamic Slip in Even Number of Laminates*

The relative slip displacement at the interfaces for even number of laminates is found out by combining expressions (5.7), (5.8) and (5.44) and simplifying the same we get;

$$\Delta u_x=\frac{\mathrm{m}(\mathrm{m}-1)h}{Rl}\left[\frac{-Q}{2}+\frac{3Rf(t)}{\mathrm{m}^2}\right]\left(\frac{2x}{l}-\frac{x^2}{l^2}\right)$$
$$+h\sum_i b_i k_i\left[\sinh k_i l\cos k_i(l-x)-\sin k_i l\cosh k_i(l-x)\right]\times\left[f(t)-p_i\int_0^t f(\tau)\sin p_i(t-\tau)\,d\tau\right] \tag{5.45}$$

5.2.2.3.2 *Dynamic Slip in Odd Number of Laminates*

The relative slip displacement at the interfaces for odd number of laminates is found out by combining expressions (5.8), (5.10) and (5.44) and simplifying we get;

$$\Delta u_x=\frac{\mathrm{m}h}{2Rl}\left[-(\mathrm{m}-2)Q+\frac{6(\mathrm{m}-1)Rf(t)}{\mathrm{m}^2}\right]\left(\frac{2x}{l}-\frac{x^2}{l^2}\right)$$
$$+h\sum_i b_i k_i\left[\sinh k_i l\cos k_i(l-x)-\sin k_i l\cosh k_i(l-x)\right]\times\left[f(t)-p_i\int_0^t f(\tau)\sin p_i(t-\tau)\,d\tau\right] \tag{5.46}$$

5.2.2.4 Analysis of Energy Dissipated

The energy dissipation in multilayered welded beams subjected to forced vibration is also dependent on the even and odd number of layers of the beam.

5.2.2.4.1 *Energy loss in Even Number of Laminates*

The energy loss in jointed beam with even number of laminates is evaluated by considering relative dynamic slip developed at the interfaces of even number of laminates under dynamic loading.

Substituting the expression (5.45) in (4.13) considering the beam to be excited with time dependent displacement '*f*(t)' at the free end of the welded beams and integrating, the energy dissipation per cycle in terms of initial excitation of amplitude for even number of laminates is given by;

$$E_{loss}=4\mu pb\int_0^l\left\{\begin{array}{l}\dfrac{\mathrm{m}(\mathrm{m}-1)h}{Rl}\left[\dfrac{-Q}{2}+\dfrac{3Rf(t)}{\mathrm{m}^2}\right]\left(\dfrac{2x}{l}-\dfrac{x^2}{l^2}\right)\\+h\sum_i b_ik_i\left[\sinh k_il\cos k_i(l-x)-\sin k_il\cosh k_i(l-x)\right]\\\times\left[f(t)-p_i\int_0^t f(\tau)\sin p_i(t-\tau)\,\mathrm{d}\tau\right]\end{array}\right\}\mathrm{d}x \qquad (5.47)$$

Rearranging expression (5.47) we get;

$$\begin{aligned}E_{loss}&=4\mu pb\int_0^l\left\{\frac{\mathrm{m}(\mathrm{m}-1)h}{Rl}\left[\frac{-Q}{2}+\frac{3Rf(t)}{\mathrm{m}^2}\right]\left(\frac{2x}{l}-\frac{x^2}{l^2}\right)\right\}\mathrm{d}x\\&+4\mu pbh\sum_i b_ik_i\int_0^l\left\{\begin{array}{l}\left[\sinh k_il\cos k_i(l-x)-\sin k_il\cosh k_i(l-x)\right]\\\times\left[f(t)-p_i\int_0^t f(\tau)\sin p_i(t-\tau)\,\mathrm{d}\tau\right]\end{array}\right\}\mathrm{d}x\end{aligned} \qquad (5.48)$$

Modifying expression (5.48) we have;

$$\begin{aligned}E_{loss}&=4\mu pb\int_0^l\left\{\frac{\mathrm{m}(\mathrm{m}-1)h}{Rl}\left[\frac{-Q}{2}+\frac{3Rf(t)}{\mathrm{m}^2}\right]\left(\frac{2x}{l}-\frac{x^2}{l^2}\right)\right\}\mathrm{d}x\\&+4\mu pbh\sum_i\left\{\begin{array}{l}b_ik_i\left[\int_0^l\left\{\sinh k_il\cos k_i(l-x)\,\mathrm{d}x\right\}-\int_0^l\left\{\sin k_il\cosh k_i(l-x)\,\mathrm{d}x\right\}\right]\\\times\left[f(t)-p_i\int_0^t f(\tau)\sin p_i(t-\tau)\,\mathrm{d}\tau\right]\end{array}\right\}\end{aligned} \qquad (5.49)$$

Integrating the expression (5.49) we get;

$$\begin{aligned}E_{loss}&=4\mu pb\left[\frac{\mathrm{m}(\mathrm{m}-1)h}{Rl}\left[\frac{-Q}{2}+\frac{3Rf(t)}{\mathrm{m}^2}\right]\left(\frac{2x}{l}-\frac{x^2}{l^2}\right)\right]\left[\frac{2l}{3}\right]\\&+4\mu pbh\sum_i\left\{b_ik_i\left[\frac{\sinh k_il\sin k_il}{k_i}-\frac{\sin k_il\sinh k_il}{k_i}\right]\times\left[f(t)-p_i\int_0^t f(\tau)\sin p_i(t-\tau)\,\mathrm{d}\tau\right]\right\}\end{aligned} \qquad (5.50)$$

Simplification of expression (5.50) yields;

$$E_{loss} = 4\mu pb\left\{\frac{\mathrm{m}(\mathrm{m}-1)h}{Rl}\left[\frac{-Q}{2}+\frac{3Rf(t)}{\mathrm{m}^2}\right]\right\}\left[\frac{2l}{3}\right] \tag{5.51}$$

Rearranging the expression (5.51) we get;

$$E_{loss} = \frac{8(\mathrm{m}-1)Q}{\mathrm{m}}\left[f(t)-\frac{\mathrm{m}^2 Q}{6R}\right] \tag{5.52}$$

5.2.2.4.2 *Energy loss in Odd Number of Laminates*

The energy loss in jointed beam with odd number of laminates is evaluated by considering the friction force and relative dynamic slip developed at the interfaces of odd number of laminates under dynamic loading.

Substituting the expression (5.46) in (4.12) and integrating, the energy dissipation per cycle in terms of initial excitation of amplitude for odd number of laminates is given by;

$$E_{loss} = 4\mu pb\int_0^l \left\{\begin{array}{l} \dfrac{\mathrm{m}\,h}{2Rl}\left[-(\mathrm{m}-2)Q+\dfrac{6(\mathrm{m}-1)Rf(t)}{\mathrm{m}^2}\right]\left(\dfrac{2x}{l}-\dfrac{x^2}{l^2}\right) \\ +h\sum_i b_i k_i\left[\sinh k_i l\cos k_i(l-x)-\sin k_i l\cosh k_i(l-x)\right] \\ \times\left[f(t)-p_i\int_0^t f(\tau)\sin p_i(t-\tau)\,\mathrm{d}\tau\right] \end{array}\right\}\mathrm{d}x \tag{5.53}$$

Rearranging expression (5.53) we get;

$$\begin{aligned} E_{loss} &= 4\mu pb\int_0^l \left\{\frac{\mathrm{m}\,h}{2Rl}\left[-(\mathrm{m}-2)Q+\frac{6(\mathrm{m}-1)Rf(t)}{\mathrm{m}^2}\right]\left(\frac{2x}{l}-\frac{x^2}{l^2}\right)\right\}\mathrm{d}x \\ &+4\mu pbh\sum_i b_i k_i\int_0^l \left\{\begin{array}{l} \left[\sinh k_i l\cos k_i(l-x)-\sin k_i l\cosh k_i(l-x)\right] \\ \times\left[f(t)-p_i\int_0^t f(\tau)\sin p_i(t-\tau)\,\mathrm{d}\tau\right] \end{array}\right\}\mathrm{d}x \end{aligned} \tag{5.54}$$

Modifying expression (5.54) we have;

$$E_{loss} = 4\mu pb\int_0^l \left\{ \frac{\mathrm{m}\,h}{2Rl}\left[-(\mathrm{m}-2)Q + \frac{6(\mathrm{m}-1)Rf(t)}{\mathrm{m}^2}\right]\left(\frac{2x}{l} - \frac{x^2}{l^2}\right)\right\}\mathrm{d}\,x$$
$$+4\mu pbh\sum_i \left\{ \begin{array}{l} b_i k_i \left[\int_0^l \left\{ \sinh k_i l \cos k_i (l-x)\,\mathrm{d}\,x \right\} - \int_0^l \left\{ \sin k_i l \cosh k_i (l-x)\,\mathrm{d}\,x \right\} \right] \\ \times \left[f(t) - p_i \int_0^t f(\tau) \sin p_i (t-\tau)\,\mathrm{d}\,\tau \right] \end{array} \right\} \qquad (5.55)$$

Integrating the expression (5.55) we get;

$$E_{loss} = 4\mu pb\left[\frac{\mathrm{m}\,h}{2Rl}\left[-(\mathrm{m}-2)Q + \frac{6(\mathrm{m}-1)Rf(t)}{\mathrm{m}^2}\right]\left(\frac{2x}{l} - \frac{x^2}{l^2}\right)\right]\left[\frac{2l}{3}\right]$$
$$+4\mu pbh\sum_i \left\{ b_i k_i \left[\frac{\sinh k_i l \sin k_i l}{k_i} - \frac{\sin k_i l \sinh k_i l}{k_i} \right] \times \left[f(t) - p_i \int_0^t f(\tau) \sin p_i (t-\tau)\,\mathrm{d}\,\tau \right] \right\} \qquad (5.56)$$

Simplifying expression (5.56) we get;

$$E_{loss} = 4\mu pb\left\{ \frac{\mathrm{m}\,h}{2Rl}\left[-(\mathrm{m}-2)Q + \frac{6(\mathrm{m}-1)Rf(t)}{\mathrm{m}^2}\right]\right\}\left[\frac{2l}{3}\right] \qquad (5.57)$$

Rearranging the expression (5.57) we get;

$$E_{loss} = \frac{8(\mathrm{m}-1)Q}{\mathrm{m}}\left[f(t) - \frac{\mathrm{m}^2(\mathrm{m}-2)Q}{6(\mathrm{m}-1)R}\right] \qquad (5.58)$$

5.2.2.5 Evaluation of Loss Factor

The damping capacity of the multilayered structures subjected to forced vibration is evaluated considering the energy losses under forced vibration conditions in even and odd number of laminates. The maximum strain energy stored in the system in terms of time dependent displacement at the tip of the beam is given by;

$$E_{ne} = \frac{1}{4R}\left(\frac{Rf(t)}{2} + Q \right)^2 \qquad (5.59)$$

5.2.2.5.1 *Loss Factor in Even Number of Laminates*

The loss factor in terms of dynamic tip displacement for even number of laminates is evaluated by putting expressions (5.52) and (5.59) in expression (4.17). The loss factor in terms of dynamic tip displacement for even number of laminates is given by;

$$\eta_s = \frac{64(\mathrm{m}-1)\left(\frac{Rf(t)}{Q} - \frac{\mathrm{m}^2}{6}\right)}{\mathrm{m}\pi\left(\frac{Rf(t)}{Q}+2\right)^2} \tag{5.60}$$

5.2.2.5.2 *Loss Factor in Odd Number of Laminates*

The loss factor in terms of dynamic tip displacement for odd number of laminates is evaluated by putting expressions (5.58) and (5.59) in expression (4.17) and the same is given by;

$$\eta_s = \frac{64(\mathrm{m}-1)\left(\frac{Rf(t)}{Q} - \frac{\mathrm{m}^2(\mathrm{m}-2)}{6(\mathrm{m}-1)}\right)}{\mathrm{m}\pi\left(\frac{Rf(t)}{Q}+2\right)^2} \tag{5.61}$$

5.3 Summary

Mechanism of slip damping in multilayered beams is a very complex and nonlinear phenomenon. Despite many arduous researches still many aspects related to phenomenon of damping in these structures remains poorly examined and require further investigations. In the present study, a detailed analysis has been carried out to explore the mechanism of damping in multilayered welded structures and means to improve it. In actual working conditions the structures are subjected to the various complex and unpredictable nature of forces that cannot be averted. Hence, the present analysis has been carried out considering both free and forced vibration conditions in order to get an insight into the behavior of multilayered welded structures in such ambiguous environments. It is observed that the relative slip and energy dissipation depend on both the even and odd number of laminates. It is further found that the damping is more pronounced in even number of laminates as compared to the odd number of laminates for the same overall jointed beam configuration. Loss factor

have been evaluated theoretically for various configuration and number of layers. The loss factor for two layered and welded beam is estimated to be same as found in the previous chapter by putting the value of number of layers (m) equal to two in the expression (5.60) for loss factor of multilayered welded beams. However, a detailed analysis has been elaborated in the present chapter as the slip mechanism and its formulation are entirely different for that of the symmetrical welded beams with single interface. Validation of the developed model has been ascertained by comparing the theoretical results for loss factor with the experimental ones.

6

DAMPING ESTIMATION OF WELDED UNSYMMETRICAL BEAMS CONSIDERING IN-PLANE BENDING STRESS

6.1 Introduction

In many systems, the assembled structures are fabricated using the layered constructions. As discussed in the preceding chapters, layered construction is another means of improving the damping capacity of the structural systems. Depending upon the use, layered structures can be fabricated using symmetrical and unsymmetrical beams. Substantial work has been reported on the damping mechanism of two layered jointed beams with equal thickness. The mechanism of damping in layered and welded structures with unequal beam thickness is yet to be explored. In the present chapter, a detailed analysis has been presented for the estimation of damping in layered and welded beams with unequal thickness. The factors governing the damping capacity of welded unsymmetrical beams are identified for both free and forced vibration conditions. Further, the findings are compared with that of the equivalent welded symmetrical beams.

6.2 Static Analysis

The two layered and tack welded cantilever beam model with overall thickness $2h$, width b, and length l as shown in Fig. 6.1(a) is considered to find out the damping ratio. Each of the two halves of thickness h_1 and h_2 is considered separately as depicted in the Fig. 6.1(b). The cross-sectional dimension of the beam considered is small compared to the length and therefore the effect due to vertical shear and rotary inertia has been neglected in the present analysis.

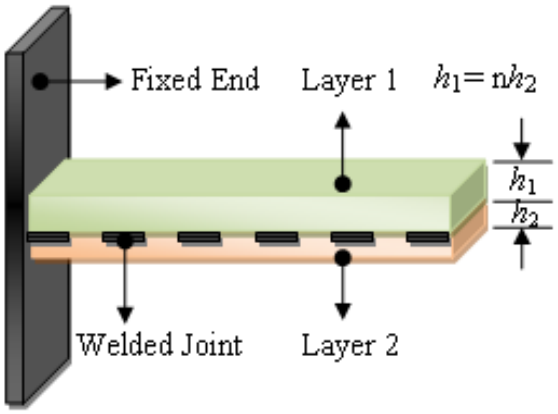

Fig. 6.1(a) Two layered tack welded cantilever beam model

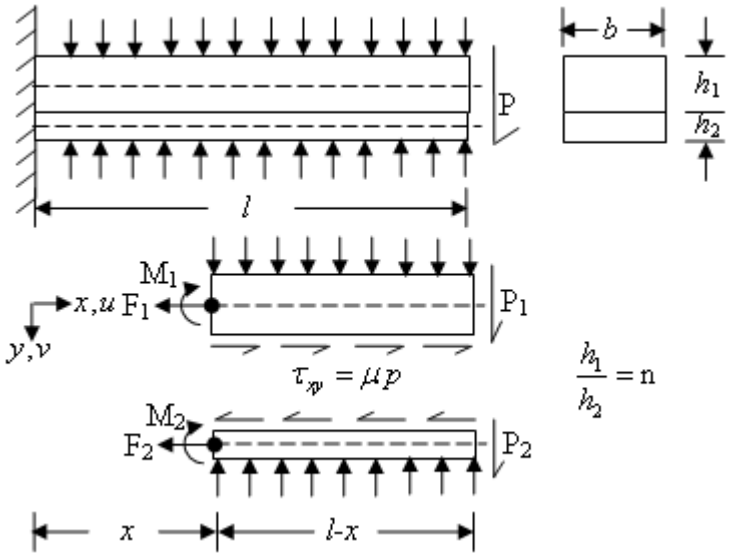

Fig. 6.1(b) Two halves of the beam depicting load and co-ordinates

6.2.1 Analysis of Static Response

The layered and jointed welded beam of unequal thickness as shown in Fig. 6.1 is initially subjected to a static load "*P*" at the tip. The ratio of the two layers as shown in Fig. 6.1(a) is given by;

$$\frac{h_1}{h_2} = \text{n} \tag{6.1}$$

where 'n' is the thickness ratio.

Furthermore,

$$h_1 + h_2 = 2h \tag{6.2}$$

Solving expressions (6.1) and (6.2), thickness of the upper and lower layers is given by;

$$h_1 = 2h\,\mathrm{n}/_{\mathrm{n}+1} \tag{6.3a}$$

$$h_2 = 2h/_{\mathrm{n}+1} \tag{6.3b}$$

The resultant moment at the centroid of each laminate as shown in Fig. 6.1(b) is given by;

$$M_1 = P_1(l-x) - \mu pb\frac{\mathrm{n}\,h}{\mathrm{n}+1}(l-x) \tag{6.4a}$$

$$M_2 = P_2(l-x) - \mu pb\frac{h}{\mathrm{n}+1}(l-x) \tag{6.4b}$$

where the subscripts 1 and 2 refer to the upper and lower laminates, respectively. Moreover, P_1 and P_2 are the static forces acting on the laminates 1 and 2, respectively as shown in Fig. 6.1(b).

Further,

$$P_1 + P_2 = P \tag{6.5}$$

Invoking the relation between bending moment and curvature as derived by Warburton [177], we get;

$$M = -EI\frac{\mathrm{d}^2 v}{\mathrm{d}x^2} \tag{6.6}$$

where E is the modulus of elasticity

Putting expression (6.4) in (6.6), the following expression is obtained;

$$\frac{\mathrm{d}^2 v_1}{\mathrm{d}x^2} = \frac{1}{EI_1}\left(P_1 - \frac{\mu pb\,\mathrm{n}\,h}{\mathrm{n}+1}\right)(l-x) \tag{6.7a}$$

$$\frac{\mathrm{d}^2 v_2}{\mathrm{d}x^2} = \frac{1}{EI_2}\left(P_2 - \frac{\mu pbh}{\mathrm{n}+1}\right)(l-x) \tag{6.7b}$$

where $I_1\left(bh_1^3/12\right), I_2\left(bh_2^3/12\right), v_1$ and v_2 are the moment of inertia and static response of the laminates 1 and 2, respectively.

Integrating expression (6.7) once we get;

$$\frac{\mathrm{d}v_1}{\mathrm{d}x} = \frac{1}{EI_1}\left(P_1 - \frac{\mu pb\,\mathrm{n}\,h}{\mathrm{n}+1}\right)\left(lx - \frac{x^2}{2}\right) + C_{1a} \tag{6.8a}$$

$$\frac{\mathrm{d}v_2}{\mathrm{d}x} = \frac{1}{EI_2}\left(P_2 - \frac{\mu pbh}{\mathrm{n}+1}\right)\left(lx - \frac{x^2}{2}\right) + C_{1b} \tag{6.8b}$$

where C_{1a}, C_{1b} are the integration constants and are evaluated to be zero by putting the boundary condition, $\left(\mathrm{d}v_1/\mathrm{d}x\right)\Big|_{x=0} = \left(\mathrm{d}v_2/\mathrm{d}x\right)\Big|_{x=0} = 0$ in the expression (6.8).

Further, integration of expression (6.8) yields;

$$v_1 = \frac{3\left(\mathrm{n}+1\right)^3}{2Ebh^3\,\mathrm{n}^3}\left(P_1 - \frac{\mu pbh\,\mathrm{n}}{\mathrm{n}+1}\right)\left(\frac{lx^2}{2} - \frac{x^3}{6}\right) + C_{2a} \tag{6.9a}$$

$$v_2 = \frac{3\left(\mathrm{n}+1\right)^3}{2Ebh^3}\left(P_2 - \frac{\mu pbh}{\mathrm{n}+1}\right)\left(\frac{lx^2}{2} - \frac{x^3}{6}\right) + C_{2b} \tag{6.9b}$$

where the integration constants, $C_{2a} = C_{2b} = 0$ since $v_1\big|_{x=0} = v_2\big|_{x=0} = 0$.

Assuming that the continuity equation prevails, we get;

$$v_1 = v_2 \tag{6.10}$$

Solving expressions (6.9) and (6.10), we get;

$$P_1 = \frac{\mathrm{n}^3 P + \mathrm{n}\left(2\,\mathrm{n}^3 - \mathrm{n} + 1\right)Q}{\mathrm{n}^3 + 1} \tag{6.11a}$$

$$P_2 = \frac{P + \mathrm{n}\left(\mathrm{n}-1\right)Q}{\mathrm{n}^3 + 1} \tag{6.11b}$$

The two dimensional parameters “Q” and “R” as defined in expression (4.7) in the previous chapter is given by;

$$Q = \mu p b h$$

$$R = \frac{E b h^3}{l^3}$$

Using the expressions (6.9), (6.11) and (4.7), the static response in terms of “Q” and “R” is finally found to be;

$$v_1 = v_2 = \frac{(\mathrm{n}+1)^3}{4R(\mathrm{n}^3+1)}(P-Q)\left[3\left(\frac{x}{l}\right)^2 - \left(\frac{x}{l}\right)^3\right] \tag{6.12}$$

6.2.2 Evaluation of Relative Slip

Relative slip is dependent on the thickness ratio of the beam laminates. In the present analysis, the relative slip at the interfaces has been evaluated considering the thickness ratio, slope, transverse deflection and in-plane bending stress.

The displacements at any axial position x and $y_{1,2} = \mp h/2$ are given by;

$$u_1 = \frac{1}{E}\int_0^x \sigma_{x_1}\,\mathrm{d}x - \frac{h_1}{2}\frac{\mathrm{d}v_1}{\mathrm{d}x} \tag{6.13a}$$

$$u_2 = \frac{1}{E}\int_0^x \sigma_{x_2}\,\mathrm{d}x + \frac{h_2}{2}\frac{\mathrm{d}v_2}{\mathrm{d}x} \tag{6.13b}$$

These displacements are produced by the resultant axial force $F_{1,2}$ and moment $M_{1,2}$ about the centroid of each half of the beam as shown in Fig. 6.1(b). σ_{x_1} and σ_{x_2} are the in-plane bending stresses.

From the force equilibrium, the in-plane bending stresses in the upper and lower laminates are computed in terms of thickness ratio as given by:

$$\sigma_{x_1} = \frac{\mu p(\mathrm{n}+1)}{2\,\mathrm{n}\,h}(l-x) \tag{6.14a}$$

$$\sigma_{x_2} = -\frac{\mu p(\mathrm{n}+1)}{2h}(l-x) \tag{6.14b}$$

Combining expressions (6.12), (6.13) and (6.14), the relative slip displacement at the interfaces is given by;

$$\Delta u = u_2 - u_1 = \frac{3(\mathrm{n}+1)^3 h}{4(\mathrm{n}^3+1)Rl}\left[P - \frac{(\mathrm{n}^3+3\mathrm{n}^2+3\mathrm{n}+1)}{3\mathrm{n}(\mathrm{n}+1)}Q\right]\left[2\left(\frac{x}{l}\right)-\left(\frac{x}{l}\right)^2\right] \tag{6.15}$$

Slip will occur only if $P > P_c = \frac{(\mathrm{n}^3+3\mathrm{n}^2+3\mathrm{n}+1)}{3\mathrm{n}(\mathrm{n}+1)}Q$.

where P_c is the critical static load applied at the tip of the welded cantilever beams.

6.2.3 Analysis of Energy Dissipated

Energy dissipation in the multilayered jointed beams is evaluated by considering the expression for energy loss developed by Goodman and Klumpp [17] as discussed in details (expression 4.13) in the previous chapter.

Substituting the expression (6.15) in (4.12) considering the beam to be loaded cyclically between the loads $\pm P_m$ and integrating, the energy dissipation per cycle in terms of static load is given by;

$$E_{loss} = \frac{2(\mathrm{n}+1)^3 Q}{(\mathrm{n}^3+1)R}\left(P_m - \frac{(\mathrm{n}^3+3\mathrm{n}^2+3\mathrm{n}+1)Q}{3\mathrm{n}(\mathrm{n}+1)}\right) \tag{6.17}$$

where P_m is the maximum static load applied at the tip of the welded cantilever beams. The maximum tip displacement v_m, corresponding to $P = P_m$ is obtained from (6.12) by putting $x = l$ as follows;

$$v_m = \frac{(\mathrm{n}+1)^3}{2(\mathrm{n}^3+1)R}(P_m - Q) \tag{6.18a}$$

On rearranging expression (6.18a), P_m in terms of v_m is given by;

$$P_m = \frac{2(\mathrm{n}^3+1)Rv_m}{(\mathrm{n}+1)^3} + Q \tag{6.18b}$$

Putting the expression (6.18b) in (6.17), the energy dissipation in terms of displacement is given by;

$$E_{loss} = 4Q\left(v_m - \frac{(\mathrm{n}+1)^2}{6\,\mathrm{n}} \frac{Q}{R} \right) \tag{6.19}$$

From the expression (6.19), it is evident that the slip will occur only if $v \geq v_c = \frac{(\mathrm{n}+1)^2}{6\,\mathrm{n}} \frac{Q}{R}$, where v_c is the critical tip displacement.

6.2.4 Evaluation of Damping Capacity

In the present analysis, the damping capacity of welded structures is expressed in terms of non-dimensional quantities such as the damping ratio (ψ) and loss factor (η_s), defined by;

$$\psi = \frac{E_{loss}}{E_{ne}} \tag{6.20a}$$

$$\eta_s = \frac{E_{loss}}{2\pi E_{ne}} = \frac{\psi}{2\pi} \tag{6.20b}$$

where E_{ne} is the maximum strain energy stored in the system.

The maximum strain energy stored in the system in terms of maximum load and tip deflection is given by;

$$E_{ne} = \frac{1}{2} P_m \left(\frac{v_c}{P_c} \right) P_m = \frac{P_m^2}{4R} \tag{6.21a}$$

Inserting expression (6.18b) in (6.21a) and simplifying we get;

$$E_{ne} = \frac{1}{4R} \left(\frac{2\left(n^3+1\right) R v_m}{(n+1)^3} + Q \right)^2 \tag{6.21b}$$

Putting expressions (6.19) and (6.20) in expression (6.21), the damping ratio in terms of tip displacement is given by;

$$\psi = \frac{16Q}{R} \frac{\left[v_m - \frac{(n+1)^2}{6n} \left(\frac{Q}{R} \right) \right]}{\left[\frac{2\left(n^3+1\right) R v_m}{(n+1)^3} + Q \right]^2} \tag{6.22}$$

Putting expression (6.22) in (6.20b), the loss factor for two layered welded structures with unequal thickness is evaluated to be;

$$\eta_s = \frac{8Q}{\pi R} \frac{\left[v_m - \frac{(n+1)^2}{6n} \left(\frac{Q}{R} \right) \right]}{\left[\frac{2\left(n^3+1\right) R v_m}{(n+1)^3} + Q \right]^2} \tag{6.23}$$

6.3 Dynamic Analysis

In the present section, a detailed analysis has been presented for the dynamic analysis of the layered welded beams with unequal thickness. The analysis developed follows the static analysis presented in the preceding sections for the unsymmetrical welded beam as shown in Fig. 6.1.

6.3.1 Types of Loading Considered In the Analysis

The following displacement function $f(t)$ has been considered for the forced vibration analysis of unsymmetrical welded beams;

(a) $f(t) = F_0 H(t - t_0)$ (6.24a)

where $H(t)$ is the Heaviside function and F_0 is the amplitude

(b) $f(t) = F_0 \, e^{i\omega t}$ (6.24b)

where ω is the excitation frequency

6.3.2 Analysis of Dynamic Response

The forced vibration of the beam produced by the displacement f (t) is applied at the unsupported end such that;

$$v\big|_{x=l} = f(t) \tag{6.25}$$

The dynamic displacement is composed of two parts;

$$v = v_{\mathrm{I}} + v_{\mathrm{II}} \tag{6.26}$$

where

$$v_{\mathrm{I}} = \frac{9}{8}\frac{(n+1)^3}{(n^3+1)}\left[\frac{3}{2}\left(\frac{x}{l}\right)^2 - \frac{1}{2}\left(\frac{x}{l}\right)^3\right] f(t) \tag{6.27}$$

The term in the bracket represents the static mode function and satisfies the end conditions;

$$v_{\mathrm{I}}\big|_{x=0} = 0; \left.\frac{\mathrm{d}\, v_{\mathrm{I}}}{\mathrm{d}\, x}\right|_{x=0} = 0; \left.\frac{\mathrm{d}^2 v_{\mathrm{I}}}{\mathrm{d}\, x^2}\right|_{x=l} = 0; v_{\mathrm{I}}\big|_{x=l} = 0; \tag{6.28}$$

but does not satisfies the dynamic equilibrium equation;

$$EI\frac{\partial^4 v}{\partial x^4} + \rho A\frac{\partial^2 v}{\partial t^2} = 0 \tag{6.29}$$

where EI and ρ are the flexural rigidity and density of the beam, respectively.

The displacement v_{I} produces the dynamic loads as given by;

$$-\frac{9}{8}\frac{(n+1)^3}{(n^3+1)} A\rho\left[\frac{3}{2}\left(\frac{x}{l}\right)^2 - \frac{1}{2}\left(\frac{x}{l}\right)^3\right] \ddot{f}(t) \tag{6.30}$$

where A is the cross-sectional area of the beam.

The displacement (v_{II}) representing vibrations produced by the force function given in expression (6.30) is expressed as;

$$v_{\mathrm{II}} = \sum_i \varphi_i(t) X_i(x) \tag{6.31}$$

where $X_i(x)$ and $\varphi_i(t)$ are the modal and time-dependent functions, respectively. v_{II} must satisfy the end conditions;

$$v_{\mathrm{II}}\big|_{x=0} = 0; \left.\frac{\mathrm{d}\, v_{\mathrm{II}}}{\mathrm{d}\, x}\right|_{x=0} = 0; \left.\frac{\mathrm{d}^2 v_{II}}{\mathrm{d}\, x^2}\right|_{x=l} = 0; v_{\mathrm{II}}\big|_{x=l} = 0; \tag{6.32}$$

$X_i(x)$ are the solutions of the expression (6.29) and satisfies the end condition as given in (6.32). Thus, we get;

$$X_i = \sinh k_i l \sin k_i(l-x) - \sin k_i l \sinh k_i(l-x) \tag{6.33}$$

where k_i are the roots of the following expression;

$$\tanh k_i l = \tan k_i l \tag{6.34}$$

The total displacement is obtained by putting expressions (6.27) and (6.31) in (6.26) and is given by;

$$v = \frac{9}{8}\frac{(n+1)^3}{(n^3+1)}\left[\frac{3}{2}\left(\frac{x}{l}\right)^2 - \frac{1}{2}\left(\frac{x}{l}\right)^3\right] f(t) + \sum_i \varphi_i(t) X_i(x) \tag{6.35}$$

The time-dependent functions $\varphi_i(t)$ must satisfy the differential equation;

$$\ddot{\varphi}_i + \frac{EIk_i^4}{A\rho}\varphi_i = -b_i \ddot{f}(t) \tag{6.36}$$

where the dot superscripts denote differentiation with respect to time. The coefficients b_i are obtained by expanding the force function given in expression (6.30) in a series of the normal functions, X_i. Thus,

$$-\frac{9}{8}\frac{(n+1)^3}{(n^3+1)} A\rho \ddot{f}(t)\left[\frac{3}{2}\left(\frac{x}{l}\right)^2 - \frac{1}{2}\left(\frac{x}{l}\right)^3\right] = -A\rho \ddot{f}(t)\sum_i b_i X_i \tag{6.37}$$

The coefficients b_i are obtained from the following expression;

$$b_i = \frac{\int_0^l \frac{9}{8}\frac{(n+1)^3}{(n^3+1)}\{X_i\}\left[\frac{3}{2}\left(\frac{x}{l}\right)^2 - \frac{1}{2}\left(\frac{x}{l}\right)^3\right] \mathrm{d}x}{\int_0^l X_i^2 \,\mathrm{d}x} \tag{6.38}$$

Integrating the expression (6.38), b_i is finally found to be;

$$b_i = \frac{9(n+1)^3}{4(n^3+1)k_i l(\sinh k_i l - \sin k_i l)} \tag{6.39}$$

The general solution of expression (6.36) is given by;

$$\varphi_i(t) = A_i \cos p_i t + B_i \sin p_i t - \frac{b_i}{p_i}\int_0^t \ddot{f}(t) \sin p_i (t-\tau)\,\mathrm{d}\tau \tag{6.40}$$

where $p_i = \left(\frac{EI}{A\rho}\right)^{1/2} k_i^2$

Constants A_i and B_i are evaluated from the initial conditions;

$$v(0) = U(x,0) \tag{6.41a}$$

$$\dot{v}(0) = V(x,0) \tag{6.41b}$$

Putting expression (6.35) in (6.41), U and V are evaluated as;

$$U = \frac{9}{8}\frac{(n+1)^3}{(n^3+1)}\left[\frac{3}{2}\left(\frac{x}{l}\right)^2 - \frac{1}{2}\left(\frac{x}{l}\right)^3\right] f(0) + \sum_i X_i \{A_i\} \tag{6.42a}$$

$$V = \frac{9}{8}\frac{(n+1)^3}{(n^3+1)}\left[\frac{3}{2}\left(\frac{x}{l}\right)^2 - \frac{1}{2}\left(\frac{x}{l}\right)^3\right] \dot{f}(0) + \sum_i X_i \{B_i p_i\} \tag{6.42b}$$

Moreover, the static mode shape is expressed as;

$$\frac{9}{8}\frac{(n+1)^3}{(n^3+1)}\left[\frac{3}{2}\left(\frac{x}{l}\right)^2 - \frac{1}{2}\left(\frac{x}{l}\right)^3\right] = \sum_i b_i X_i \tag{6.43}$$

Putting expression (6.43) in (6.42), we obtain;

$$U(x,0) = \sum_i X_i \{A_i + b_i f(0)\} \tag{6.44a}$$

$$V(x,0) = \sum_i X_i \{B_i p_i + b_i \dot{f}(0)\} \tag{6.44b}$$

Putting the initial conditions U=V=0, the constants A_i and B_i are found as;

$$A_i = -b_i f(0) \tag{6.45a}$$

$$B_i = -\frac{b_i}{p_i}\dot{f}(0) \tag{6.45b}$$

Substitution of expressions (6.40) and (6.45) in (6.35) yields;

$$\begin{aligned} v(x,t) = {} & \frac{9}{8}\frac{(n+1)^3}{(n^3+1)}\left[\frac{3}{2}\left(\frac{x}{l}\right)^2 - \frac{1}{2}\left(\frac{x}{l}\right)^3\right] f(t) - f(0)\sum_i b_i X_i \cos p_i t \\ & - \dot{f}(0)\sum_i \frac{b_i}{p_i} X_i \sin p_i t - \sum_i \frac{b_i}{p_i} X_i \int_0^t \ddot{f}(\tau) \sin p_i (t-\tau)\, \mathrm{d}\tau \end{aligned} \tag{6.46}$$

Integrating the expression (6.46), the transverse deflection is finally found to be;

$$v(x,t)=\frac{9}{8}\frac{(n+1)^3}{\left(n^3+1\right)}\left[\frac{3}{2}\left(\frac{x}{l}\right)^2-\frac{1}{2}\left(\frac{x}{l}\right)^3\right]f(t)-\sum_i b_i X_i f(t)$$
$$+\sum_i b_i X_i p_i \int_0^t f(\tau)\sin p_i(t-\tau)\,\mathrm{d}\tau \tag{6.47}$$

6.3.3 Evaluation of Dynamic Slip

In the present section, the relative dynamic slip at the interface of welded beams of unequal thickness has been evaluated considering the thickness ratio, external loading and in-plane bending stresses developed during this loading.

The relative slip at the interfaces under dynamic condition is evaluated combining the expressions (6.13), (6.14) and (6.47). The relative slip at the interfaces is given by;

$$\Delta u_x = u_2 - u_1 = -\frac{9(n+1)^3\,\mu p l^2}{8\left(n^3+1\right)Eh}\left(\frac{2x}{l}-\frac{x^2}{l^2}\right)+h\frac{\mathrm{d}v}{\mathrm{d}x} \tag{6.48}$$

Utilizing the expression for mode shape as given by (6.47) in (6.48), the relative slip is modified as;

$$\Delta u_x = \frac{3(n+1)^2}{4}\left[-\frac{\mu p l^2}{3nEh}+\frac{2h}{(n+1)^2 l}f(t)\right]\left(\frac{2x}{l}-\frac{x^2}{l^2}\right)$$
$$+h\sum_i b_i k_i\left[\sinh k_i l\cos k_i(l-x)-\sin k_i l\cosh k_i(l-x)\right]\times\left[f(t)-p_i\int_0^t f(\tau)\sin p_i(t-\tau)\,\mathrm{d}\tau\right] \tag{6.49}$$

6.3.4 Analysis of Energy Dissipated

The energy dissipation per cycle has been evaluated considering the relation developed by Goodman and Klumpp [17]. Substituting the expression (6.49) in (4.13), the energy dissipation per cycle is given by;

$$E_{loss}=4\mu p b\int_0^l\left\{\begin{aligned}&\left[\frac{3(n+1)^2}{4}\left(-\frac{\mu p l^2}{3nEh}+\frac{2h}{(n+1)^2 l}f(t)\right)\right]\left(\frac{2x}{l}-\frac{x^2}{l^2}\right)\\&+h\sum_i b_i k_i\left[\sinh k_i l\cos k_i(l-x)-\sin k_i l\cosh k_i(l-x)\right]\\&\times\left[f(t)-p_i\int_0^t f(\tau)\sin p_i(t-\tau)\,\mathrm{d}\tau\right]\end{aligned}\right\}\mathrm{d}x \tag{6.50}$$

Rearranging expression (6.50) we obtain;

$$E_{loss} = 4\mu pb\int_0^l \left\{\left[\frac{3(n+1)^2}{4}\left(-\frac{\mu pl^2}{3nEh}+\frac{2h}{(n+1)^2 l}f(t)\right)\right]\left(\frac{2x}{l}-\frac{x^2}{l^2}\right)\right\}\mathrm{d}x$$
$$+4\mu pbh\sum_i b_i k_i \int_0^l \left\{\begin{array}{l}\left[\sinh k_i l\cos k_i(l-x)-\sin k_i l\cosh k_i(l-x)\right] \\ \times\left[f(t)-p_i\int_0^t f(\tau)\sin p_i(t-\tau)\,\mathrm{d}\tau\right]\end{array}\right\}\mathrm{d}x \tag{6.51}$$

Modification of expression (6.51) yields;

$$E_{loss} = 4\mu pb\int_0^l \left\{\left[\frac{3(n+1)^2}{4}\left(-\frac{\mu pl^2}{3nEh}+\frac{2h}{(n+1)^2 l}f(t)\right)\right]\left(\frac{2x}{l}-\frac{x^2}{l^2}\right)\right\}\mathrm{d}x$$
$$+4\mu pbh\sum_i \left\{\begin{array}{l} b_i k_i\left[\int_0^l\left\{\sinh k_i l\cos k_i(l-x)\,\mathrm{d}x\right\}-\int_0^l\left\{\sin k_i l\cosh k_i(l-x)\,\mathrm{d}x\right\}\right] \\ \times\left[f(t)-p_i\int_0^t f(\tau)\sin p_i(t-\tau)\,\mathrm{d}\tau\right]\end{array}\right\} \tag{6.52}$$

Integrating the expression (6.52) we get;

$$E_{loss} = 4\mu pb\left\{\left[\frac{3(n+1)^2}{4}\left(-\frac{\mu pl^2}{3nEh}+\frac{2h}{(n+1)^2 l}f(t)\right)\right]\right\}\left[\frac{2l}{3}\right]$$
$$+4\mu pbh\sum_i\left\{b_i k_i\left[\frac{\sinh k_i l\sin k_i l}{k_i}-\frac{\sin k_i l\sinh k_i l}{k_i}\right]\times\left[f(t)-p_i\int_0^t f(\tau)\sin p_i(t-\tau)\,\mathrm{d}\tau\right]\right\} \tag{6.53}$$

Simplifying expression (6.53), energy loss is found to be;

$$E_{loss} = 4\mu pb\left\{\frac{3(n+1)^2}{4}\left(-\frac{\mu pl^2}{3nEh}+\frac{2h}{(n+1)^2 l}f(t)\right)\right\}\left[\frac{2l}{3}\right] \tag{6.54}$$

The expression (6.54) is modified putting two dimensional parameters “Q” and “R” as given by expressions 4.7(a) and 4.7(b) and the same is given as;

$$E_{loss} = 4Q\left(f(t)-\frac{(n+1)^2}{6n}\frac{Q}{R}\right) \tag{6.55}$$

6.3.5 Evaluation of Loss Factor

The maximum strain energy stored in the system in terms of dynamic deflection at the tip of the beam is given by;

$$E_{ne} = \frac{1}{2} k \left[f(t) \right]^2 = R \left[f(t) \right]^2 \tag{6.56}$$

where $\left(k = \frac{3EI}{l^3} \right)$ is the bending stiffness

Putting expressions (6.55) and (6.56) in expression (6.20a), the damping ratio in terms of dynamic tip displacement is given by;

$$\psi = \frac{4Q}{R \left[f(t) \right]^2} \left(f(t) - \frac{(n+1)^2}{6n} \frac{Q}{R} \right) \tag{6.57}$$

Putting expression (6.57) in expression (6.27b), the loss factor in terms of dynamic tip displacement is given by;

$$\eta_s = \frac{2Q}{\pi R \left[f(t) \right]^2} \left(f(t) - \frac{(n+1)^2}{6n} \frac{Q}{R} \right) \tag{6.58}$$

6.4 Summary

In the present chapter, an elaborate static and dynamic analysis for the damping mechanism of layered and welded beams with unequal thickness has been dealt. The governing equations for the transverse vibration and relative dynamic slip during static and dynamic loading have been derived considering the thickness ratio and in-plane bending stress neglecting the effects of shear deformation and rotary inertia. It is found that the total slip is a function of the distance from the fixed end and thickness ratio of the laminates in the welded beams. All other parameters remaining constant, with thickness ratio greater than one, initiation of slip requires a larger displacement and the energy loss reduces compared to the jointed beam of equal thickness. The reason being, slip interface is not at the centroid of the beam in case of layered and welded non-symmetric beams thereby raising the critical load and amplitude. In other words, energy dissipation is maximized by having the slip interface at the centroid of the total beam cross-section. The critical load and amplitude increases with the increase in thickness ratio. It is also deduced that the loss coefficient becomes more for the symmetrical beam (thickness ratio one) compared to that of the equivalent unsymmetrical beam (thickness ratio other than one) with same

overall thickness. Loss factor have been evaluated theoretically for various configurations and thickness ratio. Validation of the developed model has been ascertained comparing these theoretical results for loss factor with the experimental ones.

7

DAMPING ESTIMATION OF WELDED BEAMS USING FINITE ELEMENT METHOD

7.1 Introduction

In the previous chapters, the analysis of a layered and welded cantilever beam has been dealt in detail considering the jointed beam model as a distributed-parameter system. Although a distributed-parameter model accurately reflects the real situation thus giving an exact solution, but its application is restricted to relatively simple systems. In fact, many practical problems in engineering deal with complicated shapes with arbitrary boundary conditions whose analysis becomes extremely difficult and in a few cases almost impossible by the conventional methods. Therefore, various numerical techniques have been developed to solve all these complicated engineering problems. One of such numerical techniques used is the finite element method in which an approximate solution is achieved by discretizing the problem domain into many subdomains and this subdomain is called a finite element. In contrast to the analytical solutions which show the exact behavior of a system at any point within the system, numerical solutions are approximate ones agreeing with the exact solutions at some discrete points.

There are two common types of numerical methods: (1) finite difference methods and (2) finite element methods. In the finite difference methods, the differential equation is written for each node and the derivatives are replaced by difference equations. This approach results in a set of simultaneous linear equations. Although finite difference methods are easy to adopt in simple problems, but their application becomes difficult to problems with complex geometries or boundary conditions.

Contrary to this, the finite element method uses integral formulations to create a system of algebraic equations. In this technique, all the complexities of the problems such as varying shape, boundary conditions and loads are maintained as usual and the

solutions are obtained in an approximate manner. The finite character of the structural connectivity makes it possible to obtain a solution by means of simultaneous algebraic equations. Because of its diversity and flexibility, it receives much attention in present day engineering problems. Over the years, this technique has been well established so that it is considered to be one of the best methods for solving a wide variety of practical problems efficiently. Both the static and dynamic problems are effectively analyzed by this method.

7.2 Finite Element Method

In finite element method, the actual continuum is represented as an assemblage of subdivisions called finite elements. Each element is free to deform and may have different material and geometrical properties. The proper choice of the element varies from one-dimensional axial element to three-dimensional solid element depending upon the nature of problem. The elements considered in the present investigation are one-dimensional beam elements representing the neutral axis of the beam. These elements are considered to be interconnected at specified joints called nodes. These nodes usually lie on the element boundaries where adjacent elements are considered to be connected.

The actual variation of the field variable (e.g., displacement) inside an element is not known. Instead, the field variable within an element is normally expressed in terms of nodal values. The variation of this field variable within a finite element is approximated by a simple function called shape function. The shape function dictates the size of these nodal contributions. Further, the element stiffness and mass matrices of the individual elements are evaluated. The governing equations for each element are derived and assembled to find out the system equations describing the behavior of the body. Thus, each individual element and its contributions are considered adequately in obtaining a global model for a structure.

Summarizing the above, the finite element analysis consists of the following steps:

• Discretization of the domain into a finite number of elements

• Selection of proper shape functions

• Development of the element stiffness and mass matrices

• Assembly of the element matrices to obtain the global matrix for the entire domain

• Imposition of the boundary conditions

• Solution of equations

In general, there are several approaches to formulate finite element problems; (1) Direct Formulation, (2) Minimum Potential Energy Formulation and (3) Weighted Residual Formulations. In the present analysis, the "Minimum Potential Energy Formulation" approach has been adopted. In this approach the total potential energy of the system is evaluated. It is assumed that all the kinematically admissible displacement fields, those corresponding to equilibrium, extremize the total potential energy. If the extremum condition is a minimum, the equilibrium state is stable. This principle has been utilized to evaluate the element stiffness and mass matrices. The damping matrix has been evaluated considering the Rayleigh damping matrix. These stiffness, mass and damping matrices are further used to evaluate the natural frequency, mode shapes and loss factor of the layered and welded cantilever beams.

7.3 Formulation Using Finite Element Method

A layered and tack welded cantilever beam model with uniform pressure distribution at the interfaces as shown in Fig. 7.1 is considered in the present investigation in order to evaluate the loss factor of the welded and layered structures using finite element approach. The particular beam is divided into a number of elements equal to the number of tack welded joints in the specimen. Each element is considered as one-dimensional of equal length. A standard beam element is modeled using two nodes with three degrees of freedom per node (transverse, axial and rotation) as shown in Fig. 7.2. The contribution of each element depends on both the displacements and rotations at the nodes associated with the corresponding element.

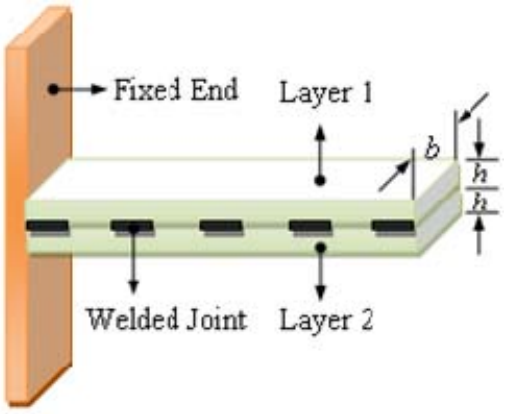

Fig. 7.1 Two layered tack welded cantilever beam model

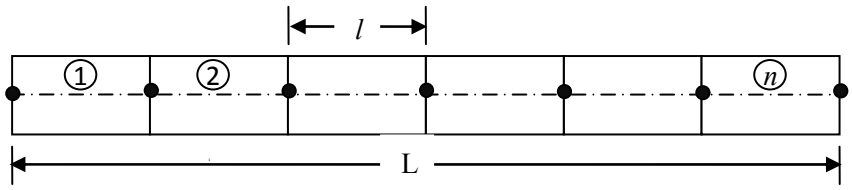

Fig. 7.2 Mesh of *n* number of beam elements

7.3.1 The Displacement Description

The layered beam as shown in Fig. 7.1 is considered to be made up of a number of linear elements of equal size connected at their nodal points. Each element is defined by two nodes and has three degrees of freedom, i.e., transverse displacement, axial displacement and rotation at each node. The geometry of an element displaying the nodes and degrees of freedom is shown in Fig. 7.3. It is assumed that the continuity equation prevails and every layer has the same transverse displacement. At each node *n*, four displacements $\{q_n\}$ are introduced, these being the transverse displacement w_n, the rotation θ_n and the axial displacements u_{n1}, u_{n2} of the middle planes of these elastic layers.

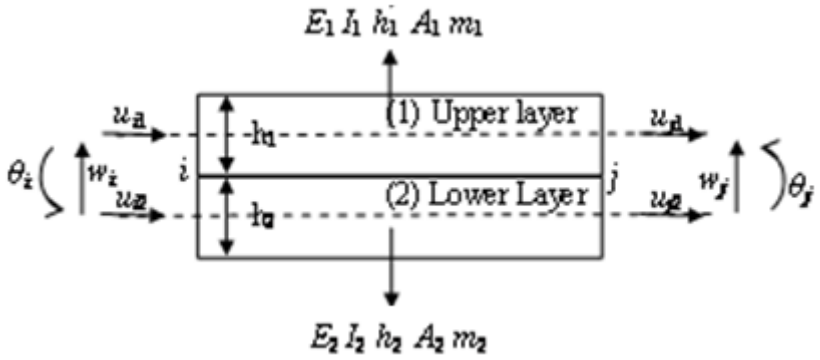

Fig. 7.3 Finite element model for the damped layered and welded beams

The total set of nodal displacements for the element is given by:

$$\left\{\mathbf{q}^{\mathbf{e}}\right\} = \begin{bmatrix} w_i & \theta_i & u_{i1} & u_{i2} & w_j & \theta_j & u_{j1} & u_{j2} \end{bmatrix}^T \tag{7.1}$$

The displacement field vector {d} is expressed in terms of the polynomial shape functions as;

$$\begin{Bmatrix} w \\ \theta \\ u_1 \\ u_2 \end{Bmatrix} = \begin{bmatrix} N \\ N^{'} \\ N_1 \\ N_2 \end{bmatrix} \left\{ \mathbf{q}^{\mathbf{e}} \right\} \tag{7.2}$$

$\begin{bmatrix} N_1 & N_2 & N & N^{'} \end{bmatrix}$ are the cubic shape functions given by;

$$\begin{bmatrix} N_1 \end{bmatrix} = \begin{Bmatrix} 0 & 0 & 1-\xi & 0 & 0 & 0 & \xi & 0 \end{Bmatrix} \tag{7.3a}$$

$$\begin{bmatrix} N_2 \end{bmatrix} = \begin{Bmatrix} 0 & 0 & 0 & 1-\xi & 0 & 0 & 0 & \xi \end{Bmatrix} \tag{7.3b}$$

$$\begin{bmatrix} N \end{bmatrix} = \begin{Bmatrix} 1-3\xi^2+\xi^3 & \left(\xi-2\xi^2+\xi^3\right)l & 0 & 0 & 3\xi^2-2\xi^3 & \left(-\xi^2+\xi^3\right)l & 0 & 0 \end{Bmatrix} \tag{7.3c}$$

$$\begin{bmatrix} N' \end{bmatrix} = \begin{bmatrix} \frac{\partial N}{\partial x} \end{bmatrix} = \frac{1}{l} \begin{bmatrix} \frac{\partial N}{\partial \xi} \end{bmatrix} \tag{7.3d}$$

where $\xi = x/l$, l =element length.

7.3.2 Element Stiffness Matrix

The stiffness matrix for the jointed element is obtained from the bending and extensional strain energies as follows:

$$U_{be} = \frac{1}{2} \int_V \left(\varepsilon_1 \sigma_1 + \varepsilon_2 \sigma_2 \right) dV \tag{7.4}$$

$$U_{be} = \frac{1}{2} \int_0^l \left\{ E_1 A_1 \left(\frac{\partial u_1}{\partial x} \right)^2 + E_2 A_2 \left(\frac{\partial u_2}{\partial x} \right)^2 + \left(E_1 I_1 + E_2 I_2 \right) \left(\frac{\partial^2 w}{\partial x^2} \right)^2 \right\} dx \tag{7.5}$$

$$U_{be} = \frac{1}{2} \left\{ \mathbf{q}^{\mathbf{e}} \right\}^T \int_0^1 \left\{ \frac{E_1 A_1}{l} \left[N_1' \right]^T \left[N_1' \right] + \frac{E_2 A_2}{l} \left[N_2' \right]^T \left[N_2' \right] + \left(\frac{E_1 I_1 + E_2 I_2}{l^3} \right) \left[N'' \right]^T \left[N'' \right] \right\} d\xi \left\{ \mathbf{q}^{\mathbf{e}} \right\} \tag{7.6}$$

$$U_{be} = \frac{1}{2} \left\{ \mathbf{q}^{\mathbf{e}} \right\}^T \left[\mathbf{k} \right]^{\mathbf{e}} \left\{ \mathbf{q}^{\mathbf{e}} \right\} \tag{7.7}$$

Therefore, element stiffness matrix is given by;

$$\left[\mathbf{k}\right]^{\mathrm{e}} = \int_0^1 \left\{ \begin{array}{l} \dfrac{E_1 A_1}{l}\left[N_1'\right]^T\left[N_1'\right] + \dfrac{E_2 A_2}{l}\left[N_2'\right]^T\left[N_2'\right] \\ + \dfrac{E_1 I_1}{l^3}\left[N''\right]^T\left[N''\right] + \dfrac{E_2 I_2}{l^3}\left[N''\right]^T\left[N''\right] \end{array} \right\} d\xi \tag{7.8}$$

where, E_i, A_i, I_i are the modulus of elasticity, cross-section area and moment of inertia of the ith layer of the beam. Integrating the expression (7.8), the element stiffness matrix is found to be;

$$\left[\mathbf{k}\right]^{\mathrm{e}} = \begin{bmatrix} \frac{12EI}{l^3} & \frac{6EI}{l^2} & 0 & 0 & \frac{-12EI}{l^3} & \frac{6EI}{l^3} & 0 & 0 \\ \frac{6EI}{l^2} & \frac{4EI}{l} & 0 & 0 & \frac{-6EI}{l^2} & \frac{2EI}{l} & 0 & 0 \\ 0 & 0 & \frac{E_1A_1}{l} & 0 & 0 & 0 & \frac{-E_1A_1}{l} & 0 \\ 0 & 0 & 0 & \frac{E_2A_2}{l} & 0 & 0 & 0 & \frac{-E_2A_2}{l} \\ \frac{-12EI}{l^3} & \frac{-6EI}{l^2} & 0 & 0 & \frac{12EI}{l^3} & \frac{-6EI}{l^2} & 0 & 0 \\ \frac{6EI}{l^3} & \frac{2EI}{l} & 0 & 0 & \frac{-6EI}{l^2} & \frac{4EI}{l} & 0 & 0 \\ 0 & 0 & \frac{-E_1A_1}{l} & 0 & 0 & 0 & \frac{E_1A_1}{l} & 0 \\ 0 & 0 & 0 & \frac{-E_2A_2}{l} & 0 & 0 & 0 & \frac{E_2A_2}{l} \end{bmatrix} \tag{7.9}$$

where $EI = E_1 I_1 + E_2 I_2$

7.3.3 Element Mass Matrix

Following a similar procedure, the mass matrix for the jointed and welded beam element is obtained from the kinetic energy as follows:

$$T = \frac{1}{2}\int_0^l \left(m_0 \dot{w}^2 + m_1 \dot{u}_1^2 + m_2 \dot{u}_2^2 \right) dx \tag{7.10}$$

where, m_i is the mass per unit length of the ith layer of the beam element and $m_0 = m_1 + m_2$

$$T = \frac{l}{2}\left\{\dot{\mathbf{q}}^{\mathbf{e}}\right\}^T \int_0^1 \left(m_0 \left[N\right]^T \left[N\right] + m_1 \left[N_1\right]^T \left[N_1\right] + m_2 \left[N_2\right]^T \left[N\right] \right) d\xi \left\{\dot{\mathbf{q}}^{\mathbf{e}}\right\} \tag{7.11}$$

$$T = \frac{1}{2}\left\{\dot{\mathbf{q}}^{\mathbf{e}}\right\}^T \left[m\right]^e \left\{\dot{\mathbf{q}}^{\mathbf{e}}\right\} \tag{7.12}$$

Therefore, element mass matrix is given by;

$$\left[\mathbf{m}\right]^{\mathbf{e}} = \int_0^1 \left(m_1 \left[N\right]^T \left[N\right] + m_2 \left[N\right]^T \left[N\right] + m_1 \left[N_1\right]^T \left[N_1\right] + m_2 \left[N_2\right]^T \left[N_2\right] \right) d\xi \tag{7.13}$$

Integrating the expression (13), the element mass matrix is found to be;

$$\left[\mathbf{m}\right]^{\mathbf{e}} = \begin{bmatrix} \frac{13m_0l}{35} & \frac{11m_0l^2}{210} & 0 & 0 & \frac{9m_0l}{70} & \frac{-13m_0l^2}{420} & 0 & 0 \\ \frac{11m_0l^2}{210} & \frac{m_0l^3}{105} & 0 & 0 & \frac{13m_0l^2}{140} & \frac{-m_0l^3}{140} & 0 & 0 \\ 0 & 0 & \frac{m_1l}{3} & 0 & 0 & 0 & \frac{m_1l}{6} & 0 \\ 0 & 0 & 0 & \frac{m_2l}{3} & 0 & 0 & 0 & \frac{-m_2l}{6} \\ \frac{9m_0l}{70} & \frac{13m_0l^2}{140} & 0 & 0 & \frac{13m_0l}{35} & \frac{-11m_0l^2}{210} & 0 & 0 \\ \frac{-13m_0l^2}{420} & \frac{-m_0l^3}{140} & 0 & 0 & \frac{-11m_0l^2}{210} & \frac{m_0l^3}{105} & 0 & 0 \\ 0 & 0 & \frac{m_1l}{6} & 0 & 0 & 0 & \frac{m_1l}{3} & 0 \\ 0 & 0 & 0 & \frac{-m_2l}{6} & 0 & 0 & 0 & \frac{m_2l}{3} \end{bmatrix} \tag{7.14}$$

7.3.4 Global Stiffness and Mass Matrix

The individual element stiffness and mass matrices are assembled by taking into account the element connectivity to obtain the global stiffness and mass matrix for the jointed .beam.

While adding the element-stiffness matrices, the elements of $\mathbf{k}^{\mathbf{e}}$ are placed in the appropriate locations of the global **K** matrix, based on the element connectivity; overlapping elements are simply added. This assembly is denoted symbolically as;

$$\sum_{e} \mathbf{k}^{e} \rightarrow \mathbf{K} \tag{7.15}$$

Similarly, the global mass matrix is assembled using the element mass matrices as given by;

$$\sum_{e} \mathbf{m}^{e} \rightarrow \mathbf{M} \tag{7.16}$$

7.3.5 Natural Frequencies and Mode Shapes

The finite element method can be advantageously used to evaluate the natural frequencies and mode shapes of a dynamic system. If an elastic structure is excited, it oscillates harmonically depending on the distribution of the mass and stiffness in the structure. The amplitude of oscillations will decay progressively in the presence of damping and if the magnitude of damping exceeds a certain critical value, the oscillatory character of the motion will cease altogether. On the other hand, if damping is absent, the oscillatory motion will continue indefinitely with the same initial amplitude of excitation. In all practical cases, the vibration always occurs at certain frequencies known as natural frequencies which follow the well defined deformation patterns known as mode shapes. The study of natural frequencies and mode shapes in a vibrating system is known as modal analysis.

For multiple degrees of freedom systems, the modes essentially describe the nature of motion and provide physical understanding of their dynamic behavior. The modes are characterized by the eigenvalues and eigenvectors representing the natural frequencies and mode shapes, respectively. The global mass and stiffness matrices are utilized to determine the natural frequencies of vibration and mode shapes. Depending on the damping, the eigenvalues and eigenvectors can be real or complex. However, the effect of damping is generally neglected in the determination of natural frequencies and mode shapes of a lightly vibrating system. Therefore, real eigenvalues and eigenvectors are derived from the assumed undamped equation of motion. This assumption fairly holds well in most of the practical cases where damping is less pronounced.

7.3.5.1 Evaluation of Eigenvalues and Eigenvectors

The basic computational eigen-solution is determined in terms of mode shape by solving the expression as given by;

$$\mathbf{M}\ddot{\mathbf{D}} + \mathbf{K}\mathbf{D} = 0 \tag{7.17}$$

where $\mathbf{D}$ and $\ddot{\mathbf{D}}$ are the displacement and acceleration vectors of all the nodes of the entire structure; $\mathbf{K}$ and $\mathbf{M}$ are the global stiffness and mass matrices, respectively. The above equation represents the required dynamic equation for the free undamped vibration of the cantilever beam.

The effect of damping has not been considered in the above derivation since the direct formation of damping matrix due to interfacial slip is very difficult in actual practice. Instead, an alternative approach has been used to account for damping in terms of natural frequency, global stiffness and mass matrices. The detailed procedure for evaluating damping in a layered and welded structure has been discussed in the subsequent section.

7.3.5.2 Determination of Natural Frequencies

The natural frequency is an important parameter in the dynamic analysis of structures. If such a system is excited by an external force and both the exciting and natural frequencies are very close to each other, the resonant condition will prevail, thereby resulting violent vibration of the structure. This condition often leads to the catastrophic failure of the system. Therefore, it becomes imperative to design the dynamic system for its safe operation. The structure generally possesses as many natural frequencies as its degrees of freedom (also modes of vibration). In fact, it is not necessary to calculate all the natural frequencies since many of the frequencies do not get excited in actual practice.

Generally, the micro-slip at the interfaces due to initial excitation of the jointed beam is more at lower modes than the higher ones as established by Nishiwaki et al. [22]. Moreover, Clough and Penzien [178] have shown that the mathematical idealization of any structural system is more reliable at lower modes of vibration. Considering all these, the higher modes are usually ignored in the dynamic analysis of structures.

Therefore, the few modes of vibration have been taken into account in the present investigation neglecting the effect of higher modes.

The equation of motion for free vibration as given in expression (7.17) represents a generalized linear eigenvalue problem and its solution is given by;

$$\boldsymbol{D} = \boldsymbol{\phi} \mathrm{e}^{i\omega t} \tag{7.18}$$

where $\boldsymbol{\phi}$ and ω are the mode shapes (eigenvector) and natural frequency (eigenvalue) of vibration, respectively.

Substituting expression (7.18) in (7.17) results;

$$\left[\mathbf{K} - \omega^2 \mathbf{M}\right] \boldsymbol{\phi} = \boldsymbol{0} \tag{7.19}$$

In order to obtain a non-trivial solution, the coefficient matrix must be singular, which means its determinant must be equal to zero, i.e.

$$\left|\mathbf{K} - \omega^2 \mathbf{M}\right| = \boldsymbol{0} \tag{7.20}$$

An algebraic polynomial equation is obtained in ω^2 after expanding the above determinant. The roots of this equation give the eigenvalues representing natural frequencies of the system. The solution for ω produces pairs of positive and negative values of equal magnitude. The negative values of ω are usually ignored. The positive values of ω must be ordered so that the first lowest frequency is the fundamental frequency.

7.3.5.3 Determination of Mode Shapes

The structures usually vibrate in a definite way depending upon its natural frequency so that the characteristic shape or mode of vibration is established distinctly. Therefore, the information regarding the deflection pattern associated with each natural frequency is to be known for accurate dynamic analysis.

The mode shapes in the form of eigenvectors are found out from expression (7.19) as;

$$\left[\mathbf{K} - \omega_i^2 \mathbf{M}\right] \boldsymbol{\phi}_i = \boldsymbol{0} \tag{7.21}$$

where ω_i and $\boldsymbol{\phi}_i$ are the eigenvalues and eigenvectors representing the natural frequencies and mode shapes of the vibrating system at *i*th mode, respectively.

Since the system of equations represented in expression (7.21) is homogeneous, the mode shape is not unique. The first and second mode shapes along with its natural frequency of a particular cantilever beam specimen is shown in Fig. 7.4.

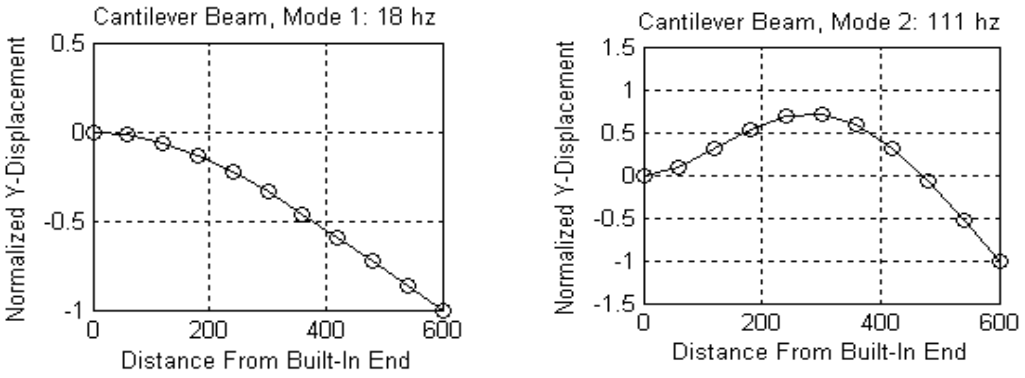

Fig. 7.4 Mode shapes

7.3.6 Damping Matrix

In the present analysis, Rayleigh damping is assumed. The element damping matrix is given by;

$$[\mathbf{C}] = \alpha[\mathbf{M}] + \beta[\mathbf{K}] \tag{7.22}$$

where α and β are the Rayleigh damping coefficients and are determined from the experimental results. For the layered and welded beam, the first two computed natural frequencies are;

$\omega_1 = 154.6$ rad/s, $\omega_2 = 432.3$ rad/s

and the first two experimentally determined damping ratios are;

$\xi_1 = 0.0257$ $\xi_2 = 0.0123$

The Rayleigh damping coefficients are evaluated using the values of natural frequencies and damping ratios as follows;

$$\alpha = \frac{2\omega_1\omega_2\left(\xi_1\omega_2 - \xi_2\omega_1\right)}{\omega_2^2 - \omega_1^2} = 7.55\,\mathrm{s}^{-1}$$

$$\beta = \frac{2\left(\xi_2\omega_2 - \xi_1\omega_1\right)}{\omega_2^2 - \omega_1^2} = 1.65\times10^{-5}\,\mathrm{s}$$

7.3.7 Evaluation of Loss Factor

The eigenvalue problem is solved with a real stiffness matrix to obtain the real modal parameters for the undamped structure. The loss factor for the damped structure is obtained using the modal strain energy method as given by;

$$\eta_s = \frac{\sum_e \left\{\mathbf{X}^e\right\}^T \left\{\mathbf{C}^e\right\} \left\{\mathbf{X}^e\right\}}{\sum_e \left\{\mathbf{X}^e\right\}^T \left\{\mathbf{K}^e\right\} \left\{\mathbf{X}^e\right\}} \tag{7.23}$$

where $\{\mathbf{X}^e\}$, $\{\mathbf{C}^e\}$ and $\{\mathbf{K}^e\}$ are the mode shape vector, element damping and stiffness matrices, respectively.

7.4 Summary

In the present work, a new technique of analyzing layered and jointed beams with slip damping at the interfaces has been proposed considering the finite element method. Unlike finite element method, existing classical methods use displacement models defined over the whole structure for analysis of slip damping. An approximate solution is obtained considering the beam model as a discrete system. The basic concept of this method is that a body is considered to consist of an assemblage of individual elements interconnected at finite number of nodal points. In the present problem, a given beam is discretized into finite number of one-dimensional elements of equal length. The element length considered is the distance between the consecutive welded joints. In principle, rapid convergence to the exact solution occurs with an increasing number of finite elements. However, no significant improvement in convergence is observed with further increase in the number of element thus establishing the optimality condition. Further, each element consists of two nodes with each node having three degrees of freedom, i.e., rotation, axial and transverse

displacement. Cubic shape functions are considered for the transverse vibration of the beam in terms of nodal variables.

The consistent stiffness and mass matrices have been evaluate in the present formulation with the inclusion of all rotational, axial and translational degrees of freedom. The damping has been defined in terms of loss factor as this can be determined experimentally or computed numerically with adequate precision. The formulation of damping matrix in case of slip damping has not yet been available in the literature and this study is another piece of work for future researchers. For this reason, it is generally more convenient and physically reasonable to assess the damping effect considering the Rayleigh damping matrix. The important parameters have been identified and their effect on damping has been evaluated. Theoretical loss factor has been evaluated considering finite element damping model and compared with the experimental ones in the results and discussion section for the validation of the developed model.

8

DAMPING ANALYSIS USING RESPONSE SURFACE METHODOLOGY (RSM)

8.1 Introduction

Slip damping mechanism in layered and welded structures is a non linear phenomenon and dependent on a number of parameters. Correct assessment of these parameters is essential to quantify the damping capacity of these structures. There are a number of parameters affecting slip damping in jointed structures which cannot be assessed correctly using the classical theory. Alternatively, experiments are performed to ascertain the effectiveness of these parameters on the damping of layered and jointed structures. Welded joints are used extensively in many modern industries to fabricate jointed structures that contribute significantly to the inherent slip damping. The main problem faced in the manufacture of these structures is the selection of optimum combination of input variables for achieving the required damping. This problem can be solved by developing the mathematical models through effective and strategic planning and executing experiments by RSM. Response surface methodology (RSM) is a technique used to determine and represent the cause and effect of relationship between true mean responses and input control variables influencing the responses as a n-dimensional hyper surface. The present investigation highlights the use of RSM by designing a three-factor three-level Full Factorial and Central Composite rotatable design matrix with full replication of planning, conducting, executing and developing the mathematical models. This is useful for predicting the mechanism of interfacial slip damping in layered and welded structures. The design utilizes the number of tack welded joints, initial amplitude of excitation, natural frequency and surface roughness at the interfaces as well as the material property to develop a damping model for the layered and welded structures.

8.2 Response Surface Methodology (RSM)

RSM is a collection of mathematical and statistical data that are useful for the modelling and analysis of problems in which a response of interest is influenced by several variables with an objective to optimize the response [179]. RSM also quantifies the relationships among one or more measured responses and the input factors. Response surface methodology (RSM) explores the relationships between several control variables to develop a mathematical model for the response. However, an experimental design involves choosing the appropriate combination of various factors and the levels of each factor for developing a model. Since experimental runs cost both time and money, it is pertinent to minimize the number of runs without compromising the desired goals. In order to achieve this, some strategies such as; Full Factorial (FF), Box–Benhken (BB), Central Composite Designs (CCD) etc. are frequently used.

The CCD design of experiment (DOE) allows the designer to utilize 3 levels for each factor (with each factor placed at one of each equally spaced value to ensure orthogonality and near rotatability) to adequately quantify second-order response models in 15 runs, inclusive of 3-replicated center points of a cubical design region. However, Full Factorial (FF) designs use different levels of various factors with every level of each factor combining with those of other factors. They are good for first-order response models, enabling the estimation of main and interaction effects. However, as the number of factors and levels increase, the number of requisite runs becomes cost and time prohibitive, and therefore the Taguchi designs, and fractional factorial design are utilized for product improvement and cost reduction. However, the Taguchi designs suffer a major inadequacy of handling interaction and confounding effects. Montgomery [179], Hunter [180] and Sukthomya and Tannock [181] have highlighted other weaknesses of the Taguchi designs such as;

- Unnecessary complication using inner and outer arrays.
- Non-recognition of randomized experiments to save the cost of changing level settings.
- Non- applicability of orthogonal arrays to processes involving factors that vary with time and cannot be quantified exactly, and noise factors may not always be independent of one another.

- The techniques require the designer to be aware of all control and noise factors affecting a product or process.

Design Expert-8 [182] and Minitab-14 [183] software are used to develop the experimental plan for RSM. The same software was also used to analyze the data collected by following the steps as follows:

1) Choose a transformation if desired. Otherwise, leave the option at "None".
2) Select the appropriate model to be used. The Fit Summary button displays the sequential *F*-tests, lack-of-fit tests and other adequacy measures that could be used to assist in selecting the appropriate model.
3) Perform the analysis of variance (ANOVA), post-ANOVA analysis of individual model coefficients and case statistics for analysis of residuals and outlier detection.
4) Inspect various diagnostic plots to statistically validate the model.
5) If the model looks good, generate model graphs, i.e., the Contour and 3D graphs, for interpretation. The analysis and inspection performed in steps (3) and (4) above will show whether the model is good or otherwise. Very briefly, a good model must be significant and the lack-of-fit must be insignificant. The various coefficient of determination, R^2 values should be close to 1. The diagnostic plots should also exhibit trends associated with a good model and these have been elaborated subsequently.

Multiple response optimizations are performed either by inspecting each response on the interpretation plots or using the graphical and numerical tools. Moreover, RSM designs also help to quantify the relationships between one or more measured responses and the input factors. The data collected is analyzed statistically using regression analysis to establish a relationship between the input factors and response variables. Regression is performed in order to develop a functional relationship between the estimated variables. The performance of the model depends on a large number of factors which interact in a complex manner. A second order response surface model is usually expressed as:

$$R = \beta_0 + \sum_{i=1}^{z} \eta_i x_i + \sum_{i=1}^{z} \lambda_i x_i^2 + \sum_{i=1}^{z-1} \sum_{j=2}^{z} \phi_{ij} x_i x_j \tag{8.1}$$

where, β_0, $\eta_i (i = 1, 2 \ldots z)$, $\lambda_i (i = 1, 2 \ldots z)$ and $\phi_{ij} (i = 1, 2 \ldots z\text{-}1, j = 2,3 \ldots z)$ are the unknown regression coefficients to be estimated by using the method of least squares. In this expression; x_1, x_2. . . x_z are the input variables that influence the response (R), z is the number of input factors. The response surface analysis is then done in terms of the fitted surface. The method of least squares is used to estimate the coefficients of the second order model. The response surface analysis is then carried out in terms of the fitted surface. The least square technique is used to fit a model equation containing the input variables by minimizing the residual errors measured by the sum of square deviations between the actual and the estimated responses. This involves the calculation of estimates for the regression coefficients, i.e., the coefficients of the model variables including the intercept or constant term. The calculated coefficients or the model equation is to be tested for statistical significance. In this respect, the following tests are performed.

8.2.1 Test for Significance of the Regression Model

This test is performed as an ANOVA procedure by calculating the F-ratio, which is the ratio between the regression mean square and the mean square error. The F-ratio, also called the variance ratio, is the ratio of variance due to the effect of a factor (in this case the model) and variance due to the error term. The F-ratio representing the test statistics for multiple independent variables is mathematically expressed by;

$$F - ratio = \frac{(MS)_{Model}}{(MS)_{Residual}} \tag{8.2}$$

where $(MS)_{Model}$ and $(MS)_{Residual}$ are the mean square of the model and residual, respectively. Mean square (MS) is mathematically defined as the difference between the individual experimental values and the mean of all the experimental values in the set of experimental data.

The mean square of the model is used to estimate the model variance given by the model sum of squares divided by the model degrees of freedom. The mean square of the residual is used to estimate the process variance.

The *significance level* "β" for a given hypothesis test is a value for which a *P-value* less than or equal to "β" is considered to be statistically significant. Typical value for

"β" considered in the present study is 0.05. This value corresponds to the probability of observing an extreme value by chance.

8.2.2 Test for Significance on Individual Model Coefficients

This test forms the basis for model optimization by adding or deleting coefficients through backward elimination, forward addition or stepwise elimination/addition/exchange. It involves the determination of the *P*-value or probability value relating the risk of falsely rejecting a given hypothesis. The *P*-value is the probability of rejecting the hypothesis. In statistics, a given hypothesis is rejected if the *P*- value is more than 0.05. "Prob. > *F*" value on an *F*-test indicates the proportion of time expected to get the stated *F*-value if no factor effects are significant. In general, the lowest order polynomial is considered for adequately describing the system.

8.2.3 Test for Lack-of-Fit

As replicate measurements are available, a test indicating the significance of the replicate error compared to the model dependent error can be performed. This test splits the residual or error sum of squares into two portions; one is due to pure error based on the replicate measurements and the other due to lack-of-fit because of model performance. The test statistic for lack-of-fit is the ratio between the lack-of-fit mean square and the pure error mean square. As established, this *F*-test statistic can be used to determine whether the lack-of-fit error is significant or not at the desired significance level, β. Insignificant lack-of-fit is desired as significant lack-of-fit indicates that there might be contributions in the input variables–response relationship that are not accounted for in the model. Additional checks are required to determine whether the model actually describes the experimental data or not. The checks performed include determining the variance coefficient of determination, R^2. These R^2 coefficients have values between 0 and 1.

R^2 is the variation between the mean of the residuals and the individual parameters. It is mathematically expressed by;

$$R^2 = 1 - \left[\frac{(SS)_{Residual}}{(SS)_{Residual} + (SS)_{Model}} \right] \tag{8.3}$$

where $(SS)_{Model}$ is the summation of the squares of the individual experimental values that are included in the model. $(SS)_{Residual}$ is the summation of the squares of the individual experimental values which are not included in the model.

In addition to the above, the adequacy of the model is also investigated by examining the residuals. The residuals represent the differences between the observed and predicted responses. It is examined using the normal probability plots and the plots of the residuals versus the predicted response. If the model is adequate, the points on the normal probability plot should form a straight line. On the other hand, the plots of the residuals versus the predicted response normally do not follow any definite pattern.

In the present study RSM has been adopted to ascertain the influence of various parameters on the damping mechanism in layered and welded beams. The analysis has been done in two steps;

(1) Natural frequency (f), initial amplitude of excitation (y) and surface roughness (Ra) as the input control variables and logarithmic damping decrement (δ) as the response.

(2) The input variables are the number of tack welds (N), initial amplitude of vibration (y), surface roughness (Ra) and Young's Modulus (Y) and the output response is the logarithmic damping decrement (δ).

8.3 Frequency, Amplitude and Surface Roughness as Input Variables

The layered and tack welded cantilever beam model that develops uniform pressure distribution at the interfaces due to perfect contact between two flat bodies as shown in Fig. 8.1 has been considered to find out the logarithmic damping decrement. The layered and tack welded cantilever beam considered in the present analysis is a lightly damped structure. In lightly damped structures, the damping mechanism is most effective at low frequencies and first few modes of vibration as the vibration amplitudes are large enough to allow significant slip [38]. It is justified to consider the logarithmic damping decrement to estimate the damping capacity [19] in these structures for the first few modes of vibration. Hence, the free vibration tests are performed instead of harmonic test as the damping capacity of such structures can be

well estimated at lower modes of free vibration instead of higher modes under harmonic loads.

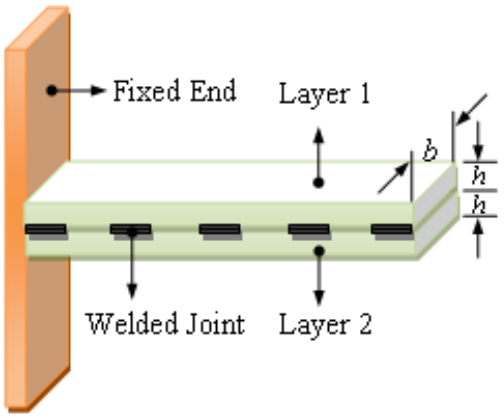

Fig. 8.1 Two layered tack welded cantilever beam model

8.3.1 Theoretical Analysis

The logarithmic damping decrement (δ) is used as a measure of the damping capacity of the jointed structures considering E_n and E_{n+1} as the energy stored in the system with the amplitudes of vibration (y_n) and (y_{n+1}) at nth and (n+1)th cycle, respectively as;

$$\delta = \ln\left(E_n / E_{n+1}\right)^{1/2} = \left[\ln\left\{1/(1-\psi)\right\}\right]/2 \tag{8.4}$$

where 'ψ' is the damping ratio as found in chapter (3) is given by;

$$\psi = \frac{1}{1+\left[ky(l,0)\right]/\left[4\mu bph\alpha\right]} \tag{8.5}$$

The exact values of dynamic slip ratio, α, and kinematic coefficient of friction, μ, are difficult to assess because of their complicated behavior under dynamic condition. The dynamic slip ratio decreases with the increase in the kinematic coefficient of friction and vice versa, the product of these two parameters $\alpha.\mu$ is assumed to be constant and is evaluated modifying expressions (8.4) and (8.5) as given by;

$$\alpha.\mu = k\left(1-e^{-2\delta}\right)y(l,0)\Big/4bphe^{-2\delta}. \tag{8.6}$$

This product $\alpha.\mu$ has been found out from the experimental results of the logarithmic damping decrement (δ) for 3 mm thickness cantilever beams of various surface roughness with tack welding using expression (8.6).

8.3.2 Response Surface Regression for $\alpha.\mu$

A polynomial model of second order type has been proposed to represent the relationship between the product $\alpha.\mu$ and independent input variables. The performance of the model depends on a large number of factors that can interact in a complex manner. In the present work, the input variables are natural frequency of vibration (*f*), initial amplitude of excitation (*y*), and surface roughness (*Ra*) and the outputs (responses) are the logarithmic damping decrement (δ) and the product $\alpha.\mu$. A full factorial design is used with three design factors for each of five levels to describe responses: the logarithmic damping decrement (δ) and the product $\alpha.\mu$, to estimate the parameters in the second-order model. Overall 5^3 = 125 free vibration experiments have been conducted to evaluate the responses. The important factors and their levels are shown in Table 8.1.

Table 8.1 Important factors and their levels

Sl.No	Factor	Notation	Unit	Levels				
1	Natural frequency	*f*	Hz	19.5	23.5	27.5	31.5	35.5
2	Amplitude	*y*	mm	0.1	0.2	0.3	0.4	0.5
3	Surface roughness	*Ra*	μm	0.81	1.14	1.47	1.8	2.13

The full models for $\alpha.\mu$ are expressed in term of the uncoded values of the independent variables as;

$$\begin{aligned}\alpha.\mu &= 0.009569 - 0.000166\times f - 0.002406\times y - 0.000035\times Ra + 0.000003\times f^2 \\ &+0.000097\times y^2 + 0.000013\times Ra^2 + 0.000152\times f\times y \\ &+0.000003\times f\times Ra - 0.000096\times y\times Ra\end{aligned} \quad (8.7)$$

8.3.2.1 Analysis of Variance (ANOVA) for $\alpha.\mu$

Analysis of variance (ANOVA) has been performed to determine the significant and non-significant parameters as well as to validate the full model as given in expression (8.7). The ANOVA has been carried out on the model for a confidence level of 95%. The results of ANOVA performed on the full model for $\alpha.\mu$ have been listed in Tables 8.2 and 8.3.

Table 8.2 Estimated regression coefficients for $\alpha.\mu$ (Full model)

Term	Coef	SE Coef	T	P
Constant	0.009569	0.000230	41.64	0.000
f	-0.000166	0.000014	-11.97	0.000
y	-0.002406	0.000352	-6.844	0.000
Ra	-0.000035	0.000127	-0.276	0.783
f×*f*	0.000003	0.000000	13.09	0.000
y×*y*	0.000097	0.000383	0.255	0.800
Ra×*Ra*	0.000013	0.000035	0.380	0.705
f×*y*	0.000152	0.000008	19.01	0.000
f×*Ra*	0.000003	0.000002	1.319	0.190
y×*Ra*	-0.000096	0.000097	-0.994	0.322

In Table 8.2, the value of '*P*' is less than 0.05. This is desirable as it indicates that the terms in the model have a significant effect on the response. The ANOVA (Table 8.3) demonstrates that the model is highly significant. The smaller values of ''*P*" indicates that the corresponding coefficients are highly significant. Hence, the results given in Table 8.2 suggest that the influence of surface roughness (Ra), square of amplitude (y^2), square of surface roughness (Ra^2), product of frequency and surface roughness ($f \times Ra$) and the product of amplitude and surface roughness ($y \times Ra$) are non-

significant and therefore has been removed from the full model for further improvement. By doing so, the full model for $\alpha.\mu$ reduces to:

$$\alpha.\mu = 0.009543 - 0.000161 \times f - 0.002489 \times y + 0.000003 \times f^2 + 0.000152 \times f \times y \quad (8.8)$$

Furthermore, the significance of each coefficient in the full model has been examined by the *P*-values and the results are listed in Table 8.3.

Table 8.3 Analysis of Variance for $\alpha.\mu$ (Full model)

Source	**DF**	**Seq SS**	**Adj SS**	**Adj MS**	**F**	**P**
Regression	9	0.000023	0.000023	0.000003	492.5	0.000
Linear	3	0.000020	0.000001	0.000000	59.19	0.000
Square	3	0.000001	0.000001	0.000000	57.15	0.000
Interaction	3	0.000002	0.000002	0.000001	121.3	0.000
Residual Error	115	0.000001	0.000001	0.000000		
Total	124	0.000023				

Further, ANOVA has been performed on the reduced model and the results are presented in Tables 8.4 and 8.5 which establishes that the model is highly significant. Thus, expression (8.8) represents the uncoded form of final empirical model for $\alpha.\mu$.

Table 8.4 Estimated Regression Coefficients for $\alpha.\mu$ (Reduced model)

Term	**Coef**	**SE Coef**	**T**	**P**
Constant	0.009543	0.000203	46.987	0.000
f	-0.000161	0.000014	-11.173	0.000
y	-0.002489	0.000242	-10.286	0.000
f×*f*	0.000003	0.000000	12.153	0.000
f×*y*	0.000152	0.000009	17.650	0.000
S = 0.00007710 R-Sq = 96.9% R-Sq (adj) = 96.8%				

Table 8.5 Analysis of Variance for $\alpha.\mu$ (Reduced model)

Source	DF	Seq SS	Adj SS	Adj MS	F	P
Regression	4	0.000023	0.000023	0.000006	950.6	0.000
Linear	2	0.000020	0.000001	0.000001	98.19	0.000
Square	1	0.000001	0.000001	0.000001	147.7	0.000
Interaction	1	0.000002	0.000002	0.000002	311.5	0.000
Residual Error	120	0.000001	0.000001	0.000000		
Lack-of-Fit	20	0.000001	0.000001	0.000000	14.51	0.000
Pure Error	100	0.000000	0.000000	0.000000		
Total	124	0.000023				

8.3.3 Response Surface Regression for Logarithmic Decrement (δ)

Response surface regression analysis has been carried out using the experimental values obtained for logarithmic damping decrement.

8.3.3.1 Analysis of Variance (ANOVA) for "δ"

Analysis of variance (ANOVA) has been performed to determine the significant and non-significant parameters affecting the logarithmic damping decrement. The ANOVA is carried out on the model for a confidence level of 95%. Estimated Regression Coefficients for δ are shown in Table 8.6 which depicts both the significant and non-significant parameters. Hence, the results given in Table 8.6 suggest that the influence of surface roughness (Ra), square of natural frequency (f^2), square of surface roughness (Ra^2), product of frequency and surface roughness ($f \times Ra$) and the product of amplitude and surface roughness ($y \times Ra$) are non-significant.

Table 8.6 Estimated Regression Coefficients for "δ"

Term	Coef	SE Coef	T	P
Constant	0.006004	0.000569	10.56	0.000
f	-0.000082	0.000034	-2.395	0.018
y	-0.018793	0.000870	-21.59	0.000
Ra	0.000049	0.000315	0.157	0.876
f×*f*	-0.000001	0.000001	-1.418	0.159
y×*y*	0.014343	0.000947	15.14	0.000
Ra×*Ra*	-0.000011	0.000087	-0.121	0.904
f×*y*	0.000233	0.000020	11.78	0.000
f×*Ra*	-0.000000	0.000006	-0.002	0.998
y×*Ra*	-0.000026	0.000240	0.110	0.913
S = 0.0001772 R-Sq = 94.5% R-Sq (adj) = 94.0%				

8.3.4 Surface and Contour Plots for $\alpha.\mu$

The effects of the parameter interactions in the form of response surfaces and contour plots on $\alpha.\mu$ are shown in Figs. 8.2–8.4. From Figs. 8.2–8.4, it is inferred that the effect of surface roughness on $\alpha.\mu$ is almost negligible. With the increase in surface roughness, kinematic coefficient of friction increases simultaneously thereby decreasing the dynamic slip and vice versa. Since the above parameters are interdependent, the product of these two is assumed to be constant irrespective of the surface roughness. During experimentation, each test has been performed for particular initial amplitude and frequency of excitation and the corresponding product of kinematic coefficient of friction and dynamic slip ratio are obtained. Several experiments have been carried out by varying these parameters and the corresponding values of the product have been ascertained. The averages of at least five readings have been taken to find out the product. The variations of kinematic coefficient of friction and dynamic slip ratio with natural frequency of vibration at the first mode of transverse vibration have been determined under different initial amplitudes of excitation and plotted as shown in Fig. 8.5. From the Fig. 8.5, it is evident that the product of coefficient of friction and slip ratio increases with the increase in the frequency and amplitude of vibration. These plots have been further used for

determining the theoretical values of logarithmic damping decrement using expression (8.4) and (8.5) for various specimens vibrating under different conditions of vibration. Furthermore, Tables 8.2-8.5 shows that the surface roughness is not the significant parameter.

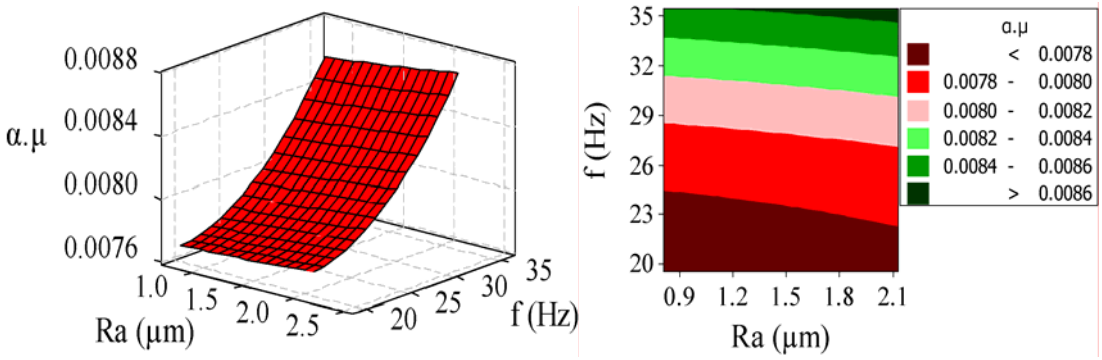

(a) Response surface plot (b) Contour plot

Fig. 8.2 Effect of surface roughness (Ra) and natural frequency (f) on the $\alpha.\mu$

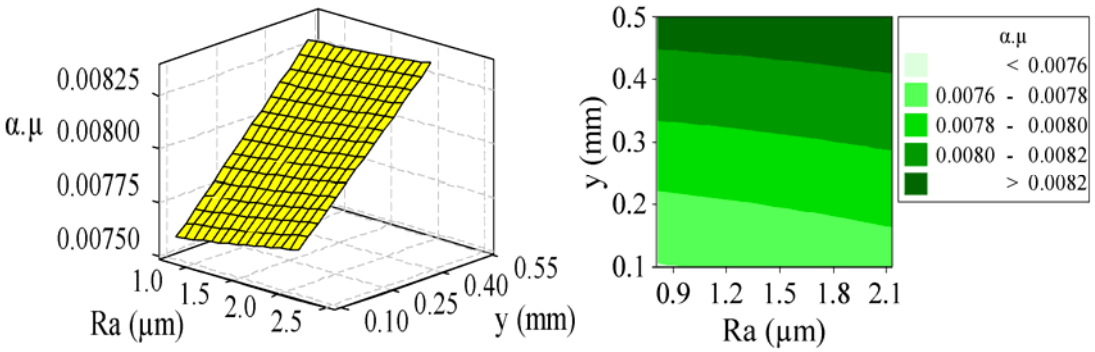

(a) Response surface plot (b) Contour plot

Fig. 8.3 Effect of surface roughness (Ra) and amplitude (y) on the $\alpha.\mu$

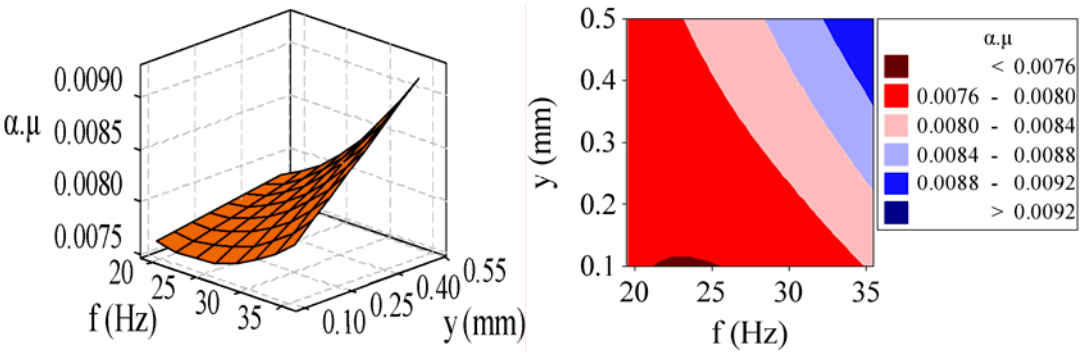

(a) Response surface plot (b) Contour plot

Fig. 8.4 Effect of natural frequency (f) and amplitude (y) on the $\alpha.\mu$

8.3.5 Surface and Contour Plots for "δ"

The effects of the parameter interactions in the form of response surfaces and contour plots on the logarithmic damping decrement are shown in Figs. 8.5–8.7.

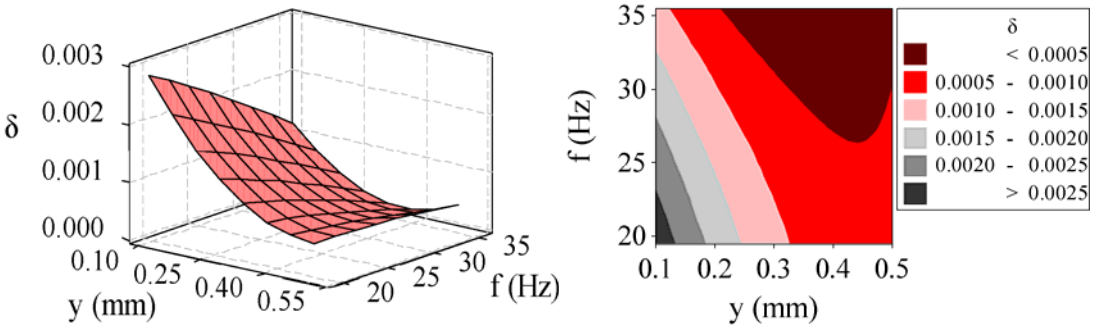

(a) Response surface plot (b) Contour plot

Fig. 8.5 Effect of natural frequency (f) and amplitude (y) on "δ"

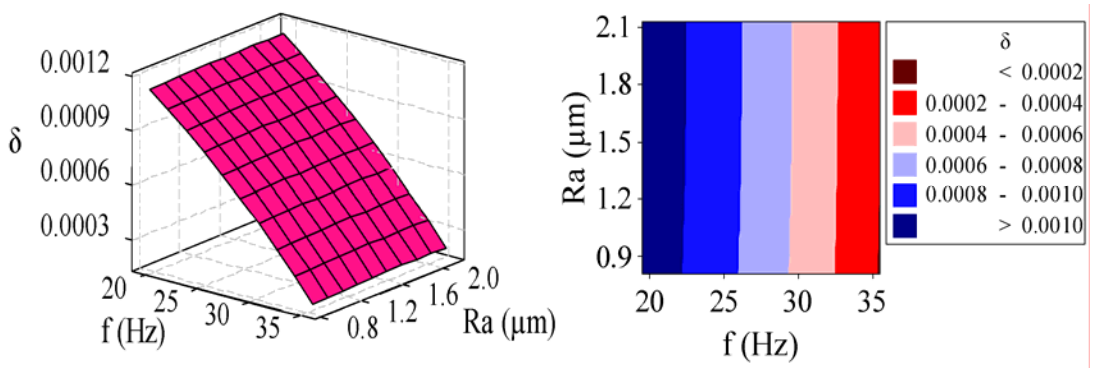

(a) Response surface plot (b) Contour plot

Fig. 8.6 Effect of surface roughness (Ra) and natural frequency (f) on "δ"

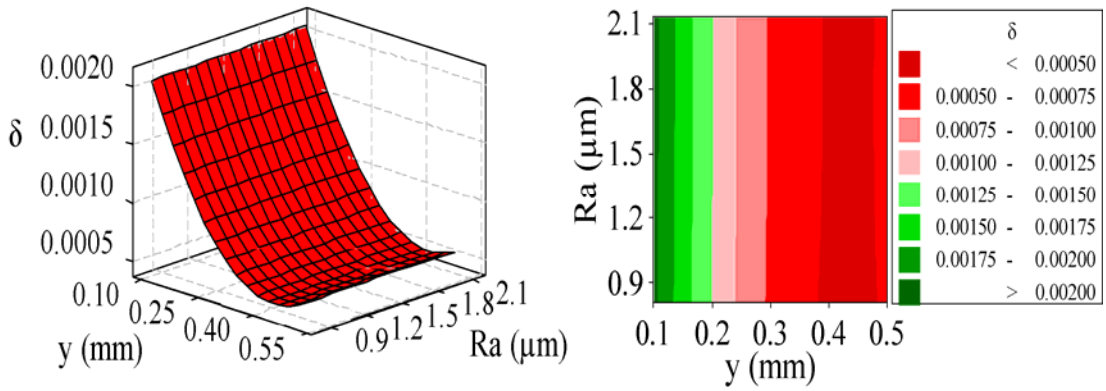

(a) Response surface plot (b) Contour plot

Fig. 8.7 Effect of surface roughness (Ra) and amplitude (y) on "δ"

The logarithmic damping decrement of layered and tack welded structures decreases with an increase in amplitude of excitation. This decrease is due to introduction of higher strain energy into the system compared to that of the dissipated energy due to interface friction as evident from expression (8.5). The parameter $\alpha.\mu$ is the key factor in the determination of damping capacity of layered and welded structures as evident from expression (8.5). It has been shown that $\alpha.\mu$ remains almost constant with respect to the surface roughness and the logarithmic damping decrement are constant for a given jointed interface of same material irrespective of the surface roughness. Normally, the logarithmic damping decrement increases with increase in kinematic coefficient of friction at the interfaces due to enhanced interfacial frictional energy loss. With increase in kinematic coefficient of friction, the friction force at the jointed interfaces increases resulting in an increase in the logarithmic damping decrement. However, the increase in kinematic coefficient of friction decreases the relative dynamic slip at the interfaces with a net result that the logarithmic damping decrement remains constant as evident from Figs. 8.6-8.7.

8.3.6 Plots of Main Effects of Interaction Parameters on $\alpha.\mu$ and δ

The plot of main effects for $\alpha.\mu$ and δ are shown in Fig. 8.8. These plots are used to compare the changes in the mean levels to know the factors which influence the response the most. The surface roughness effect line is almost parallel to the X-axis which indicates that the effect of surface roughness on $\alpha.\mu$ and δ is almost negligible. Further, the slope of amplitude is more than the frequency line with respect to the X-axis which shows that the effect of amplitude is more pronounced than frequency on both the responses as evident from Fig. 8.8.

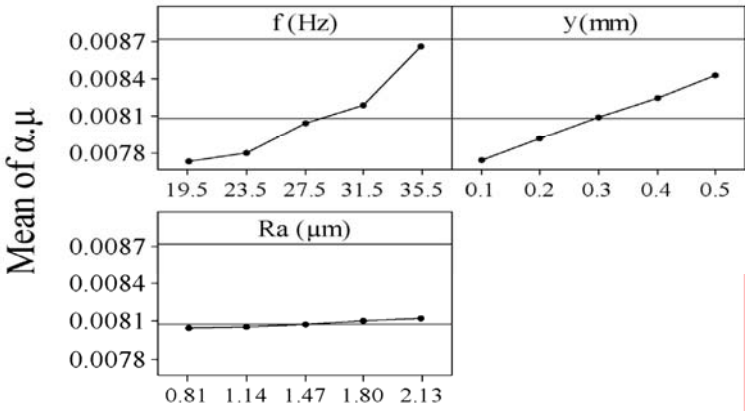

Fig. 8.8 Main effects plot: (a) Response is $\alpha.\mu$

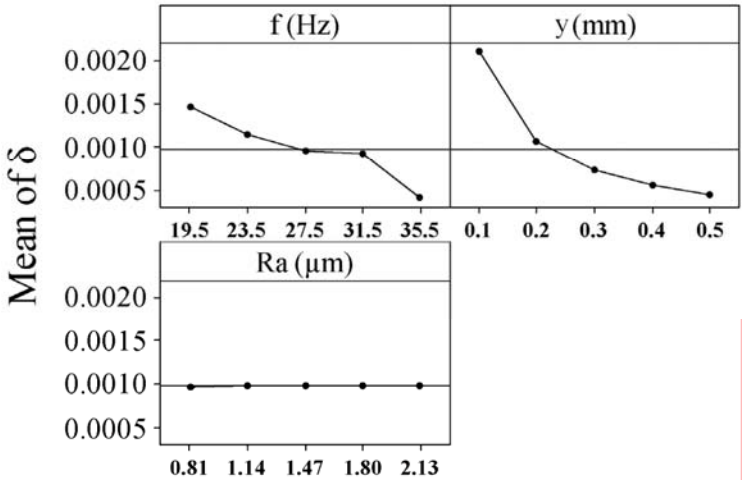

Fig. 8.8 Main effects plot: (b) Response is "δ"

8.3.7 Residual Plots for $\alpha.\mu$ and δ

The regression model is used for determining the residuals of each individual experimental run. The difference between the measured values and predicted values are called residuals. The residuals are calculated and ranked in ascending order. The normal probabilities of residuals for both the responses are shown in Fig. 8.9.

The normal probability plot is used to vary the normality assumptions. As shown in Fig. 8.9, the data are spread roughly along the straight line for both $\alpha.\mu$ and δ indicating that the data are normally distributed.

Fig. 8.10 shows the residuals against the observation order. Fig. 8.10 is used to show the correlation between the residuals. From the Fig. 8.10, it is emphasized that a tendency to have runs of positive and negative residuals indicates the existence of a certain correlation. Also the plots show that the residuals are distributed evenly in both positive and negative directions along the run. Hence, the data is said to be independent.

Fig. 8.11 indicates the residuals versus fitted values, showing the maximum variation of -0.0002 to 0.0002 and -0.0004 to 0.0004 for $\alpha.\mu$ and δ, respectively between the measured and the fitted values. These plots do not reveal any obvious pattern and therefore the fitted models are ample.

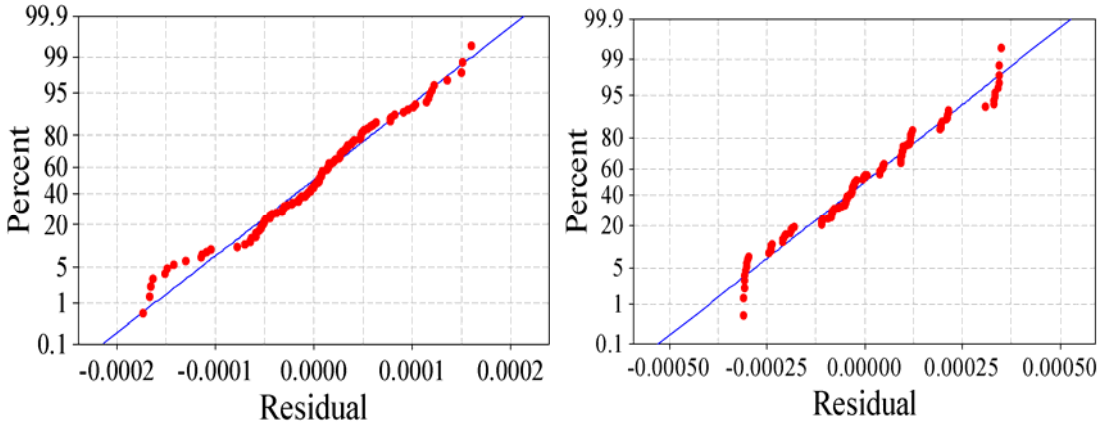

(a) Response is "$\alpha.\mu$" (b) Response is "δ"

Fig. 8.9 Normal probability plot of the residuals

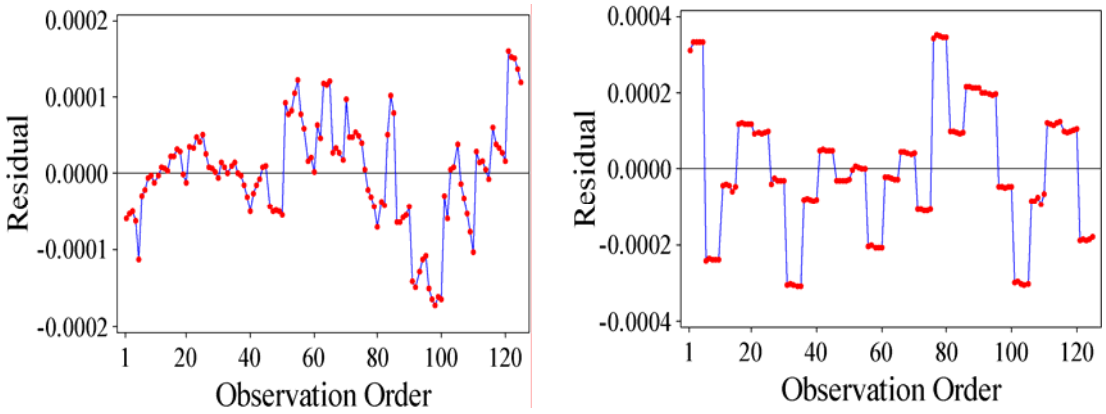

(a) Response is "$\alpha.\mu$" (b) Response is "δ"

Fig. 8.10 Residual versus order of the data

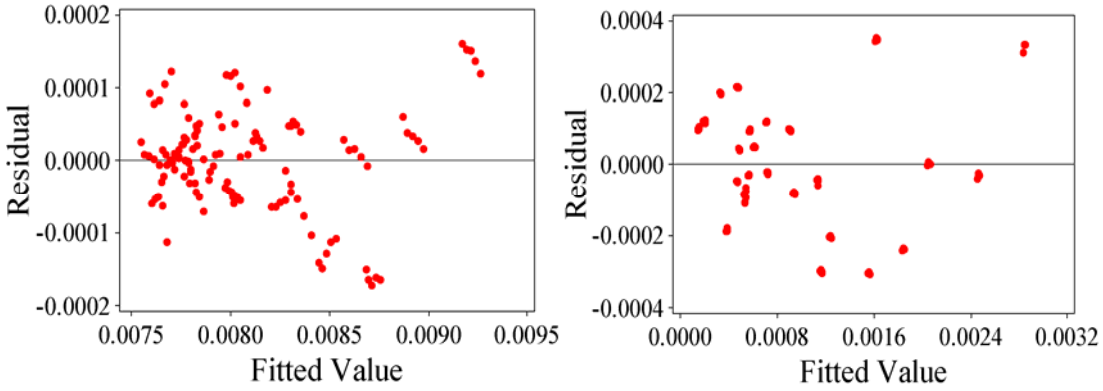

(a) Response is "$\alpha.\mu$" (b) Response is "δ"

Fig. 8.11 Residuals versus the fitted values

8.3.8 Checking Adequacy of Mathematical Models

The goodness of fit for the mathematical models has also been tested by coefficient of determination (R^2) and adjusted coefficient of determination (R^2_{adj}). The R^2 is the proportion of the variation in the dependent variable explained by the regression model. On the other hand, R^2_{adj} is the coefficient of determination adjusted for the number of independent variables in the regression model. Unlike R^2, the R^2_{adj} may decrease if the variables considered in the model do not add significantly to the model fit. The R^2 and R^2_{adj} values of mathematical models for $\alpha.\mu$ are found to be 96.9 and 96.8%, respectively which clearly establish the excellent correlation between the experimental and the predicted values of the responses.

8.3.9 Validity of the $\alpha.\mu$ Model

The performance of the developed model has been tested using five experimental data which has not been used in the modeling process. The results for $\alpha.\mu$ as predicted by the developed model in expression (8.8) have been used to evaluate the theoretical values of the logarithmic damping decrement using the expression (8.5) and compared with the experimental ones. Further, the average percentage deviation between the experimental and theoretical values of logarithmic damping decrement has been calculated and presented in the Table 8.7.

Table 8.7 Comparison of the theoretical and experimental logarithmic decrement

Parameters				**Logarithmic damping decrement**		
f **(Hz)**	***y*** **(mm)**	***Ra*** **(μm)**	$\alpha.\mu$	**Experimental**	**Theoretical**	**Deviation (%)**
24.7	0.3	0.92	0.00777	0.000982	0.00093	5.6
30.6	0.5	1.52	0.00851	0.000642	0.00059	8.8
18.2	0.1	1.24	0.00763	0.00348	0.00321	8.4
20.4	0.2	1.76	0.00772	0.00198	0.00184	7.6
27.3	0.4	1.98	0.00851	0.000522	0.000483	8.1

Avg. deviation: 7.7 %

The results indicate that the model predicting the values of $\alpha.\mu$ has good validity with acceptable percentage deviation. Moreover, the Fig. 8.12 has been plotted between the theoretical and measured logarithmic damping decrement for comparison. Since the points are very close to form a straight line implying that the data is normal and validates the model developed.

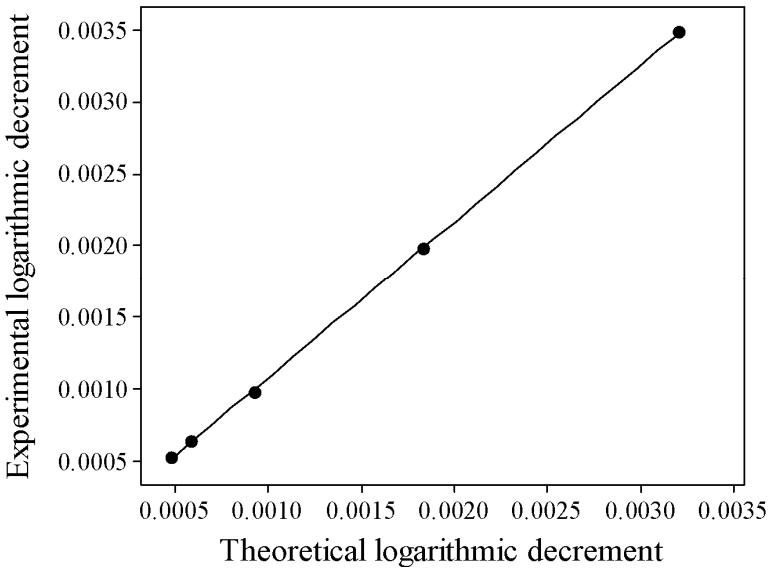

Fig. 8.12 Theoretical and experimental logarithmic damping decrement

8.4 Tack Number, Amplitude, Surface Roughness and Young's Modulus as Input Variables

The layered and tack welded cantilever beam model with uniform pressure distribution at the interfaces as shown in Fig. 8.1 has been considered to find out the logarithmic damping decrement. The details of the specimen are given in Table 8.8.

Table 8.8 Details of specimens used for layered and jointed beams

Thickness of the specimen (mm)	Width of the specimen (mm)	Number of layers	Cantilever length (mm)	Type of Welding	Number of Tack Welds	Material and Modulus of elasticity (GPa)
3	40.2	2	520.6	Tack Weld	10,20,30	Mild Steel (203.41)
3	40.2	2	520.6	Tack Weld	10,20,30	Aluminium (69.45)

In the present section, RSM approach has been implemented to evaluate the mathematical models of logarithmic damping decrement for mild steel and aluminium specimens considering various input control variables.

The logarithmic damping decrement is influenced by number of tack joints, initial amplitude of excitation, surface roughness and Young's Modulus. The relationship of logarithmic damping decrement with respect to the first two variables could be estimated by a first-degree model. For the surface roughness and Young's Modulus of the material, a second and third degree model is necessary. A suitable second and third order polynomial involving linear, quadratic, cubic and cross terms has been selected considering the statistical parameters; coefficient of determination (R^2), adjusted R^2, standard error of regression and analysis of variance (ANOVA). In the present work, the input variables are tack number (N), initial amplitude of vibration (y), surface roughness (Ra) and Young's Modulus (Y) and the output response is the logarithmic damping decrement (δ).

The logarithmic damping decrement is analyzed with a standard central composite design (CCD) technique. The star points are at the face of the cube portion which corresponds to the β-value of 1 and this is commonly referred to as a face-centered CCD and the centre points are the locations with coded value set to 0.

The important factors and their levels are shown in Table 8.9. The response surface analysis is carried out in terms of the fitted surface. The lack of fit and the degree of significance of the model are tested by the analysis of variance (ANOVA) using the Design Expert-8 software. The CCD design of experimental runs with independent control variables in uncoded forms and responses are shown in Table 8.10

Table 8.9 Important factors and their levels

Sl. No	Factor	Notation	Unit	Levels		
1	Modulus of Elasticity	Y	GPa	69.45	110.32	203.41
2	Tack number	N		10	20	30
3	Amplitude	y	mm	0.1	0.2	0.3
4	Surface roughness	Ra	μm	0.88	1.53	2.18

Table 8.10 Logarithmic decrement (δ) response for CCD design of experiment

Runs	Factors				Response
	Y **(GPa)**	***N***	***y*** **(mm)**	***Ra*** **(μm)**	δ
1	110.32	10	0.3	1.53	0.00379
2	110.32	20	0.2	1.53	0.00537
3	110.32	30	0.2	2.18	0.00397
4	110.32	20	0.1	0.88	0.00896
5	110.32	10	0.2	1.53	0.00624
6	203.41	20	0.2	1.53	0.00268
7	110.32	20	0.1	1.53	0.00874
8	110.32	30	0.2	1.53	0.00378
9	69.45	20	0.2	1.53	0.00778
10	110.32	20	0.3	1.53	0.00366
11	69.45	30	0.1	0.88	0.01152
12	69.45	30	0.3	0.88	0.00437
13	110.32	20	0.2	1.53	0.00485
14	69.45	10	0.1	2.18	0.01711
15	203.41	30	0.1	0.88	0.00411
16	69.45	30	0.1	2.18	0.01138
17	203.41	30	0.1	2.18	0.00408
18	110.32	20	0.3	1.53	0.00333
19	110.32	30	0.3	1.53	0.00284
20	203.41	10	0.1	2.18	0.00629
21	203.41	10	0.3	2.18	0.00212
22	69.45	10	0.1	0.88	0.01781
23	69.45	10	0.3	0.88	0.00596
24	203.41	10	0.1	0.88	0.00634
25	203.41	10	0.3	0.88	0.00211
26	69.45	10	0.3	2.18	0.00599
27	203.41	30	0.3	2.18	0.00153
28	69.45	30	0.3	2.18	0.00433
29	110.32	20	0.2	1.53	0.00493
30	203.41	30	0.3	0.88	0.00151

8.4.1 Quadratic and Cubic Response surface models

The results as shown in Table 8.10 are used as the input data to the Design Expert-8 software for further analysis. Initially, the sequential or extra sums of squares for the linear, quadratic and cubic terms in the model are computed and a fit summary based on this has been generated as presented in the Table 8.11.

Table 8.11 Model Fit summary

	Sequential	**Lack of Fit**	**Adjusted**	**Predicted**	
Source	**p-value**	**p-value**	**R-Squared**	**R-Squared**	
Linear	< 0.0001	< 0.0001	0.8456	0.7569	Not-suggested
2FI	0.2409	< 0.0001	0.8608	0.4358	Not-suggested
Quadratic	< 0.0001	0.0058	0.9841	0.9782	Suggested
Cubic	0.0013	0.8792	0.9996	0.9990	Suggested

The Fit Summary output as shown in Table 8.11 has been examined without performing any transformation of the response. The summary revealed that the quadratic and cubic models are statistically significant and therefore used for fitting the data. Figs. 8.13 and 8.14 show the standard error of the design which is found to be uniform and thus favorable. The Central composite design space cube representing the input variables at the star points and the face of the cube is shown in Fig. 8.15.

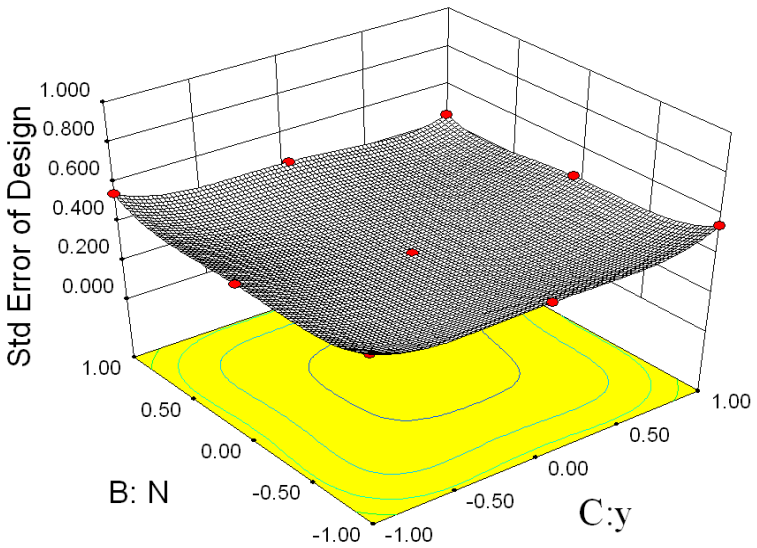

Fig. 8.13 Surface plot for the variation of standard error in the design space

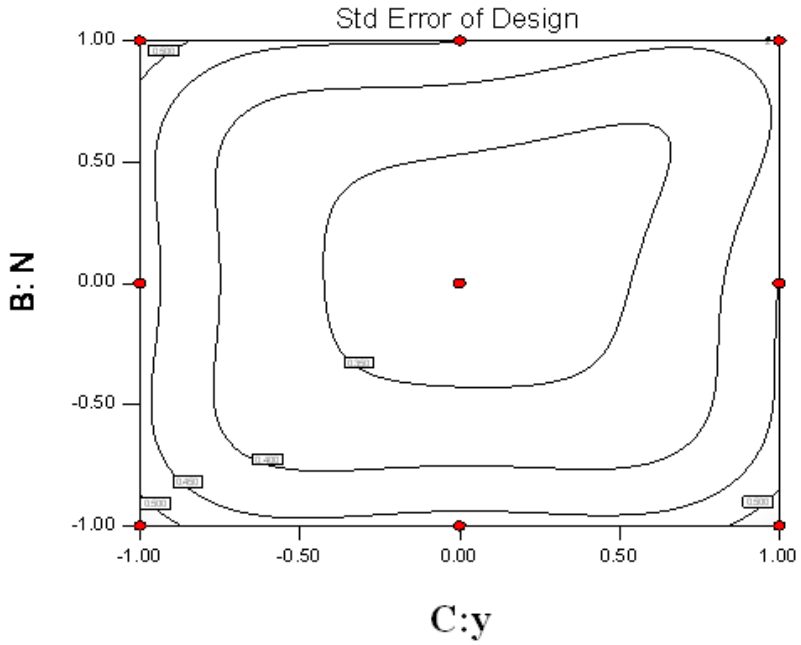

Fig. 8.14 Contour plot for the variation of standard error in the design space

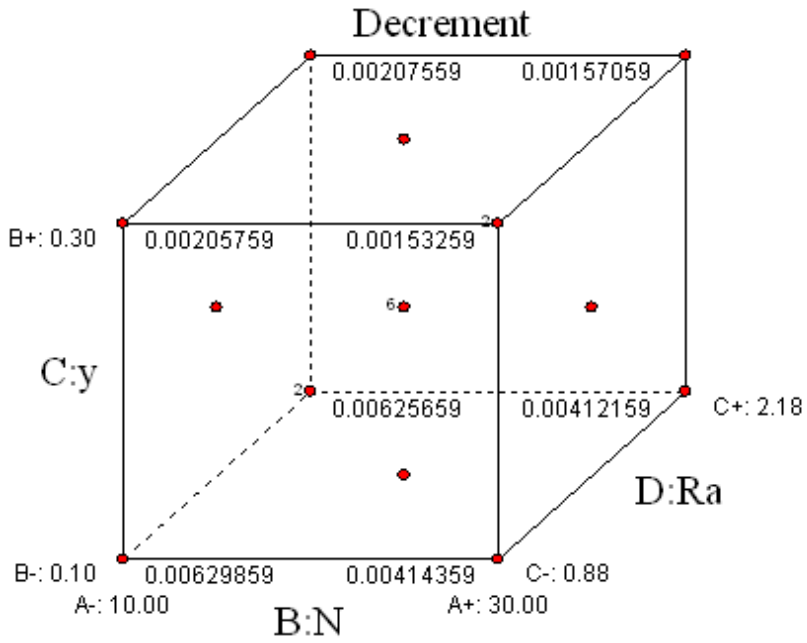

Fig. 8.15 Central composite design space cube

The following expression of quadratic model in terms of the uncoded factors has been found out for the logarithmic damping decrement:

$$\begin{aligned}\delta = {} & 0.042 - 2.16\,\mathrm{E}{-4}\times Y - 5.73\,\mathrm{E}{-4}\times N - 1.3\,\mathrm{E}{-1}\times y + 2.67\,\mathrm{E}{-3}\times Ra \\ & +4\,\mathrm{E}{-6}\times N\times N + 1.39\,\mathrm{E}{-1}\times y\times y - 9.89\,\mathrm{E}{-4}\times Ra\times Ra + 1\,\mathrm{E}{-6}\times Y\times N \\ & +2.09\,\mathrm{E}{-4}\times Y\times y + 7.77\,\mathrm{E}{-4}\times N\times y + 9\,\mathrm{E}{-6}\times N\times Ra + 4.26\,\mathrm{E}{-4}\times y\times Ra\end{aligned} \tag{8.9}$$

The analysis has been further carried out for the cubic model and the following expression of cubic model in terms of the uncoded factors has been found out for the logarithmic damping decrement of welded beam:

$$\begin{aligned}\delta = &+5.11\text{E}-3-2.39\text{E}-3\times Y-1.06\text{E}-3\times N-3.03\text{E}-3\times y\\ &+3.06\text{E}-5\times Ra+6.69\text{E}-4\times Y\times N+1.56\text{E}-3\times Y\times y\\ &+7.83\text{E}-7\times Y\times Ra+8.44\text{E}-4\times N\times y-5.33\text{E}\\ &-6\times N\times Ra+2.12\text{E}-5\times y\times Ra+1.86\text{E}-4\times Y^2\\ &-2.82\text{E}-5\times N^2+1.46\text{E}-3\times y^2+5.29\text{E}-6\times Ra^2\\ &-4.02\text{E}-4\times Y\times N\times y+1.18\text{E}-6\times Y\times N\times Ra\\ &-1.47\text{E}-6\times Y\times y\times Ra+1.86\text{E}-6\times N\times y\times Ra\\ &+1.92\text{E}-4\times Y^2\times N-1.89\text{E}-4\times Y^2\times y\\ &-1.69\text{E}-5\times Y^2\times Ra+2.49\text{E}-4\times Y\times N^2\\ &-1.01\text{E}-3\times Y\times y^2-8.74\text{E}-6\times Y\times Ra^2\\ &-1.10\text{E}-4\times N^2\times y+3.01\text{E}-6\times N^2\times Ra\\ &-4.43\text{E}-4\times N\times y^2-5.40\text{E}-6\times N\times Ra^2\\ &-2.73\text{E}-5\times y^2\times Ra-6.05\text{E}-8\times y\times Ra^2\end{aligned} \tag{8.10}$$

8.4.2 Analysis of variance (ANOVA) for full quadratic and cubic models

The tests for significance of the regression model, individual model coefficients and lack-of-fit are performed to ensure adequacy of the model. Usually an ANOVA table is used to summarize the statistical data obtained from the tests.

8.4.2.1 Quadratic Model

The ANOVA result for the quadratic response full model of logarithmic damping decrement is presented in Table 8.13. The value of "P" in Table 8.12 is less than 0.05 indicating that the model and its terms have a significant effect on the response. The Model F-value of 73.29 as given in Table 8.12 implies that the model is significant. There is only 0.01% chance that a high "Model F-Value" could occur due to noise. Model F-value is calculated to test the adequacy of the model and is mathematically expressed as;

$$Model F-value=\frac{R^2/k}{\left(1-R^2\right)/\left[z-\left(k+1\right)\right]} \tag{8.11}$$

where k and z are degrees of freedom and number of experimental runs for RSM analysis, respectively.

Table 8.12 Analysis of Variance for full quadratic model

Source	Sum of Squares	df	Mean Square	F Value	p-value Prob > F
Regression	0.000469	14	0.000033	73.29	0.0000
Linear	0.000385	4	0.000023	49.86	0.0000
Square	0.000036	4	0.000009	19.19	0.0000
Interaction	0.000048	6	0.000008	17.48	0.0000
Residual Error	0.000007	15	0.000000		
Lack of Fit	0.000007	12	0.000001	7.86	0.0058
Pure Error	0.000000	3	0.000000		
Total	0.000475	29			

Further, the significance of each coefficient in the full model has been examined by the P-values and the results are listed in Table 8.13. The value of "Prob > F" less than 0.050 indicates that the model terms are significant as shown in Table 8.13. In this case Y, N, a, Y^2, a^2, $Y \times N$, $Y \times a$ and $N \times a$ are significant model terms.Values greater than 0.05 indicate that the model terms are insignificant. The reduction of terms may improve the model further if there are many insignificant terms.The "Lack of Fit F-value" of 7.86 implies that this is significant. There is only 0.5% chance that a "Lack of Fit F-value" is insignificant and could occur due to noise. The model can be improved further by eliminating the insignificant interaction terms from it. Insignificant factors are removed from the full model by implementing the backward elimination technique for its improvement. Thus, the full quadratic model for the logarithmic decrement (δ) has been reduced to:

$$\begin{aligned}\delta = {} & 0.042 - 1.33\,\mathrm{E}{-4} \times Y - 3.95\,\mathrm{E}{-4} \times N - 1.26\,\mathrm{E}{-1} \times y + 1.33\,\mathrm{E}{-1} \times y \times y \\ & + 1\mathrm{E}{-6} \times Y \times N + 2.06\,\mathrm{E}{-4} \times Y \times y + 7.77\,\mathrm{E}{-4} \times N \times y\end{aligned} \tag{8.12}$$

Table 8.13 Estimated Regression Coefficients for full quadratic model

Factor	Coefficient Estimate	Standard Error	Probability (P)	
Intercept	0.042202	0.002295	0.000	
A-Y	-0.000216	0.000029	0.000	
B-N	-0.000573	0.000162	0.003	
C-y	-0.130057	0.016008	0.000	
D-Ra	0.002671	0.003474	0.454	(Not-Significant)
A^2	0.000000	0.000000	0.001	
B^2	0.000004	0.000004	0.284	(Not-Significant)
C^2	0.139127	0.035910	0.001	
D^2	-0.000989	0.001136	0.398	(Not-Significant)
AB	0.000001	0.000000	0.004	
AC	0.000209	0.000025	0.000	
AD	0.000001	0.000004	0.865	(Not-Significant)
BC	0.000777	0.000160	0.000	
BD	0.000009	0.000026	0.723	(Not-Significant)
CD	0.000426	0.002564	0.870	(Not-Significant)

8.4.2.2 Cubic Model

The ANOVA result for the cubic response full model of logarithmic damping decrement is presented in Table 8.14. The value of "P" in Table 8.14 is less than 0.05 indicating that the model and its terms have a significant effect on the response. Further, the significance of each coefficient in the full cubic model has been examined by the P-values and the results are listed in Table 8.14.

Table 8.14 Analysis of Variance for full cubic model

Source	Sum of Squares	df	Mean Square	F -Value	p-value Prob > F
Model	1.378E-003	30	4.593E-005	466.64	0.0001
A-Y	4.625E-005	1	4.625E-005	469.95	0.0001
B-N	9.140E-006	1	9.140E-006	92.86	0.0001
C-y	7.224E-005	1	7.224E-005	733.97	0.0001
D-Ra	7.392E-009	1	7.392E-009	0.075	0.7851
AB	1.771E-005	1	1.771E-005	179.97	0.0001
AC	9.172E-005	1	9.172E-005	931.98	0.0001
AD	2.369E-011	1	2.369E-011	2.407E-004	0.9877
BC	2.688E-005	1	2.688E-005	273.16	0.0001
BD	1.096E-009	1	1.096E-009	0.011	0.9164
CD	1.688E-008	1	1.688E-008	0.17	0.6803
A^2	6.180E-007	1	6.180E-007	6.28	0.0151
B^2	1.461E-008	1	1.461E-008	0.15	0.7015
C^2	4.108E-005	1	4.108E-005	417.42	0.0001
D^2	5.331E-010	1	5.331E-010	5.416E-003	0.9416
ABC	4.161E-006	1	4.161E-006	42.28	0.0001
ABD	3.686E-011	1	3.686E-011	3.746E-004	0.9846
ACD	5.490E-011	1	5.490E-011	5.578E-004	0.9812
BCD	8.844E-011	1	8.844E-011	8.986E-004	0.9762
A^2B	4.552E-007	1	4.552E-007	4.62	0.0358
A^2C	4.370E-007	1	4.370E-007	4.44	0.0396
A^2D	3.545E-009	1	3.545E-009	0.036	0.8502
AB^2	7.637E-007	1	7.637E-007	7.76	0.0073
AC^2	1.348E-005	1	1.348E-005	136.95	0.0001

Source	Sum of Squares	df	Mean Square	F -Value	p-value Prob > F
AD^2	9.996E-010	1	9.996E-010	0.010	0.9201
B^2C	1.480E-007	1	1.480E-007	1.50	0.2253
B^2D	1.109E-010	1	1.109E-010	1.127E-003	0.9201
BC^2	2.587E-006	1	2.587E-006	26.29	0.0001
BD^2	3.823E-010	1	3.823E-010	3.884E-003	0.9505
C^2D	9.687E-009	1	9.687E-009	0.098	0.7549
CD^2	4.611E-014	1	4.611E-014	4.685E-007	0.995
A^3	0.000	0			
B^3	0.000	0			
C^3	0.000	0			
D^3	0.000	0			
Residual	5.511E-006	56	9.842E-008		
Lack of Fit	5.511E-006	50	1.102E-007	21.54	0.0073
Pure Error	0.000	6	0.000		
Cor Total	1.383E-003	86			

The Model F-value of 466.64 as given in Table 8.14 implies that the model is significant. There is only 0.01% chance that a high "Model F-Value" could occur due to noise. Values of “P” for model terms, greater than 0.05 indicate that the model terms are insignificant. In this case, Ra, $Y{\times}Ra$, $N{\times}Ra$, $y{\times}Ra$, Y^2, N^2, Ra^2, $Y{\times}N{\times}Ra$, $Y{\times}y{\times}Ra$, $N{\times}y{\times}Ra$, $Y^2{\times}N$, $Y^2{\times}y$, $Y^2{\times}Ra$, $Y{\times}N^2$, $Y{\times}Ra^2$, $N^2{\times}y$, $N^2{\times}Ra$, $N{\times}Ra^2$, $y^2{\times}Ra$, $y{\times}Ra^2$ are the insignificant terms. The elimination of these terms may improve the model further. The "Lack of Fit F-value" of 21.54 implies that this is significant. There is only 0.3% chance that a "Lack of Fit F-value" is insignificant and could occur due to noise.

The model can be improved further by eliminating the insignificant interaction terms from it. Insignificant factors are removed from the full model by implementing

the backward elimination technique for its improvement. Thus, the full cubic model for the logarithmic decrement *(δ)* has been reduced to:

$$\begin{aligned}\delta = {} & 5.10\text{E}-3-2.22\text{E}-3\times Y-1.06\text{E}-3\times N-3.11\text{E}-3\times y+6.75\text{E}-4\times Y\times N \\ & +1.56\text{E}-3\times Y\times y+8.45\text{E}-4\times N\times y+1.87\text{E}-4\times Y^2 \\ & +1.46\text{E}-3\times y^2-3.99\text{E}-4\times Y\times N\times y+1.97\text{E}-4\times Y^2\times N \\ & -1.88\text{E}-4\times Y^2\times y-1.02\text{E}-3\times Y\times y^2-4.49\text{E}-4\times N\times y^2\end{aligned} \tag{8.13}$$

8.4.3 Analysis of variance (ANOVA) for reduced quadratic and cubic models

The tests for significance of the reduced quadratic and cubic regression models, individual model coefficients and lack-of-fit have been performed to check adequacy of the models. The resulting ANOVA tables have been used to summarize the statistical data obtained from these tests.

8.4.3.1 Quadratic Model

The resulting ANOVA table for the reduced quadratic model for logarithmic damping decrement is shown in Table 8.15. The Estimated Regression Coefficients in the reduced quadratic model for logarithmic damping decrement is shown in Table 8.16.

The Model F-value of 162.60 in Table 8.15 implies that the model is significant. There is only 0.01% chance that this high "Model F-Value" might be due to noise. The value of "Prob > F" less than 0.050 indicate that the model terms are significant. The "Lack of Fit F-value" of 22.37 implies that this is significant. There is only 0.01% chance that a "Lack of Fit F-value" is large due to noise

Table 8.15 Analysis of Variance for reduced quadratic model

Source	Sum of Squares	df	Mean Square	F -Value	p-value Prob > F
Regression	0.000468	8	0.000058	162.60	0.000
Linear	0.000384	3	0.000042	117.66	0.000
Square	0.000036	2	0.000017	47.92	0.000
Interaction	0.000047	3	0.000016	43.85	0.000

Source	Sum of Squares	df	Mean Square	F -Value	p-value Prob > F
Residual Error	0.000008	21	0.000000		
Lack of Fit	0.000007	8	0.000001	22.37	0.000
Pure Error	0.000001	13	0.000000		
Total	0.000475	29			

Table 8.16 Estimated Regression Coefficients for reduced quadratic model

Factor	Coefficient Estimate	df	Standard Error	Probability (P)
Intercept	0.041678	1	0.001545	0.000
A-Y	-0.000134	1	0.000020	0.000
B-N	-0.000395	1	0.000044	0.000
C-y	-0.126231	1	0.012020	0.000
A^2	0.000000	1	0.000000	0.000
C^2	0.133252	1	0.027624	0.000
AB	0.000001	1	0.000000	0.001
AC	0.000206	1	0.000022	0.000
BC	0.000777	1	0.000142	0.000

8.4.3.2 Cubic Model.

The ANOVA table for the reduced cubic model for logarithmic damping decrement is shown in Table 8.17. The Model F-value of 1197.31 in Table 8.17 implies that the model is significant. There is only 0.01% chance that this high "Model F-Value" might be due to noise.

Table 8.17 Analysis of Variance for reduced cubic model

Source	Sum of Squares	df	Mean Square	F Value	p-value Prob > F
Model	1.377E-003	13	1.059E-004	1197.31	0.000
A-Y	9.920E-005	1	9.920E-005	1121.43	0.000
B-N	1.261E-005	1	1.261E-005	142.56	0.000
C-y	1.737E-004	1	1.737E-004	1963.25	0.000
AB	1.810E-005	1	1.810E-005	204.56	0.000
AC	9.207E-005	1	9.207E-005	1040.88	0.000
BC	2.703E-005	1	2.703E-005	305.57	0.000
A^2	6.426E-007	1	6.426E-007	7.26	0.000
C^2	4.088E-005	1	4.088E-005	462.17	0.000
ABC	4.127E-006	1	4.127E-006	46.65	0.000
A^2B	4.813E-007	1	4.813E-007	5.44	0.000
A^2C	4.304E-007	1	4.304E-007	4.87	0.000
AC^2	1.365E-005	1	1.365E-005	154.35	0.000
BC^2	2.661E-006	1	2.661E-006	30.08	0.000
Residual	6.457E-006	73	8.846E-008		
Lack of Fit	6.457E-006	67	9.638E-008	27.64	0.000
Pure Error	0.000	6	0.000		
Cor Total	1.383E-003	86			

8.4.4 Surface and Contour plots for logarithmic damping decrement (δ)

The effects of the interactions of the parameter such as; tack number/amplitude, tack number/surface roughness, and amplitude/surface roughness on the logarithmic damping decrement are shown in Figs. 8.16–8.21. The initial amplitude of excitation of free vibration is an important parameter influencing the logarithmic damping decrement of layered and welded structures. The logarithmic damping decrement of such structures decreases with an increase in initial amplitude of excitation. This

decrease is due to the introduction of higher strain energy into the system compared to that of the dissipated energy due to interface friction.

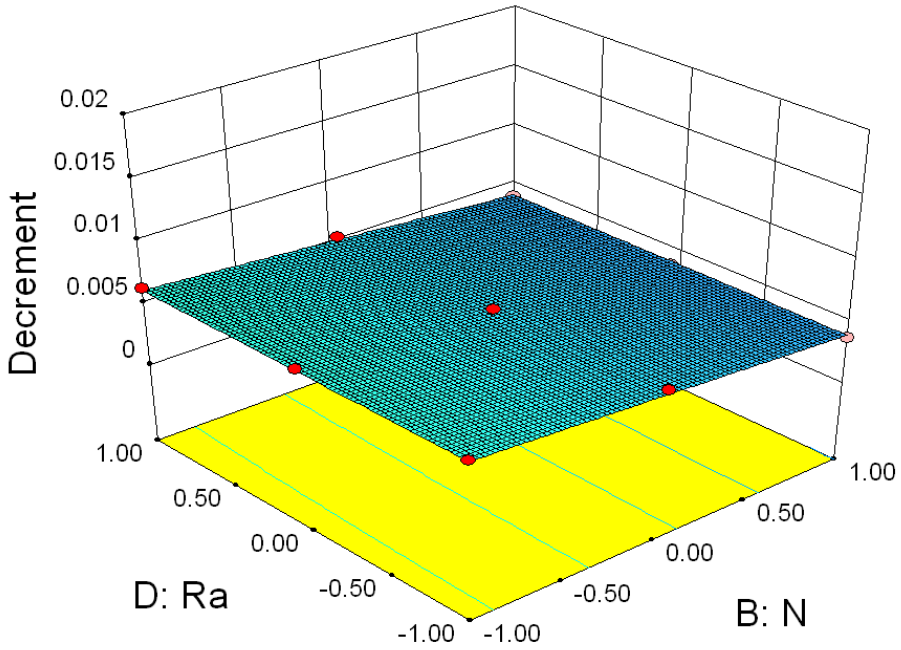

Fig. 8.16 Response surface plot: effect of tack number and surface roughness on "δ"

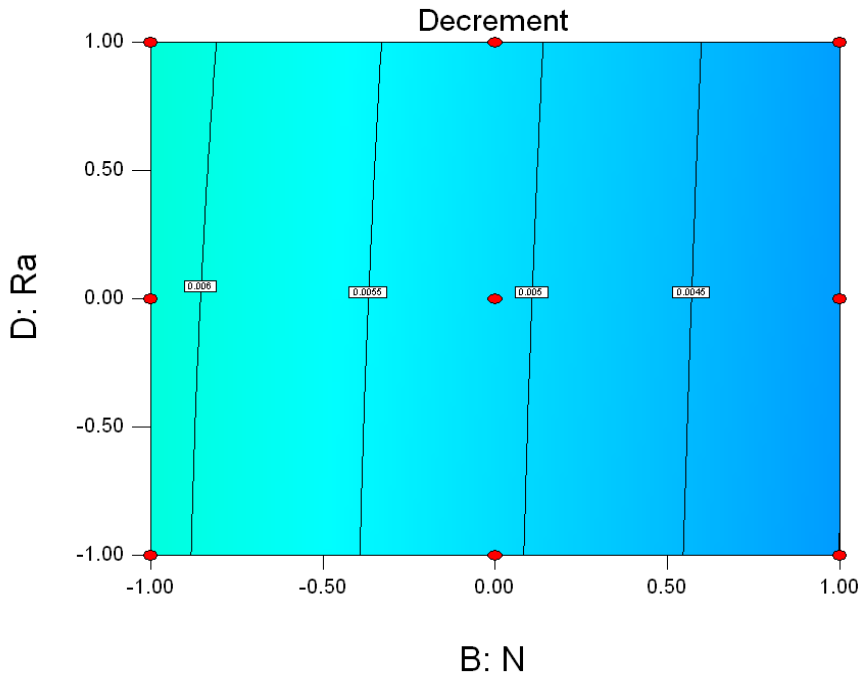

Fig. 8.17 Contour plot: effect of tack number and surface roughness on "δ"

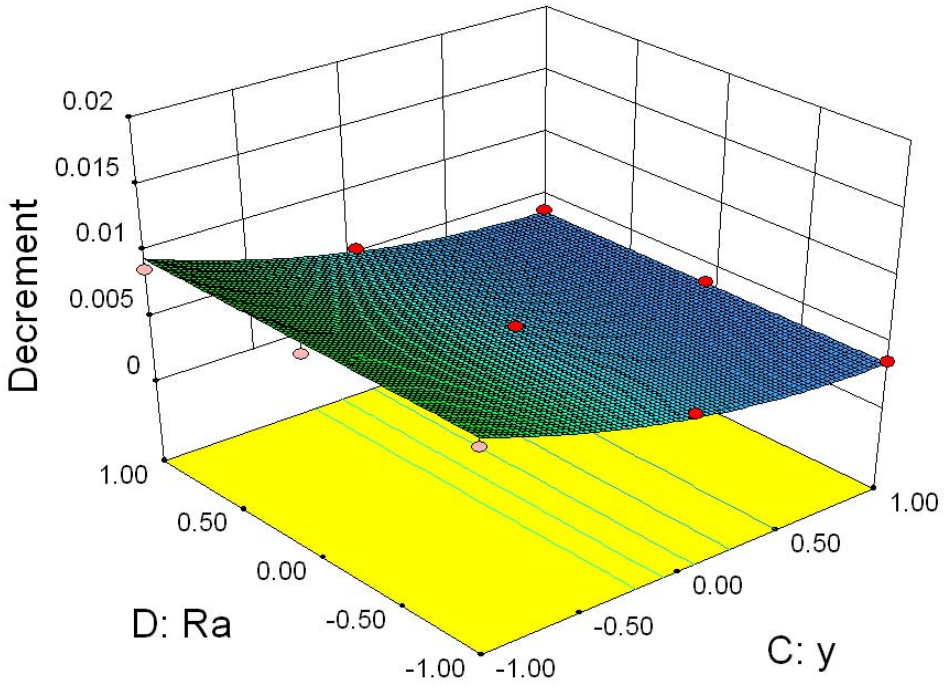

Fig. 8.18 Response surface plot: Effect of amplitude and surface roughness on "δ"

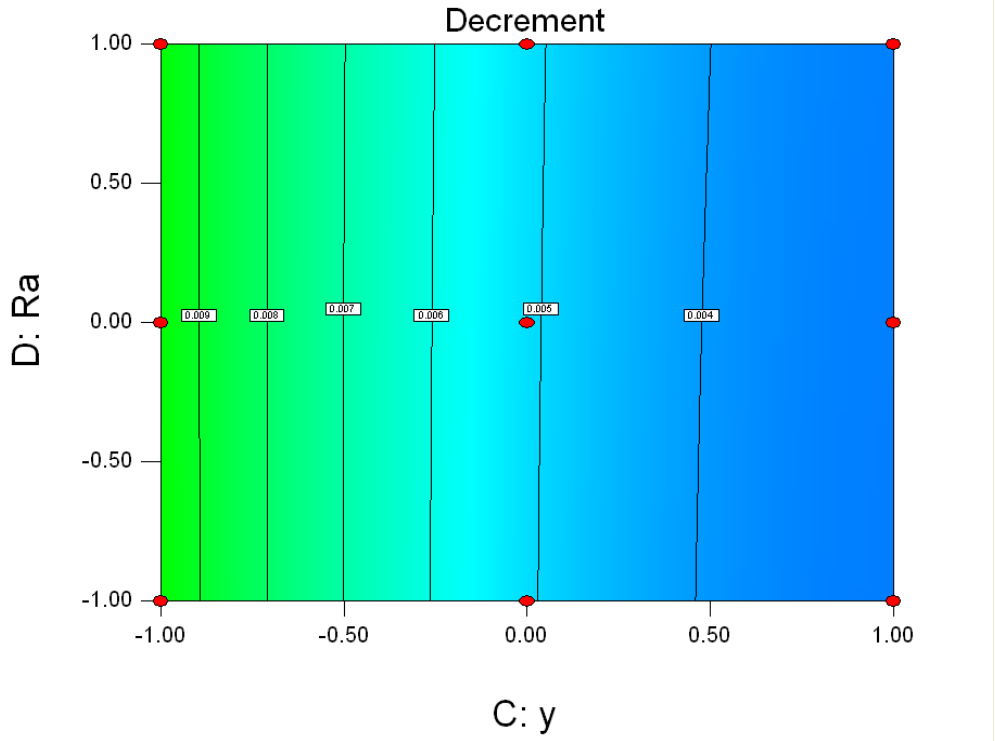

Fig. 8.19 Contour plot: Effect of amplitude and surface roughness on "δ"

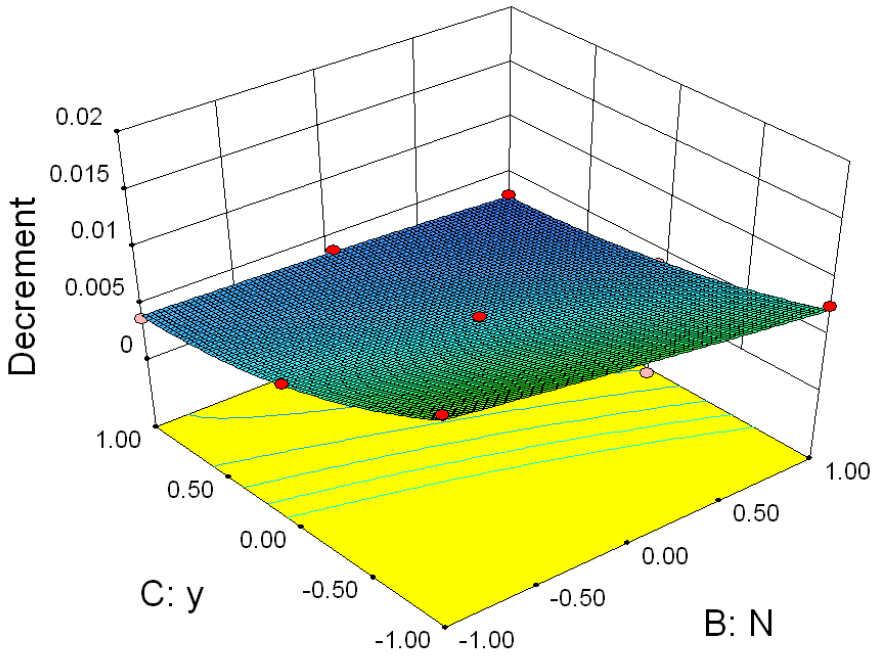

Fig. 8.20 Response surface plot: Effect of amplitude and tack number on "δ"

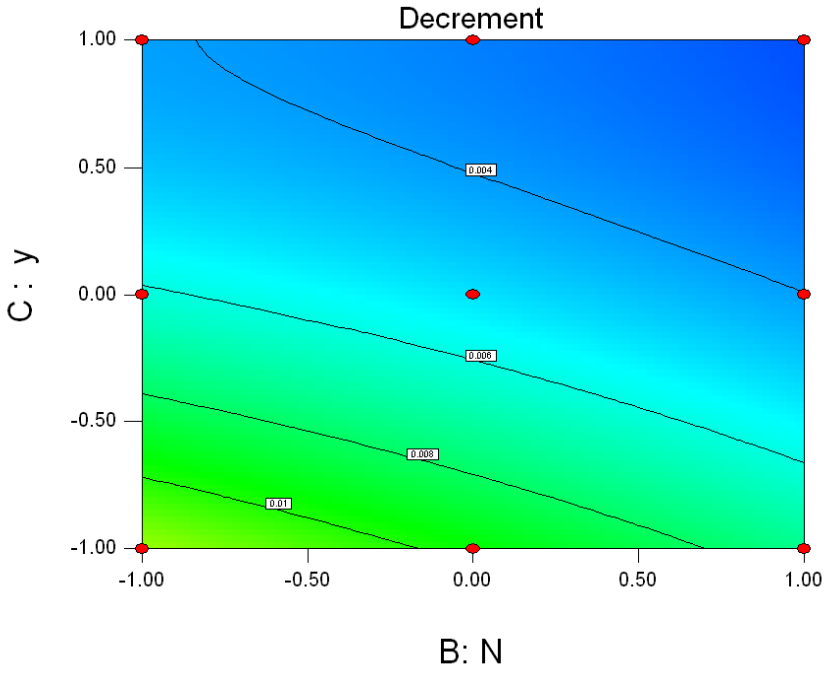

Fig. 8.21 Contour plot: Effect of amplitude and tack number on "δ"

The product of the kinematic coefficient of friction and dynamic slip ratio $\alpha.\mu$ is the key factor in the determination of damping capacity of layered and jointed welded structures. The product $\alpha.\mu$ depends on the initial amplitude of excitation and frequency of vibration. This product increases with the increase in the natural frequency of vibration and the initial amplitude of excitation. The product $\alpha.\mu$

remains almost constant with respect to the surface roughness and thereby the logarithmic damping decrement remains constant for a given jointed interface of same material irrespective of the surface roughness as shown in Figs. 8.16-8.21.

The logarithmic damping decrement increases with a decrease in the number of tack joints. The frequency of vibration depends on stiffness and mass. With a decrease in the number of the tack welds, the static bending stiffness remains the same, but the overall mass decreases since there is less weld material. The frequency of vibration increases due to decrease in mass deposition in case of tack welded joints. Hence, the product $\alpha.\mu$ is enhanced resulting in an increase in the logarithmic damping decrement. Further, the relative spacing between the consecutive tacks is increased with the decrease in the number of tack weld joints for a particular length of the structure. Thus, the dynamic slip at the interfaces increases causing an increase in the logarithmic damping decrement of the layered and jointed tack welded structure.

8.4.5 Perturbation plot

The perturbation plot for logarithmic damping decrement is shown in Fig. 8.22. The surface roughness effect line is almost parallel to the X-axis implying that the effect of surface roughness on logarithmic decrement is almost negligible. Further, the slope of the amplitude is greater compared to the number of tack welds indicating that the effect of the amplitude is more predominant.

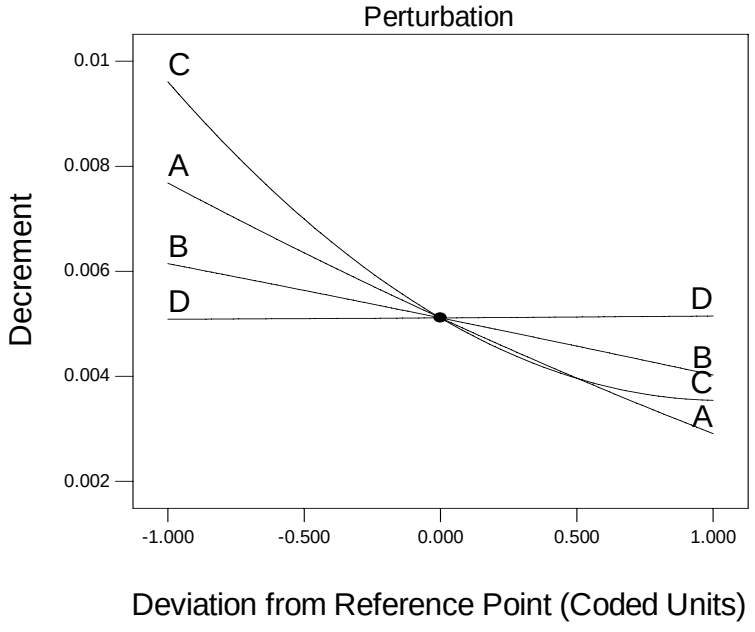

Fig. 8.22 Main effects plot for logarithmic damping decrement (δ)

8.4.6 Residual Plots for logarithmic damping decrement (δ)

The regression model is used for determining the residuals of each individual experimental run. The normal probability plot indicates whether the residuals follow a normal or random distribution. The points follow a straight and zigzag line in case of normal and random distributions, respectively. If a pattern like "S-shape" is obtained, the transformation of response may provide a better fitting analysis. The normal probability of residuals for the response is shown in Fig. 8.23. The normal probability plot is used to verify the adequacy of normality. The data is spread roughly along the straight line for the response as shown in Fig. 8.23 establishing that the residuals are normally distributed.

Further, the plot for the residuals versus the experimental run order is shown in Fig. 8.24 to check the influence of lurking variables on the response. The plot shows a random scatter indicating the accuracy of analysis. The correlation between the residuals is shown in Fig. 8.24 to check the independency of the variables. The plot shows that the residuals are distributed evenly in both positive and negative directions along the run signifying the independency of the variables.

The residual versus predicted response is shown in Fig. 8.25 to check the accuracy of the model. Since the plot shows a random scatter without any pattern, the fitted model is considered to be correct.

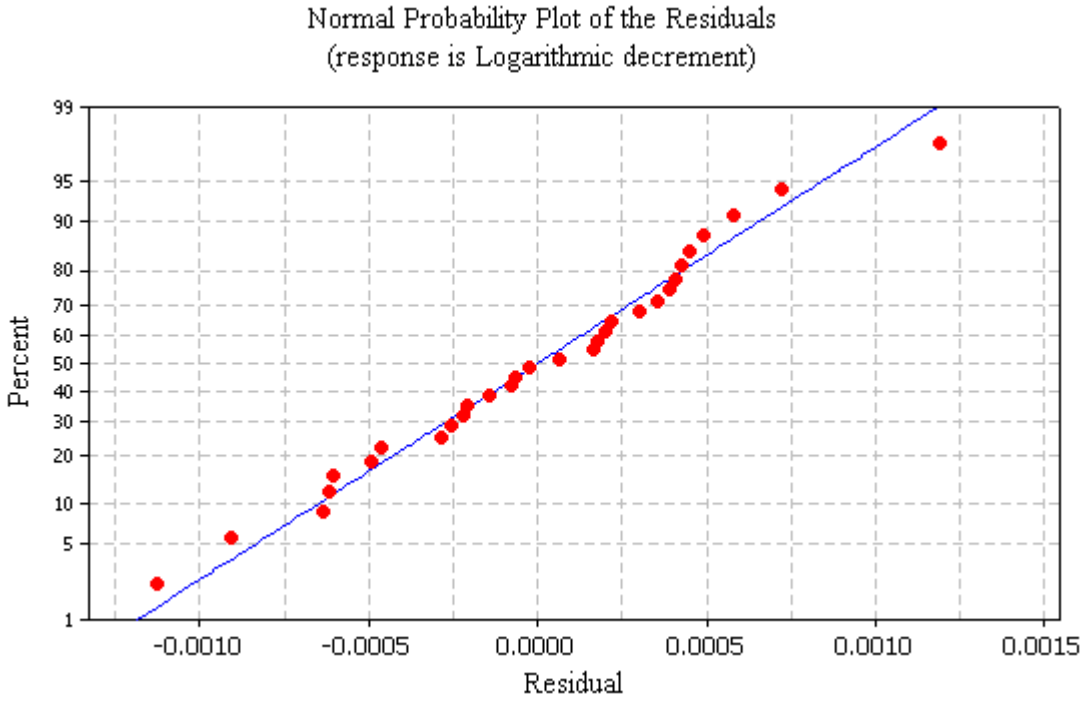

Fig. 8.23 Normal probability plot of the residuals

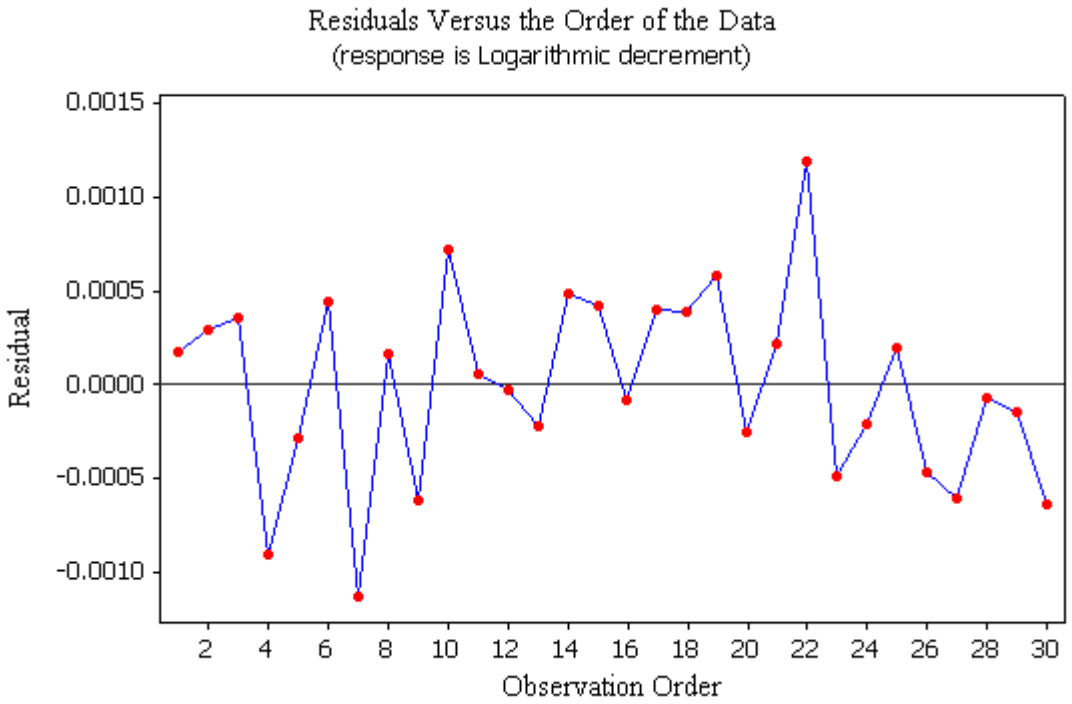

Fig. 8.24 Residuals versus order of the data

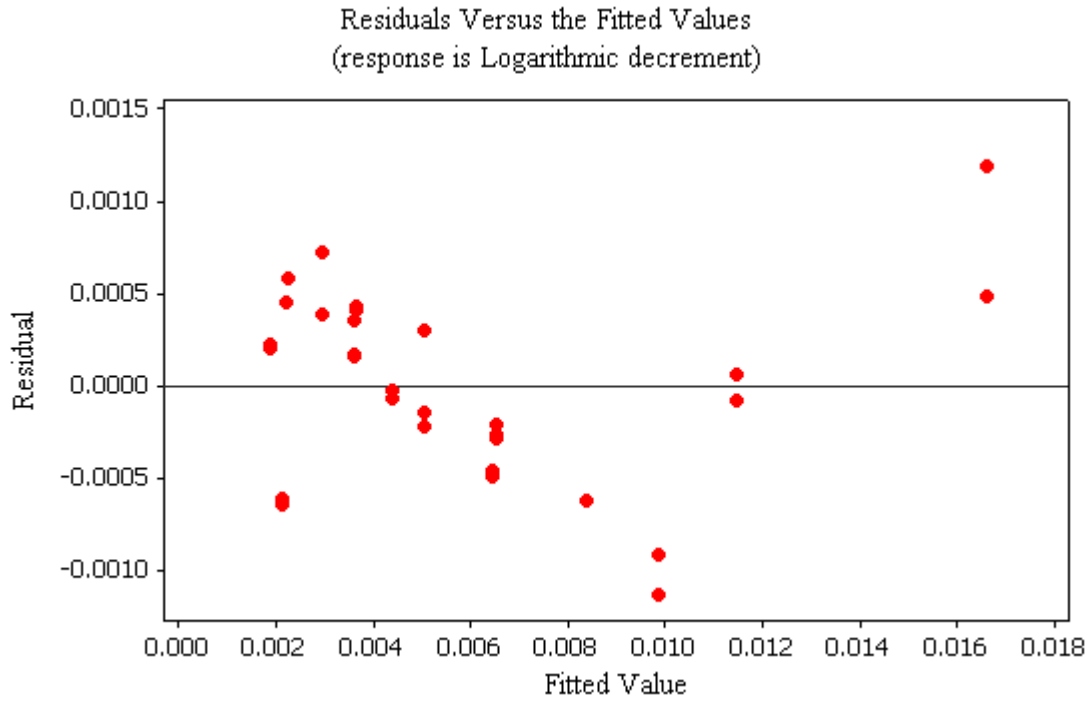

Fig. 8.25 Residuals versus the fitted values

8.4.7 Checking the Adequacy of Mathematical Models

The accuracy of the fit for the mathematical models has also been tested by coefficient of determination (R^2) and adjusted coefficient of determination (R^2_{adj}). The

R^2 is the proportion of the variation in the dependent variable indicated by the regression model. On the other hand, R^2_{adj} is the coefficient of determination adjusted for the number of independent variables in the regression model. The R^2 and R^2_{adj} values of reduced quadratic model are found to be 98.4 and 97.8%, respectively. The R^2 and R^2_{adj} values of reduced cubic model are found to be 99.53 and 99.45%, respectively establishing the excellent correlation between the predicted and experimental values of the cubic response. Thus, from the R^2 and R^2_{adj}, it is inferred that the cubic models provides better precision in evaluating the logarithmic damping decrement of layered and welded structures.

8.4.8 Validity of the model

The performance of the developed model is tested using five experimental points that has not been used during the experimentation in the modeling process. The results for the RSM response as predicted by the model in expression (8.11) are compared with the theoretical values. The time history plots as recorded in the digital storage oscilloscope for two experimental samples are presented in Figs. 8.26 and 8.27.

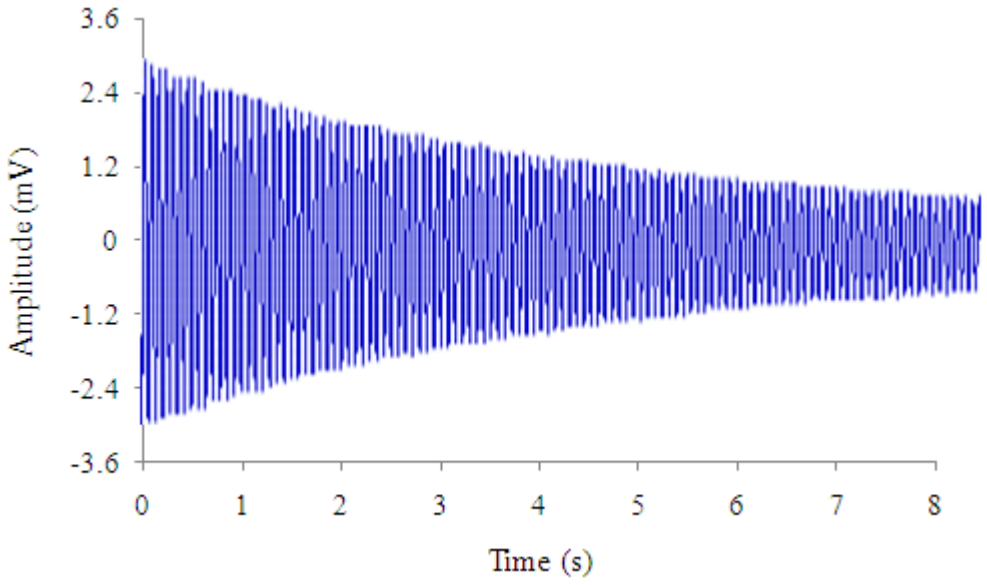

Fig. 8.26 Typical time history plot for amplitude (y): 0.1 mm, number of tack welds (N): 10 and surface roughness (Ra): 1.53 μm

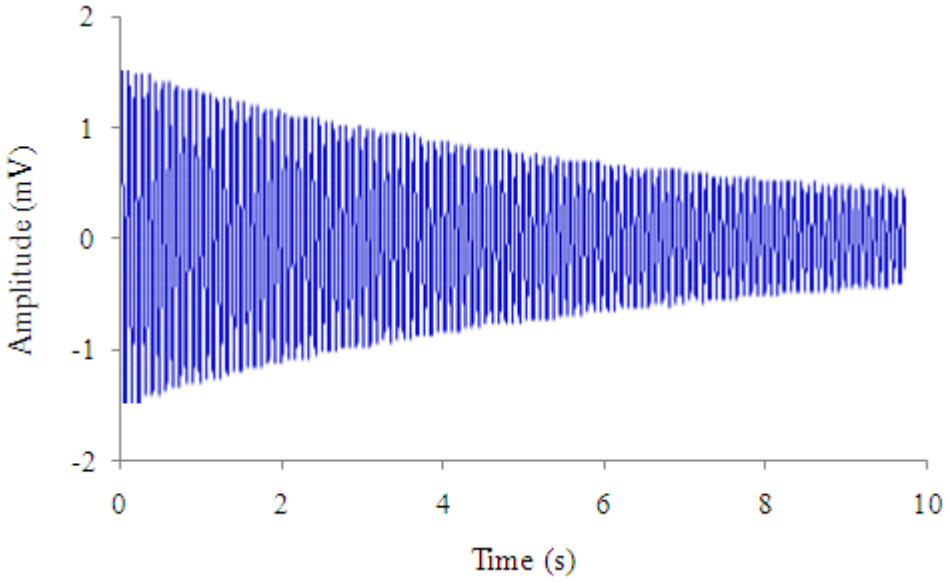

Fig. 8.27 Typical time history plot for amplitude (y): 0.1 mm, number of tack welds (N): 20 and surface roughness (Ra): 2.83 µm

8.4.8.1 Quadratic Model

The average percentage of deviation between the RSM quadratic results and theoretical values of logarithmic damping decrement for various configurations and loading conditions are evaluated for mild steel and aluminium specimens as presented in Tables 8.18-8.19. The results indicate that the RSM quadratic model predicting the values of logarithmic damping decrement has good validity with acceptable percentage deviation of 8.86 and 10.04 deviations for mild steel and aluminium beams, respectively, thereby authenticating the accuracy of the analysis.

8.4.8.2 Cubic Model

The average percentage of deviation between the RSM cubic results and theoretical values of logarithmic damping decrement for various configurations and loading conditions are evaluated for mild steel and aliminium specimens as presented in Tables 8.18-8.19. The results indicate that both the values are close to each other with 7.92 and 8.92 % deviation for mild steel and aluminium beams, respectively, thereby validating the model developed.

The average percentage of deviation between the RSM cubic results and theoretical values of logarithmic damping decrement for various configurations and loading conditions is less than that of the quadratic models thus establishing that the cubic models are more

appropriate for the estimation of logarithmic damping decrement in layered and welded structures.

It is observed that the logarithmic damping decrement is maximum in case of aluminium and minimum in mild steel beams. The present model establishes the relationship between the logarithmic damping decrement and number of tack welded joints in structures of various materials with different end conditions vibrating at various amplitudes of excitation. It is evident from this analysis that an increase in number of joints and initial amplitude of transverse excitation reduces the damping capacity.

On comparing the results of the previous works on bolted and riveted structures with welded ones, it is established that the bolted and welded joints contribute maximum and minimum damping to the system, respectively.

Table 8.18 Comparison of theoretical and RSM results for logarithmic decrement of mild steel specimens

Parameters			**Logarithmic damping decrement**				
N	***y*(mm)**	***Ra*(μm)**	**Theoretical**	**RSM (Quadrilateral)**	**RSM (Cubic)**	**%Deviation between Theoretical and RSM (Quadrilateral)**	**%Deviation between Theoretical and RSM (cubic)**
15	0.1	1.86	0.016973	0.018648	0.018335	8.90	8.02
20	0.3	0.94	0.001945	0.002123	0.002103	9.15	8.12
18	0.1	2.64	0.005271	0.005789	0.005712	9.82	8.37
12	0.4	2.88	0.003441	0.003729	0.003711	8.37	7.85
10	0.5	1.77	0.007539	0.008346	0.008086	8.07	7.26
Avg. deviation %Deviation between Theoretical and RSM (Quadrilateral): 8.862%							
Avg. deviation %Deviation between Theoretical and RSM (Cubic): 7.924 %							

Table 8.19 Comparison of the theoretical and RSM results for logarithmic decrement of aluminium specimens

Parameters			Logarithmic damping decrement				
N	*y*(mm)	*Ra*(μm)	Theoretical	RSM (Quadrilateral)	RSM (Cubic)	%Deviation between Theoretical and RSM (Quadrilateral)	%Deviation between Theoretical and RSM (cubic)
15	0.1	1.87	0.049562	0.054293	0.053972	9.55	8.89
20	0.3	0.92	0.005738	0.006266	0.006211	9.20	8.24
18	0.1	2.66	0.015444	0.017074	0.016846	10.55	9.08
12	0.4	2.87	0.010148	0.011254	0.011083	10.89	9.21
10	0.5	1.78	0.021712	0.023884	0.023702	10.00	9.17
Avg. deviation %Deviation between Theoretical and RSM (Quadrilateral): 10.038%							
Avg. deviation %Deviation between Theoretical and RSM (Cubic): 8.918%							

8.5 Summary

In this study, full factorial design of experiments has been employed to develop a second-order polynomial expression for predicting the values of $\alpha.\mu$ at different natural frequency and amplitude of vibration. The relationship of $\alpha.\mu$ with natural frequency and amplitude of vibration has been successfully obtained by using RSM at 95% confidence level. Moreover, the response regression and variance analysis of the second order model for $\alpha.\mu$ shows that surface roughness parameter is statistically insignificant and the product $\alpha.\mu$ is constant for a jointed interface of same material irrespective of the surface roughness. In the present analysis, it is shown that a considerable amount of damping can be achieved by proper selection of amplitude and frequency during the vibration conditions. The analysis has been further extended

to explore the damping mechanism in layered and welded structures by considering the effects of number of tack joints, initial amplitude of excitation and surface roughness on the logarithmic damping decrement of layered and welded mild steel and aluminium structures. The design of experiments approach has been employed to develop second and third order polynomial expressions for predicting the values of logarithmic damping decrement of such structures. Further, response regression and variance analysis has been presented to study the effect of natural frequency, amplitude of vibration, tack number and surface roughness on the logarithmic damping decrement of these structures. It is concluded from the various statistical tests that the cubic model is more accurate and statistically significant as compared to the quadratic one. From the analysis of variance (ANOVA), it is concluded that the logarithmic damping decrement decreases with the increase in amplitude, tack number and natural frequency of vibration. The logarithmic damping decrement remains almost constant with the varying surface roughness at the interfaces of tack welded cantilever beams. It is observed that the logarithmic damping decrements are maximum and minimum in case of aluminium and mild steel beams, respectively. Further, more experiments have been performed to validate the developed statistical model for logarithmic damping decrement.

9

EXPERIMENTAL ANALYSIS

9.1 Introduction

In the previous chapters, the classical, finite element and response surface methods for the evaluation of damping capacity in layered and welded cantilever beams have been discussed in details. In real working conditions, the experimental study of damping becomes necessary as the theoretically computed results may vary from that of the actual values due to the various assumptions made in the theoretical analysis. Damping is purely a dynamic characteristic of a system which needs to be measured by conducting the dynamic tests on a structure. Therefore, the purpose of this chapter is to verify the theories developed in the previous chapters by conducting experiments to assess the accuracy of the analysis. A number of experiments have been conducted using mild steel and aluminium beam specimens in order to find out the natural frequencies and damping capacity in terms of logarithmic decrement and loss factor. The details of the experimental set-up, specimens used and the procedures adopted along with the results are enumerated in the succeeding sections.

9.2 Specimen Details

The test specimens of different sizes are prepared from the stock of commercial mild steel and aluminium flats as shown in Tables 9.1-9.8. The two and multilayered specimens are prepared by tack welding at the sides of the specimens. The distance between the tacks has been varied in steps. Further, specimens of various thicknesses and length are also prepared for conduct the experiments. This variation in cantilever length and width for a particular specimen affects the static bending stiffness as well as the natural frequency of vibration of the layered and welded cantilever specimens. The photographs of a few mild steel and aluminium specimens used in the experiments are also presented in Fig. 9.1.

Top view of mild steel specimens

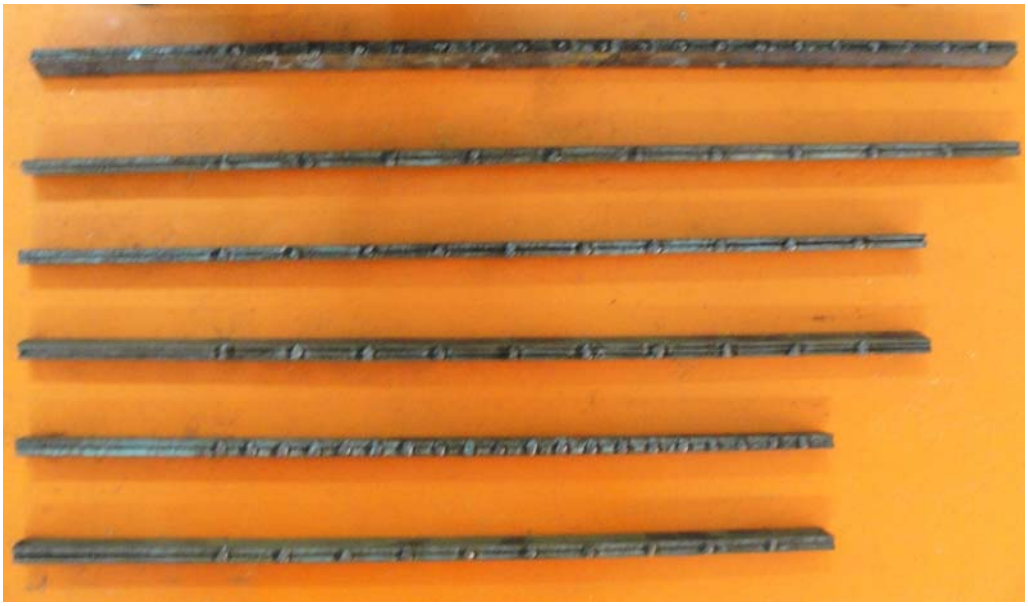

Side view of mild steel specimens

Fig. 9.1(a) Photographs of a few mild steel specimens

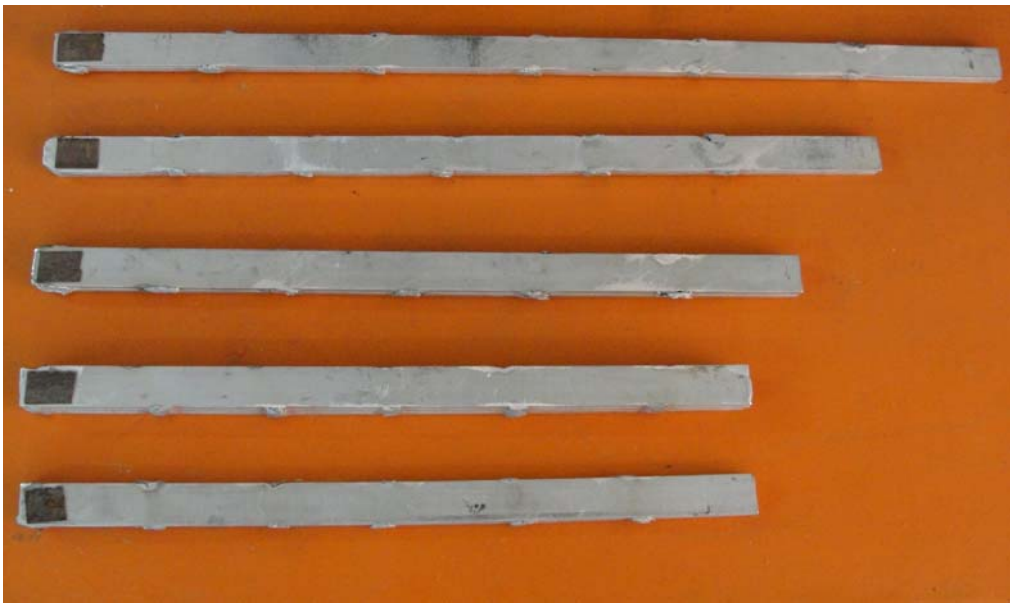

Top view of aluminium specimens

Side view of aluminium specimens

Fig. 9.1(b) Photographs of a few aluminium specimens

Sufficient care has been taken while welding in order to ensure the following salient features by the tack welded joints;

- Holds the assembled components in place and establishes their mutual location
- Ensures their alignment
- Controls movement and distortion during welding
- Sets and maintains the joint gap
- Ensures the assembly's mechanical strength against the external loading

Moreover, adequate attention has been focused while tack welding since the poorly applied tack welds frequently leads to entrapment of slag, porosity, lack of full penetration, leaks and cracks. The sequence and the direction of the tack welds are important for distortion control. Besides maintaining the joint gap, tack welds must resist transverse shrinkage to ensure sufficient rigidity. Tack welding should start at the middle and proceed along the joint length, alternating in both directions with proper back step or skip sequence for avoiding stress buildup and deformation. Tack welding can also be carried out by welding at the ends along the length first. Then, the tack welds are placed at the middle of each resulting distance between the previous welds. This procedure is repeated until the whole length at the appropriate locations is covered with the required number of welds.

9.2.1 Preparation of tack welded mild steel specimens

The specimens are prepared from the stock of mild steel flats by tack welding two and more number of layers of various thickness and cantilever length as presented in Tables 9.1-9.4. The mild steel flats are welded using the shielded metal arc welding technique. Shielded metal arc welding is performed by striking an arc between a coated-metal electrode and the base metal. Once the arc has been established, the molten metal from the tip of the electrode flows together along with the molten metal from the edges of the base metal to form a sound joint. This process is known as fusion. The coating from the electrode forms a covering over the weld deposit, shielding it from contamination; therefore the process is called shielded metal arc welding. The process requires sufficient electric current to melt both the electrode and a proper amount of base metal. It also requires an appropriate gap between the tip of the electrode and the base metal or the molten weld pool. These requirements are necessary to set the stage for coalescence. The sizes and types of electrodes for

shielded metal arc welding define the arc voltage requirements (within the overall range of 16 to 40 V) and the amperage requirements (within the overall range of 20 to 550 A). The main advantages of shielded metal arc welding are that high-quality welds are made rapidly at a low cost.

9.2.2 Preparation of tack welded aluminium steel specimens

The specimens are prepared from the stock of aluminium flats by tack welding two and more number of layers of various thickness and cantilever length. The details of the aluminium specimens used for experimentation are given in Tables 9.5-9.8. The welding of aluminium flats has met with great difficulties because of its ability to oxidation. The moment it is prepared and cleansed, the aluminium is at once covered with aluminium oxide, which prevents the pieces fusing together. By using a flux, however, the oxidation skin is dissolved, and a dross is simultaneously formed which enables the metal to flow and make a perfect weld. The commercial aluminium welding method has been employed which uses an electric arc with a permanent tungsten electrode plus filler wire (with AC current). The arc has been protected by argon gas (or argon-helium gas mix) to shield the weld pool and the electrode from the surrounding atmosphere. Arc welding is easy to use, attains a high temperature, provides high heat input and is easy to regulate. To ensure an acceptable weld quality, two basic factors have been considered - breaking loose and removing the oxide film, and preventing the formation of new oxide during the weld process. It is essential that proper preparations and precautions are to be undertaken before welding commences. The surfaces to be joined and the area around the weld zone have been degreased using a solvent (acetone or toluene) and a clean cloth. The area has been cleaned and completely dried as grease and moisture can form gases and cause pores in the welded joint. The metal surface has been lightly brushed in and around the weld, after degreasing, to remove surface oxides and avoid oxide inclusion in the weld. The high melting temperature (~2000ºC) surface oxides has been removed just prior to welding (at least within three hours or less). The weld has been properly shielded with the inert gas at the correct flow rate, and of the required purity. Care has been taken such that the nozzle distance does not vary from the weld point.

Table 9.1 Details of mild steel specimens with thickness ratio 1.0

Thickness × Width (mm × mm)	Number of layers	Type of specimen	Number of tack welds	Cantilever length (mm)
(3+3) × 40.25	2		10	440.34
(4+4) × 40.25	2		20	480.22
(6+6) × 40.25	2	Welded	30	520.32
(4+4+4) × 40.25	3		40	560.22
(3+3+3+3) × 40.25	4		50	600.61
(3+3) × 33.00	2		10	330.36
(4+4) × 33.00	2		20	363.20
(6+6) × 33.00	2	Welded	30	396.23
(4+4+4) × 33.00	3		40	429.12
(3+3+3+3) × 33.00	4		50	453.66
(3+3) × 24.00	2		10	346.50
(4+4) × 24.00	2		20	371.25
(6+6) × 24.00	2	Welded	30	396.00
(4+4+4) × 24.00	3		40	420.75
(3+3+3+3) × 24.00	4		50	460.86
6 × 40.25 8 × 40.25 12 × 40.25	-	Solid	-	440.23 480.22 520.45 560.12 600.33

Table 9.2 Details of mild steel specimens with thickness ratio 1.5

Thickness × Width (mm × mm)	Number of layers	Type of specimen	Number of tack welds	Cantilever length (mm)
(2+3) × 40.25 (2.4+3.6) × 40.25 (4+6) × 40.25	2 2 2	Welded	10 20 30 40 50	440.35 480.25 520.36 560.48 600.25
(2+3) × 33.00 (2.4+3.6) × 33.00 (4+6) × 33.00	2 2 2	Welded	10 20 30 40 50	320.25 360.26 400.46 440.58 480.66
(2+3) × 24.00 (2.4+3.6) × 24.00 (4+6) × 24.00	2 2 2	Welded	10 20 30 40 50	360.26 390.66 420.35 450.39 500.22
(2+3) × 20.00 (2.4+3.6) × 20.00 (4+6) × 20.00	2 2 2	Welded	10 20 30 40 50	375.59 400.20 425.23 450.45 525.35
6.0 × 40.25 10.0 × 40.25	-	Solid	-	440.35 480.25 520.36 560.48 600.25

Table 9.3 Details of mild steel specimens with thickness ratio 2.0

Thickness × Width (mm × mm)	Number of layers	Type of specimen	Number of tack welds	Cantilever length (mm)
(2+4) × 40.20 (3+6) × 40.20	2 2	Welded	10 20 30 40 50	440.75 480.35 520.66 560.49 600.26
(2+4) × 50.00 (3+6) × 50.00	2 2	Welded	10 20 30 40 50	280.62 336.22 392.63 448.56 488.45
(2+4) × 33.60 (3+6) × 33.60	2 2	Welded	10 20 30 40 50	336.40 369.60 403.20 436.80 480.23
(2+4) × 28.00 (3+6) × 28.00	2 2	Welded	10 20 30 40 50	364.00 392.00 420.00 448.00 520.36
6 × 40.20 9 × 40.20	-	Solid	-	440.55 480.15 520.85 560.25 600.43

Table 9.4 Details of mild steel specimens with thickness ratio 3.0

Thickness × Width (mm × mm)	Number of layers	Type of specimen	Number of tack welds	Cantilever length (mm)
(2+6) × 40.20 (3+9) × 40.20	2 2	Welded	10 20 30 40 50	440.55 480.95 520.63 560.55 600.45
(2+6) × 45.25 (3+9) × 45.25	2 2	Welded	10 20 30 40 50	280.26 336.22 392.25 448.68 488.15
(2+6) × 33.60 (3+9) × 33.60	2 2	Welded	10 20 30 40 50	336.48 369.66 403.24 436.89 480.28
(2+6) × 28.00 (3+9) × 28.00	2 2	Welded	10 20 30 40 50	364.45 392.25 420.15 448.48 520.18
8 × 40.20 9 × 40.20	-	Solid	-	440.18 480.48 520.49 560.46 600.48

Table 9.5 Details of aluminium specimens with thickness ratio 1.0

Thickness × Width (mm × mm)	Number of layers	Type of specimen	Number of tack welds	Cantilever length (mm)
(3+3) × 40.25	2		10	440.56
(4+4) × 40.25	2		20	480.52
(6+6) × 40.25	2	Welded	30	520.46
(4+4+4) × 40.25	3		40	560.55
(3+3+3+3) × 40.25	4		50	600.26
(3+3) × 33.00	2		10	330.43
(4+4) × 33.00	2		20	363.26
(6+6) × 33.00	2	Welded	30	396.29
(4+4+4) × 33.00	3		40	429.45
(3+3+3+3) × 33.00	4		50	453.33
(3+3) × 24.00	2		10	346.45
(4+4) × 24.00	2		20	371.26
(6+6) × 24.00	2	Welded	30	396.48
(4+4+4) × 24.00	3		40	420.14
(3+3+3+3) × 24.00	4		50	460.56
6 × 40.25 8 × 40.25 12 × 40.25	-	Solid	-	440.26 480.48 520.25 560.10 600.26

Table 9.6 Details of aluminium specimens with thickness ratio 1.5

Thickness × Width (mm × mm)	Number of layers	Type of specimen	Number of tack welds	Cantilever length (mm)
(2+3) × 40.25	2	Welded	10	440.23
			20	480.89
(2.4+3.6) × 40.25	2		30	520.76
(4+6) × 40.25	2		40	560.44
			50	600.55
(2+3) × 33.00	2	Welded	10	320.66
			20	360.46
(2.4+3.6) × 33.00	2		30	400.25
(4+6) × 33.00	2		40	440.88
			50	480.77
(2+3) × 24.00	2	Welded	10	360.26
			20	390.45
(2.4+3.6) × 24.00	2		30	420.32
(4+6) × 24.00	2		40	450.66
			50	500.22
(2+3) × 20.00	2	Welded	10	375.44
			20	400.55
(2.4+3.6) × 20.00	2		30	425.42
(4+6) × 20.00	2		40	450.15
			50	525.36
6.0 × 40.25	-	Solid	-	440.45
				480.56
				520.65
10.0 × 40.25				560.85
				600.69

Table 9.7 Details of aluminium specimens with thickness ratio 2.0

Thickness × Width (mm × mm)	Number of layers	Type of specimen	Number of tack welds	Cantilever length (mm)
(2+4) × 40.20 (3+6) × 40.20	2 2	Welded	10 20 30 40 50	440.55 480.66 520.33 560.35 600.25
(2+4) × 50.00 (3+6) × 50.00	2 2	Welded	10 20 30 40 50	280.65 336.45 392.65 448.45 488.55
(2+4) × 33.60 (3+6) × 33.60	2 2	Welded	10 20 30 40 50	336.58 369.90 403.45 436.25 480.14
(2+4) × 28.00 (3+6) × 28.00	2 2	Welded	10 20 30 40 50	364.36 392.56 420.45 448.45 520.42
6 × 40.20 9 × 40.20	-	Solid	-	440.56 480.65 520.88 560.77 600.45

Table 9.8 Details of aluminium specimens with thickness ratio 3.0

Thickness × Width (mm × mm)	Number of layers	Type of specimen	Number of tack welds	Cantilever length (mm)
(2+6) × 40.20 (3+9) × 40.20	2 2	Welded	10 20 30 40 50	440.56 480.36 520.45 560.22 600.55
(2+6) × 45.25 (3+9) × 45.25	2 2	Welded	10 20 30 40 50	280.45 336.25 392.36 448.44 488.56
(2+6) × 33.60 (3+9) × 33.60	2 2	Welded	10 20 30 40 50	336.65 369.66 403.54 436.22 480.44
(2+6) × 28.00 (3+9) × 28.00	2 2	Welded	10 20 30 40 50	364.33 392.66 420.78 448.88 520.12
8 × 40.20 9 × 40.20	-	Solid	-	440.22 480.33 520.56 560.45 600.52

9.3 Description of the Experimental Set-up

The schematic diagram of the experimental set-up with the instrumentation and photographic views are shown in Figs. 9.2 and 9.3, respectively. The set-up consists of a frame work fabricated from steel channel sections by welding. The frame is grouted to a heavy and rigid concrete base by means of foundation bolts which has the provision of slotted guide ways to accommodate the beams of different lengths. The frame has the provision to hold the fixed end of the cantilever beam specimens tightly and rigidly in order to ensure perfect cantilever condition. This clamping is achieved using a mechanical vice. The vice working on the screw-jack principle consists of a base plate and a spindle with internal and external threading, respectively. An arm is attached to this spindle at the upper end. On rotating the arm, it moves axially downward and imparts the necessary clamping force to the base plate thereby holding the specimen to achieve a perfect cantilever condition. The base plate prevents the rotation of the specimens while applying the fixed end load. Spring loaded exciter and vibration generators are used to initiate the vibration at the free end of the specimens with predetermined amplitudes. The use of spring in the exciter ensures zero initial velocity of the specimen at the time of excitation. It is provided with a dial gauge which is calibrated to read the initial amplitudes of excitation. The dial gauge is mounted to a vertical stand with a magnetic base.

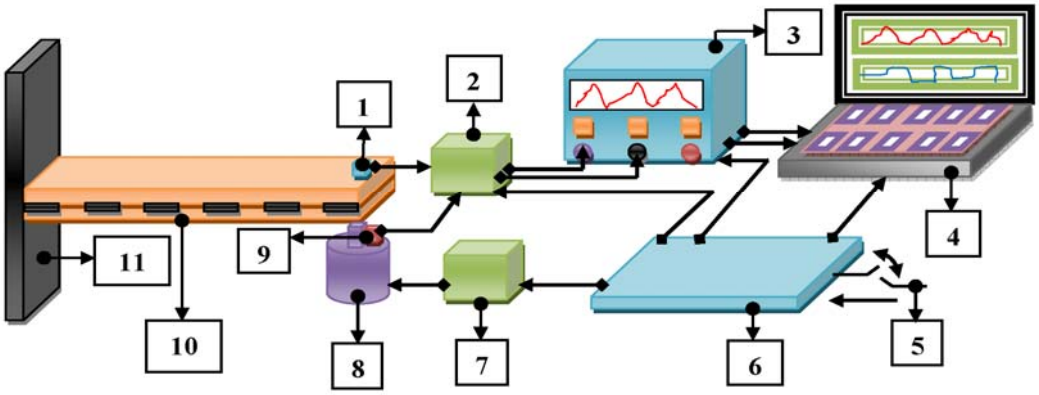

1. Output Vibration Pickup
2. Amplifier
3. Vibration Acquisition
4. Vibration Analyzer
5. Power Supply
6. Distribution Box
7. Power Amplifier
8. Vibration Generator
9. Input Excitation Pickup
10. Tack Welded Beam
11. Fixed End

Fig. 9.2 Schematic diagram of the experimental set-up

Fig. 9.3 Experimental set-up

The test rig includes the following instruments.

1. Digital Storage Oscilloscope
2. Accelerometer/Vibration Pick-Up (Contacting Type Magnetic Probe)
3. Dial Gauge
4. Distribution Box
5. Vibration Exciter
6. Power Amplifier
7. Function Generator

A brief functional description of each instrument listed above along with their specifications is presented as follows;

(1) A digital storage oscilloscope as shown in Fig. 9.4 is widely used for the processing and display of vibration signals and has a display screen, numerous input connectors, control knobs and buttons on the front panel. The signal to be measured is fed to one of the connectors. It plots a two dimensional graph of the time history curve.

Specifications:

DPO 4000 series Oscilloscope

Input Voltage: 100 V to 240 V ± 10%

Input Power Frequency: 47 Hz to 66 Hz (100 V to 240 V)
400 Hz (100 V to 132 V)

Power Consumption: 250 W maximum

Weight: 5 kg (11 lbs), standalone instrument

Clearance: 51 mm (2 inches)

Operating Temperature: 0 to 50 ^{0}C

High Operating Humidity: 40 to 50 ^{0}C, 10 to 60% RH

Low Operating Humidity: 0 to 40 ^{0}C, 10 to 90% RH

Operating Altitude: 3000 m (about 10,000 ft)

Operating Random Vibration: 0.31 G_{RMS}, 5 – 500 Hz, 10 minutes per axis, 3 axes (30 minutes total)

Pollution Degree: 2, Indoor use only

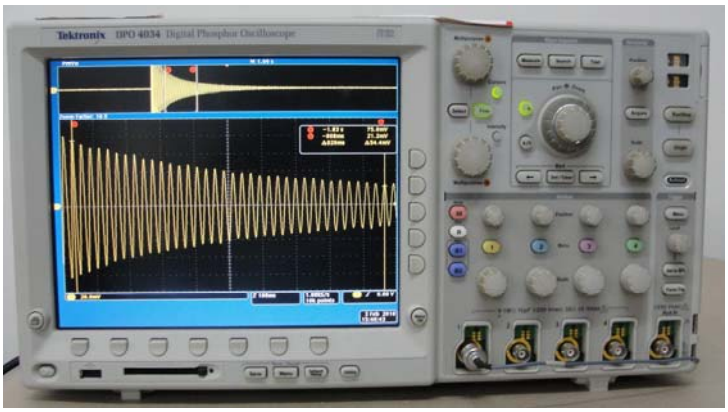

Fig. 9.4 Digital storage oscilloscope

(2) The accelerometer is a device that transforms changes in mechanical quantities (such as displacement, velocity or acceleration) into changes in electrical quantities (such as voltage or current). One end of the accelerometer is held magnetically to the vibrating surface and the other end is connected to one of the connectors of the storage oscilloscope. The accelerometer used in the experiments is of contacting-type as shown in Fig. 9.5.

Specifications:
Type: MV-2000

Make: NAL, Bangalore, India

Optional gap: 2 mm

Coil resistance: 1000 ohms

Operating temperature: 10 to 40 degree centigrade

Dynamic frequency range: 2 c/s to 1000c/s

Vibration amplitude: ± 1.5 mm maximum

Weight: 130 gm

Fig. 9.5 Accelerometer (Contacting type magnetic probe)

(3) A high precision dial gauge mounted on a stand with magnetic base is used to record the amplitude of vibration given at the tip of the specimen. The dial gauge as shown in Fig. 9.6 is shock proof and can measure the amplitude of excitation in the range of 0.01 to 10 mm.

Fig. 9.6 Dial gauge mounted on a stand with magnetic base

(4) A distribution box supplies the AC power to the storage oscilloscope at a voltage and frequency of 230V and 50Hz, respectively.
Power supply: 200-240 V, 50 Hz

(5) An RF Power Amplifier is a type of electronic amplifier used to convert a low frequency signal into a larger signal of significant power.
Type: 2719
Power Amplifier:
180VA
Make: Bruel & Kjaer

Fig. 9.7 Power Amplifier

(6) The function generator is a moving coil device with a frequency in excess of 0.2Hz to 200 KHz. The natural frequency is calculated from the function generator at the point of resonance.
Model: FG200K
Frequency Range: 0.2Hz to 200 KHz
Output attenuation up to 60dB.
Output Level: 15Vp-p into 600 ohms
Rise/Fall Time: <300nSec
Make: Aplab

Fig. 9.8 Function Generator

(7) A vibration exciter (shaker) is an electro-mechanical device which transforms electrical A.C. signals into mechanical vibrations and is used to excite vibrations in bodies or structures for testing purposes. During the past decade a wide variety of vibration exciters have been developed, their fields of application ranging from fatigue testing of automobile, missile and aircraft components to the calibration of vibration pick-ups.

Fig. 9.9 Vibration Exciter

Type: 4808

Permanent Magnetic Vibration Exciter

Force rating 112N (25 lbf) sine peak (187 N (42 lbf) with cooling)

Frequency Range: 5 Hz to 10Hz

First Axial Resonance: 10 Hz

Maximum Bare Table Acceleration: 700 m/s^2 (71 g)

Continuous 12.7 mm (0.5 in) peak-to-peak displacement with over travel stops

Two high-quality, 4-pin

Neutrik® Speakon® connectors

Make: Bruel & Kjaer

9.4 Testing Procedure

The tests are performed in the prevailing laboratory environment. In order to perform the experiments, the specimens are rigidly mounted to the support as discussed earlier. At first, the Young's modulus of elasticity and static bending stiffness are measured by carrying out the static deflection tests. These measured values are subsequently used for the theoretical evaluation of logarithmic decrement and loss factor of all the specimens. Later, the experimental logarithmic decrement and loss factor are calculated from the time history curve of decaying signals and frequency response curves, respectively. The detailed procedure to find out the above quantities is discussed in the succeeding sections.

9.4.1 Measurement of Young's Modulus of Elasticity (*E*)

As mentioned in the preceding paragraph, the Young's modulus of elasticity (E) of the specimen material is found out by conducting the static deflection tests. For this purpose, few samples of solid beams are selected from the same stock of mild steel and aluminium flats. These specimens are mounted on the same experimental set-up rigidly so as to ensure perfect cantilever conditions as mentioned earlier. Static loads (W) are applied at the free end and the corresponding deflections (Δ) are recorded. The Young's modulus for the specimen material is then determined using the expression $E = WL^3/3I\Delta$, where L and I are the free length and moment of inertia of the cantilever specimen. The average of five readings is recorded from the tests from which the average value of Young's modulus for different material is evaluated as presented in Table 9.9.

Table 9.9 Young's modulus of specimen materials

Material	Average Modulus of Elasticity (GPa)
Mild steel	203.41
Aluminium	69.45

9.4.2 Measurement of Static Bending Stiffness (*k*)

It is a well known fact that the stiffness of a jointed beam is always less compared to an equivalent solid one. It means that the incorporation of joints to assemble layers of beams is accompanied by a decrease in the stiffness. The amount of reduction in the stiffness is quantified by a factor called stiffness ratio which is defined as the ratio of the stiffness of a jointed beam (*k*) to that of an identical solid one (k'). The stiffness ratio is inversely related to the number of layers used in the jointed specimen. Its exact assessment carries much significance in the theoretical evaluation of damping capacity. The same static deflection tests as used in case of Young's modulus are performed to measure the actual stiffness (*k*) of a jointed specimen using the relation $k = W / \Delta$. However, the stiffness of an identical solid cantilever beam is theoretically calculated from the expression $k' = 3EI/L^3$. The average values of the stiffness ratios for two layered cantilever welded beams has been calculated and presented in Tables 9.10 and 9.11 as samples for mild steel and aluminium, respectively. It is seen that there is marginal variation in the stiffness ratio for the group of specimens considered in the above mentioned table.

Table 9.10 Average stiffness ratio of two layered welded mild steel beams

Thickness × Width (mm × mm)	Cantilever length (mm)	Static bending stiffness (N/mm)		Stiffness ratio (*k*/*k*')	Average stiffness ratio
		Experimental (*k*)	Theoretical (*k*')		
(3+3) ×40.25	520.36	2.6615	3.1378	0.8482	0.8503
	560.23	2.1063	2.5144	0.8377	
	600.63	1.7637	2.0404	0.8644	
(4+4) ×40.25	520.56	6.3578	7.4291	0.8558	
	560.45	5.0220	5.9530	0.8437	
	600.44	4.1101	4.8410	0.8491	
(6+6) ×40.25	520.26	21.3896	25.117	0.8516	
	560.33	17.1131	20.104	0.8512	
	600.48	14.0351	16.335	0.8592	

(2.4+3.6) ×40.25	520.65	2.6300	3.1325	0.8396	
	560.45	2.1244	2.5114	0.8459	
	600.88	1.7459	2.0378	0.8568	
(2+4) ×40.25	520.59	2.6707	3.1336	0.8523	
	560.25	2.1309	2.5141	0.8476	
	600.75	1.7358	2.0392	0.8512	

Table 9.11 Average stiffness ratio of two layered welded aluminium beams

Thickness× Width (mm × mm)	Cantilever length (mm)	Static bending stiffness (N/mm)		Stiffness ratio (k/k')	Average stiffness ratio
		Experimental (k)	Theoretical (k')		
(3+3) ×40.25	520.56	0.9429	1.0701	0.8812	0.8736
	560.25	0.7478	0.8584	0.8712	
	600.66	0.6056	0.6965	0.8723	
(2.4+3.6) ×40.25	520.25	0.9338	1.0720	0.8711	
	560.45	0.7506	0.8574	0.8754	
	600.77	0.6089	0.6961	0.8748	
(2+4) ×40.25	520.44	0.9333	1.0708	0.8714	
	560.33	0.7455	0.8580	0.8689	
	600.42	0.6109	0.6973	0.8761	

Further, the stiffness ratio of multi-layered jointed beams has been calculated in the similar manner as in case of two layered ones. The corresponding values of average stiffness ratios for jointed beams consisting of varying number of layers for a constant overall thickness are given in Table 9.12 and 9.13 for mild steel and aluminium specimens, respectively. It is observed that the stiffness ratio decreases with the increase in number of layers of the jointed construction. These calculated stiffness

ratios are utilized in determining the actual stiffness of jointed beams and further used for the theoretical evaluation of logarithmic decrement and loss factor.

Table 9.12 Average stiffness ratio of multi-layered welded mild steel beams

Number of layers used		
2 layers	3 layers	4 layers
0.8503	0.8112	0.7832

Table 9.13 Average stiffness ratio of multi-layered welded aluminium beams

Number of layers used		
2 layers	3 layers	4 layers
0.8736	0.8423	0.8012

9.4.3 Surface Roughness (SR) Measurements

The specimens are prepared from commercial mild steel flats and the roughness measurement at the interfaces have been carried out using a portable stylus type profilometer, Talysurf (Taylor Hobson, Surtronic 3+). The profilometer has been set to a cut-off length of 0.8 mm, filter 2CR with traverse speed of 1mm/second having evaluation length of 4 mm. Roughness measurements in the transverse direction on the specimens have been repeated at least for five times and the average of these measurements has been recorded. The measured profile is digitized and processed through the advanced surface finish analysis software Talyprofile for the evaluation of the roughness parameters. Surface roughness is expressed as the irregularities of material resulted from the various machining operations and is usually denoted as "*Ra*". The surface roughness is described by the height, slope and curvature of the surface profile.

Surtronic 3+ surface measuring instrument as shown in Fig. 9.10 is used for measuring the interface roughness of various mild steel and aluminium specimens.

Specification:

Make: Taylor Hobson Limited, England

Battery: Alkaline non-rechargeable battery with minimum 600 measurements of 4 mm measurement length

NiCad rechargeable battery with minimum 200 measurements of 4 mm measurement length

110/240V, 50/60 Hz

Traverse speed: 1 mm/sec

Measurement units: Metric/Inch

Cut-off values: 0.25mm, 0.80mm and 2.50mm (0.01in, 0.03in and 0.1in)

Filter: Digital Gauss filter or 2CR filter

Parameters: Ra, Rq, Rz (DIN), Ry and Sm

Calculation time: Less than reversal time or 2 sec whichever is the longer

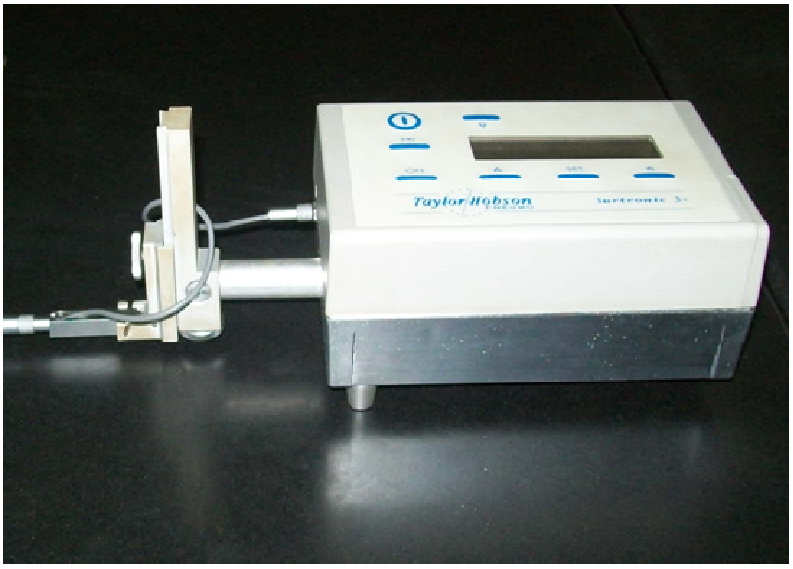

Fig. 9.10 Roughness tester

9.4.4 Measurement of Damping

Once, the Young's modulus and static bending stiffness of the specimen materials are determined, tests are further conducted on the same set of specimens for evaluating the damping capacity. In the present study, damping has been measured using the logarithmic decrement and loss factor methods based on time and frequency domains, respectively. The test specimens are first rigidly mounted on the set-up one after another. The test procedure is essentially the same for all the cases. The cause of

energy dissipation may be due to different effects such as material, joint friction and support damping. However, it is assumed that all the energy dissipation is due to the joint friction only. Design of experimental set-up for measurement of damping requires some primary consideration. It is assumed that the energy losses due to support friction, air drag, connecting wires, accelerometer mountings etc., are neglected. Secondly, proper care has been taken while preparing the specimens, assembling the test rig and conducting the experiments. The connecting members of the test specimens should be flat with perfect contact at the interfaces. This will ensure identical pressure distribution at the interfaces so that proper energy dissipation takes place. While mounting the specimen in the test rig, sufficient clamping has to be provided in order to achieve a perfect cantilever condition which will minimize the errors due to support damping. Further, some errors may build up while giving the initial excitation which may not be instantaneous. This may not ensure perfect sinusoidal waveforms thus containing some harmonic contents. All these factors have been considered during experimentation in order to minimize the errors.

9.4.4.1 Logarithmic Damping Measurement

Several techniques are used to quantify the level of damping in a structure as discussed earlier in the literature review. Out of them, the logarithmic decrement technique is the most popular time-response method used for measuring the damping. The logarithmic decrement represents the rate at which the amplitude of a free damped vibration decreases. As the structure is considered to vibrate with small excitation level in the low and moderate frequency range, this method produces fairly good results for lightly damped linear systems. In this method, the structure is set into free vibration with the fundamental mode dominating the response since all the higher modes are damped out quite quickly. The vibration response of the specimen is picked up by the accelerometer and a time history curve showing the decay of amplitude is displayed on the digital storage oscilloscope. This decay can be further used to estimate the damping in jointed specimens using the expression $\delta = \ln\left(x_1 / x_{z+1}\right)/z$, where x_1, x_{n+1} and z are the recorded values of the amplitudes of the first cycle, last cycle and the number of cycles, respectively. In the present work, the damping ratio for static loading has been evaluated considering the logarithmic damping decrement

method. A spring loaded exciter is used to excite the specimens at the free ends. The excitation is imparted for a range of beam-tip amplitudes varying from 0.1 to 0.5 mm in steps of 0.1 mm. For a particular test specimen, the beam is deflected and released to oscillate at its first mode of free vibration. The beam response is sensed by a contacting-type accelerometer attached to the tip of the beam. In view of non-magnetic property of aluminium specimen, the beam-tip is glued with a square size strip of some magnetic material for sensing of the signal. One end of the accelerometer is held magnetically to the vibrating surface of the specimen and the other is connected to one of the connectors of the storage oscilloscope. The output from the accelerometer is proportional to the frequency and amplitude of vibration. This output signal is fed to a digital storage oscilloscope for processing and display. The data is then analyzed to determine the natural frequency and damping characteristics of the beam structure. The decaying signal is recorded on the screen of the storage oscilloscope indicating that the energy dissipation is taking place. Each test during experiments is repeated at least for five times and the average value is taken for accuracy. The damped frequency of vibration (ω_d) is read directly from the data recorded on the oscilloscope. The natural frequency of vibration (ω_n) is calculated from this damped one using the expression $\omega_n = \omega_d \big/ \sqrt{1-\xi^2}$, where ξ is the damping ratio. As the value of ξ is very small for lightly damped structures, the natural frequency of vibration is fairly same as that of the damped frequency of vibration, i.e., $\omega_n \approx \omega_d$. It is observed that the natural frequency of transverse vibration vary only with the physical dimensions of the layered and jointed beam specimens. However, it is independent of the amplitudes of excitation. Some of the experimental observations using time history plots for the evaluation of logarithmic decrement have been presented in Figs. 9.11 and 9.12 as samples for mild steel and aluminium specimens, respectively. The time interval has been normalized for comparison with interval being 1 second. It is evident from these plots that the damping in jointed specimens increases with the use of more number of layers.

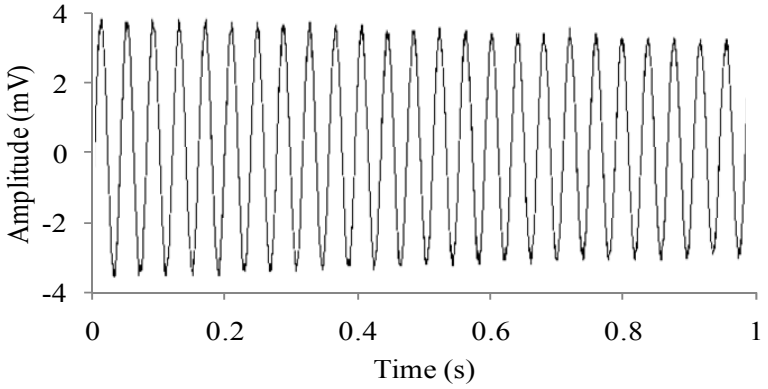

(a) Two layered mild steel specimen (520.65x40.25x6 mm)
Amplitude of excitation = 0.1 mm

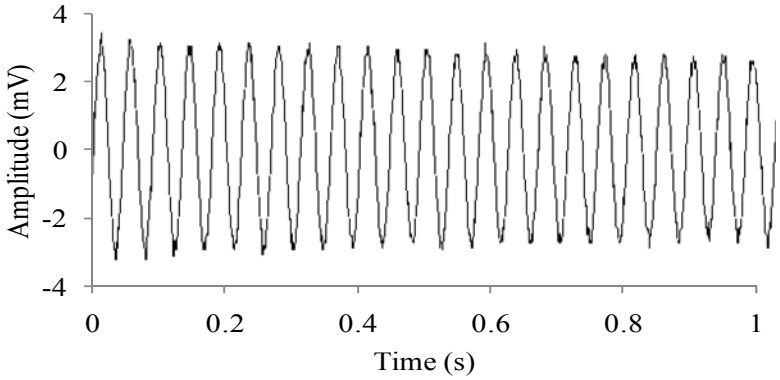

(b) Three layered mild steel specimen (520.65x40.25x6 mm)
Amplitude of excitation = 0.1 mm

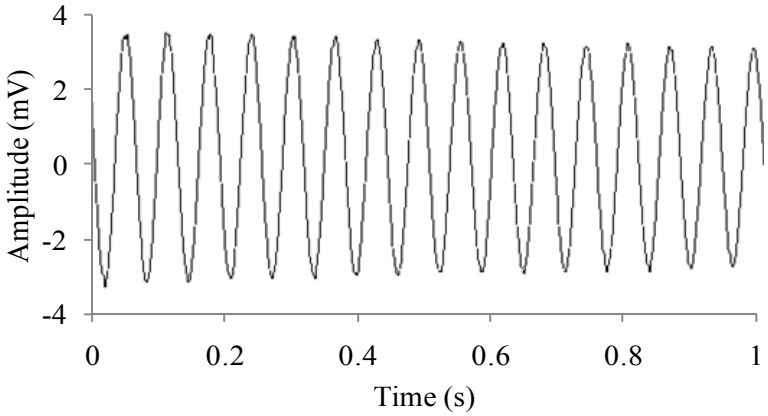

(c) Four layered mild steel specimen (520.65x40.25x6 mm)
Amplitude of excitation = 0.1 mm

Fig. 9.11 Time history curve of welded mild steel specimens under free vibration recorded by the digital storage oscilloscope

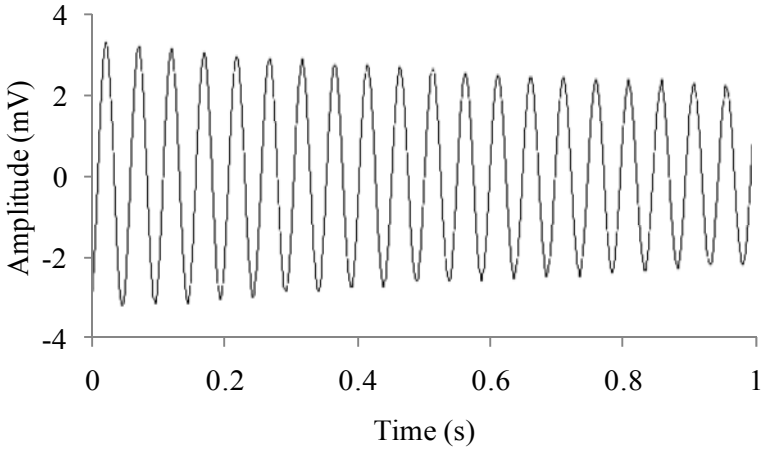

(a) Two layered Aluminium specimen (520.65x40.25x6 mm)
Amplitude of excitation = 0.1 mm

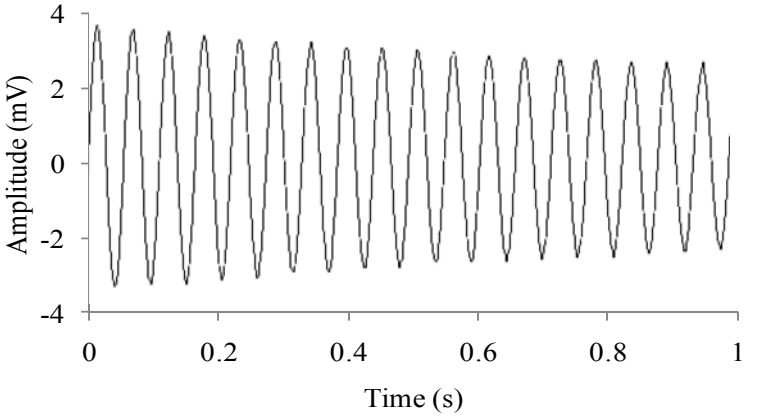

(b) Three layered Aluminium specimen (520.65x40.25x6 mm)
Amplitude of excitation = 0.1 mm

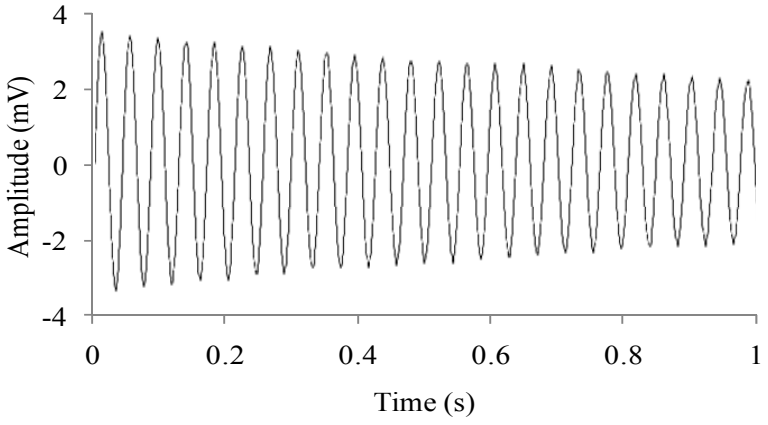

(c) Four layered Aluminium specimen (520.65x40.25x6 mm)
Amplitude of excitation = 0.1 mm

Fig. 9.12 Time history curve of welded aluminium specimens under free vibration recorded by the digital storage oscilloscope

9.4.4.1.1 Experimental Evaluation of "$\alpha.\mu$"

The energy dissipation at the interfaces of jointed structures primarily depends upon the kinematic coefficient of friction (μ) and dynamic slip ratio (α). These two vital parameters are to be correctly assessed for accurate evaluation of the logarithmic decrement. It is generally known that the dynamic slip at the interfaces increases with a decrease in coefficient of friction and vice versa. They are inter-dependent with each other and inversely related. Further, they exhibit complex behavior under dynamic condition making it difficult to assess the exact value of the individual parameters at a particular condition of excitation. In view of the above factors, it is convenient to evaluate the product $\alpha.\mu$ as a single parameter from the experimental results and use it for theoretical calculations for other conditions of the beam. However, their product $\alpha.\mu$ is found to be constant for a particular specimen under a particular condition of vibration irrespective of surface roughness.

In view of the discussions in the preceding paragraph, the product $\alpha.\mu$ has been determined from the experimental results of logarithmic decrement for two layered welded cantilever beam specimens of mild steel and aluminium using expression (3.41). Since this product is frequency and amplitude dependent, plots displaying its variation with the above two parameters are shown in Figs. 9.13 to 9.15 and 9.16 to 9.18 for mild steel and aluminium specimens, respectively. These plots are further used to find out the numerical values of the logarithmic decrement for other conditions of the beam using expressions (3.36) and (3.40). It is observed from the above plots that this product increases with an increase in both the natural frequency and amplitude of excitation. However, the product $\alpha.\mu$ is established to be constant for a particular specimen irrespective of any surface condition at the mating surfaces. In order to authenticate this, experiments are conducted with a few layered and welded beams made up of mild steel and aluminium connected with different thickness ratio and excited at 0.1 mm. The roughness values at the interfaces of the specimens have been varied. These values are measured with the help of a Surtronic 3 + surface texture measuring instrument and found to be 0.81, 1.14 and 1.47 micron for mild steel and 0.88, 1.53, and 2.13 micron for aluminium specimens. The results of the effect of surface roughness on the damping capacity of the jointed structures have been presented in Table 9.14. It is observed that the logarithmic decrement remains

almost constant irrespective of condition of roughness at the interfaces since the maximum deviation is found to be 0.65%.

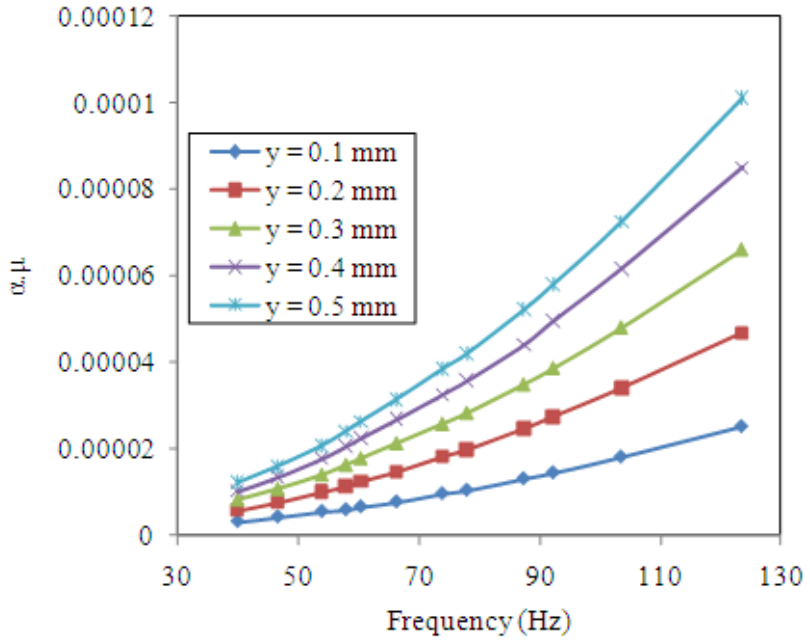

Fig. 9.13 Variation of $\alpha.\mu$ with frequency of vibration for mild steel specimens with beam thickness ratio 1.0 at different initial amplitudes of excitation (y)

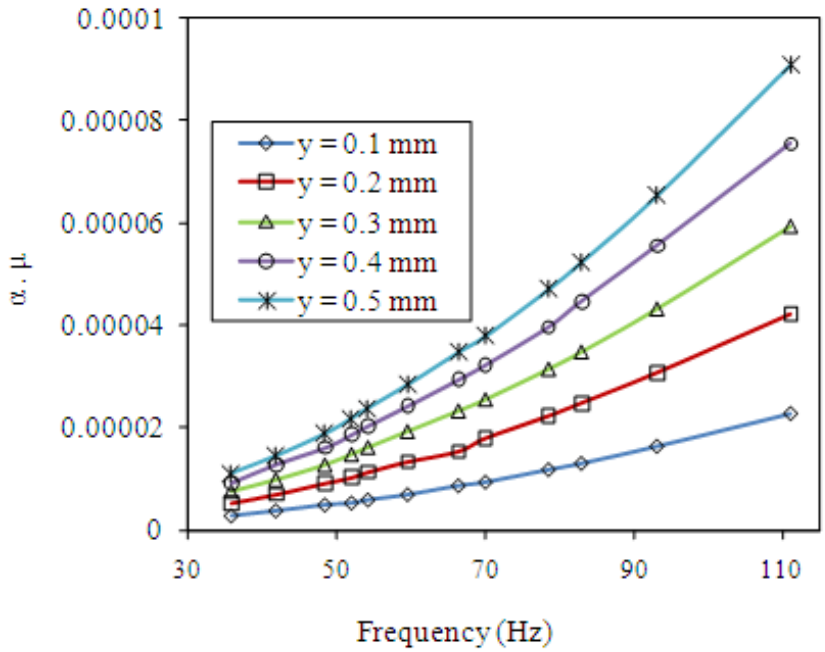

Fig. 9.14 Variation of $\alpha.\mu$ with frequency of vibration for mild steel specimens with beam thickness ratio 1.5 at different initial amplitudes of excitation (y)

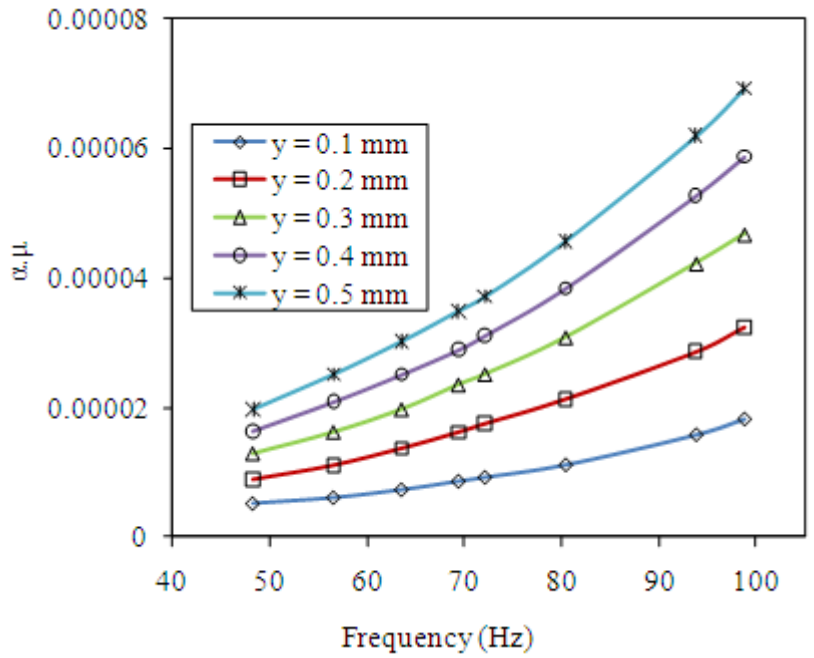

Fig. 9.15 Variation of $\alpha.\mu$ with frequency of vibration for mild steel specimens with beam thickness ratio 2.0 at different initial amplitudes of excitation (y)

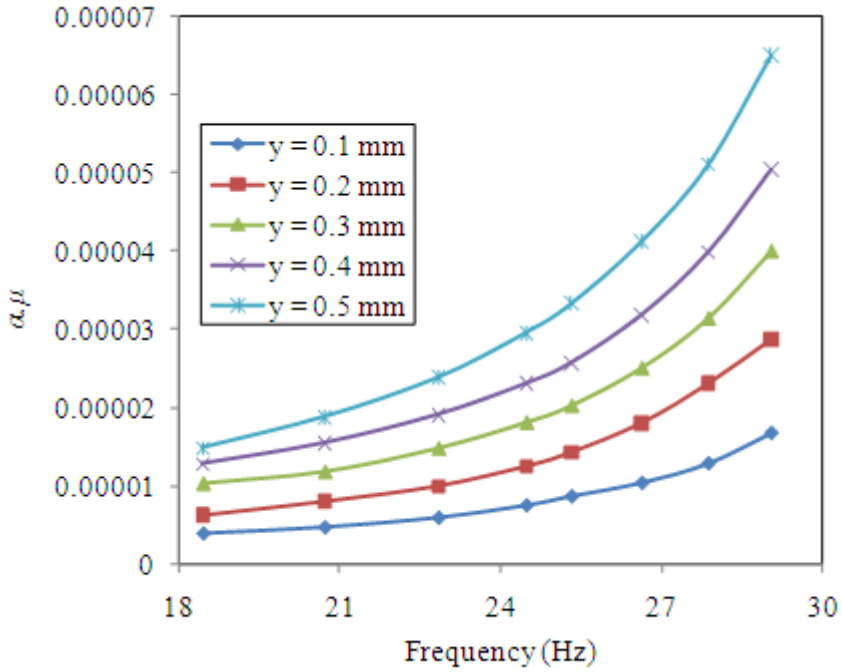

Fig. 9.16 Variation of $\alpha.\mu$ with frequency of vibration for aluminium specimens with beam thickness ratio 1.0 at different initial amplitudes of excitation (y)

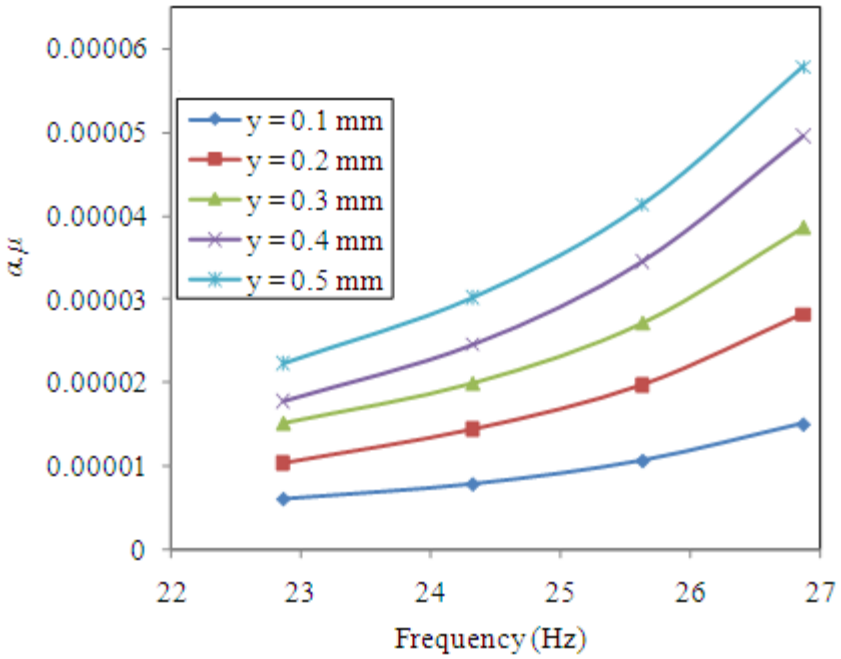

Fig. 9.17 Variation of $\alpha.\mu$ with frequency of vibration for aluminium specimens with beam thickness ratio 1.5 at different initial amplitudes of excitation (y)

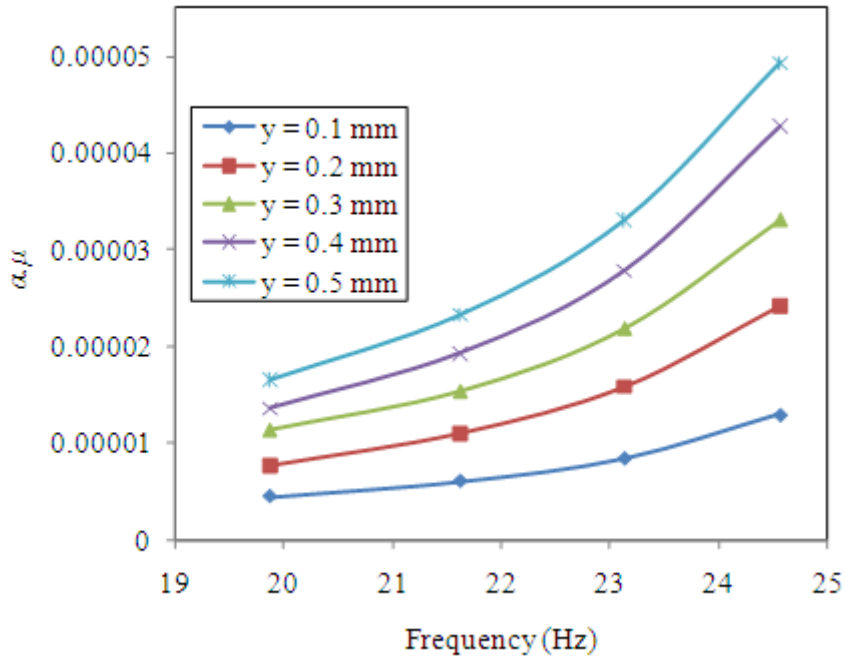

Fig. 9.18 Variation of $\alpha.\mu$ with frequency of vibration for aluminium specimens with beam thickness ratio 2.0 at different initial amplitudes of excitation (y)

The presence of joints to assemble the layered and jointed structures damp out the vibrations and reduces the stiffness. This reduction in the stiffness brings about a slight decrease in the natural frequency. It is thus observed that the jointed beam has lower frequencies compared to its equivalent solid one. This difference in frequency is fairly close at lower modes of vibration. Further, the reduction in the frequency of vibration results a change in the product of $\alpha.\mu$ under various conditions of the beam.

Table 9.14 Experimental logarithmic decrement of mild steel and aluminium welded beams with different surface roughness

Material	Length × thickness × width (mm × mm × mm)	Thickness ratio	Roughness (micron)	Logarithmic decrement
Mild Steel	520.65 × (3+3) × 40.25	1.0	0.81	0.01744
			1.14	0.01785
			1.47	0.01794
	520.65 × (2.4+3.6) × 40.25	1.5	0.81	0.01556
			1.14	0.01578
			1.47	0.01592
	520.65 × (2+4) × 40.25	2.0	0.81	0..01414
			1.14	0.01438
			1.47	0.01484
Aluminium	520.65 × (3+3) × 40.25	1.0	0.88	0.04436
			1.53	0.04459
			2.18	0.04484
	520.65 × (2.4+3.6) × 40.25	1.5	0.88	0.03890
			1.53	0.03915
			2.18	0.03937
	520.65 × (2+4) × 40.25	2.0	0.88	0.03632
			1.53	0.03656
			2.18	0.03684

Moreover, in order to compare the damping capacity of jointed beams with their equivalent solid ones, few experiments are also conducted on geometrically identical specimens of mild steel and aluminium materials excited at 0.2 mm. The experimental results of damping capacity as well as static bending stiffness for few sample specimens are presented in Table 9.15. It is observed from the results that the damping capacity of a welded beam increases with a decrease in stiffness. Due to the incorporation of joints, it is estimated that the damping capacity increases approximately by 161 and 142% for mild steel and aluminium specimens, respectively, whereas their stiffness decreases by 14 and 13% only.

Table 9.15 Comparison of experimental logarithmic decrement and stiffness of identical solid and jointed beams excited at 0.1mm

Material	Length × width × thickness (mm × mm × mm)	Type of Specimen	Stiffness (k) (N/mm)	Damping (δ)	% decrease in k	% increase in δ
Mild steel	520.65× (3+3) ×40.25	Jointed	2.6615	0.01372	13.55	161.25
	520.65×6×40.25	Solid	3.0787	0.00525		
	560× (2.4+3.6) ×40.25	Jointed	2.1244	0.01181	14.22	154.55
	560×6×40.25	Solid	2.6159	0.00464		
	600.25× (2+4) ×40.25	Jointed	1.7358	0.01047	14.78	148.26
	600.25×6×40.25	Solid	2.0373	0.00422		
Aluminium	520.65× (3+3) ×40.25	Jointed	0.9429	0.03420	13.54	142.22
	520.65×6×40.25	Solid	1.0906	0.01413		
	560× (2.4+3.6) ×40.25	Jointed	0.7506	0.02969	13.44	136.77
	560×6×40.25	Solid	0.8671	0.01254		
	600.25× (2+4) ×40.25	Jointed	0.6109	0.02449	13.12	132.85
	600.25×6×40.25	Solid	0.7032	0.01148		

9.4.4.2 Loss Factor Measurement

Loss factor for welded beams of various configurations vibrating at dynamic conditions has been evaluated experimentally using the half-power band width method. The welded beams are excited with time dependent displacement functions using the vibration exciter of type as mentioned earlier in the preceding section. Two types of displacement function (Heaviside and harmonic nature) have been generated using the function generator. The excitation is imparted for a range of beam-tip amplitudes varying from 0.1 to 0.5 mm in steps of 0.1 mm. The input excitation and output vibration are sensed with vibration pick-ups and the corresponding signal is fed to a digital storage oscilloscope which is connected to the computer with vibration analyzer software i. e., Lab View of National Instruments limited.

The acquired input and output amplitude signals are analyzed using the vibration analyzer software. The frequency response function (FRF) has been generated using the measured amplitudes of input and output signals. The damping ratio is evaluated from the frequency curves generated using the experimental data. To estimate damping ratio from frequency domain, half-power bandwidth method has been used. In this method, FRF amplitude of the system is obtained first. Corresponding to each natural frequency, there is a peak in FRF amplitude. This method requires very accurate measurement of the vibration amplitude for excitation frequencies in the region of resonance. Once the maximum dynamic displacement (X_{max}) and resonant frequency (ω_n) have been located, the half-power points are determined when the amplitude is $X_{max}/\sqrt{2}$ and the corresponding frequencies on either side of the resonant frequencies, ω_1 and ω_2 are also determined as shown in Fig. 9.19. The more the damping, the more is the frequency range between these two points. Half-power bandwidth is defined as the ratio of the frequency range between the two half power points to the natural frequency at this mode. The damping ratio is then evaluated using the half-power bandwidth expression as given by;

$$\psi = \frac{\omega_2 - \omega_1}{2\omega_n} \tag{9.1}$$

The loss factor is evaluated using the damping ratio and is given by;

$$\eta_s = \frac{\psi}{2\pi} \tag{9.2}$$

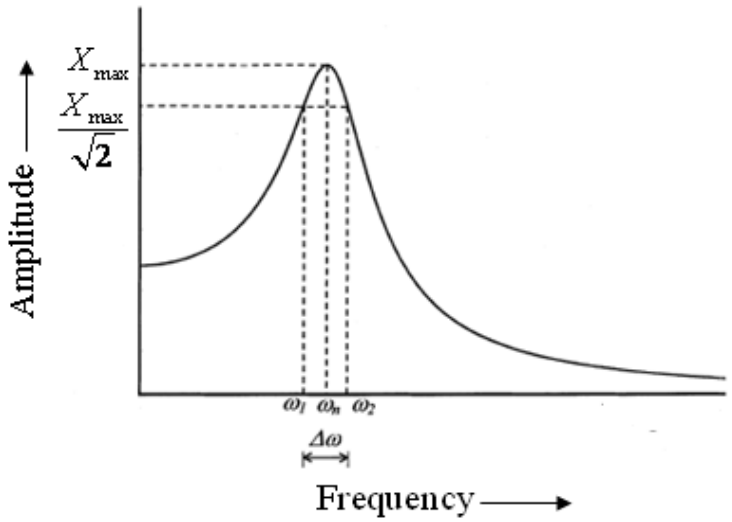

Fig. 9.19 Half-power bandwidth method for damping measurement

The damping ratio measurements are recorded for layered and welded cantilever beam specimens of mild steel and aluminium. The test specimens are fixed at one end with the help of mechanical vice as shown in Figs. 9.2 and 9.3. Proper care has been taken to ensure the perfect cantilever condition. The vibration generator is placed at the driving point just below the free end of the cantilever specimen. This shaker is used to excite the structure via a function generator with excitations in a frequency range from 0 to 800 Hz. The signal has been amplified by a power amplifier before being fed to the vibration exciter. The natural frequency is also measured under the excitation from the function generator at the point of resonance. The response is measured with an accelerometer which is placed normal to the surface at a specific point i.e., at the free end of the welded cantilever beams. The measurement configuration setup is shown in Fig. 9.3. The storage oscilloscope has been setup to measure averages of 25 readings within the frequency range of 0 to 800 Hz, in order to measure the input (channel 1) and output (channel 2) signals. The acquired input and the output signal are transmitted to the computer using the visa software and USB channel via amplifier. The amplifier is used to amplify the low frequency response. The computer is installed with the vibration analyzer software i. e., Lab View of National Instruments Limited. The Lab View software is used to analyze the acquired

vibration signals. After connecting the set-up along with the analyzer, the start button on the analyzer is pressed in order to start the averaging of the 25 readings. After finding out the averages, FRF curves are generated and the data is saved in a storage drive. FFT based measurements are subject to errors from an effect known as leakage. Appropriate window function has been applied to correct this problem. The FFT amplitude, frequency or overall shape of the spectrum may be erroneous if windowing is not applied correctly. Hanning is the most commonly used window function which has been used in the present case. It provides good frequency resolution and leakage protection with fairly accurate amplitude. The window reduces the leakage and provides more accurate amplitude measurements for the resonant frequencies. This process is repeated for the various specimens and the corresponding experimental results are recorded.

The frequency response curves at different amplitudes of excitation loadings have been generated. Some of the frequency response curves are shown in Figs. 9.20-9.27. The experimental damping ratio is then evaluated using the expression (9.2) and FRF curves. Experiments are performed to evaluate the experimental loss factors for different mild steel and aluminium specimens. These experimental results are compared with the theoretical ones and the detailed discussions are presented in the succeeding chapter.

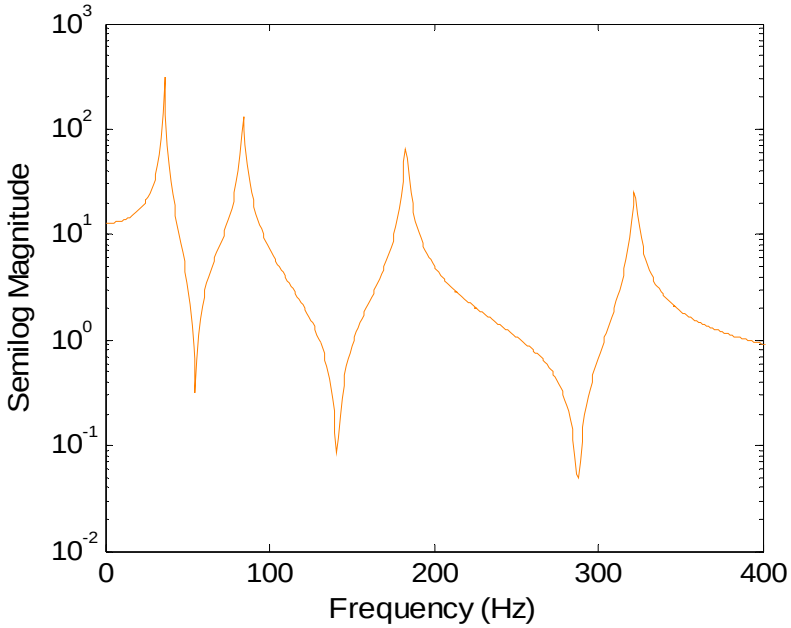

Fig. 9.20 FRF plot at Heaviside loading for welded mild steel beams of dimensions=600.6×40.2×3 and amplitude 0.1 (mm)

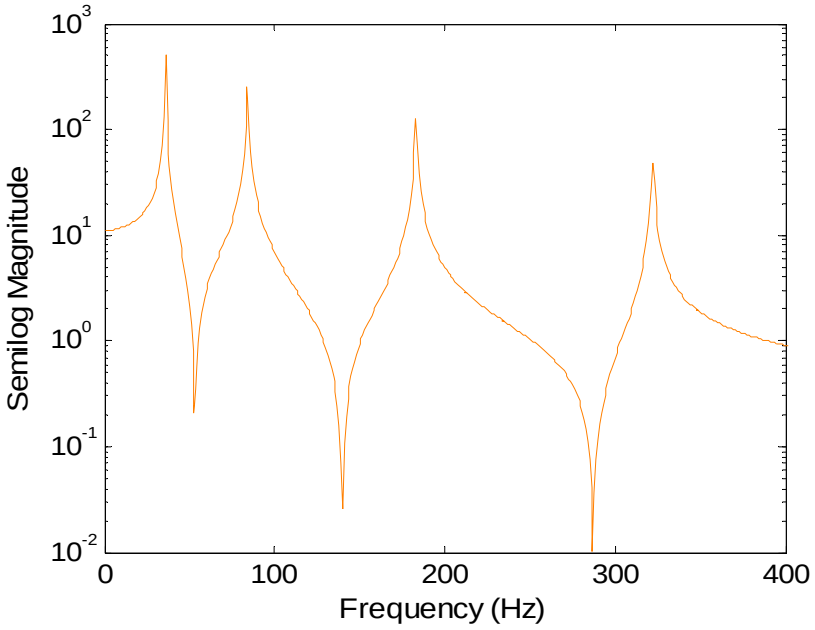

Fig. 9.21 FRF plot at Heaviside loading for welded mild steel beams of dimensions=600.6×40.2×3 and amplitude 0.2 (mm)

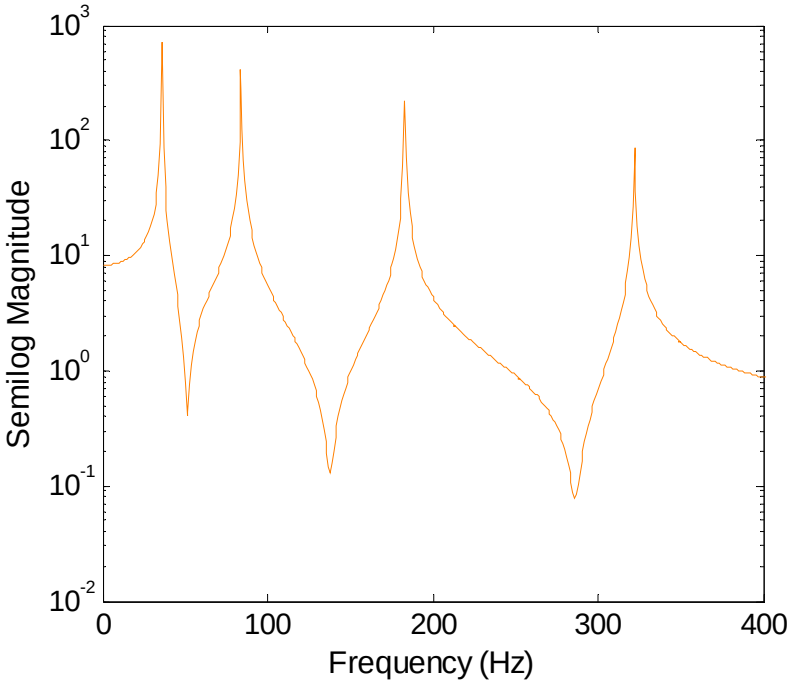

Fig. 9.22 FRF plot at harmonic loading for welded mild steel beams of dimensions=600.6×40.2×3 and amplitude 0.1 (mm)

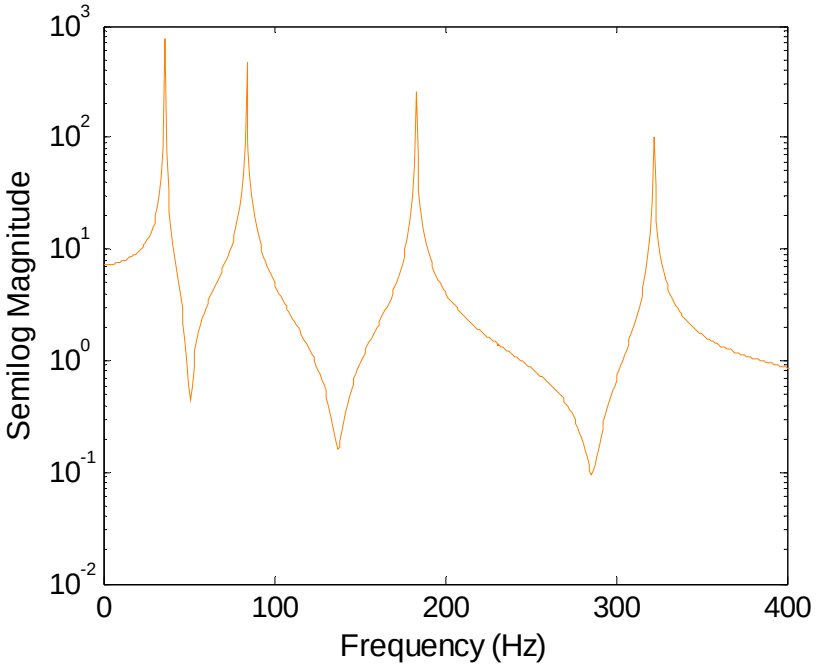

Fig. 9.23 FRF plot at harmonic loading for welded mild steel beams of dimensions=600.6×40.2×3 and amplitude 0.2 (mm)

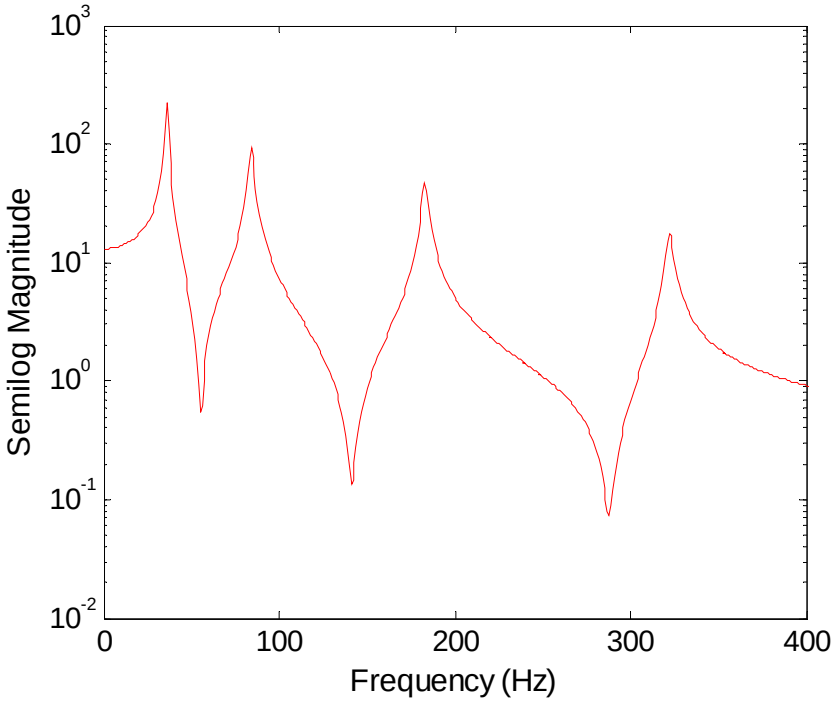

Fig. 9.24 FRF plot at Heaviside loading for welded aluminium beams of dimensions=600.6×40.2×3 and amplitude 0.1 (mm)

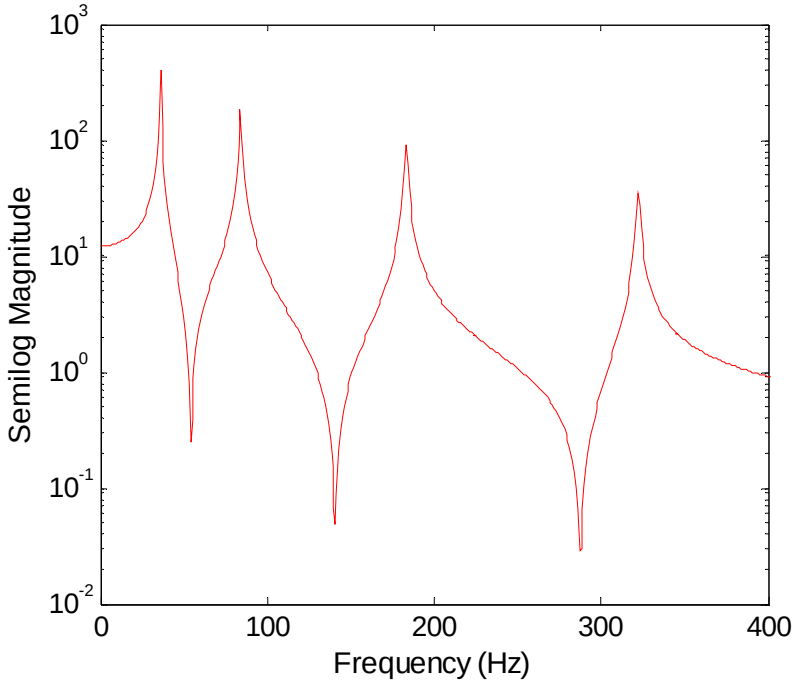

Fig. 9.25 FRF plot at Heaviside loading for welded aluminium beams of dimensions=600.6×40.2×3 and amplitude 0.2 (mm)

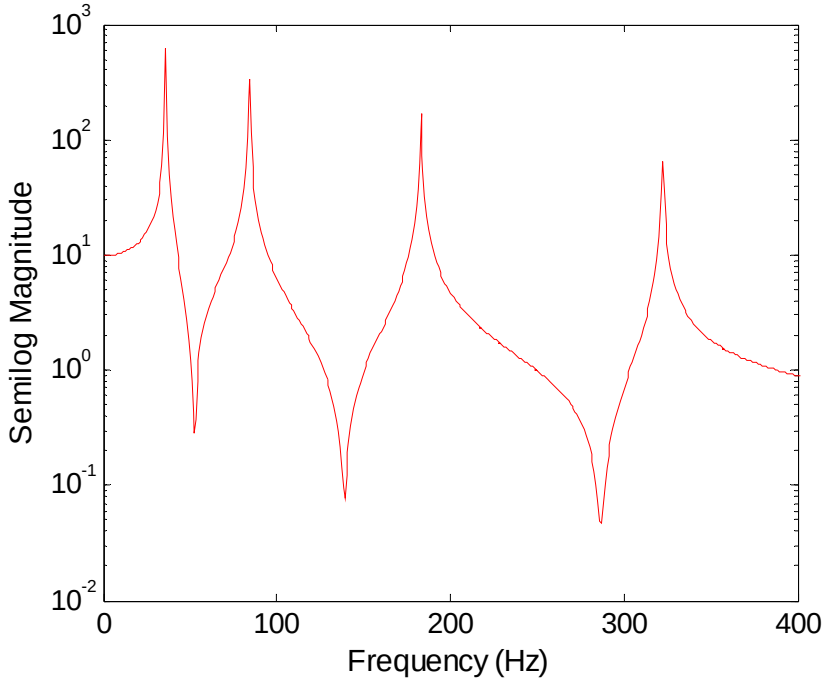

Fig. 9.26 FRF plot at harmonic loading for welded aluminium beams of dimensions=600.6×40.2×3 and amplitude 0.1 (mm)

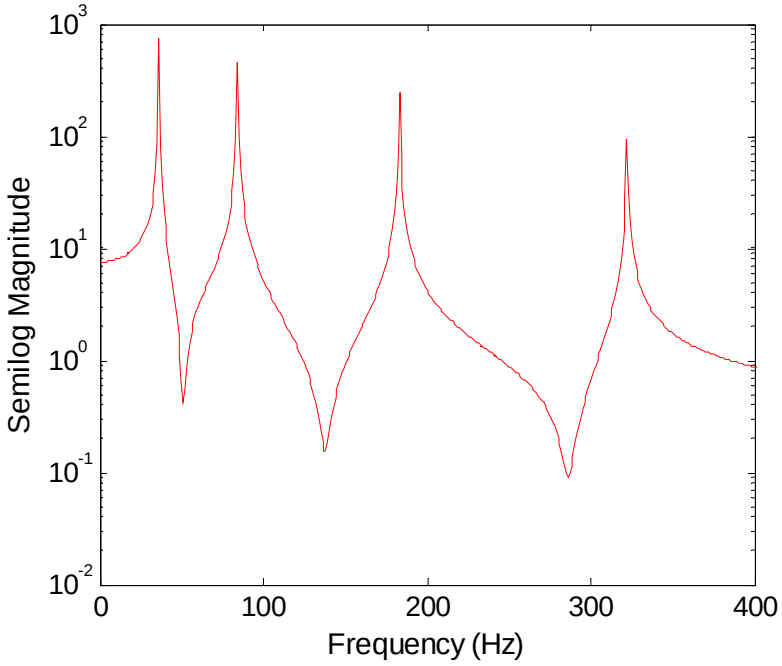

Fig. 9.27 FRF plot at harmonic loading for welded aluminium beams of dimensions=600.6×40.2×3 and amplitude 0.2 (mm)

9.5 Summary

In this chapter, a number of free and forced vibration tests have been conducted using specimens of different sizes prepared from the same stock of mild steel and aluminium commercial flats. The detailed instrumentation and necessary data for all the specimens have been presented through photographs and tables, respectively. As per the test procedure, the Young's modulus of elasticity and static bending stiffness are first found out by static deflection tests. These values are subsequently used for the theoretical evaluation of logarithmic decrement and loss factor of all the specimens. The logarithmic decrement technique, a time-response method, has been used for measuring the damping experimentally for the static loading conditions. In this method, the experimental logarithmic decrement is calculated from the time history curve of the decaying signals recorded on the screen of digital storage oscilloscope. In order to calculate the theoretical results for logarithmic decrement, the product $\alpha.\mu$ is first found out from the measured logarithmic decrement corresponding to two layered welded mild steel and aluminium beams of 3 mm thickness. This product being the frequency and amplitude dependent, plots

displaying its variation with the above two parameters have been shown in Figs. 9.11-9.16 for both mild steel and aluminium specimens with thickness ratios of 1, 1.5 and 2. Then, the product $\alpha.\mu$ of a particular test specimen is found out from the corresponding plot of the above figures at specific frequency and initial excitation of vibration. This product is then utilized to evaluate the theoretical values of logarithmic decrement at different conditions of vibration.

Moreover, this chapter also deals with the evaluation of loss factor for the welded mild steel and aluminium beams using the half-power band width method and experimentally generated frequency response curves for higher modes of vibration with thickness ratios of 1, 2, 3 and 5. The loss factor is evaluated using the frequency response functions generated experimentally. This method has the advantage over the time domain method as it is possible to evaluate the damping ratio of structures subjected to dynamic loadings and vibrating at the higher modes of vibration. Moreover, this method is employed when the structure is subjected to the forced vibration conditions. In the present study, experiments have been conducted with layered and welded beams subjected to two types of forced functions i.e., Heaviside and harmonic excitation. This method also has an advantage of capturing the resonance effects on the damping of layered and welded structures. This method is not suitable for evaluating the damping ratio of these structures subjected to static loads of low amplitudes. In case of static loading, this technique results in significant errors as the actual peak in the frequency response function is difficult to capture and much interpolation is required to estimate the half-power points.

Further, in order to study the effects of surface roughness on the damping capacity, experiments have been conducted with a few layered and welded beams made up of mild steel and aluminium. It is observed that the logarithmic decrement remains almost constant irrespective of roughness condition at the interfaces since the maximum deviation is found to be 0.65%. The experimental logarithmic decrement and loss factor have been evaluated for various mild steel and aluminium specimens. These experimental results are compared with the theoretical ones in the succeeding chapter and the necessary inferences have been drawn concerning the damping of layered and welded structures.

10

RESULTS AND DISCUSSION

10.1 Introduction

In the previous chapters, elaborate discussions have been presented for the theoretical and experimental analysis of damping mechanism of both symmetrical and unsymmetrical layered welded cantilever beams subjected to both static and dynamic vibration conditions. The theoretical part consisted of both the classical and finite element methods for measuring the damping of the layered and welded cantilever beams made up of mild steel and aluminium. Due to the assumptions made in the analysis, the theoretically computed results may be different from the actual ones. The experimental work is thus necessary for the verification of the theoretical results. For this purpose, a number of free and forced vibration tests have been conducted using specimens of different sizes prepared from the same stock of mild steel and aluminium commercial flats. The detailed instrumentation and necessary data of all specimens have been presented through photographs and tables, respectively, in Chapter 9. The damping capacity has been measured using the logarithmic damping decrement and loss factor techniques depending on the time and frequency domains, respectively. In the present chapter, both the theoretical and experimental results obtained for the damping capacity have been presented. The experimental results for logarithmic decrement and loss factor have been compared with the corresponding numerical ones obtained in chapters 3-8 for establishing the authenticity of the theory developed. Further based on the results, inferences are drawn and presented in details.

10.2 Results

In the present section, various results obtained from the theoretical and experimental analysis have been presented. These comparative results are presented in graphical forms. In all these plots, the numerical results obtained either by classical or finite element method is shown by solid lines (——) and the corresponding experimental

ones by dashed lines (-------). In presenting the results, the variation of logarithmic decrement and loss factor with respect to different influencing parameters such as; beam length, thickness ratio, amplitude of excitation and number of layers have been discussed and presented in the succeeding subsections depending on the theoretical analysis used.

10.2.1 Logarithmic Decrement of Welded Beams Based on Theoretical Analysis Considering Dynamic Slip Ratio

A classical method has been discussed in Chapter 3 for the study and evaluation of damping of two as well as multi-layered beams. First, this method is used to formulate the expressions (3.40) and (3.41) for evaluating the logarithmic decrement and product $\alpha.\mu$, respectively. The logarithmic decrements of various specimens are found out using expression (3.40) using the product $\alpha.\mu$ determined from Figs. 9.13 to 9.18 at different frequencies and amplitudes of vibration. Next, experiments have been performed on all the test specimens as discussed in the previous chapter. In this section, the comparison of the results by the classical approach and experiments has been shown in Figs. 10.1 to 10.8 for mild steel and aluminium specimens. It is observed from the above results that both the curves are close to each other with maximum variation of 12.32%.

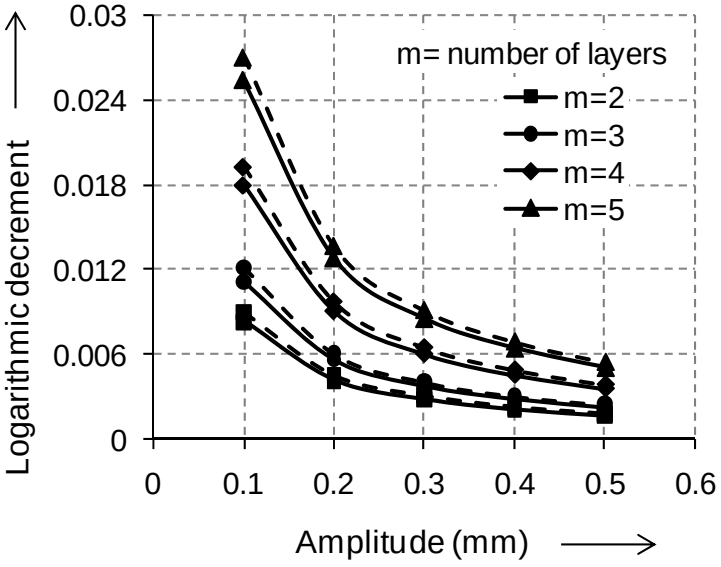

Fig. 10.1 Variation of logarithmic decrement (δ) with amplitude for welded mild steel beams of dimensions in mm (560.2x40.2x12)

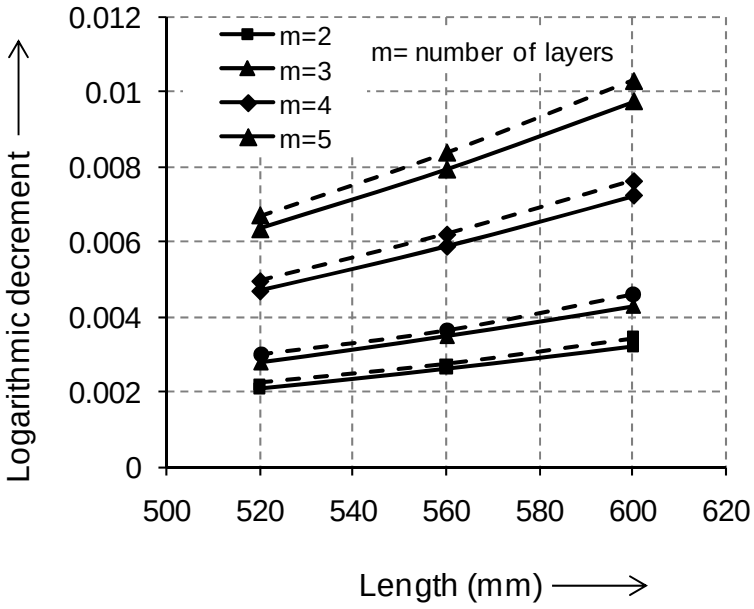

Fig. 10.2 Variation of logarithmic decrement(δ) with length for welded mild steel beams of width and thickness= 40.2 x 12 and amplitude=0.1mm

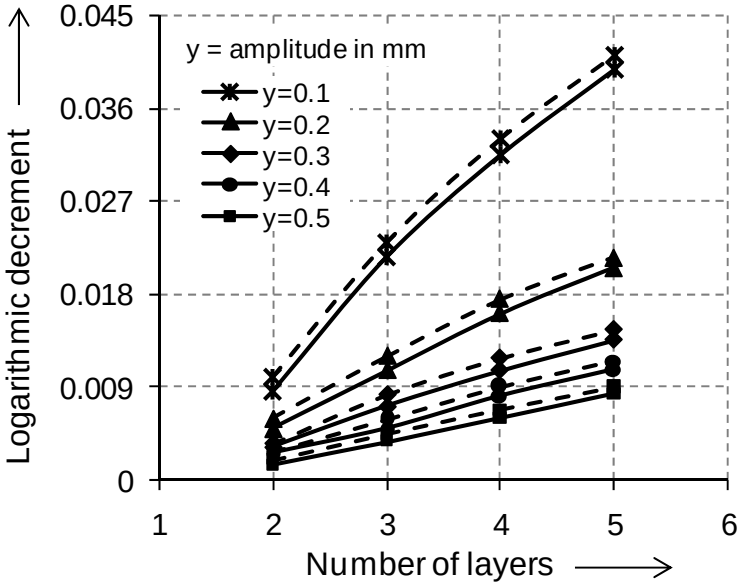

Fig. 10.3 Variation of logarithmic decrement (δ) with no. of layers for welded mild steel beams with dimension in mm=520.36 x 40.2 x 12

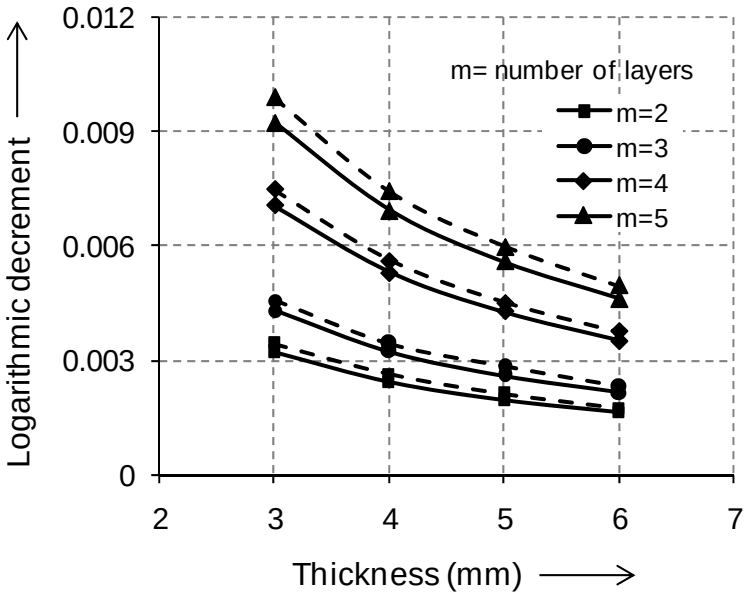

Fig. 10.4 Variation of logarithmic decrement (δ) with thickness for mild steel beams of length and width = 600.4 x 40.2 and amplitude=0.1mm

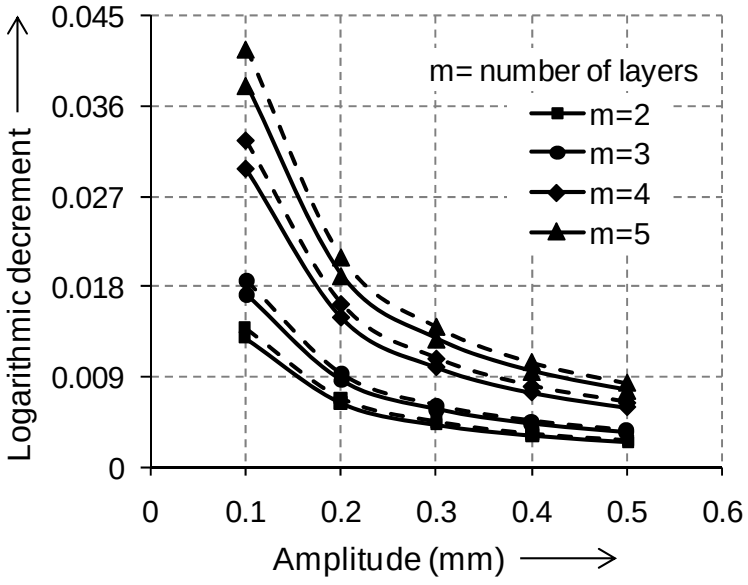

Fig. 10.5 Variation of logarithmic decrement (δ) with amplitude for welded aluminium beams of dimensions in mm = (520.2 x 40.2 x 12)

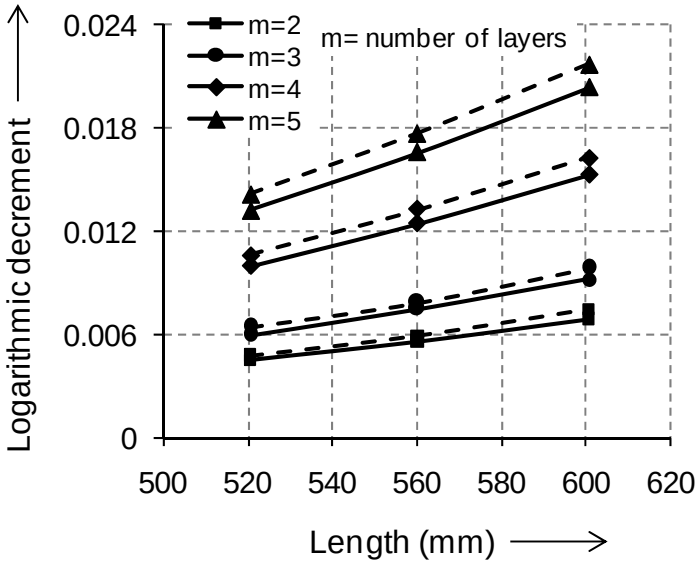

Fig. 10.6 Variation of logarithmic decrement (δ) with length for welded aluminium beams of width and thickness= 40.2x 12 and amplitude=0.2mm

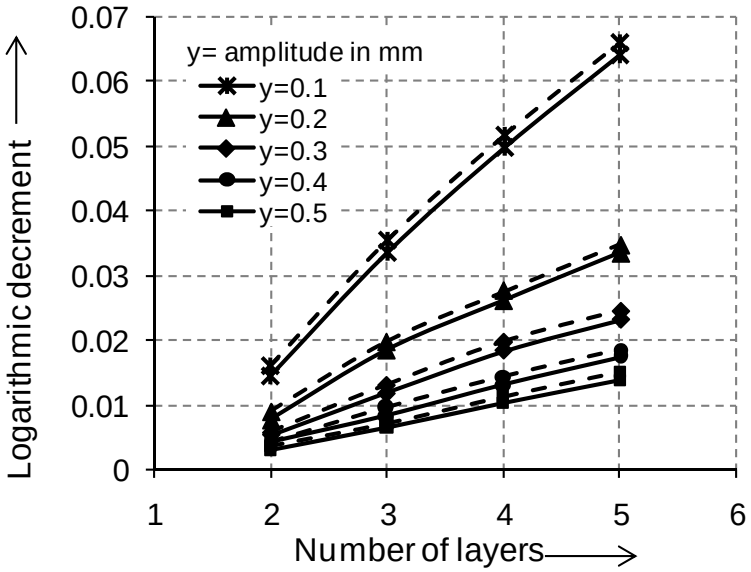

Fig. 10.7 Variation of logarithmic decrement (δ) with no. of layers for welded aluminium beams with dimension in mm=560.2x40.2x12

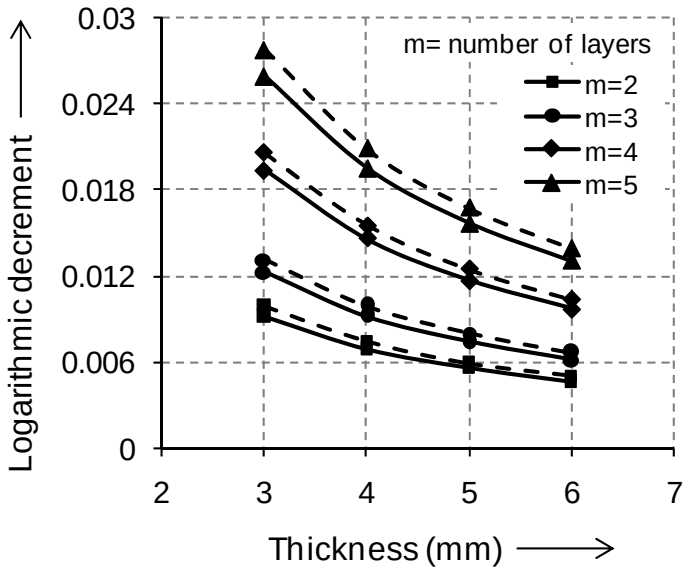

Fig. 10.8 Variation of logarithmic decrement (δ) with thickness for aluminium beams of length and width = 560.4 x 40.2 and amplitude=0.1mm

10.2.2 Loss Factor of Welded Beams with Equal Thickness Based on Theoretical Analysis Considering In-Plane Bending Stress

Theoretical analysis has been discussed in Chapters 4 and 5 for the study and evaluation of damping of two as well as multi-layered symmetrical beams. The loss factors of various specimens are found out using expressions (4.55), (5.60) and (5.61). Next, experiments are performed on all the test specimens as discussed in the previous chapter. In this section, the comparison of the theoretical results and experimental ones for loss factor are shown in Figs. 10.9 to 10.14 for mild steel and aluminium specimens. It is observed from the above results that both the curves are close to each other with maximum variation of 9.54%. Further, plots of critical load and amplitude, energy loss, dynamic response and slip with respect to the various parameters are shown in Figs. 10.15 to 10.28.

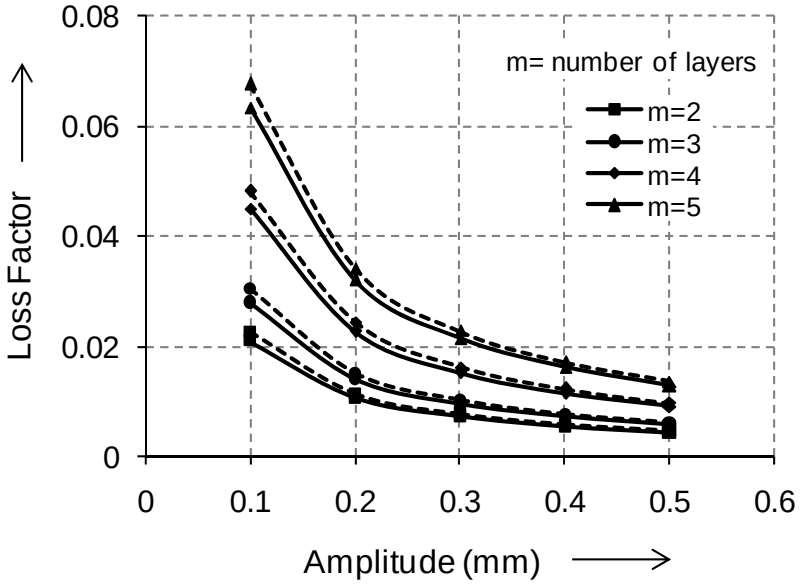

Fig. 10.9 Variation of loss factor (η_s) with amplitude for welded mild steel beam of dimensions in mm=600.2×40.2×12

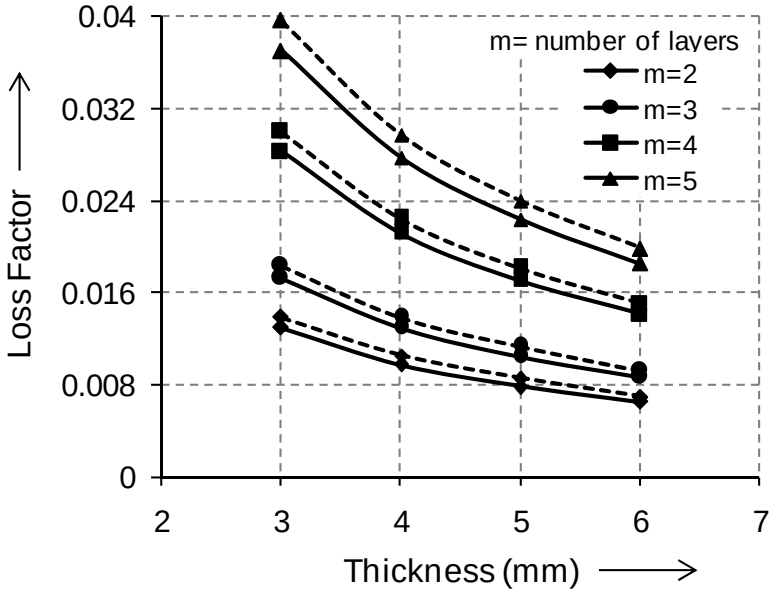

Fig. 10.10 Variation of loss factor (η_s) with thickness for mild steel beams of dimensions =600.6×40.2 and amplitude=0.1mm

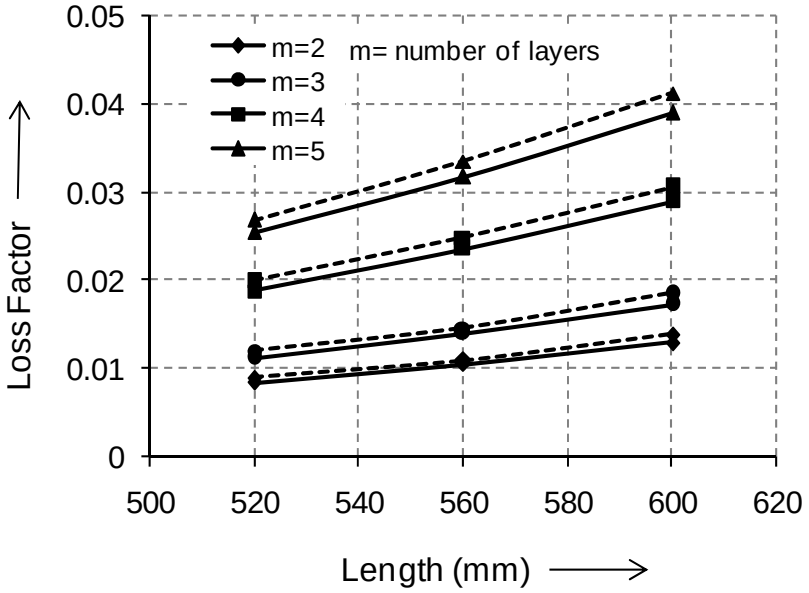

Fig. 10.11 Variation of loss factor (η_s) with length for welded mild steel beams of dimensions=40.2×12 and amplitude=0.1mm

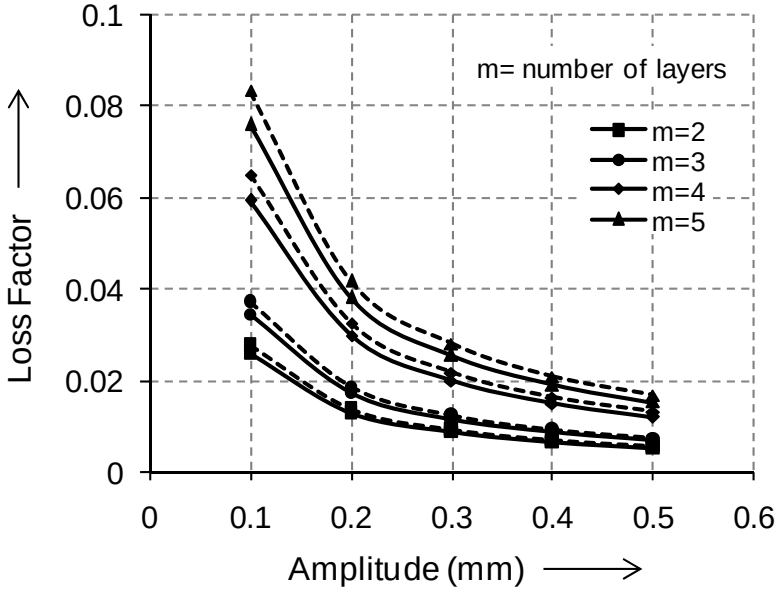

Fig. 10.12 Variation of loss factor (η_s) with amplitude for welded aluminium beams of dimensions in mm=600.6×40.2×12

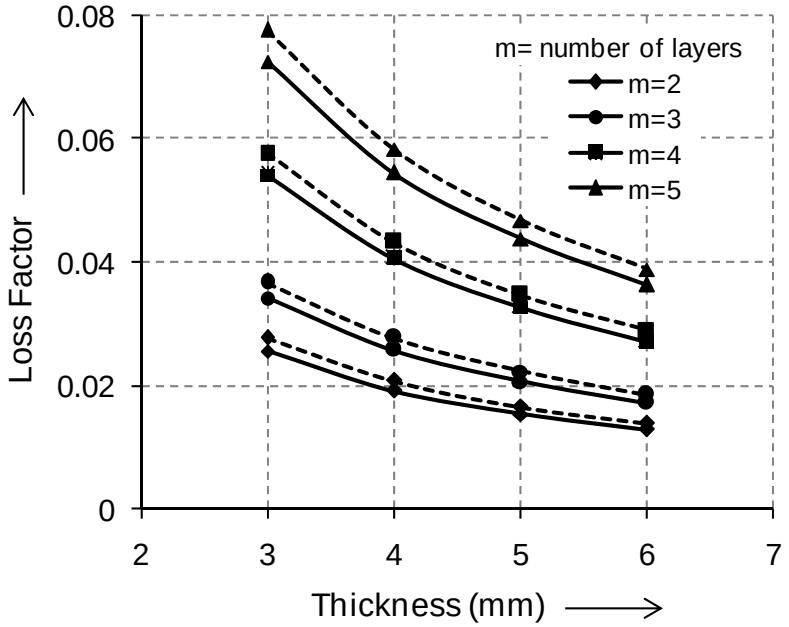

Fig. 10.13 Variation of loss factor (η_s) with thickness for aluminium beams of dimensions=600.6×40.2 and amplitude=0.1mm

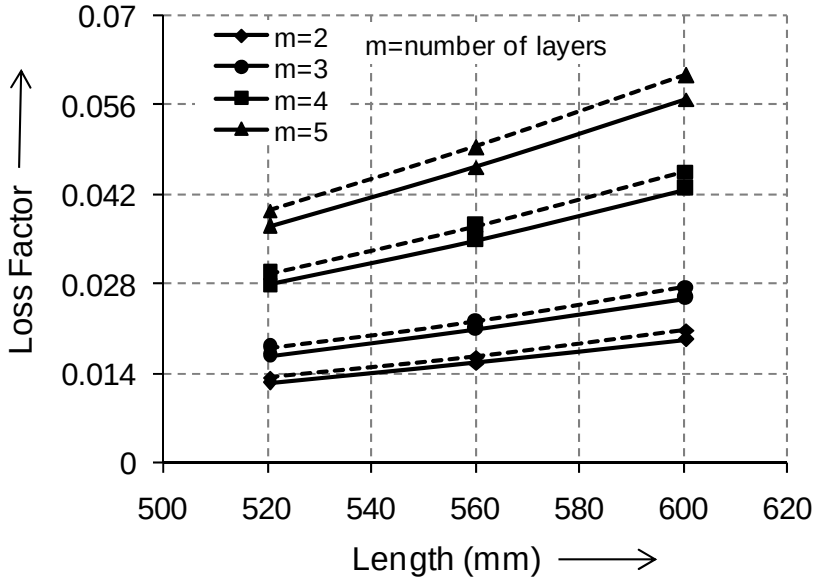

Fig. 10.14 Variation of loss factor (η_s) with length for welded aluminium beams of dimensions=40.2×12 and amplitude=0.1mm

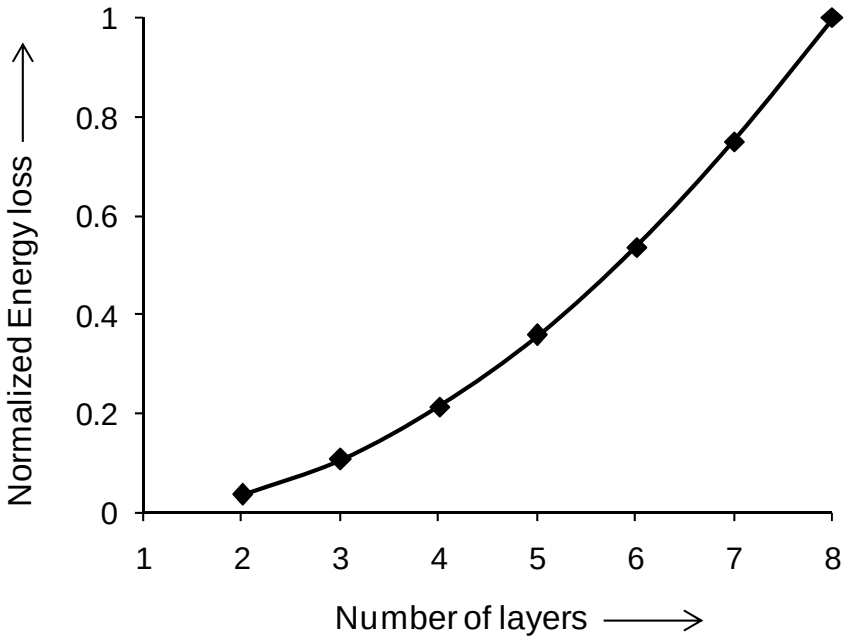

Fig. 10.15 Variation of energy loss with number of layers for welded beams

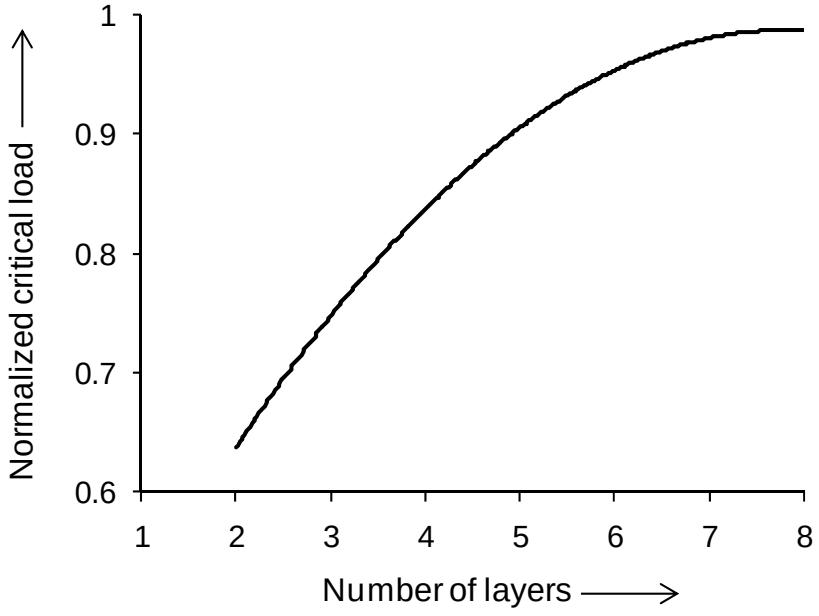

Fig. 10.16 Variation of critical load with number of layers for welded beams

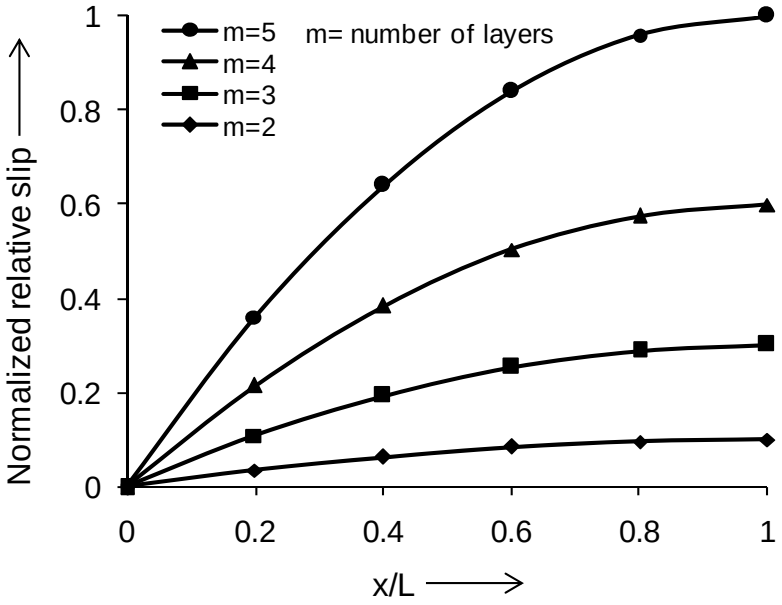

Fig. 10.17 Relative slip versus axial position

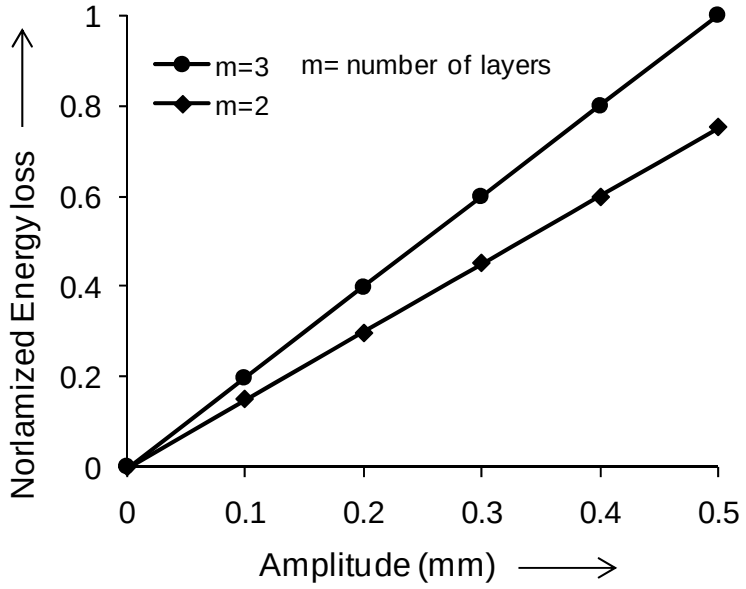

Fig. 10.18 Energy loss versus amplitude

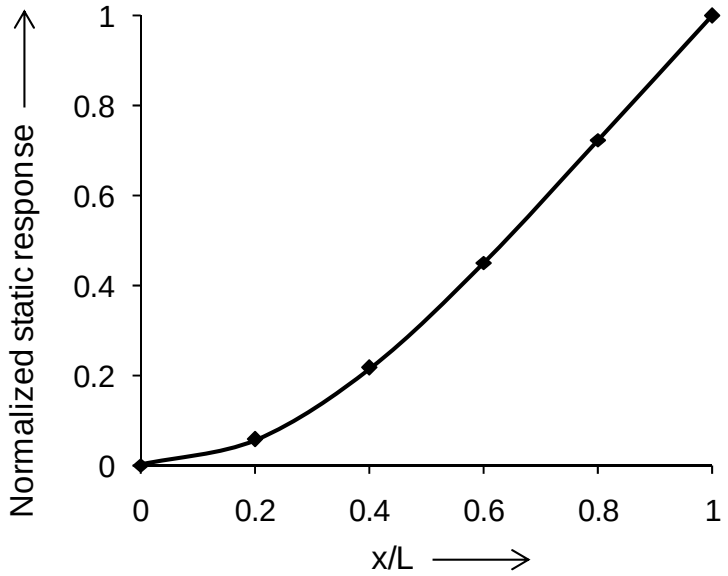

Fig. 10.19 Mode shape of the jointed and welded beam of two layers

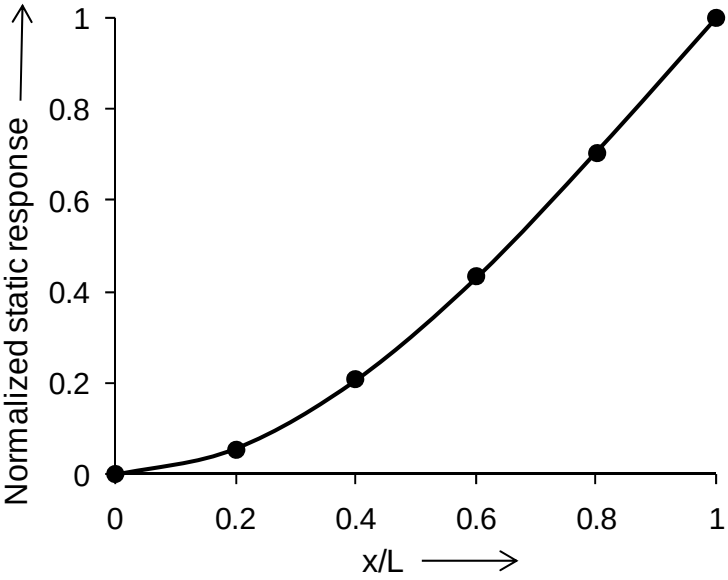

Fig. 10.20 Mode shape of the jointed and welded beam of three layers

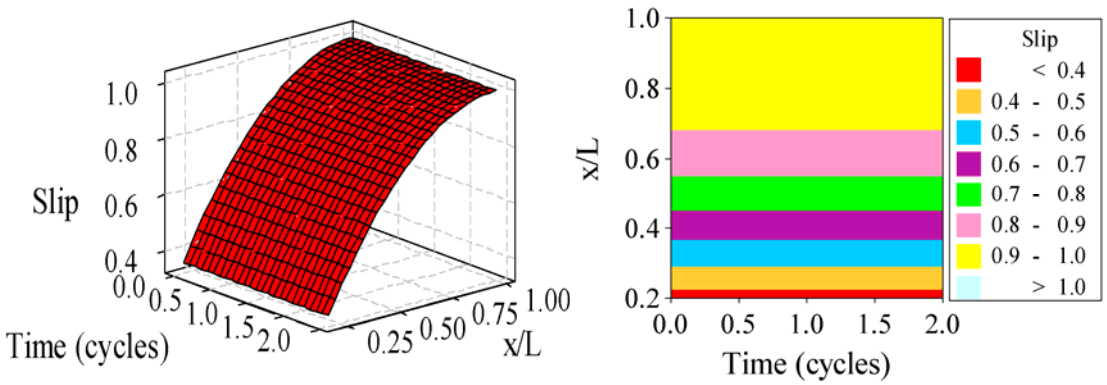

(a) Surface plot (b) Contour plot

Fig. 10.21 Normalized slip (u) profile at Heaviside loading for welded beams

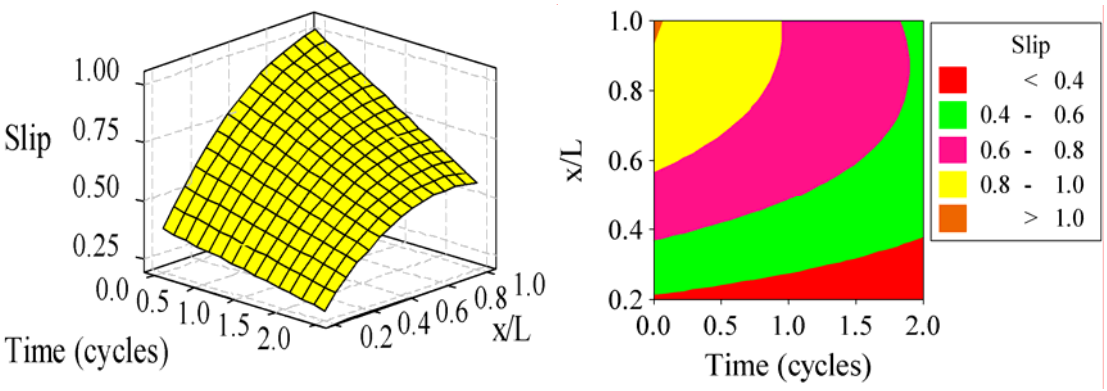

(a) Surface plot (b) Contour plot

Fig. 10.22 Normalized slip (u) profile at harmonic loading for welded beams

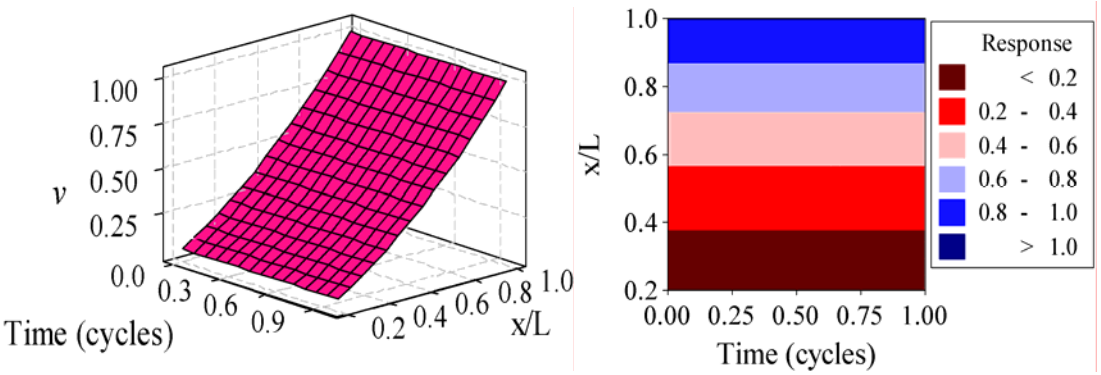

(a) Surface plot (b) Contour plot

Fig. 10.23 Normalized dynamic response (v) at Heaviside loading for welded beams

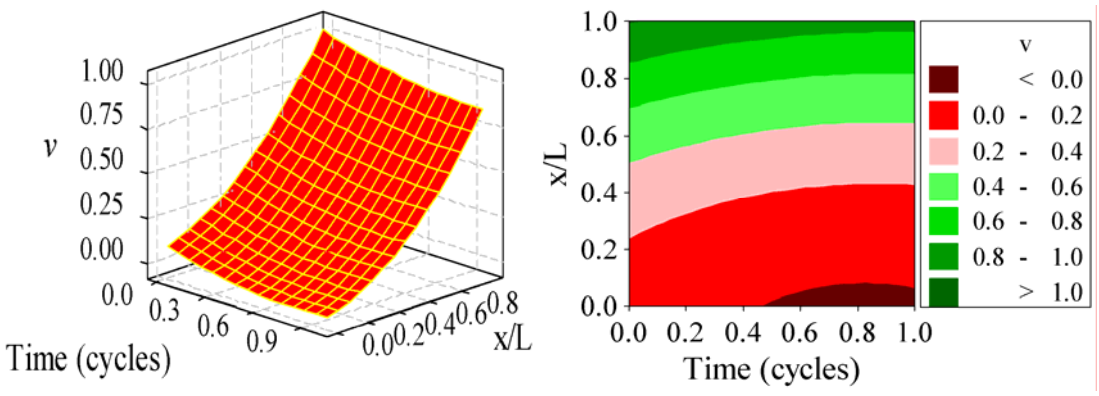

(a) Surface plot (b) Contour plot

Fig. 10.24 Normalized dynamic response (v) at harmonic loading for welded beams

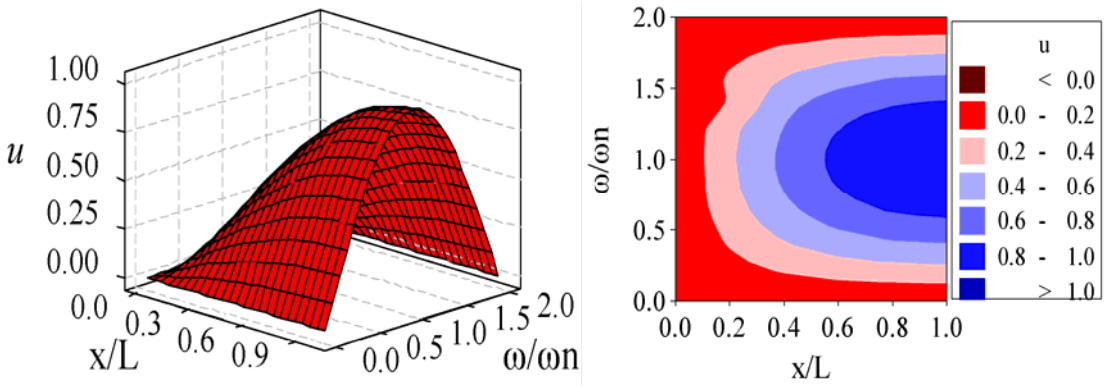

(a) Surface plot (b) Contour plot

Fig. 10.25 Normalized slip (u) at Heaviside loading with respect to frequency ratio

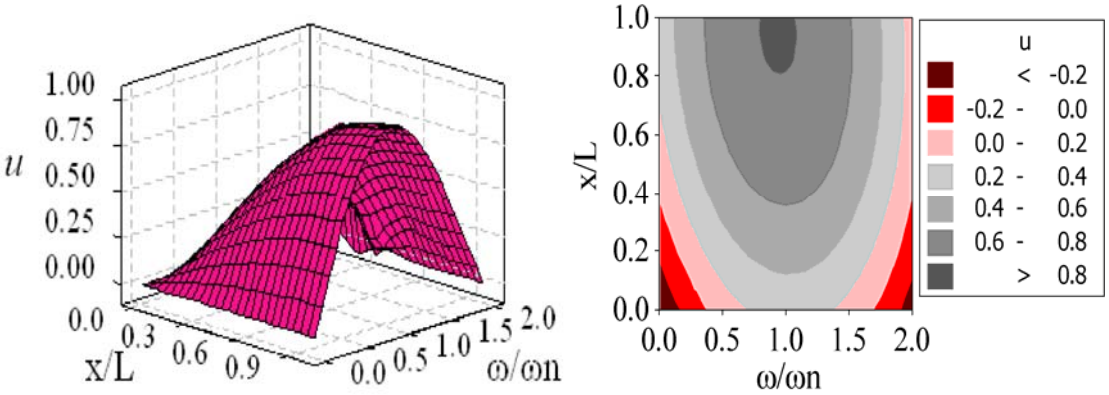

(a) Surface plot (b) Contour plot

Fig. 10.26 Normalized slip (u) at harmonic loading with respect to frequency ratio

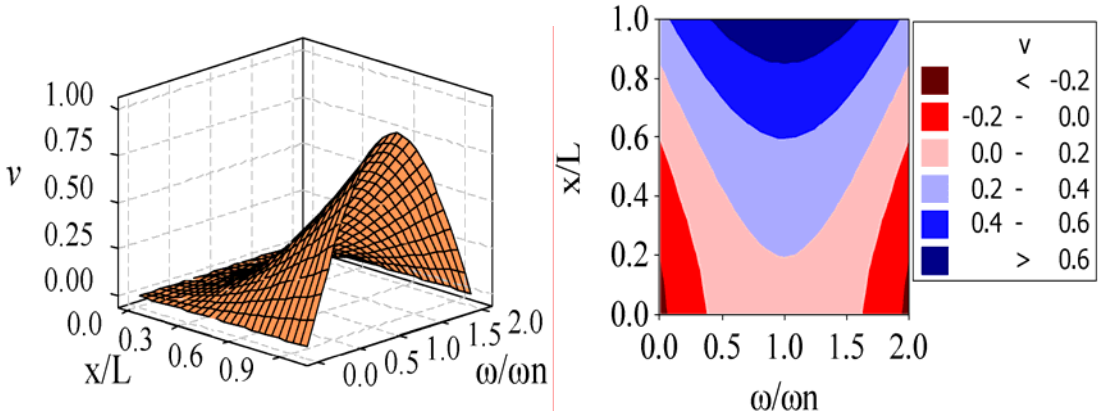

(a) Surface plot (b) Contour plot

Fig. 10.27 Normalized dynamic response(v) at Heaviside loading with frequency ratio

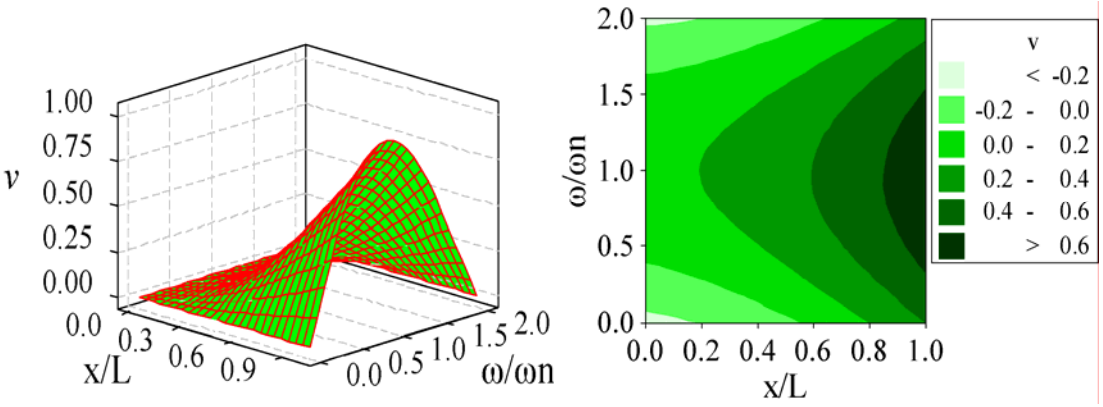

(a) Surface plot (b) Contour plot

Fig. 10.28 Normalized dynamic response(v) at harmonic loading with frequency ratio

10.2.3 Loss Factor of Welded Beams with Unequal Thickness Based on Theoretical Analysis Considering In-Plane Bending Stress

For the study and evaluation of damping of layered and welded beams of unequal thickness, theoretical analysis has been developed and discussed in Chapter 6. The loss factors of various specimens are found out using expressions (6.23) and (6.58). Next, experiments are performed on all the test specimens as discussed in the previous chapter. In this section, the comparison of the theoretical results and experimental ones are shown in Figs. 10.29 to 10.34 for mild steel and aluminium specimens. It is observed from the above results that both the curves are close to each other with

maximum variation of 10.26%. Further, plots of energy loss, dynamic response and slip with respect to the various parameters are shown in Figs. 10.35 to 10.42.

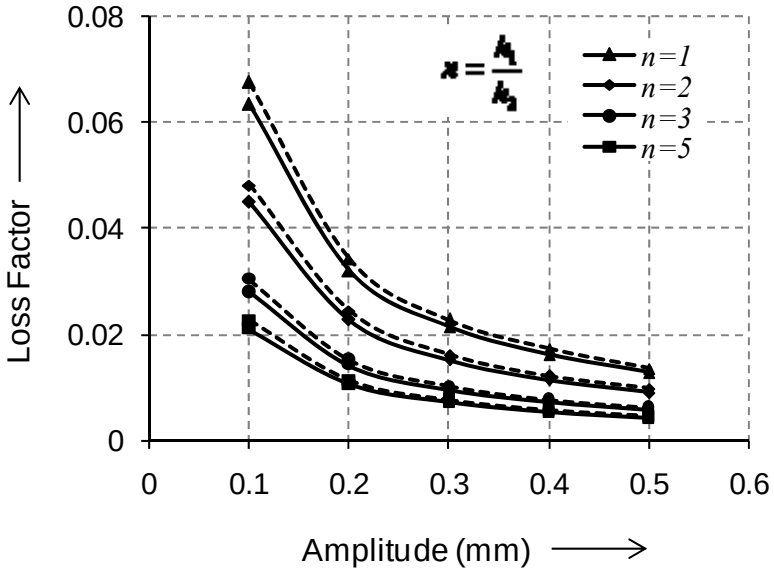

Fig. 10.29 Variation of loss factor (η_s) with amplitude for welded mild steel beam of dimensions in mm=560.2×40.2×12

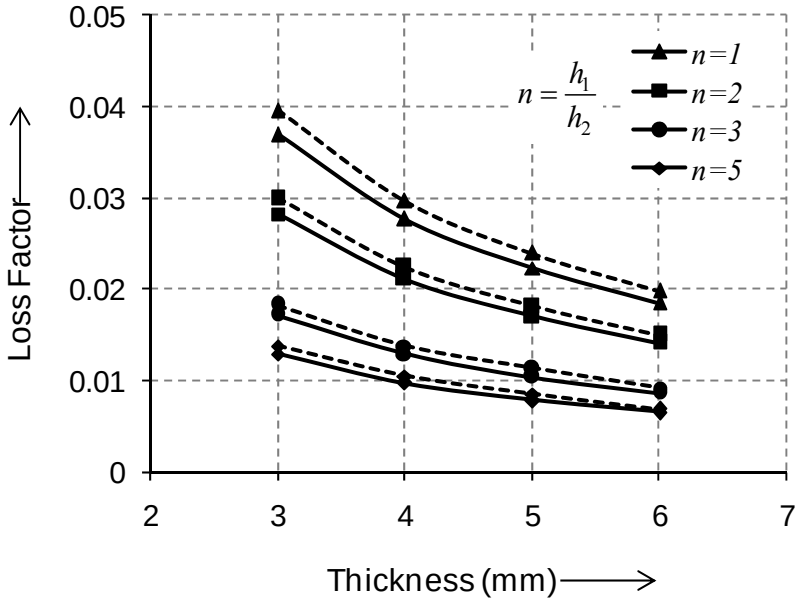

Fig. 10.30 Variation of loss factor (η_s) with thickness for mild steel beams of dimensions=560.2×40.2 and amplitude=0.1mm

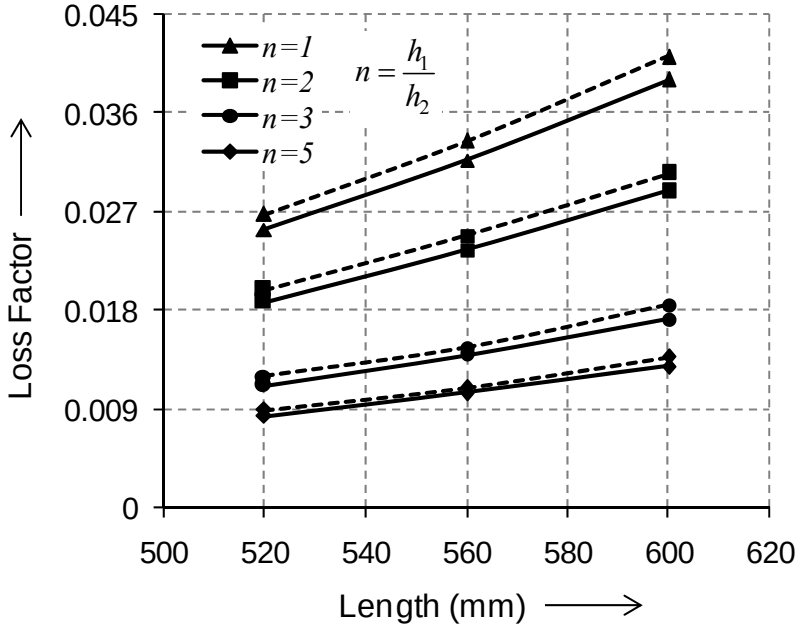

Fig. 10.31 Variation of loss factor (η_s) with length for welded mild steel beams of dimensions=40.2×12 and amplitude=0.1mm

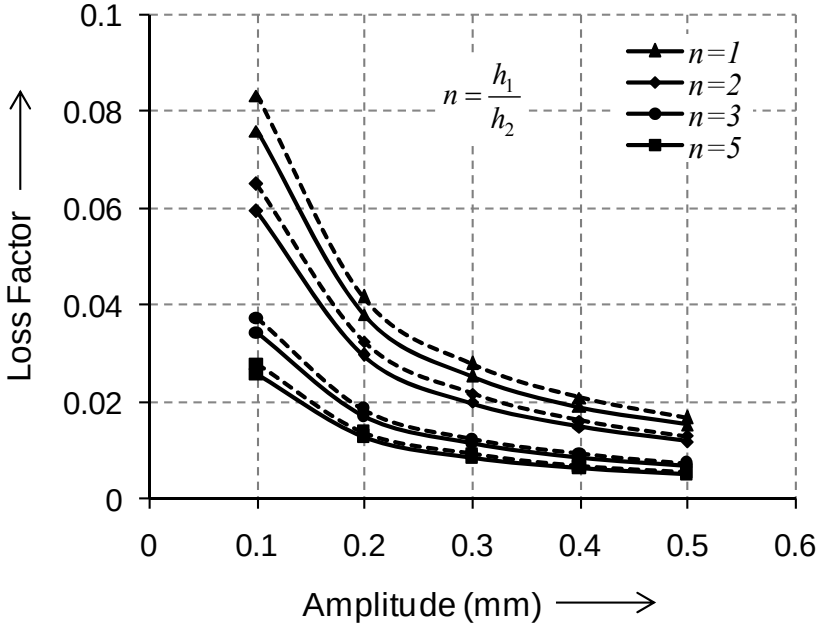

Fig. 10.32 Variation of loss factor (η_s) with amplitude for welded aluminium beams of dimensions in mm=560.6×40.2×12

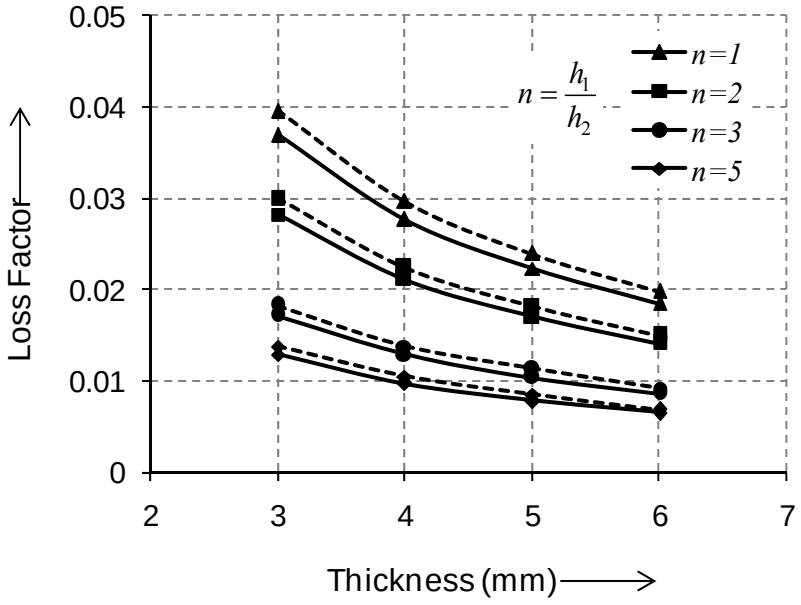

Fig. 10.33 Variation of loss factor (η_s) with thickness for aluminium beam of dimensions=560.6×40.2 and amplitude=0.1mm

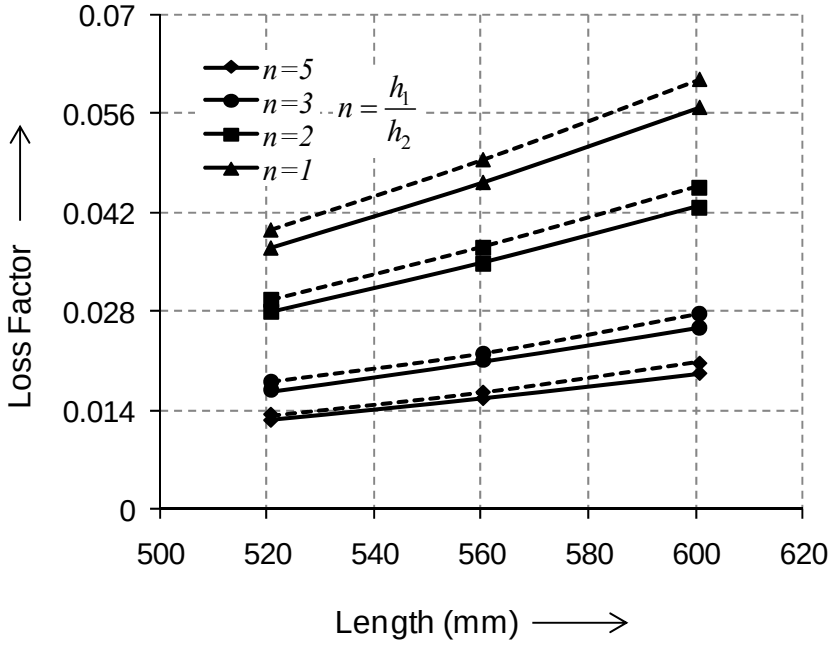

Fig. 10.34 Variation of loss factor (η_s) with length for welded aluminium beams of dimensions=40.2×12 and amplitude=0.1mm

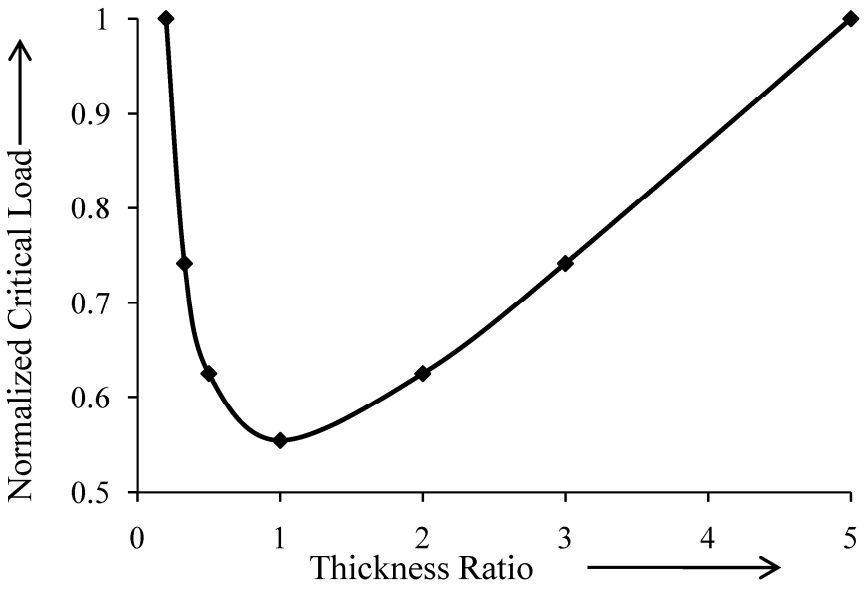

Fig. 10.35 Variation of critical load with thickness ratio for welded beams

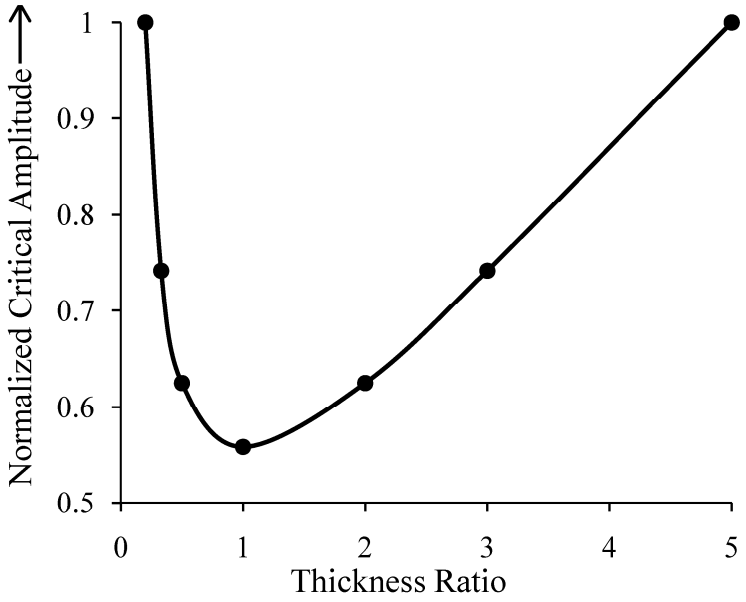

Fig. 10.36 Variation of critical amplitude with thickness ratio for welded beams

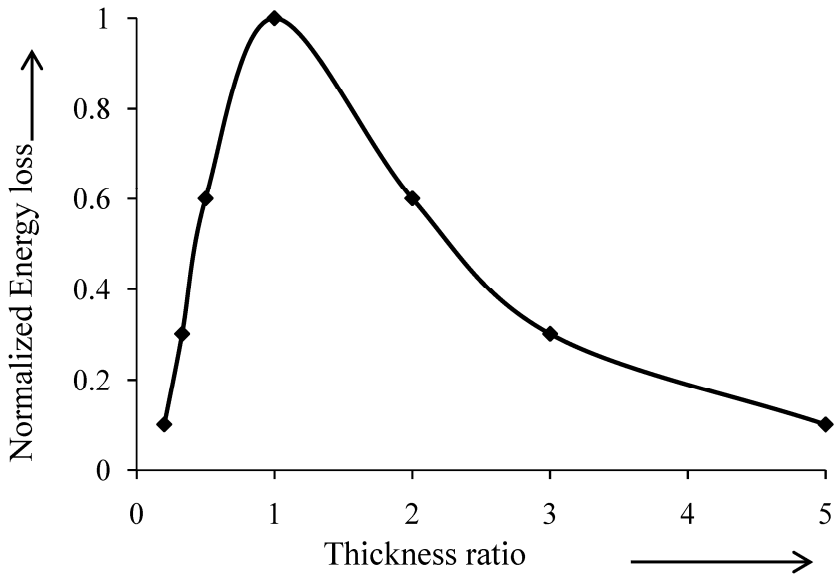

Fig. 10.37 Variation of Energy loss with thickness ratio (*n*) for welded beams

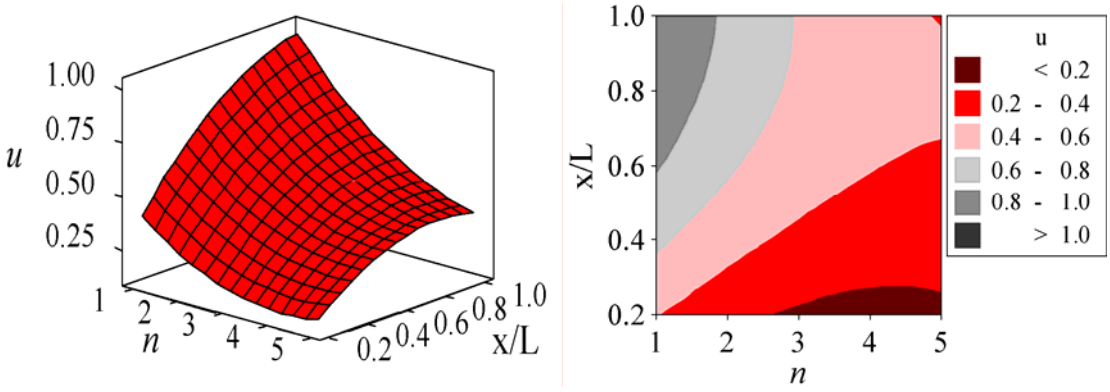

(a) Surface plot (b) Contour plot

Fig. 10.38 Normalized slip with axial position and thickness ratio (*n*) more than one

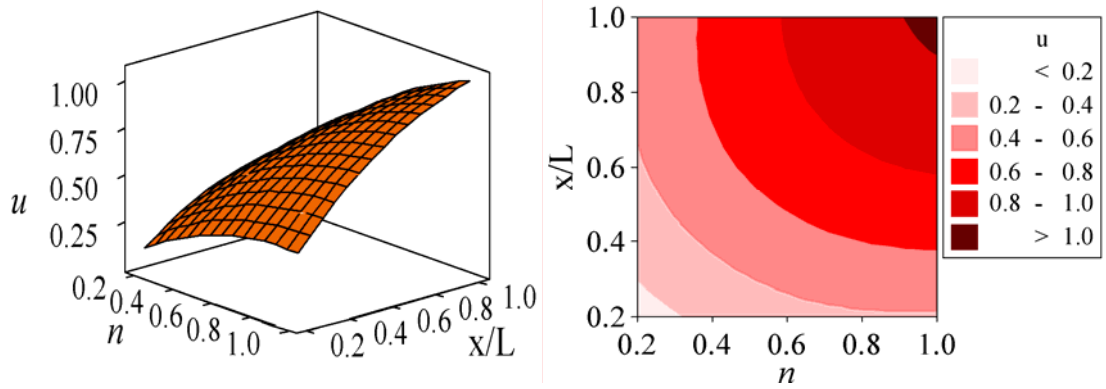

(a) Surface plot (b) Contour plot

Fig. 10.39 Normalized slip with axial position and thickness ratio (*n*) less than one

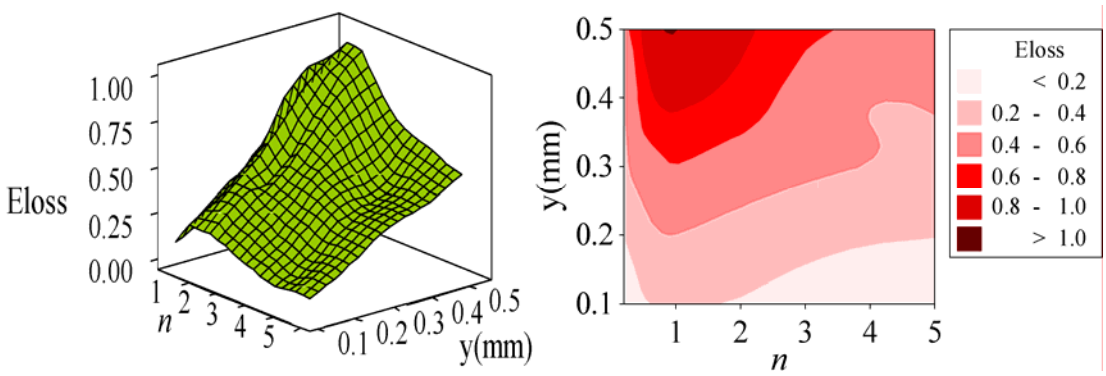

(a) Surface plot (b) Contour plot

Fig. 10.40 Normalized energy loss with amplitude (y) and thickness ratio (n)

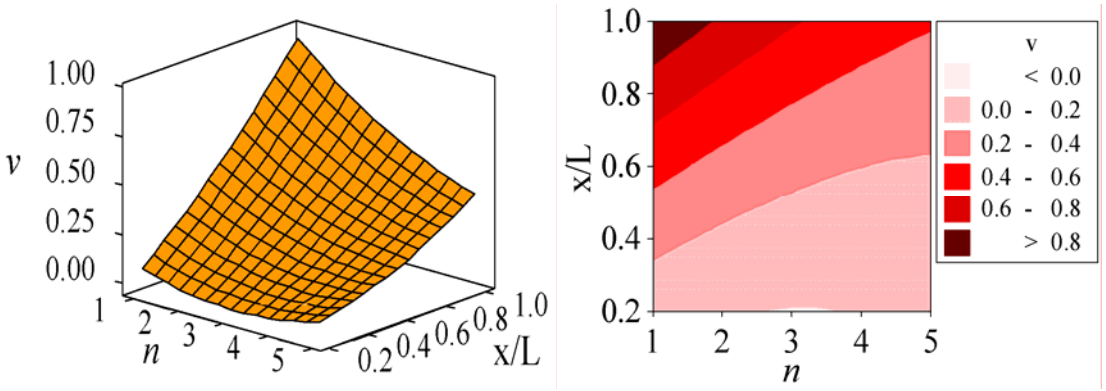

(a) Surface plot (b) Contour plot

Fig. 10.41 Dynamic response with axial position and thickness ratio greater than one

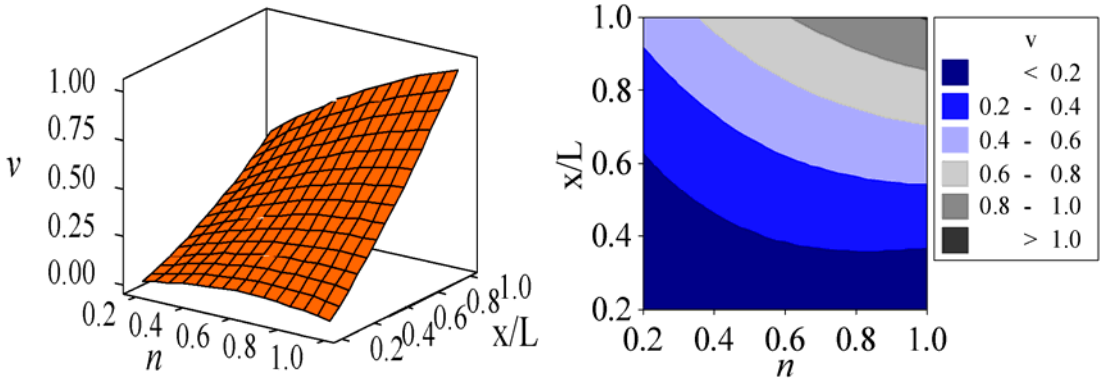

(a) Surface plot (b) Contour plot

Fig. 10.42 Dynamic response with axial position and thickness ratio less than one

10.2.4 Loss Factor of Welded Beams Based on Finite Element Analysis

Finite element analysis has been discussed in Chapter 7 for the study and evaluation of damping of layered and welded beams. The loss factors of various specimens are found out using expression (7.23). Further, experiments are also performed on all the test specimens as discussed in the previous chapter. In this section, the comparison of the theoretical results and experimental ones are presented in Figs. 10.43 to 10.48 for mild steel and aluminium specimens. It is observed from the above results that both the curves are close to each other with maximum variation of 13.42%.

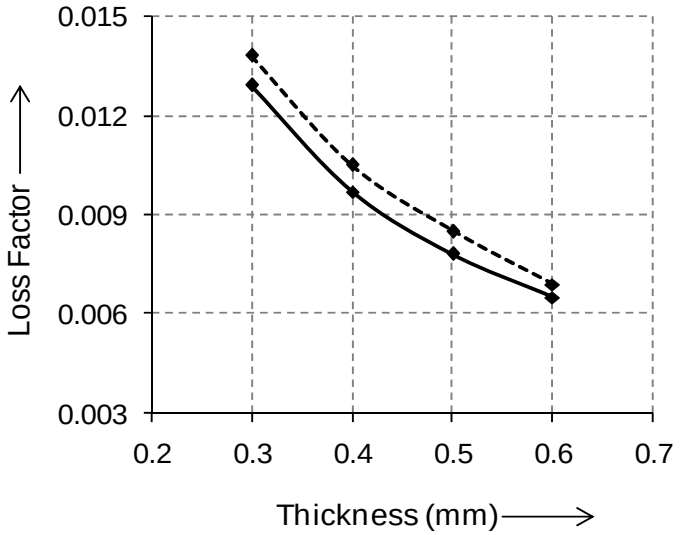

Fig. 10.43 Variation of loss factor (η_s)with thickness for mild steel beams of dimensions=520.4×40.2 and amplitude=0.2 mm

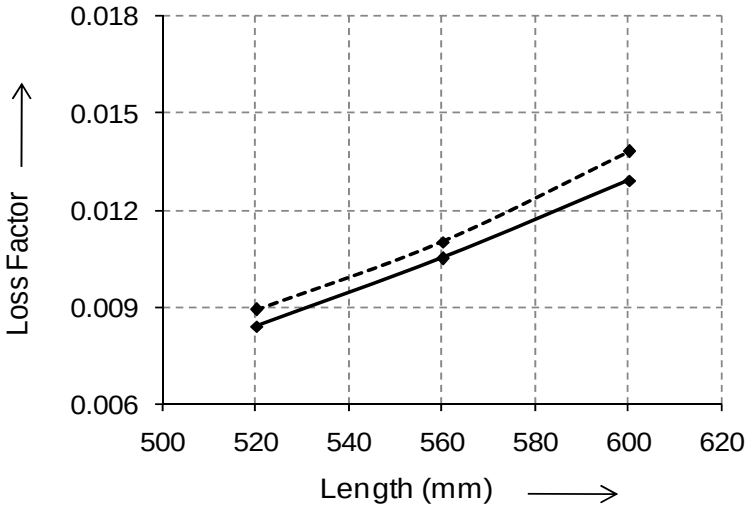

Fig. 10.44 Variation of loss factor (η_s) with length for welded mild steel beams of dimensions=40.2×12 and amplitude=0.2 mm

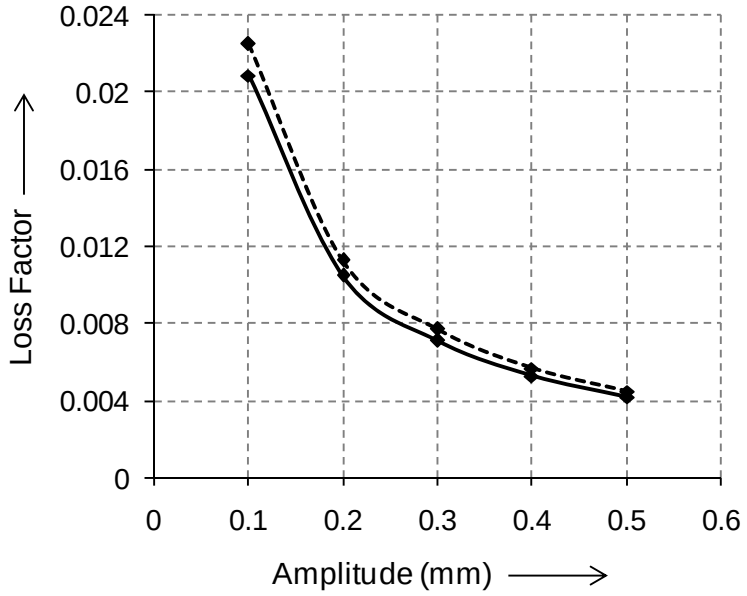

Fig. 10.45 Variation of loss factor (η_s) with amplitude for welded mild steel beams of dimensions in mm=520.4×40.2×12

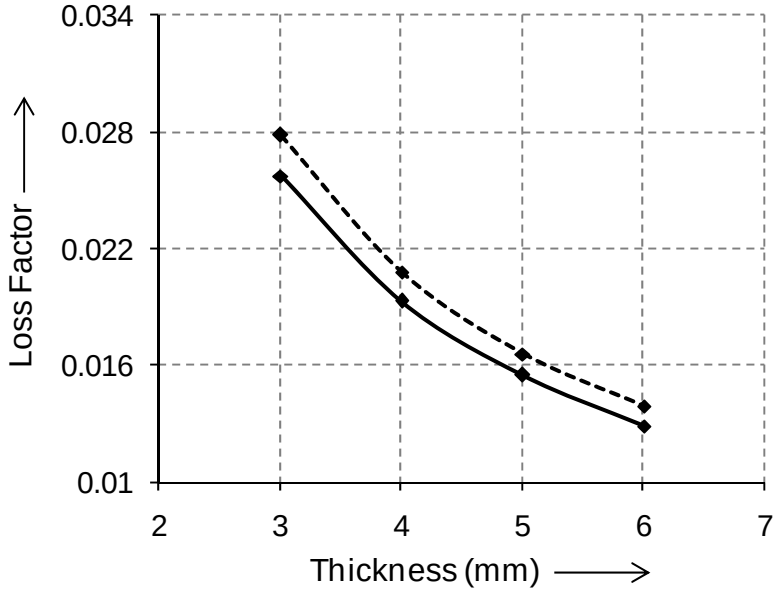

Fig. 10.46 Variation of loss factor (η_s) with thickness for aluminium beams of dimensions =520.4×40.2 and amplitude=0.2mm

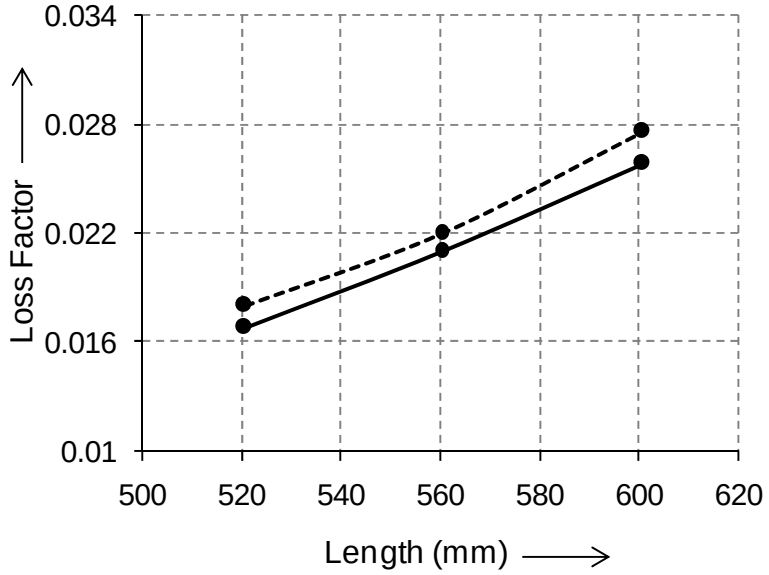

Fig. 10.47 Variation of loss factor (η_s) with length for welded aluminium beams of dimensions=40.2×12 and amplitude=0.2 mm

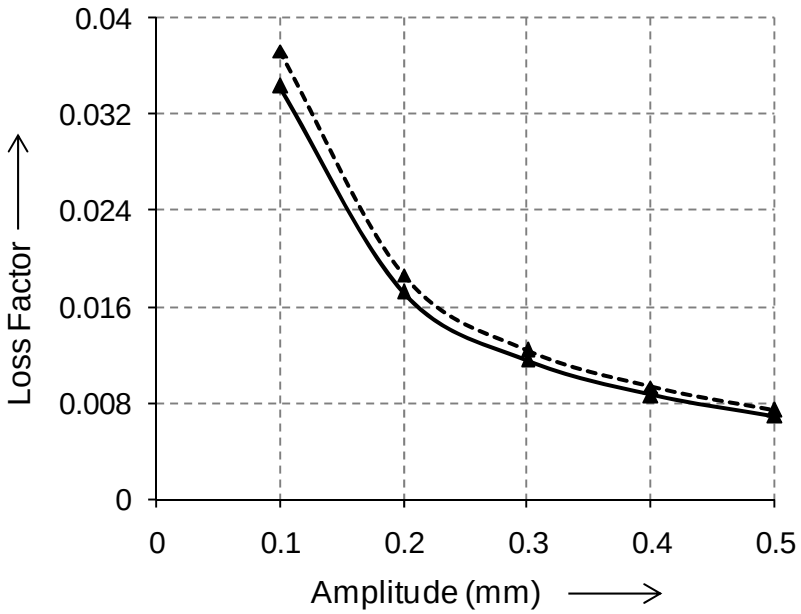

Fig. 10.48 Variation of loss factor (η_s) with amplitude for welded aluminium beams of dimensions in mm=520.4×40.2×12

In gist, the influence of various parameters on the damping capacity of layered and welded symmetrical and unsymmetrical structures at different modes of vibration are presented in Tables 10.1-10.3 for mild steel and aluminium specimens.

Table 10.1 Effect of influencing parameters on the damping capacity of mild steel beams

Length × thickness × width (mm × mm × mm)	Influencing parameter	Variation of influencing parameter	Variation in damping capacity
440× (3+3) ×40.25 (with 0.1 mm amplitude)	Beam length	Increases from 440 to 600 mm	Increases by 39.24%
520× (3+3) ×40.25	Amplitude of vibration	Increases from 0.1 to 0.5 mm	Decreases by 24.78%
560×6×40.25 (with 0.1 mm amplitude)	Beam thickness ratio	Increases from 1.0 to 2.0	Decreases by 23.26%
600.6×12×40.25 (with 0.3 mm amplitude)	Number of layers	Two layers	Increase by 149.42% compared to equivalent solid one
		Three layers	Increases by 32.16% compared to that of two layers
		Four layers	Increases by 61.58% compared to that of two layers

Table 10.2 Effect of influencing parameters on the damping capacity of aluminium beams

Length × thickness × width (mm × mm × mm)	Influencing parameter	Variation of influencing parameter	Variation in damping capacity
440× (3+3) ×40.25 (with 0.1 mm amplitude)	Beam length	Increases from 440 to 600 mm	Increases by 28.46%
520× (3+3) ×40.25	Amplitude of vibration	Increases from 0.1 to 0.5 mm	Decreases by 23.24%
560×6×40.25 (with 0.1 mm amplitude)	Beam thickness ratio	Increases from 1.0 to 2.0	Decreases by 19.94%
600×12×40.25 (with 0.3 mm amplitude)	Number of layers	Two layers	Increase by 125.33% compared to equivalent solid one
		Three layers	Increases by 19.14% compared to that of two layers
		Four layers	Increases by 54.78% compared to that of two layers

Table 10.3 Experimental loss factor of mild steel and aluminium welded beams at different modes of vibration

Material	Length × thickness × width (mm × mm × mm)	Modes of Vibration	Natural Frequency (Hz)	Loss Factor
Mild Steel	520.65 × (3+3) × 40.25	1	18.59	0.04360
		2	116.55	0.01981
		3	326.38	0.00853
		4	639.48	0.00318
	560.65 × (2.4+3.6) × 40.25	1	16.04	0.05439
		2	100.49	0.02497
		3	281.43	0.01041
		4	551.39	0.00389
	600.65 × (2+4) × 40.25	1	13.97	0.06356
		2	87.54	0.02893
		3	245.15	0.01204
		4	480.32	0.00463
Aluminium	520.65 × (3+3) × 40.25	1	18.12	0.09744
		2	113.55	0.04418
		3	317.99	0.01842
		4	623.03	0.00706
	560.65 × (2.4+3.6) × 40.25	1	15.62	0.11508
		2	97.91	0.05243
		3	274.18	0.02178
		4	537.20	0.00824
	600.65 × (2+4) × 40.25	1	13.61	0.13448
		2	85.29	0.06112
		3	238.84	0.02534
		4	467.96	0.00964

10.3 Discussion

The damping mechanism in welded structures is influenced by the intensity of pressure distribution, micro-slip and kinematic coefficient of friction at the interfaces. All the above vital parameters are largely influenced by the thickness ratio of the beam and thereby affect the damping capacity of the structures. Moreover, the damping in layered and welded structures is dependent on various dimensional parameters such as; length and thickness of the specimen, amplitude of vibration, number of layers and thickness ratio of the welded beam laminates. In the previous section, both the theoretical and experimental results for different specimens with all the influencing parameters have been compared for authenticating the numerical analyses. The following observations have been made from the theoretical and experimental analyses in the process of investigation.

1. The exact nature of the interface pressure profile and its magnitude across a beam layer is necessary for the correct assessment of the damping capacity of welded structures. This contact pressure between the surfaces is generated by the welding of the beams and plays a vital role on the joint properties. The welded beams are considered to be in contact with each other because of perfect flatness and same condition of flatness is maintained under excitation due to welding. Since perfect contact is maintained under both the static and dynamic conditions, the pressure at the interfaces is uniform. In the present investigation the pressure distribution given by Johnson [130] and Giannakopoulos et al. [131] for flat surfaces in contact with each other has been used for the analysis.

2. The presence of friction at the interfaces due to the welded joints has a strong influence on the system dynamics and largely contributes to the majority of the damping capacity of the system. The friction force at the interfaces arises from the shearing action between the parts and is governed by the interfacial pressure and friction coefficient. It is understood that the interface friction comes into play only when the contacting layers tend to move relatively under the action of transverse vibration and serves as a catalyst for energy dissipation. In the present analysis, the Coulomb's friction law is used to represent the friction at the contacting surfaces.

3. The friction, micro-slip, and surface roughness are the major factors affecting the joint behavior and each factor varies from joint to joint because of manufacturing tolerances. As a result, all the joints and jointed structures exhibit non-linear behavior. However, the assumption of linear vibration theory is justified when the beam is vibrated at lower amplitudes and mode of vibration.

4. The energy dissipation at the interfaces of jointed structures primarily depends upon the kinematic coefficient of friction *(*μ) and dynamic slip ratio *(*α). These two parameters being interdependent with each other exhibit complicated behavior under dynamic conditions. In view of the above facts, it is more appropriate to evaluate the product $\alpha.\mu$ as a single parameter from the experimental logarithmic decrement corresponding to welded beam of particular thickness. Since this product is frequency and amplitude dependent, plots exhibiting its variation with the above two parameters have been displayed in Figs. 9.13 to 9.18 for both mild steel and aluminium specimens. These plots have been further used for the theoretical evaluation of logarithmic decrements of layered and welded beams with respect to other dimensions and conditions of vibration. Moreover, the evaluation of the product $\alpha.\mu$ from the experimental result takes care of the effect of non-linearity, various modes of vibration, support, material and environmental damping effects in the results.

5. The average value of Young's modulus of elasticity (*E*) for both mild steel and aluminium specimens has been found out experimentally by conducting static deflection tests as presented in Table 9.9. These values are observed to be slightly less compared to their standard values and are subsequently used in all the theoretical works. As the specimens used in all the experiments are from the same stock of commercial flats, the use of these average values of Young's modulus in the theoretical computations is appropriate.

6. It is observed that the incorporation of joints in layered structures reduces the stiffness. It means that the ratio of the stiffness of a jointed beam to that of an identical solid one is always less than one. This ratio has been calculated by carrying out the same static deflection tests as used in case of Young's modulus and is found to be decreased with the number of layers used in the jointed specimen. Few samples of the average values of the stiffness ratio for two and

multi-layered mild steel and aluminium specimens are presented in Tables 9.10 to 9.13. This ratio shows the extent of reduction in the stiffness due to the inclusion of joints and its exact assessment carries much significance in the theoretical evaluation of damping ratio. It is estimated that the maximum decrease in the stiffness is approximately 15 and 14% for two layered mild steel and aluminium specimens, respectively, as compared to their equivalent solid ones. This observation is presented in Table 9.15. This stiffness decreases further by 19 and 20% for mild steel 17 and 19% for aluminium specimens with three and four layers, respectively, compared to their equivalent solid ones. It is further observed that the stiffness ratio for aluminium specimens is always more compared to that of similar mild steel ones because of the higher coefficient of interface friction for aluminium.

7. It is now a well known fact that the inclusion of joints in a fabricated structure not only damps out the structure but also reduces the structural stiffness. This reduction in the stiffness brings about a slight decrease in the natural frequency. The same has been observed during experimentation by comparing the frequency between a jointed beam and an equivalent solid one. This difference in frequency is fairly close at lower modes of vibration. Further, the variation in the frequency of vibration brings about a change in the product $\alpha.\mu$ as evident from Figs. 9.13 to 9.18 and hence the damping capacity.

8. It is found from the experiments that the surface roughness at the jointed interfaces has no effect on the damping capacity of layered and jointed structures. In order to authenticate this, experiments are conducted with a few layered and jointed beams made up of mild steel and aluminium specimens with varying surface roughness. Further, Response Surface Methodology has been applied to ascertain the role of surface roughness in the damping of layered and welded structures as presented in chapter 8. From the analysis, it is inferred that the damping ratio remains almost constant with the varying surface roughness at the interfaces of tack welded cantilever beams. Usually, the kinematic coefficient of friction is more and dynamic slip ratio is less with the higher surface roughness at the interfaces and vice versa. However, it is interesting to observe that the product of the kinematic coefficient of friction and dynamic slip ratio is almost constant

for any surface condition of a particular specimen at similar conditions of vibration since the maximum deviation for damping ratio is found to be 0.65% as presented in Table 9.14. Hence, it is found that the damping capacity remains constant irrespective of condition of roughness at the interfaces.

9. In order to compare the damping capacity of a jointed beam with its equivalent solid one, experiments are conducted with two geometrically identical specimens. It is observed that the damping ratio is always more in case of layered and jointed structures. It is estimated that the maximum increase in the loss factor is about 150 and 126% for two layered mild steel and aluminium specimens with thickness ratio 1.0, respectively, compared to its equivalent solid ones. The loss factor further increases by 32.16 and 61.58% for mild steel and 19.14 and 54.78% for aluminium structures with three and four layers with thickness ratio 1.0, respectively, compared to similar specimens of two layered beams. This increase is due to the presence of more interface friction layers and reduction in the joint stiffness.

10. It is observed that the damping capacity of aluminium specimens is always more compared to similar mild steel specimens. This is due to lower static bending stiffness of aluminium compared to identical mild steel specimens which results in the lower strain energy. Moreover, the energy loss due to friction at the interfaces of aluminium specimens is more than that of the equivalent mild steel because of higher kinematic coefficient of interface friction for aluminium. Thus, the net effect of the decrease in the input strain energy and increase in energy loss result in the higher damping capacity for aluminium specimens compared to mild steel for similar conditions of beam dimension and vibration.

11. The joints usually do not form a rigid connection and thus allow a relative motion at the interfaces of the connecting members. As the beam vibrates, it bends in the transverse direction. This beam bending causes the generation of shear stresses at the contact surfaces. When the limiting friction force is high, no slippage occurs at the interfaces and the damping due to joints is ignored. However, the slippage occurs when the transverse load exceeds the critical load as discussed in the previous chapters. This slippage being of exceedingly small amount is termed as micro-slip and occurs only at the lower level of excitation. This small relative

displacement at the interfaces causes energy dissipation due to friction thereby contributing large amount of damping to the system. When the excitation level is increased, the macro-slip is developed due to which the entire jointed interface will slip as a whole. Usually, the macro-slip is avoided as it leads to structural damage of the joints.

12. The onset of micro slip at the interfaces is governed by the critical load and amplitude. The critical load is defined as the minimum load, applied at the free end of the layered and welded cantilever beam, which initiates the relative slip at the interfaces. The critical amplitude is defined as the minimum initial excitation, provided at the free end of the layered and welded cantilever beam that initiates the relative slip at the interfaces. These critical load and amplitude of excitation are dependent on the dimensional properties, number of layers and thickness ratio of the layered and welded beams as derived in expressions (4.11), (4.16), (5.9), (5.11) and (6.15).

13. The critical load and amplitude are non-linearly dependent on the number of layers in jointed beams as depicted in Fig. 10.16. From the Fig. 10.16 it is evident that the critical load increases with the increase in number of layers which implies that greater transverse load has to be applied at the free end in case of multilayered welded cantilever beams in order to initiate micro slip at the interfaces.

14. The critical load and amplitude is also nonlinearly dependent on the thickness ratio as shown in the Figs. 10.35 and 10.36, respectively. From these figures, it is quite evident that the critical load and amplitude is minimum at the thickness ratio of 1.0 i.e., in welded beams of equal thickness as the slip surface is at the centroid of the total beam cross-section. It is evident from the Figs. 10.29-10.34 that for the beam with the same total thickness, the loss coefficient is increased by having laminates of equal thickness. Moreover, for layered and welded beam with laminates of unequal thickness, the onset of slip is delayed due to higher critical load, as compared to that of the laminates of equal thickness as evident from the Figs. 10.35 and 10.36. The reason being, slip interface is not at the centroidal plane of the welded beam in case of layered and welded non-symmetric beams thereby raising the critical load.

15. In the previous chapters, expression for the relative slip at the interfaces has been developed for both symmetrical and unsymmetrical welded beams. It is found that the relative slip is dependent on the axial distance from the fixed end of the welded cantilever beams. The variation of relative slip with an axial distance from the fixed end has been plotted in Figs. 10.21, 10.22, 10.38, and 10.39. From the figures, it is evident that the relative slip increases with the distance from the fixed end and attains the maximum value at the free end of the layered and welded cantilever beams.

16. The relative slip has been derived for layered and welded beams for both equal and unequal thickness. The relative slip is more for the welded beams of equal thickness compared to equivalent welded beams of unequal thickness with same overall thickness. In order to illustrate the above mentioned fact relative slip has been plotted with respect to the different thickness ratio, as depicted in Figs. 10.38 and 10.39. From the figures it is evident that the relative slip achieves the maximum value at thickness ratio of one and decreases as the ratio is increased. The reason being, in welded beams of equal thickness the slip surface is at the centroid of the total beam cross-section thereby offering greater relative slip at the interfaces.

17. The variation of relative slip for the multilayered welded beams has been plotted with respect to the number of laminates as presented in Fig. 10.17. From the figure, it is obvious that the total relative slip increases with the number of layers. The reason is that the mating surface is increased due to increase in number of layers thereby offering more interfaces for the resultant slip.

18. In the previous chapters, expression for the transverse response at the interfaces has been developed for both symmetrical and unsymmetrical welded beams. It is found that the response is dependent on the axial distance from the fixed end of the welded cantilever beams. The variation of relative slip with an axial distance from the fixed end has been plotted in Figs. 10.19, 10.20, 10.23, 10.24, 10.41, and 10.42. From the figures it is quite evident that the transverse response increases with the distance from the fixed end and attains the maximum value at the free end of layered and welded cantilever beams.

19. The transverse response has been derived for layered and welded beams of both equal and unequal thickness. The response is more for the welded beams of equal thickness compared to equivalent welded beams of unequal thickness with same overall thickness. In order to illustrate the above mentioned fact response has been plotted with respect to the different thickness ratio, as depicted in Figs. 10.41 and 10.42. From the figures it is evident that the response achieves the maximum value at thickness ratio of one and decreases as the ratio is increased.

20. The variation of transverse response for the multilayered welded beams has been derived in chapter 5. From the expression (5.6) it is evident that the transverse deflection decreases with the number of layers. The reason is being, with the increase in number of layers the mating surfaces is increased thereby offering more relative slip. This increased relative slip results in greater energy dissipation thereby lowering the transverse response.

21. The variation of dynamic slip and transverse response at different locations along the cantilever beam length at various excitation frequencies for Heaviside and harmonic loading have been plotted in Figs. 10.25-10.28, respectively. It is evident from the figures that the transverse response of vibration and the complementary interfacial slip increases with higher frequency ratio in the pre-resonance regime on one hand and behaves conversely in the post-resonance zone. Moreover, the dynamic response and relative slip increases in the pre-resonance region with the increasing frequency and attains the maximum value at the frequency ratio of 1.0, i. e., at the resonant frequency.

22. The values of loss factor and frequency for the welded mild steel and aluminium beams have been presented in Table 10.3. From the table it is evident that the damping capacity of the jointed structures is insignificant at the higher modes of vibration. The structure considered in the present analysis is a lightly damped structures and most of the damping takes place at the lower modes of vibration.

23. The variation of energy dissipation with the initial amplitude of excitation for the layered and jointed beams of symmetric and non-symmetric beams has been plotted in Figs. 10.18 and 10.40. From the figures it is apparent that the energy dissipation increases with the increase in initial amplitude of excitation. From the

expressions (4.16), (5.15), (5.17) and (6.19), it is deduced that the energy loss due to friction is directly proportional to the initial amplitude of excitation which establishes that the energy dissipation is enhanced with increase in initial amplitude of excitation. Further, the relative slip at the interfaces is increased due to increase in initial amplitude of excitation as shown in expressions (4.11), (5.9), (5.11) and (6.15) thereby enhancing the energy loss due to friction.

24. The variation of energy dissipation with the number of layers for the multilayered welded beams has been plotted in Figs. 10.15 and 10.18. From the figures, it is evident that the energy dissipation increases with increase in number of layers. From the expressions (5.15) and (5.17) it is deduced that the energy loss due to friction is directly proportional to the number of layers which establishes that the energy dissipation is enhanced with increase in number of layers. Moreover, with the increase in number of layers the number of frictional interfaces is increased thereby resulting in more frictional energy loss. Further, the relative slip at the interfaces is increased due to increase in number of layers as shown in expressions (5.9) and (5.11) thereby enhancing the energy loss due to friction.

25. The variation of energy dissipation with the thickness ratio for the layered and welded unsymmetrical beams has been plotted in Figs. 10.37 and 10.40. From the figures it is evident that the energy dissipation decreases with the increase in thickness ratio. Energy loss is maximum at the thickness ratio of 1.0 i.e., in welded beams of equal thickness. The reason being, the relative slip in layered and welded beams of equal thickness is maximum thereby resulting in more energy loss compared to welded beams of unequal thicknesses. Energy dissipation is maximized by having the slip interface at the centroid of the total beam cross-section which occurs particularly in case of jointed beams of equal thickness. Thus, it is inferred that the damping capacity of layered and welded structures is enhanced substantially by fabricating the structures with symmetric beams.

26. In the present work, damping capacity of layered and welded structures has been examined for the following variables: length and thickness of the specimen, amplitude of vibration, number of layers and thickness ratio. The dependency of the damping on each of these variables is enumerated from the theoretical and experimental results as discussed below.

(a) The damping capacity of the welded mild steel and aluminium structures increases with the increase in length as presented in Table 6.1 and 6.2. The variation of damping capacity with length of welded symmetrical and unsymmetrical mild steel and aluminium specimens are plotted as shown in Figs. 10.2, 10.6, 10.11, 10.14, 10.31, 10.34, 10.44 and 10.47. From the figures, it is evident that the damping capacity increases with the increase in length. With the increase in length, the interface area is increased resulting in greater dissipation of the energy due to friction. Furthermore, with increase in the length of the jointed beam, strain energy introduced into the system is reduced as evident from the expressions (4.18), (5.18) and (6.21). Hence, the overall effect is an increase in the damping capacity of the system.

(b) The overall thickness of the beam influences the damping capacity of the welded structures. The damping capacity of the welded mild steel and aluminium structures decreases with an increase in overall thickness as presented in Table 6.1 and 6.2. The variation of damping capacity with thickness of welded symmetrical and unsymmetrical mild steel and aluminium specimens are plotted as shown in Figs. 10.4, 10.8, 10.10, 10.13, 10.33, 10.43 and 10.46. From the figures, it is evident that the damping capacity decreases with the increase in overall thickness. The larger beam thickness is accompanied by an increase in the static bending stiffness and also the input strain energy into the system. Expressions (4.11), (5.9), (5.11) and (6.15) reveal that the increase in thickness increases the relative slip thereby raising the energy loss. Although the energy loss is enhanced with the increase in thickness but the damping capacity is reduced as the dissipation of energy is at a slower rate compared to that of the input strain energy.

(c) The damping capacity of the welded mild steel and aluminium structures decreases with the increase in initial amplitude of excitation as presented in Table 6.1 and 6.2. The variation of damping capacity with initial amplitude of excitation for welded symmetrical and unsymmetrical mild steel and aluminium specimens are plotted as shown in Figs. 10.1, 10.5, 10.9, 10.12, 10.29, 10.32, 10.45 and 10.48. From the figures, it is evident that the damping capacity decreases with the increase in initial amplitude of vibration at the free

end of the beam model although increase in the amplitude of vibration raises energy loss due to friction. The strain energy introduced into the system is proportional to square of the amplitude as given by expressions (4.18), (5.18) and (6.21). The increase in amplitude of excitation increases the input strain energy at a higher rate compared to the energy loss due to friction which is linearly proportional to the initial amplitude as given by expressions (4.16), (5.15), (5.17) and (6.19), thereby reducing the damping capacity. This fact suggests that the damping is amplitude dependent.

(d) The variation of damping capacity with the number of layers for the multilayered welded beams has been plotted in Figs. 10.3-10.14. From the figures it is evident that the damping ratio increases with the increase in number of layers. From the expressions (5.15) and (5.17), it is deduced that the energy loss due to friction is directly proportional to the number of layers which establishes that the damping ratio is enhanced with increase in number of layers. Moreover, with the increase in number of layers, the number of frictional interfaces is increased thereby resulting in more frictional energy loss. Further, the relative slip at the interfaces is increased due to increase in number of layers as shown in expressions (5.9) and (5.11) thereby enhancing the energy loss due to friction.

(e) The variation of damping capacity with the thickness ratio for the layered and welded unsymmetrical beams has been plotted in Figs. 10.29-10.34. From the figures, it is evident that the energy dissipation decreases with the increase in thickness ratio. Energy loss is maximum at the thickness ratio of 1.0 i.e., in welded beams of equal thickness. The reason being, the relative slip in layered and welded beams of equal thickness is maximum thereby resulting in more energy loss compared to welded beams of unequal thicknesses. Energy dissipation is maximized by having the slip interface at the centroid of the total beam cross-section as in case of jointed beams of equal thickness. Thus, it is inferred that the damping capacity of layered and welded structures is enhanced substantially by fabricating the structures with symmetric beams.

10.4 Summary

In the present chapter, both the theoretical and experimental results for the damping capacity of welded symmetrical and unsymmetrical beams have been presented. The experimental results for logarithmic decrement and loss factor have been compared with the corresponding numerical ones obtained in chapters 3-8 for establishing the authenticity of the theory developed. In the present work, damping of the welded beams has been examined for the following variables: length and thickness of the specimen, amplitude of vibration, thickness ratio, number of layers and thickness ratio. The dependency of the damping on each of these variables has been properly addressed. Finally, useful conclusions have been drawn from both the theoretical and experimental results as presented below.

The damping capacity of a layered beam jointed with tack weld increases with:

- an increase in the cantilever length
- a decrease in the thickness of the cantilever beam
- a decrease in initial amplitude of excitation
- an increase in the number of layers of the cantilever structure
- a decrease in the beam thickness ratio of constant overall thickness

11

SUMMARY AND SCOPE FOR FURTHER RESEARCH

The aim of this thesis is to explore the mechanism of slip damping in layered and welded structures. Motivation for this study stems from the need to meliorate the damping capacity in built-up structures in order to improve its dynamic performance and longevity. Keeping these objectives in view, theoretical and experimental analyses have been carried out in chapters 3-9. In depth discussions of the theoretical and experimental results have been presented in chapter 10. This chapter summarizes the important conclusions drawn from the observations discussed in the previous chapter along with some suggestions for continuing future research in this field.

11.1 Summary and Conclusions

An extensive study has been done to find out the effects of various influencing parameters on the damping capacity of layered and welded structures. The damping of welded structures in the present investigation has been examined for the following variables: intensity of pressure distribution, dynamic slip ratio, surface roughness and kinematic coefficient of friction at the interfaces, thickness ratio, length of the specimen, amplitude of vibration, number of layers and overall beam thickness. The effect of all these parameters on the damping capacity of layered and welded structures is enumerated from the theoretical and experimental results as detailed below.

- The exact nature of the interface pressure profile and its magnitude across a beam layer is significant for the correct assessment of damping capacity in layered and welded structures. In these structures, the nature of interface pressure is uniformly distributed owing to the perfect contact between the flat bodies.

- The dynamic slip ratio (α) plays an important role in estimating the damping of layered and jointed structures and is largely influenced by the surface texture of

the joint interface. Therefore, it is more appropriate to consider the combined effect of both the dynamic slip ratio and coefficient of friction in the evaluation of damping because of their interdependencies and complicated behavior under dynamic conditions as elaborated earlier. Indeed, the logarithmic decrement increases with increase in dynamic slip ratio.

- It is found from the experiments that the surface roughness at the jointed interfaces has no effect on the damping of layered and jointed structures. The effect of surface roughness has been further examined applying Response Surface Methodology (RSM) and finally inferred that the damping capacity remains constant irrespective of condition of roughness at the interfaces.

- The friction force at the interfaces arises from the shearing action between the parts and is governed by the interface pressure and friction coefficient. In the present work, the well-known Coulomb friction model has been used to quantify the friction force. It is established that the energy is dissipated through this frictional effects and is a function of both the micro-slip and friction at the interfaces. As already discussed, both dynamic slip ratio (α) and coefficient of friction (μ) are interdependent and show complicated behavior under dynamic condition. In view of this, their product $\alpha.\mu$ is considered as a single parameter in the theory as evident from the fact that the energy dissipation is a function of the above product.

- Energy dissipation is maximized by having the slip interface at the centroid of the total beam cross-section which occurs in case of jointed beams of equal thickness. Thus, it is inferred that the damping capacity of layered and welded structures is enhanced substantially by fabricating the structures with symmetric beams.

- The damping capacity increases with the increase in length of the welded structures. With the increase in length, the interface area is increased resulting in greater dissipation of the energy due to friction. Furthermore, with increase in the length of the jointed beam, strain energy introduced into the system is reduced. Hence, the overall effect is an increase in the damping capacity of the system.

- The damping capacity decreases with increase in initial amplitude of excitation at the free end of the beam model although increase in the amplitude of vibration raises energy loss due to friction. The strain energy introduced into the system is proportional to square of the amplitude. The increase in amplitude of excitation increases the input strain energy at a higher rate compared to the energy loss due to friction thereby reducing the damping capacity. This fact suggests that the damping is amplitude dependent.

- The damping capacity is enhanced with the use of more number of layers compared to the solid beam of same overall thickness due to more friction interfaces as it produces higher energy loss at the interfaces. Moreover, the stiffness as well as strain energy is reduced with the increased number of layers, thus increasing the logarithmic decrement.

- The damping capacity of the welded structures decreases with the increase in overall thickness. The larger beam thickness is accompanied by an increase in the static bending stiffness and also the input strain energy into the system. Increase in the overall thickness increases the relative slip at the interfaces thereby raising the energy loss. Although the energy loss is enhanced with the increase in thickness but the damping capacity is reduced as the dissipation of energy is at a slower rate compared to that of the input strain energy.

The main purpose of the structural design is to control the vibration of structures at a desirable level as per the requirements. In fact, most monolithic structures possess low inherent damping thereby posing serious problems which will impair the function and life of structures leading to their ultimate failure. It is always desirable to keep the vibration level as low as possible by introducing damping so that the performance and useful life of structures are enhanced largely. Since many decades, it has been a biggest challenge for the practicing engineers and designers to limit this unwanted vibration in structures. The sole contribution of the present investigation is intended in this direction only. The design concept evolved from this research work by using layered structures with welded joints can be effectively utilized in trusses, frames, aircraft and aerospace structures, automobiles, bridges, machine members, robots and many other applications where higher damping is essentially required.

11.2 Scope for Further Research

In the present investigation, the mechanism of damping and the various parameters affecting the damping capacity of layered and welded structures have been presented in details to enable the engineers for designing the structures depending upon their damping capacity in real applications. However, the present study can be extended for further research as enumerated below.

- Timoshenko beam theory can be used for analysis instead of Euler-Bernoulli beam theory.
- The problem can be studied considering the nonlinearity effects of slip, friction and joint properties.
- The analysis can be extended to other boundary conditions such as fixed-fixed, fixed-hinged, hinged - hinged etc.
- The analysis can be made for layered and jointed beams of dissimilar materials.
- The analysis can be made for layered and jointed plates
- The analysis can be extended to other forcing functions such as impact hammer testing etc.

References

[1] Goodman, L.E., 1959, A review of progress in analysis of interfacial slip damping, Edited by Ruzicka, J.E., Structural Damping, New York, ASME, pp. 35–48.

[2] Ungar, E.E., 1973, The status of engineering knowledge concerning the damping of built-up structures, Journal of Sound and Vibration, Vol. 26, No. 1, pp. 141-154.

[3] Gaul, L. and Nitsche, R., 2000, Friction control for vibration suppression, Mechanical Systems and Signal Processing, Vol. 14, No. 2, pp. 139-150.

[4] Chen, W. and Deng, X., 2005, Structural damping caused by micro-slip along frictional interfaces, International Journal of Mechanical Sciences, Vol. 47, No. 8, pp. 1191-1211.

[5] Beards, C.F., 1985, Damping in structural joints, The Shock and Vibration Digest, Vol. 17, No. 11, pp. 17-20.

[6] Earles, S.W.E. and Mansoor, F.S., 1974, Frictional damping applied to a cantilever-beam structure: A theoretical and experimental response comparison, International Journal of Machine Tool Design and Research, Vo1. 14, No. 1, pp. 111-124.

[7] Beards, C.F., 1975, Some effects of interface preparation on frictional damping in joints, International Journal of Machine Tool Design and Research, Vo1.15, No. 1, pp. 77-83.

[8] Beards, C.F. and Williams, J., 1977, The damping of structural vibration by rotational slip in joints, Journal of Sound and Vibration, Vol. 53, No. 3, pp. 333–340.

[9] Beards, C.F. and Imam, I.M.A., 1978, The damping of plate vibration by interfacial slip between layers, International Journal of Machine Tool Design and Research, Vol. 18, No. 3, pp. 131-137.

[10] Menq, C.H. and Griffin, J.H., 1985, A comparison of transient and steady state finite element analyses of the forced response of a frictionally damped beam, Journal of Vibration, Acoustics, Stress and Reliability in Design, ASME, Vol. 107, No. 1, pp. 19–25.

[11] Menq, C.H., Bielak, J. and Griffin, J.H., 1986, The influence of microslip on vibratory response, Part I: A new microslip model, Journal of Sound and Vibration, Vol. 107, No. 2, pp. 279-293.

[12] Menq, C.H., Griffin, J.H. and Bielak, J., 1986, The influence of microslip on vibratory response, Part II: A comparison with experimental results, Journal of Sound and Vibration, Vol. 107, No. 2, pp. 295-307.

[13] Menq, C.H., Griffin, J.H. and Bielak, J., 1986, The forced response of shrouded fan stages, Journal of Vibration, Acoustics, Stress, and Reliability in Design, ASME, Vol. 108, No. 1, pp. 50-55.

[14] Menq, C.H., Griffin, J.H. and Bielak, J., 1986, The influence of a variable normal load on the forced vibration of a frictionally damped structure, Journal of Engineering for Gas Turbines and Power, ASME, Vol. 108, No. 2, pp. 300-305.

[15] Ren, Y., 1988, Damping in structural joints, M.Sc. Thesis. Imperial College, London University.

[16] Hansen, S.W. and Spies, R.D., 1997, Structural damping in laminated beams due to interfacial slip, Journal of Sound and Vibration, Vol. 204, No. 2, pp. 183-202.

[17] Goodman, L.E. and Klumpp, J.H., 1956, Analysis of slip damping with reference to turbine-blade vibration, Journal of Applied Mechanics, ASME, Vol. 23, pp. 421–429.

[18] Pian, T.H.H., 1957, Structural damping of a simple built-up beam with riveted joints in bending, Journal of Applied Mechanics, ASME, Vol. 24, pp. 35–38.

[19] Masuko, M., Ito, Y. and Yoshida, K., 1973, Theoretical analysis for a damping ratio of a jointed cantibeam, Bulletin of JSME, Vol. 16, No. 99, pp. 1421-1432.

[20] Motosh, N., 1975, Stress distribution in joints of bolted or riveted connections, Journal of Engineering for Industry, ASME, Vol. 97, No. 1, pp. 157-161.

[21] Nishiwaki, N., Masuko, M., Ito, Y. and Okumura, I., 1978, A study on damping capacity of a jointed cantilever beam, 1st Report: Experimental results, Bulletin of JSME, Vol. 21, No. 153, pp. 524-531.

[22] Nishiwaki, N., Masuko, M., Ito, Y. and Okumura, I., 1980, A study on damping capacity of a jointed cantilever beam, 2nd Report: Comparison between theoretical and experimental values, Bulletin of JSME, Vol. 23, No. 177, pp. 469-475.

[23] Beards, C.F., 1992, Damping in structural joints, The Shock and Vibration Digest, Vol. 24, No. 7, pp. 3-7.

[24] Ibrahim, R. A., 1994, Friction-induced vibration, chatter, squeal and chaos: Part I – Mechanics of contact and friction, Applied Mechanics Reviews, ASME, Vol. 47, No. 7, pp. 209-226.

[25] Gaul, L. and Nitsche, R., 2001, The role of friction in mechanical joints, Applied Mechanics Reviews, ASME, Vol. 54, No. 2, pp. 93-106.

[26] Groper, M., 1985, Microslip and macroslip in bolted joints, Experimental Mechanics, Vol. 25, No. 2, pp. 171-174.

[27] Beards, C.F., 1996, Structural Vibration: Analysis and Damping, Butterworth-Heinemann, Oxford.

[28] Timoshenko, S., 1955, Vibration Problems in Engineering, 3rd Edition, Van Norstrand Co. Inc., pp. 371.

[29] Argoul, P. and Le, T.P., 2003, Instantaneous indicators of structural behaviour based on continuous Cauchy wavelet transform, Mechanical Systems and Signal Processing, Vol. 17, No. 1, pp. 423–250.

[30] Ren, Y. and Beards, C., 1995, Identification of joint properties of a structure using FRF data, Journal of Sound Vibration, Vol. 186, No. 4, pp. 567–587.

[31] Grandhi, R.V., 1990, Optimum design of space structures with active and passive damping, Engineering with Computers, Vol. 6, No. 3, pp. 177-183.

[32] Ferri, A.A. and Heck, B.S., 1992, Analytical investigation of damping enhancement using active and passive structural joints, Journal of Guidance, Control and Dynamics, Vol. 15, No. 5, pp. 1258-1264.

[33] Park, J.T. and Choi, N.S., 2004, Flexural vibration analyses of a sandwich beam specimen with a partially inserted viscoelastic layer, KSME Journal of Mechanical Science and Technology, Vol. 18, No. 3, pp. 347-356.

[34] Lazan, B.J., 1968, Damping of Materials and Members in Structural Mechanics, London, Pergamon Press.

[35] Bert, C.W., 1973, Material damping: An introductory review of mathematical models, measures and experimental techniques, Journal of Sound and Vibration, Vol. 29, No. 2, pp. 129–153.

[36] Clarence W. de Silva, 2000, Vibration: Fundamentals and Practice, CRC Press LLC, Boca Raton.

[37] Clarence W. de Silva, 2007, Vibration Damping, Control, and Design, CRC Press, Taylor and Francis Group LLC, Boca Raton.

[38] Kelly, S.G., 2000, Fundamentals of Mechanical Vibrations, McGraw-Hill International Editions, Singapore.

[39] Waterhouse, R.B., 1981, Fretting Fatigue, Applied Science Publishers, Essex, England.

[40] Inman, D.J., 1994, Engineering Vibration, Prentice Hall, Englewood Cliffs.

[41] Sun, C.T. and Lu, Y.P., 1995, Vibration Damping of Structural Elements, Prentice Hall PTR, Englewood Cliffs, New Jersey.

[42] Nashif, A.D., Jones, D.I.G. and Henderson, J.P., 1985, Vibration Damping, John Wiley and Sons, NY.

[43] Ross, D., Ungar, E.E. and Kerwin, E.M. Jr., 1959, Damping of plate flexural vibrations by means of viscoelastic laminate, ASME Colloquium on Structural Damping, pp. 49-87.

[44] Pearce, B.K. and Baumgarten, J.R., 1971, The damping effects of viscoelastic materials, Part 2: Transverse vibration of plates with viscoelastic coatings, Journal of Engineering for Industry, ASME, Vol. 93, No. 2, pp. 645-655.

[45] Reddy, C.V.R. and Narayanan, S., 1980, Response of plates with unconstrained layer damping treatment to random acoustic excitation, Part I: Damping and frequency evaluations, Journal of Sound and Vibration, Vol. 69, No. 1, pp. 35-43.

[46] Parthasarathy, G., Reddy, C.V.R. and Ganesan, N., 1985, Partial coverage of rectangular plates by unconstrained layer damping treatments, Journal of Sound and Vibration, Vol. 102, No. 2, pp. 203-216.

[47] Kerwin Jr., E.M., 1959, Damping of flexural waves by a constrained viscoelastic layer, Journal of the Acoustical Society of America, Vol. 31, No. 7, pp. 952–962.

[48] DiTaranto, R.A., 1965, Theory of vibratory bending for elastic and viscoelastic layered finite-length beams, Journal of Applied Mechanics, ASME, Vol. 32, No. 4, pp. 881–886.

[49] Mead, D.J. and Markus, S., 1969, The forced vibration of a three-layer, damped sandwich beam with arbitrary boundary conditions, Journal of Sound and Vibration, Vol. 10, No. 2, pp. 163–175.

[50] Mead, D.J. and Markus, S., 1970, Loss factors and resonant frequencies of encastre damped sandwich beams, Journal of Sound and Vibration, Vol. 12, No. 1, pp. 99–112.

[51] Mead, D.J., 1982, A comparison of some equations for the flexural vibration of damped sandwich beams, Journal of Sound and Vibration, Vol. 83, No. 3, pp. 363–377.

[52] Rao, D.K., 1978, Frequency and loss factors of sandwich beams under various boundary conditions, Journal of Mechanical Engineering Science, Vol. 20, No. 5, pp. 271–282.

[53] Douglas, B.E. and Yang, J.C.S., 1978, Transverse compressional damping in the vibratory response of elastic–viscoelastic–elastic beams, AIAA Journal, Vol. 16, No. 9, pp. 925–930.

[54] Douglas, B.E., 1986, Compressional damping in three-layer beams incorporating nearly incompressible viscoelastic cores, Journal of Sound and Vibration, Vol. 104, No. 2, pp. 343–347.

[55] Sylwan, O., 1987, Shear and compressional damping effects of constrained layered beams, Journal of Sound and Vibration, Vol. 118, No. 1, pp. 35–45.

[56] Lee, B.C. and Kim, K.J., 1995, Consideration of both extensional and shear strain of core material in modal property estimation of sandwich plates, Design Engineering Technical Conferences 3, ASME, pp. 701–708.

[57] Mallik, A.K. and Ghosh, A., 1970, Improvement of damping capacity with introduced stress concentration, Indian Journal of Technology, Vol. 8, pp. 113-119.

[58] Mallik, A.K. and Ghosh, A., 1971, Improvement of dynamic rigidity of structural members with introduced stress concentration, Journal of Technology, Vol. 13, pp. 19-26.

[59] Mallik, A.K. and Ghosh, A., 1973, Improvement of damping characteristics of structural members with high damping elastic inserts, Journal of Sound and Vibration, Vol. 27, No. 1, pp. 25-36.

[60] Rahmathullah, R. and Mallik, A.K., 1979, Damping of cantilever strips with inserts, Journal of Sound and Vibration, Vol. 66, No. 1, pp. 109-117.

[61] Williams, E.J. and Earles, S.W.E., 1974, Optimization of the response of frictionally damped beam type structures with reference to gas turbine compressor blading, Journal of Engineering for Industry, ASME, Vol. 76, pp. 471-476.

[62] Dowell, E.H. and Schwartz, H.B., 1983, Forced response of a cantilever beam with a dry friction damper attached, Part I: Theory, Journal of Sound and Vibration, Vo1. 91, No. 2, pp. 255-267.

[63] Beards, C.F., 1983, The damping of structural vibration by controlled interface slip in joints, Journal of Vibration, Acoustics, Stress and Reliability and in Design, ASME, Vol. 105, No. 3, pp. 369–373.

[64] Murty, A.S.R. and Padmanabhan, K.K., 1982, Effect of surface topography on damping in machine joints, Precision Engineering, Vol. 4, pp. 185-190.

[65] Sextro, W., 2002, Dynamical contact problems with friction: Models, methods, experiments and applications, Lecture notes in Applied Mechanics, Vol. 3, Series editor, Pfeiffer, F., Springer.

[66] Yoshimura, M., 1977, Measurement of dynamic rigidity and damping property for simplified joint models and simulation by computer, Annals of the CIRP, Vol. 25, No. 1, pp. 193-198.

[67] Tsutsumi, M. and Ito, Y., 1979, Damping mechanism of a bolted joint in machine tools, Proceedings of the 20th International Machine Tool Design and Research Conference, Birmingham, U.K., pp. 443-448.

[68] Padmanabhan, K.K. and Murty, A.S.R., 1991, Evaluation of frictional damping by response surface methodology, International Journal of Machine Tools and Manufacture, Vol. 31, No. 1, pp. 95-105.

[69] Padmanabhan, K.K. and Murty, A.S.R., 1991, Damping in structural joints subjected to tangential loads, Journal of the Structural Division, Proceedings of Institute of mechanical Engineers, Vol. 205(C2), pp. 121–129.

[70] Lenz, J. and Gaul, L., 1995, The influence of micro-slip on the dynamic behavior of bolted joints, 13th International Modal Analysis Conference, Nashville, Vol. 3, pp. 248-254.

[71] Cochardt, A.W., 1954, A method for determining the internal damping of machine members, Journal of Applied Mechanics, ASME, Vol. 76, No. 9, pp. 257-262.

[72] Goodman, L.E. and Brown, C.B., 1962, Energy dissipation in contact friction: Constant normal and cyclic tangential loading, Journal of Applied Mechanics, ASME, Vol. 29, No. 1, pp. 17-22.

[73] Earles, S.W.E. and Philpot, M.G., 1967, Energy dissipation at plane surfaces in contact, Journal of Mechanical Engineering Science, Vo1. 9, No. 2, pp. 86-97.

[74] Dekoninck, C., 1972, Deformation properties of metallic contact surfaces of joints under the influence of dynamic tangential loads, International Journal of Machine Tool Design and Research, Vol. 12, No. 3, pp. 193-199.

[75] Masuko, M., Ito, Y. and Koizumi, T., 1974, Horizontal stiffness and micro-slip on a bolted joint subjected to repeated tangential static loads, Bulletin of JSME, Vol. 17, No. 113, pp. 1494-1501.

[76] Rogers, P.F. and Boothroyd, G., 1975, Damping at metallic interfaces subjected to oscillating tangential loads, Journal of Engineering for Industry, ASME, Vo1. 97, pp. 1087-1093.

[77] Burdekin, M., Back, N. and Cowley, A., 1978, Experimental study of normal and shear characteristics of machined surfaces in contact, Journal of Mechanical Engineering Science, Vo1. 20, No. 3, pp. 129-132.

[78] Vinogradov, O., 1989, Effect of frequency on losses in a dry friction joint, Proceedings of the 89th Conference, The Damping, pp.2-10, Florida, U.S.A.

[79] Anderson, J.R. and Ferri, A.A., 1990, Behaviour of a single-degree-of-freedom system with a generalized friction law, Journal of Sound and Vibration, Vol. 140, No. 2, pp. 287-304.

[80] Griffin, J.H. and Menq, C.H., 1991, Friction damping of circular motion and its implication to vibration control, Journal of Vibration and Acoustics, ASME, Vo1. 113, No. 2, pp. 225-229.

[81] Menq, C.H. and Chidamparma, P., 1991, Friction damping of two dimensional motion and its application in vibration control, Journal of Sound and Vibration, Vol. 144, No. 3, pp. 427-447.

[82] Sinha, A. and Griffin, J.H., 1985, Stability of limit cycles in frictionally damped and aerodynamically unstable rotor stages, Journal of Sound and Vibration, Vol. 103, No. 3, pp. 341-356.

[83] Dweib, A.H. and D'Souza, A.F., 1990, Self-excited vibrations induced by dry friction, Part 1: Experimental Study, Journal of Sound and Vibration, Vol. 137, No. 2, pp. 163-175.

[84] Cheng, S.P. and Perkins, N.C., 1991, The vibration and stability of a friction-guided translating string, Journal of Sound and Vibration, Vol. 144, No. 2, pp. 281-292.

[85] Shaw, S.W., 1986, On the dynamic response of a system with dry friction, Journal of Sound and Vibration, Vo1. 108, No. 2, pp. 305-325.

[86] Gregory, D.L., Smallwood, D.O., Coleman, R.G. and Nusser, M.A., 1999, Experimental studies to investigate damping in frictional shear joints, Proceedings of the 70th Shock and Vibration Symposium, NM.

[87] Smallwood, D.O., Gregory, D.L. and Coleman, R.G., 2000, Damping investigations of a simplified frictional shear joint, Proceedings of the 71st Shock and Vibration Symposium, Alexandria, Virginia.

[88] Smallwood, D.O., Gregory, D.L. and Coleman, R.G., 2001, A three parameter constitutive model for a joint which exhibits a power law relationship between energy loss and relative displacement, Proceedings of the 72nd Shock and Vibration Symposium, Destin FL.

[89] Ferri, A.A., 1995, Friction damping and isolation systems, Journal of vibration and acoustics, ASME, Vol. 117(B), pp. 196-206.

[90] Gaul, L. and Lenz, J., 1997, Nonlinear dynamics of structures assembled by bolted joints, Acta Mechanica, Vol. 125, No. 1-4, pp. 169-181.

[91] Ibrahim, R.A. and Pettit, C.L., 2005, Uncertainties and dynamic problems of bolted joints and other fasteners, Journal of Sound and Vibration, Vol. 279, No. 3-5, pp. 857-936.

[92] Song, Y., Hartwigsen, C.J., McFarland, D.M., Vakakis, A.F. and Bergman, L.A., 2004, Simulation of dynamics of beam structures with bolted joints using adjusted Iwan beam elements, Journal of Sound and Vibration, Vol. 273, No. 1-2, pp. 249-276.

[93] Hartwigsen, C.J., Song, Y., Mcfarland, D.M., Bergman, L.A. and Vakakis, A.F., 2004, Experimental study of non-linear effects in a typical shear lap joint configuration, Journal of Sound and Vibration, Vol. 277, No. 1-2, pp. 327-351.

[94] Miller, J.D. and Quinn, D.D., 2009, A two-sided interface model for dissipation in structural systems with frictional joints, Journal of Sound and Vibration, Vol. 321, No. 1-2, pp. 201-219.

[95] Khattak, A.R., Garvey, S. and Popov, A., 2010, Proper orthogonal decomposition of the dynamics in bolted joints, Journal of Sound and Vibration, Vol. 329, No. 9, pp. 1480-1498.

[96] Den Hartog, J.P., 1931, Forced vibrations with combined coulomb and viscous friction, ASME, Vol. 53, No. 9, pp. 107-115.

[97] Pratt, T.K. and Williams, R., 1981, Nonlinear analysis of stick/slip motion, Journal of Sound and Vibration, Vol. 74, No. 4, pp. 531-542.

[98] Liang, J.W. and Feeny, B.F., 1998, Identifying Coulomb and viscous friction from free-vibration decrements, Nonlinear Dynamics, Vol. 16, No. 4, pp. 337-347.

[99] Awrejcewicz, J. and Olejnik, P., 2007, Occurrence of stick-slip phenomenon, Journal of Theoretical and Applied Mechanics, Vol. 45, No. 1, pp. 33-40.

[100] Pratt, J.D. and Pardoen, G., 2002, Numerical modeling of bolted lap joint behavior, Journal of Aerospace Engineering, Vol. 15, No. 1, pp. 20-31.

[101] Chen, S. and Sinha, A., 1990, Probabilistic method to compute the optimal slip load for a mistuned bladed disk assembly with friction dampers, Journal of Vibration and Acoustics, ASME, Vol. 112, No. 2, pp. 214–221.

[102] Wang, J.H. and Chen, W.K., 1993, Investigation of the vibration of a blade with friction damper by HBM, Journal of Engineering for Gas Turbines and Power, ASME, Vol. 115, No. 2, pp. 294–299.

[103] Whiteman, W. and Ferri, A., 1996, Displacement-dependent dry friction damping of a beam-like structure, Journal of Sound Vibration, Vol. 198, No. 3, pp. 313–329.

[104] Berthillier, M., Dupont, C., Mondal, R. and Barrau, J., 1998, Blades forced response analysis with friction dampers, Journal of Vibration and Acoustics, ASME, Vol. 120, No. 2, pp. 468–474.

[105] Sanliturk, K.Y., Ewins, D.J., Elliott, R. and Green, J.S., 2001, Friction damper optimization: Simulation of rainbow tests, Journal of Engineering for Gas Turbines and Power, ASME, Vol. 123, No. 4, pp. 930–939.

[106] Cigeroglu, E., 2002, Nonlinear vibration analysis of bladed disks with dry friction dampers, MS Thesis, Middle East Technical University, Ankara.

[107] Poudou, O. and Pierre, C., 2007, Blades forced response analysis with friction dampers, Ph.D. thesis, University of Michigan.

[108] Sanliturk, K.Y., Imregun, M. and Ewins, D.J., 1997, Harmonic balance vibration analysis of turbine blades with friction dampers, Journal of Vibration and Acoustics, ASME, Vol. 119, No. 1, pp. 96–103.

[109] Csaba, G., 1998, Forced response analysis in time and frequency domains of a tuned bladed disk with friction dampers, Journal of Sound and Vibration, Vol. 214, No. 3, pp. 395–412.

[110] Nanda, B.K. and Behera, A.K., 1999, Study of damping in layered and jointed structures with uniform pressure distribution at the interfaces, Journal of Sound and Vibration, Vol. 226, No. 4, pp. 607-624.

[111] Esteban, J. and Rogers, C.A., 2000, Energy dissipation through joints: theory and experiments, Computers and. Structures, Vol. 75, No. 4, pp. 347–359.

[112] Lu, W., 2001, Modeling of microslip friction and design of frictionally constrained turbine blade systems, PhD Thesis, The Ohio State University.

[113] Nanda, B.K., 2006, Study of the effect of bolt diameter and washer on damping in layered and jointed structures, Journal of Sound and Vibration, Vol. 290, No. 3-5, pp. 1290-1314.

[114] Cigeroglu, E., Lu, W. and Menq, C.H., 2006, One-dimensional dynamic microslip friction model, Journal of Sound and Vibration, Vol. 292, No. 3-5, pp. 881-898.

[115] Olofsson, U. and Hagman, L., 1997, A model for micro-slip between flat surfaces based on deformation of ellipsoidal elastic bodies, Tribology International, Vol. 30, No. 8, pp. 599-603.

[116] Sidorov, O.T., 1983, Change of the damping of vibrations in the course of operation in dependence on the parameters of bolted joints, Strength of Materials, Vol. 14, pp. 671–674.

[117] El-Zahry, R.M., 1985, Investigation of the vibration behavior of pre-loaded bolted joints, Dirasat-Engineering Technology, Vol. 12, pp. 201–223.

[118] Kaboyashi, T. and Matsubayashi, T., 1986, Consideration on the improvement of the stiffness of bolted joints in machine tools, Bulletin of JSME, Vol. 29, pp. 3934–3937.

[119] Tsai, J.S. and Chou, Y.F., 1988, Modelling of dynamic characteristics of two-bolted joints, Journal of Chinese Institute of Engineering, Vol. 11, pp. 235–245.

[120] Tsai, J.S. and Chou, Y.F., 1988, The identification of dynamic characteristics of a single bolt joint, Journal of Sound and Vibration, Vol. 125, No. 3, pp. 487-502.

[121] Shin, Y.S., Iverson, J.C. and Kim, K.S., 1991, Experimental studies on damping characteristics of bolted joints for plates and shells, Journal of Pressure Vessel Technology, ASME, Vol. 113, No. 3, pp. 402–408.

[122] Marshall, M.B., Lewis, R. and Dwyer-Joyce, R.S., 2006, Characterization of contact pressure distribution in bolted joints, Strain, Vol. 42, No. 1, pp. 31-43.

[123] Gould, H.H. and Mikic, B.B., 1972, Areas of contact and pressure distribution in bolted joints, Journal of Engineering for Industry, ASME, Vol. 94, No. 3, pp. 864–870.

[124] Ziada, H.H. and Abd, A.K., 1980, Load pressure distribution and contact areas in bolted joints, Institute of Engineers, India, Vol. 61, pp. 93–100.

[125] Hisakado, T. and Tsukizoe, T., 1978, Measurent of the interface pressure distribution of flat metallic joints, Wear, Vol. 48, No. 1, pp. 209-212.

[126] Damisa, O., Olunloyo, V.O.S., Osheku, C.A. and Oyediran, A.A., 2007, Static analysis of slip damping with clamped laminated beams, European Journal of Scientific Research, Vol. 17, No. 4, pp. 455-476.

[127] Damisa, O., Olunloyo, V.O.S., Osheku, C.A. and Oyediran, A.A., 2008, Dynamic analysis of slip damping in clamped layered beams with non-uniform pressure distribution at the interface, Journal of Sound and Vibration, Vol. 309, No. 3-5, pp. 349-374.

[128] Olunloyo, V.O.S., Damisa, O., Osheku, C.A. and Oyediran, A.A., 2007, Further results on static analysis of slip damping with clamped laminated beams, European Journal of Scientific Research, Vol. 17, No. 4, pp. 491-508.

[129] Ciavarella, M., Hills, D.A. and Monno, G., 1998, The influence of rounded edges on indentation by flat punch, Proceedings of the Institution of Mechanical Engineers, Part C: Journal of Mechanical Engineering Science, Vol. 212, No. 4, pp. 319–327.

[130] Johnson K. L., 1985, Contact mechanics, Cambridge University Press, New York.

[131] Giannakopoulos, A.E., Lindley, T.C., Suresh, S. and Chenut, C., 2000, Similarities of stress concentrations in contact at round punches and fatigue at notches: Implications to fretting fatigue crack initiation, Fatigue and Fracture of Engineering Materials and Structures, Vol. 23, No. 7, pp. 561–571.

[132] Earles, S.W.E., 1966, Theoretical estimation of the frictional energy dissipation in a simple lap joint, IMechE, Part C: Journal of Mechanical Engineering Science, Vol. 8, No. 2, pp. 207–214.

[133] Richardson, R.S.H. and Nolle, H., 1977, Energy dissipation in rotary structural joints, Journal of Sound and Vibration, Vol. 54, No. 4, pp. 577–588.

[134] Jezequel, L., 1983, Structural damping by slip in joints, , Journal of Vibration, Acoustics Stress, Reliability and Design, ASME, Vol. 105, No. 4, pp. 497–504.

[135] Hanks, B.R. and Stephens, D.G., 1967, Mechanisms and scaling of damping in a practical structural joint, Shock and Vibration Bulletin, Vol. 36, pp. 1–8.

[136] Brown, C.B., 1968, Factors affecting the damping in a lap joint, Journal of Structural Division, ASCE, Vol. 94, No. 5, pp. 1197–1218.

[137] Hertz, T.J. and Crawley, E.F., 1985, Displacement dependent friction in space structure joints, AIAA Journal, Vol. 23, No. 12, pp. 1998–2000.

[138] Ferri, A.A., 1988, Modeling and analysis of nonlinear sleeve joints of large space structures, Journal of Spacecraft and Rockets, AIAA, Vol. 25, No. 5, pp. 354–360.

[139] Folkman, S.L. and Redd, F.J., 1990, Gravity effects on damping of a space structure with pinned joints, Journal of Guidance and Control Dynamics, AIAA, Vol. 13, No. 2, pp. 228–233.

[140] Ferri, A.A. and Bindemann, A.C., 1992, Damping and vibration of beams with various types of frictional support conditions, Journal of Vibration and Acoustics, ASME, Vol. 114, No. 3, pp. 289–296.

[141] Folkman, S.L., Roswell, E.A. and Ferney, G.D., 1995, Influence of pinned joints on damping and dynamic behavior of a truss, Journal of Guidance and Control Dynamics, AIAA, Vol. 18, No. 6, pp. 1398–1403.

[142] Heller, L., Foltete, E. and Piranda, J., 2009, Experimental identification of nonlinear dynamic properties of built-up structures, Journal of Sound and Vibration, Vol. 327, No. 1-2, pp. 183-196.

[143] Walker, S.J.I., Aglietti, G.S. and Cunningham, P., 2009, A study of joint damping in metal plates, Acta Astronautica, Vol. 65, No. 1-2, pp. 184-191.

[144] Mohanty, R.C. and Nanda, B.K., 2009, Damping in layered and jointed riveted structures with equal thickness, Journal of Mechanical Engineering Science, Part C, IMechE, Vol. 223, No. 2, pp. 319-328.

[145] Mohanty, R.C. and Nanda, B.K., 2011, Effect of micro-slip on the damping capacity of jointed riveted structures with unequal thickness, Journal of Vibration and Control, Vol. 17, No. 2, pp. 235-244.

[146] Metherell, A. and Diller, S., 1968, Instantaneous energy dissipation rate in a lap joint uniform clamping pressure, Journal of Applied Mechanics, ASME, Vol. 35, No. 1, pp. 123–128.

[147] Heller, L., 2005, Damping in assemblies structures, Ph.D. thesis (Universite de Franche- Comte).

[148] Caignot, A., Ladeveze, P., Neron, D. and Durand, J.F., 2010, Virtual testing for the prediction of damping in joints, Engineering Computations, Vol. 27, No. 5, pp. 621–644.

[149] Yang, B., Chu, M. and Menq, C.F., 1998, Stick-slip-separation analysis and nonlinear stiffness and damping characterization of friction contacts having variable normal load, Journal of Sound and Vibration, Vol. 210, No. 4, pp. 461-481.

[150] Sainsbury, M.G. and Zhang, Q.J., 1999, The Galerkin element method applied to the vibration of damped sandwich beams, Computers and Structures, Vol. 71, No. 3, pp. 239-256.

[151] Lee, S.Y., Ko, K.H. and Lee, J.M., 2000, Analysis of dynamic characteristics of structural joints using stiffness influence coefficients, KSME International Journal, Vol. 14, No. 12, pp. 1319-1327.

[152] Oldfield, M., Ouyang, H. and Mottershead, J.E., 2005, Simplified models of bolted joints under harmonic loading, Computers and Structures, Vol. 84, No. 1-2, pp. 25-33.

[153] Mohanty, R.C. and Nanda, B.K., 2010, Investigation into the dynamics of layered and jointed cantilevered beams, Proceedings of the Institution of Mechanical Engineers, Part C: Journal of Mechanical Engineering Science, Vol. 224, No. 10, pp. 2129-2139.

[154] Escobar, R.L. and Cavalca, K.L., 2007, Parameter prediction in dynamic analysis using response surface method and multi-objective genetic algorithms, 12th IFToMM World Congress, Besançon, France.

[155] Abdo, J. and Tahat, M., 2008, The effect of frequency and amplitude of vibration on the coefficient of friction for metals, WSEAS Transactions on Applied and Theoretical Mechanics, Vol. 3, No.7, pp. 265-274.

[156] Guillaume, B. and Chanet, M., 2010, Improving the accuracy of large-dimension response surface models: application to the vibration behaviour of a car body, 2nd International Conference on Engineering Optimization, September 6 - 9, Lisbon, Portugal.

[157] Liang, X., Lin, Z. and Zhu, P., 2007, Acoustic analysis of damping structure with response surface method, Applied Acoustics, Vol. 68, No. 9, pp. 1036-1053.

[158] Li, Z. and Liang, X., 2007, Vibro-acoustic analysis and optimization of damping structure with response surface method, Materials and Design, Vol. 28, No. 7, pp. 1999-2007.

[159] Ren, W.X. and Chen, H.B., 2010, Finite element model updating in structural dynamics by using the response surface method, Engineering Structures, Vol. 32, No. 8, pp. 2455-2465.

[160] Olunloyo, V.O.S., Osheku, C.A. and Damisa, O., 2008, Vibration damping in structures with layered viscoelastic beam-plate, Journal of Vibration and Acoustics, ASME, Vol. 130, No. 6, pp. 061002-(1-26).

[161] Yoshimura, M., 1980, Computer design improvement of machine tool structure incorporation joint dynamics data, Annals CIRP, Vol. 28, pp. 241–246.

[162] Wang, J.H. and Chuang, S.C., 2004, Reducing errors in the identification of structural joint parameters using error functions, Journal of Sound and Vibration, Vol. 273, No. 1-2, pp. 295-316.

[163] Yin, H.P., Duhamel, D. and Argoul, P., 2004, Natural frequencies and damping estimation using wavelet transform of a frequency response function, Journal of Sound and Vibration, Vol. 271, No. 3-5, pp. 999-1014.

[164] Hwang, H.Y., 1998, Identification techniques of structure connection parameters using frequency response functions, Journal of Sound and Vibration, Vol. 212, No. 3, pp. 469-479.

[165] Ahmadian, H. and Jalali, H., 2007, Identification of bolted lap joints parameters in assembled structures, Mechanical Systems and Signal Processing, Vol. 21, No. 2, pp. 1041-1050.

[166] Good, M.R. and Marioce, D.J., 1989, Using experimental modal analysis to characterize automobile body joints and improve finite element analysis, Proceedings of the Seventh International Modal Analysis Conference, Las Vegas, NV, pp. 106–110.

[167] Young, Y.L., Baker, J.W. and Motley, M.R., 2010, Reliability-based design and optimization of adaptive marine structures, Composite Structures, Vol. 92, No. 2, pp. 244–253.

[168] Nobari, A.S., Robb, D.A. and Ewins, D.J., 1992, A new modal-based method for structural dynamic model updating and joint identification,

Proceedings of the 10th International Modal Analysis Conference, Vol. 1, San Diego, pp. 741–750.

[169] Inamura, T. and Sata, T., 1979, Stiffness and damping properties of the elements of a machine tool structure, Annals of the CIRP, Vol. 28, pp. 235–239.

[170] Yuan, J.X. and Wu, X.M., 1985, Identification of the joint structural parameters of machine tool by DDS and FEM, Journal of Engineering for Industry, ASME, Vol. 107, pp. 64–69.

[171] Kim, T.R., Wu, X.M. and Eman, K.F., 1989, Identification of the joint parameters for a taper joint, Journal of Engineering for Industry, ASME, Vol. 111, No. 3, pp. 282–287.

[172] Mottershead, J.E. and Stanway, R., 1986, Identification of structural vibration parameters by using a frequency domain filter, Journal of Sound and Vibration, Vol. 109, No. 3, pp. 495–506.

[173] Wang, J.H. and Sas, P., 1990, A new method for identifying parameters of mechanical joints, Journal of Applied Mechanics, ASME, Vol. 57, No.2, pp. 337–342.

[174] Aoki, S., 1996, Dynamic characteristics of welded structures, Nuclear Engineering and Design, Elsevier, Vol. 160, No. 3, pp. 379-385.

[175] Carey, A.E., 2002, Experimental studies of welding effects on damping for undersea warfare applications, Thesis, Naval Post Graduate School.

[176] Ehnes, C.W., 2003, Damping in Stiffener Welded Structures, Thesis, Naval Post Graduate School.

[177] Warburton, G.B., 1976, The Dynamical Behaviour of Structures, 2nd edn., Pergamon Press Ltd., Oxford, England, pp. 204-205, pp. 230-231.

[178] Clough, R.W. and Penzien, J., 2003, Dynamics of Structures, 3rd edition, Computers and Structures, Inc., Berkeley, USA.

[179] Montgomery, D.C., 1997, Design and Analysis of Experiments, 4th edn., Wiley, New York.

[180] Hunter, J.S., 1985, Statistical design applied to product design, Journal of Quality Technology, Vol. 17, No. 4, pp. 210–221.

[181] Sukthomya, W. and Tannock, J.D.T., 2005, Taguchi experimental design for manufacturing process optimization using historic data and a neural network process model, International Journal of Quality and Reliability Management, Vol. 22, No. 5, pp. 485–502.

[182] Design Expert, 2008, V8, Design expert user manual release 8, State-Ease Inc., 2021 E. Hennepin Avenue, Suite 480, Minneapolis, MN 55413-2726.

[183] Minitab14, 2003, Minitab User Manual Release 14, MINITAB Inc., State College, PA, USA.

Curriculum Vitae

Name:	BHAGAT SINGH
E-mail:	bhagatmech@gmail.com
Date of birth:	11th October 1976
Nationality:	Indian
Permanent Address:	Qr. No.-MI/231, Kalinga Vihar, Chhend phase-2 PIN: 769015, Rourkela, Odisha, India
Education:	B. Tech., in Mechanical Engineering, Regional Engineering College (REC), Kurukshetra, India, 1999 M. Tech., in M/C Design, Regional Engineering College (REC), Rourkela, India, 2002

Publications

1. Singh, B. and Nanda, B.K., 2009, Study of damping in layered and jointed welded structures, International Journal of Design Engineering, Vol. 2, No. 2, pp. 169-190.

2. Singh, B. and Nanda, B.K., Dynamic analysis of multilayered welded aluminium cantilever beams, Applied Acoustics, Elsevier. (In press)

3. Singh, B. and Nanda, B.K., Estimation of damping in layered welded structures with unequal thickness, Shock and Vibration. (In press)

4. Singh, B. and Nanda, B.K., Identification of damping mechanism in layered and welded structures, International Journal of Mechanical Sciences (IJMS), Elsevier. (In press)

5. Singh, B. and Nanda, B.K., 2010, Effect of Welding on the Slip Damping of Layered and Jointed Structures, Journal of Engineering Mechanics, ASCE, Vol. 136, No. 7, pp. 928-932.

6. Singh, B. and Nanda, B.K., 2010, Mechanism of Damping in Welded Structures using Finite Element Approach, International Journal of Information and Mathematical Sciences, Vol. 6, No. 2, pp. 138-142.

7. Singh, B. and Nanda, B.K., 2010, Damping Mechanism in Welded Structures, International Journal of Engineering and Applied Sciences, Vol. 6, No. 6, pp. 383-388.

8. Singh, B. and Nanda, B.K., 2011, Analysis of damping in layered welded structures using response surface methodology approach, International Journal of Structural Engineering. (In press)

9. Singh, B. and Nanda, B.K., 2011, Effect of interlayer slip on the damping of layered and welded aluminium beams, Journal of Aerospace Engineering, Proceedings of the Institution of Mechanical Engineers Part G, DOI: 10.1177/0954410011417346. (In press)

10. Singh, B. and Nanda, B.K., 2011, Study of damping in layered and welded aluminium cantilever beams of unequal thickness with interlayer slip, Australian Journal of Mechanical Engineering. (In press)

11. Singh, B. and Nanda, B.K., 2011, Investigation into the effect of surface roughness on the damping of tack welded structures using response surface methodology approach, Journal of Vibration and Control. (In press)

12. Singh, B. and Nanda, B.K., Slip damping mechanism in welded structures using response surface methodology, Experimental Mechanics, Springer. DOI: 10.1007/s11340-011-9563-3. (In press)

13. Singh, B. and Nanda, B.K., Study of Damping in Layered and Jointed Welded Structures, International Conference on Advances in Mechanical Engineering (ICAME ’08), December 15-17, 2008, N.I.T. Surat, India, pp. 618-623.

14. Singh, B. and Nanda, B.K., Mechanism of Slip Damping in Welded Structures, International Conference on Emerging Research and Advances in Mechanical Engineering (ERA’09), March 19-21, 2009, Chennai, India, pp. 417-422.

15. Singh, B. and Nanda, B.K., Analysis of Slip Damping in Layered and Jointed Welded Structures using Finite Element Approach, International Conference on Advances in Mechanical Engineering (ICAME '09), August 3-5, 2009, N.I.T. Surat, India, pp. 512-516.

16. Singh, B. and Nanda, B.K., Investigation of Damping Mechanism in Layered and Welded Structures Using Response Surface Methodology Approach, Fifth International Conference on Theoretical, Applied, Computational and Experimental Mechanics (ICTACEM '10), December 27-29, 2010, I.I.T. Kharagpur, India, pp. 1-12.

17. Singh, B. and Nanda, B.K., Analysis of Slip Damping in Welded Structures Using Finite Element Approach, Fifth International Conference on Theoretical, Applied, Computational and Experimental Mechanics (ICTACEM '10), December 27-29, 2010, I.I.T. Kharagpur, India, pp. 1-9.

Papers Communicated

1. Singh, B. and Nanda, B.K., Study of the mechanism of slip damping in jointed welded structures using response surface methodology approach, International Journal of Acoustics and Vibration (IJAV).

2. Singh, B. and Nanda, B.K., Investigation of damping in layered welded beams using finite element approach, International Journal of Acoustics and Vibration (IJAV).

3. Singh, B. and Nanda, B.K., Dynamic analysis of damping in layered and welded beams, Engineering Structures, Elsevier.

4. Singh, B. and Nanda, B.K., Dynamic analysis of layered and welded mild steel beams with unequal thickness, Nonlinear Mechanics, Elsevier.

5. Singh, B. and Nanda, B.K., Dynamic analysis of damping mechanism in welded multilayered mild steel beams, Aerospace Science and Technology, Elsevier.